REGIONAL CORRELATION OF DIAGENETIC COLORATION FACIES AND ANALYSIS OF IRON OXIDE CEMENTATION PROCESSES, JURASSIC NAVAJO SANDSTONE, SOUTHWESTERN UTAH

by

Gregory Barry Nielsen

A dissertation submitted to the faculty of
The University of Utah
in partial fulfillment of the requirements for the degree of

Doctor of Philosophy

in

Geology

Department of Geology and Geophysics

The University of Utah

May 2010

The Graduate School
THE UNIVERSITY OF UTAH

SUPERVISORY COMMITTEE APPROVAL

of a dissertation submitted by

Gregory Barry Nielsen

This dissertation has been read by each member of the following supervisory committee and by a majority vote has been found to be satisfactory.

3-17-10 Date	Chair: **Marjorie A. Chan**
3-18-2010 Date	**Erich U. Petersen**
3-18-2010 Date	**Allan A. Ekdale**
3-20-10 Date	**Cari L. Johnson**
4/9/2010 Date	**Brenda Beitler Bowen**

The Graduate School
THE UNIVERSITY OF UTAH

FINAL READING APPROVAL

To the Graduate Council of the University of Utah:

I have read the dissertation of **Gregory Barry Nielsen** in its final form and have found that (1) its format, citations, and bibliographic style are consistent and acceptable; (2) its illustrative materials including figures, tables, and charts are in place; (3) the final manuscript is satisfactory to the supervisory committee and is ready for submission to The Graduate School.

3-17-10 Marjorie A. Chan, Chair of the Supervisory Committee
Date **Marjorie A. Chan**

Approved for the Major Department

3-23-10 Kip Solomon, Chair / Dean
Date **D. Kip Solomon**

Please DO NOT complete this boxed section UNLESS you are requesting a publication embargo.

Request for Publication Embargo

I request that The Graduate School, the University of Utah, delay the publication of my thesis or dissertation through ProQuest/UMI and the University of Utah Libraries Institutional Repository (USpace) for a period of six months. The chair of my supervisory committee joins me in this request for an embargo.

I am requesting this embargo because (check one):
- ☐ I have a patent pending through the University of Utah Technology Transfer Office.
- ☐ I have a copyright issue with the Journal of ______________________

I understand that the embargo may be lifted at my written request. I also understand that any extension to the approved embargo must be submitted in writing before the embargo is lifted and that the extension will be for an additional six months.

______________ ______________________________, Student
Date

______________ ______________________________, Chair of the Supervisory Committee
Date

The embargo is for a period of six months beginning with the date this form is approved by the Dean of The Graduate School.

Approved for the Graduate Council

4/28/10 CAWight, Dean of The Graduate School
Date Charles A. Wight

ABSTRACT

The effects of iron chemistry dominate the visual landscape of southwestern Utah, producing not only the well-known red rock scenery, but also a broad variety of other colorful features. Diagenetic coloration is perhaps best displayed in the magnificent cliffs of the Jurassic Navajo Sandstone, where selective chemical alteration by subsurface fluids has enriched the rock with iron in some areas (iron oxide cement precipitation), and locally depleted the rock of iron in others (chemical bleaching). This study examines the complex interrelationships between these coloration facies in a regional context in order to better understand the large-scale stratigraphic, hydrodynamic, and tectonic mechanisms that produced them. Primary goals of the study are to map diagenetic coloration facies, analyze geospatial relationships, establish the timing of major diagenetic events, and evaluate the impact of iron oxide cementation on reservoir architecture.

Results indicate that the Navajo Sandstone has a prolonged and complex diagenetic history. At least four major events have occurred on a regional scale: 1) precipitation of primary grain coats to produce primary red rock; 2) bleaching of the upper Navajo Sandstone; 3) precipitation of dense concentrations of iron oxide (up to 30% by weight) in the lower formation; and 4) brightly colored secondary cementation along joints in the upper formation. Hierarchal taxonomies are presented for classifying and interpreting the major types of diagenetic features that are present.

Sandstone bleaching patterns are influenced by multiple factors including variations in eolian bedform morphology, higher percent grainflow stratification in the upper formation, and the localized superimposition of horizontally contiguous bleached facies (loosely akin to sedimentary facies relationships of Walther's law). Dense concentrations of concretionary iron oxide cement occur primarily as discontinuous subhorizontal horizons in the lower portion of the formation. The wide occurrence of these horizons in southwestern Utah may indicate a relationship with regional tectonic processes, with cementation resulting from fluctuating geochemical conditions. Iron oxide precipitation locally follows previously high-permeability bedding features that, upon cementation, become barriers to subsequent fluid flow ("permeability inversion"). These relationships have application for both characterizing reservoir architecture and understanding the diagenetic history of the region.

To my mom and dad,
who first taught me to love the red rock canyons,
and see beauty in an approaching storm.

And to my wonderful wife Brenda.
and great children Brooke, Logan, Zac, and Josh,
who were patient with the long evenings,
and helped me remember what is most important.

TABLE OF CONTENTS

LIST OF TABLES

LIST OF FIGURES

ACKNOWLEDGEMENTS

I gratefully acknowledge my advisory committee for their assistance and advice on this project. I specifically thank Marjorie A. Chan, William T. Parry, and Brenda Beitler Bowen, who pioneered the detailed study of coloration patterns in the Navajo Sandstone, and have provided helpful ideas and feedback throughout the course of this research. I also thank Erich U. Peterson who assisted me in performing laboratory work and was always willing to provide help. This study was funded primarily by the Utah Geological Survey (UGS) under the "Characterization of Utah's Natural Gas Reservoirs and Potential New Reserves" initiative. I thank Tom Chidsey, Craig Morgan, Bryce Tripp, Robert Biek, Rick Allis, and others at the UGS who have provided ideas and support. I also express my appreciation to Victor Heilweil and Kip Solomon, who answered questions regarding groundwater processes. Acknowledgement is made to Leslie Courtright at Zion National Park and Kristin Comella at Snow Canyon State Park who provided research access. I also gratefully thank David Wavrek of Petroleum Systems International, Inc. and Adolph Yonkee of Weber State University who provided laboratory analyses free of charge. Finally, I would like express my appreciation to Allan A. ("Tony") Ekdale, who has served as a close mentor throughout my research.

CHAPTER 1

INTRODUCTION

Background and Objectives

Iron is the fourth most abundant element in the crust of the earth (~5.63% by weight [Enghag, 2004]). Despite its abundance, natural iron is never found in its pure state, but instead occurs chemically bound to oxygen or other elements (Stwertka, 2002). A common result of this bonding is the formation of iron oxide and hydroxide minerals (e.g., hematite, goethite, etc.), which are important ores of considerable economic and cultural importance (about 90% of all refined metal is iron [Stwertka, 2002]). Iron oxide minerals are widely distributed in sedimentary settings (including eolian deposits), often imparting characteristic colors to rocks.

This study investigates regional-scale diagenetic processes that produced iron oxide cementation within the Jurassic Navajo Sandstone of southwestern Utah, including Zion National Park (Zion NP) and Snow Canyon State Park (Snow Canyon SP) (Fig. 1.1). It builds on the work of previous researchers who have explored the following aspects of sandstone coloration: geochemistry and mineralogy of different coloration units (Chan et. al., 2000; Parry et al., 2004; Bowen, 2005; Parry et al., 2009), spatial extent of bleaching (Bowen, 2005), micro- and macro-scale iron oxide cementation

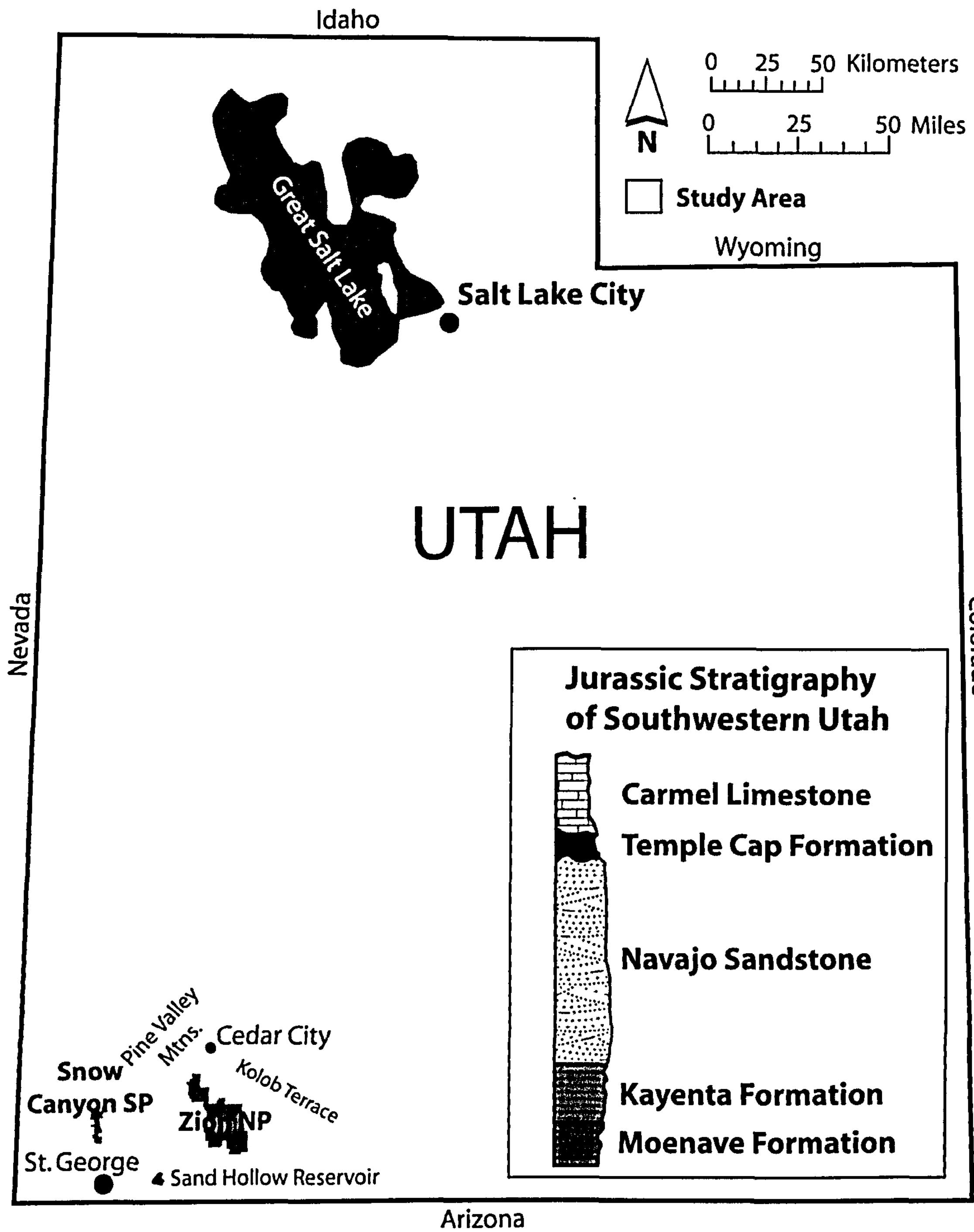

Figure 1.1
Index map shows the location of the study area (lower left) and the Jurassic stratigraphy of southwestern Utah. The locations of Zion National Park (Zion NP) and Snow Canyon State Park (Snow Canyon SP) are shown.

features such as concretions (Chan et al., 2000, Bowen, 2005; Chan et al., 2007; Potter, 2009), relationships of cementation to local stratigraphic and structural features (Net, 2003; Eichhubl et al., 2004; Parry et al., 2004; Bowen, 2005), and similarities between iron oxide features in the Navajo Sandstone and those on Mars (Chan et al., 2004; Bowen, 2005; Chan et al., 2007; Potter, 2009).

The present study expands on this previous work by taking an integrative spatial approach to understanding iron oxide cementation, comparing relationships between coloration units on an outcrop, local area, and broad regional scale. The main objective of this integrative approach is to provide a context for understanding the impact of cementation on reservoir architecture. Specific goals of the study are to: 1) analyze and describe the major diagenetic coloration units that are present in the SW Utah; 2) develop a useful system for classifying bleached and iron enriched features; 3) examine spatial relationships between coloration features using geospatial techniques; 4) establish the timing of major diagenetic events; 5) investigate potential stratigraphic, hydrodynamic, and tectonic controls on cementation; 6) evaluate the impact of iron oxide cementation on reservoir architecture; 7) explore possible correlations with analogous iron oxide features at other localities. The southwest Utah area (Fig. 1.1) is an ideal location for investigating large-scale diagenetic processes because excellent exposures of Navajo Sandstone display a broad diversity of alteration features. Concentrated iron oxide features such as iron oxide concretions and densely cemented "ironstone" layers (Fig. 1.2) are particularly abundant, and occur over a large geographic region. Large areas of relatively undisturbed strata at Zion NP and elsewhere allow for detailed analysis of

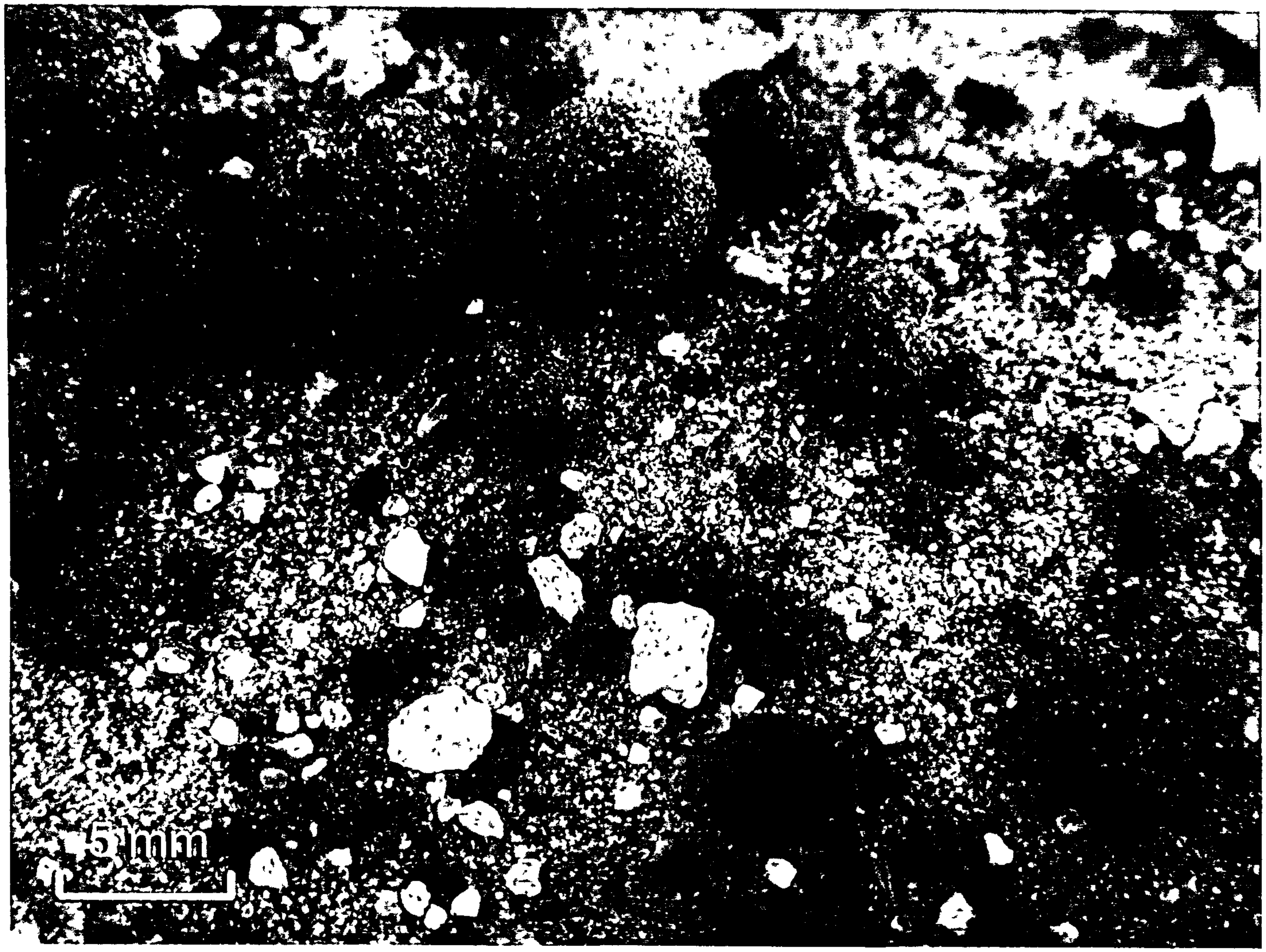

Figure 1.2
Small iron oxide concretions form a lag deposit in the Sand Hollow Reservoir area.

spatial relationships between units, while local zones of structural deformation facilitate temporal correlation.

Iron Oxide Geochemistry and Sandstone Color

Coloration and other characteristics of iron oxides in the Navajo Sandstone have their foundation in the atomic structure of iron. Because of this, a few aspects of iron oxide geochemistry that are relevant to understanding Navajo Sandstone coloration are outlined here. As with other transition elements, elemental iron (electron configuration: $[Ar]3d^6 4s^2$) has a complete outer s energy sublevel (two valence electrons) and an incomplete inner d sublevel that can gain or lose electrons. This structure helps determine many properties of the iron oxide minerals, including their oxidation states, solubility, and color.

Electrons in the outer d and s sublevel of elemental iron are loosely bound. As a result, iron commonly occurs in two oxidation states: "ferrous" iron (Fe^{2+}) and "ferric" iron (Fe^{3+}). The ability of these cations to enter into solution varies considerably, with Fe^{2+} being somewhat soluble and Fe^{3+} being essentially "insoluble" under normal surface conditions. Despite the relative insolubility of ferric oxides such as hematite, dissolution and transport of iron can (and does) occur. Cornell and Schwertmann (2003) observe:

> In natural systems where most of the iron is in the form of Fe^{3+} oxides, the iron should therefore be in immobile form. As large amounts of iron circulate in all parts of the ecosystem (biota, water and soil), however, mobilization of iron (i.e. dissolution) from the oxide reserves must take place (p. 297).

Within the Navajo Sandstone, mobilization of iron is facilitated by chemical and biological reduction (Chan et al., 2000), protonation in acid solution, and complexation with molecules or ions that weaken chemical the bonds (Cornell and Schwertmann, 2003). Dissolution is therefore favored under acidic conditions (low pH) with relatively low reduction potential (or Eh; Tucker, 1991; Parry et al., 2004; Parry et al., 2009).

Iron has precipitated from solution in the Navajo Sandstone to form widespread iron oxide cements (Fig. 1.3). Cementation occurs through either direct precipitation from iron-bearing solution, or the transformation of an iron oxide precursor (Cornell and Schwertmann, 2003). Both hematite and goethite are common cements that are stable at pH and Eh conditions commonly associated with the near-surface. It is primarily the abundance and distribution of these two minerals that gives the Navajo Sandstone its variable coloration.

The uniform, reddish coloration that characterizes the Navajo Sandstone in many areas (Fig. 1.4) is produced by low concentrations of evenly disseminated iron oxide cement (Fig. 1.3A; Bowen, 2005). The reddish hue results from selective absorption of energy (photons) in the blue-green part of the visible spectrum. This absorption occurs as a result of both charge transfer (e.g., between oxygen and iron cations) and temporary splitting of the d sublevel into multiple energy states (Clark, 1995; Schwertman and Cornell, 2000). Other colors in the same area of the visible spectrum (e.g., orange, yellow, brown) are also common (Fig. 1.5), typically resulting from differences in iron oxide concentration, crystal size and shape, and the presence of trace minerals (Schwertman and Cornell, 2000). The term "bleaching" refers to the removal of original iron oxide pigment from a sandstone or other rock (Lindquist, 1988; Chan et al., 2000; Parry, 2004; Beitler, 2005). Bleached white or pale-colored rock is common in many areas of the Navajo Sandstone (Fig. 1.6; Bowen, 2005).

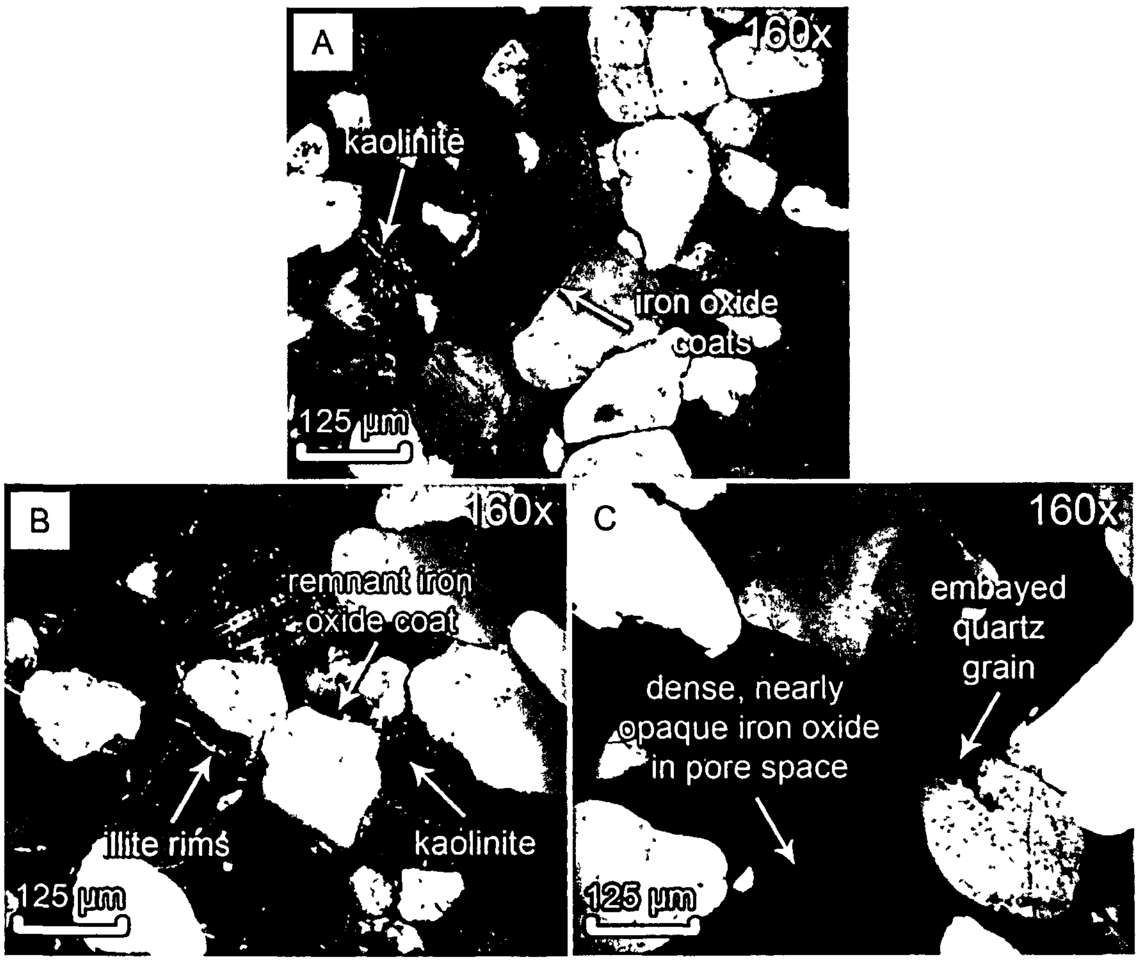

Figure 1.3
Thin section micrographs show distribution of iron oxide for different diagenetic coloration facies at Snow Canyon SP (crossed polarized light). A) Uniform red sandstone has thin coats of hematite around grains. B) Bleached sandstone lacks hematite grain rims. C) Dark colored ironstone with dense iron oxide cement between grains.

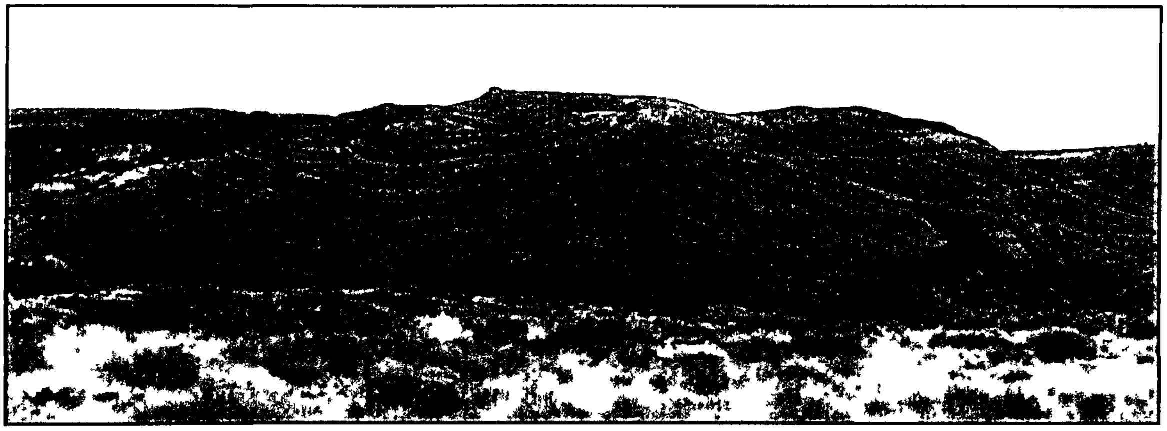

Figure 1.4
Red-colored sandstone of Snow Canyon SP shows different types of interdune bounding surfaces. Parallel, planar bounding surfaces (right of outcrop) have been scoured by a trough-shaped bounding surface (upper left).

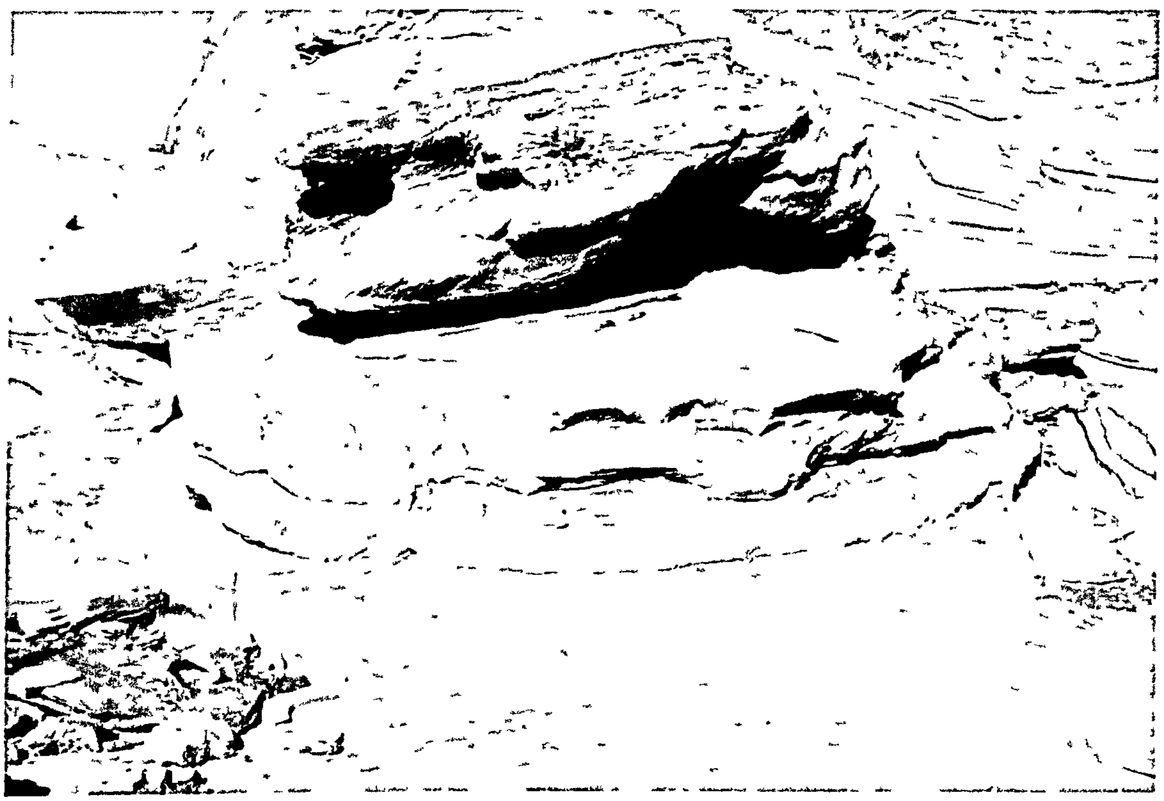

Figure 1.5
Colorful Liesegang-type bands associated with concentrated iron oxide precipitation in the Navajo Sandstone. The origin of these bands is described in Chapter 4. Unaltered "primary" red rock is visible in the rear of the photo.

Figure 1.6
Bleached white and tan rock in the upper Navajo Sandstone of Snow Canyon SP. The boundary between these two coloration facies dips gently to the northwest. Origins of the white and tan coloration subfacies are discussed in Chapter 3.

Eolian Stratification Types

The spatial distribution of diagenetic coloration units in sandstone is commonly related to primary permeability associated with different types of eolian deposition. Kocurek (1996) provides an excellent overview of major eolian transport processes and resulting bedforms. Deposition is controlled by prevailing wind systems and results in three basic types of strata: grainflow, grainfall, and wind ripple. Brief descriptions of each of these basic strata type are given below.

Grainflow strata (Fig. 1.7) are cm-scale, high-angle, lens-shaped deposits that are produced by the avalanching of sand down the slipface of a dune (Hunter, 1977). Individual beds are generally structureless, with contacts marked by thin "pinstripe lamina" (Fryberger and Schenk, 1988; Kocurek and Dott, 1981). Grain size is somewhat larger than that of other eolian deposits (typically fine- to medium- grained). As a result of poor sorting and relatively large grain size, grainflow strata typically have higher primary permeability than other eolian strata types.

Grainfall strata are mm-cm scale, intermediate-angle deposits that form as relatively small particles settle out of wind suspension in front of a dune (Hunter, 1977). Although grainfall deposition may blanket a large area, preservation potential for these strata is relatively low in large dune systems because sediment is frequently reworked by other processes (Lindquist, 1988). The reworking of fine sand by airflow in front of a dune produces wind ripple laminae (Fig. 1.8). These are mm-scale, low to intermediate angle deposits are typically fine- to very fine-grained (Kocurek and Dott, 1981; Hunter, 1977; Kocurek, 1996). Individual lamina are characterized by relatively sharp contacts

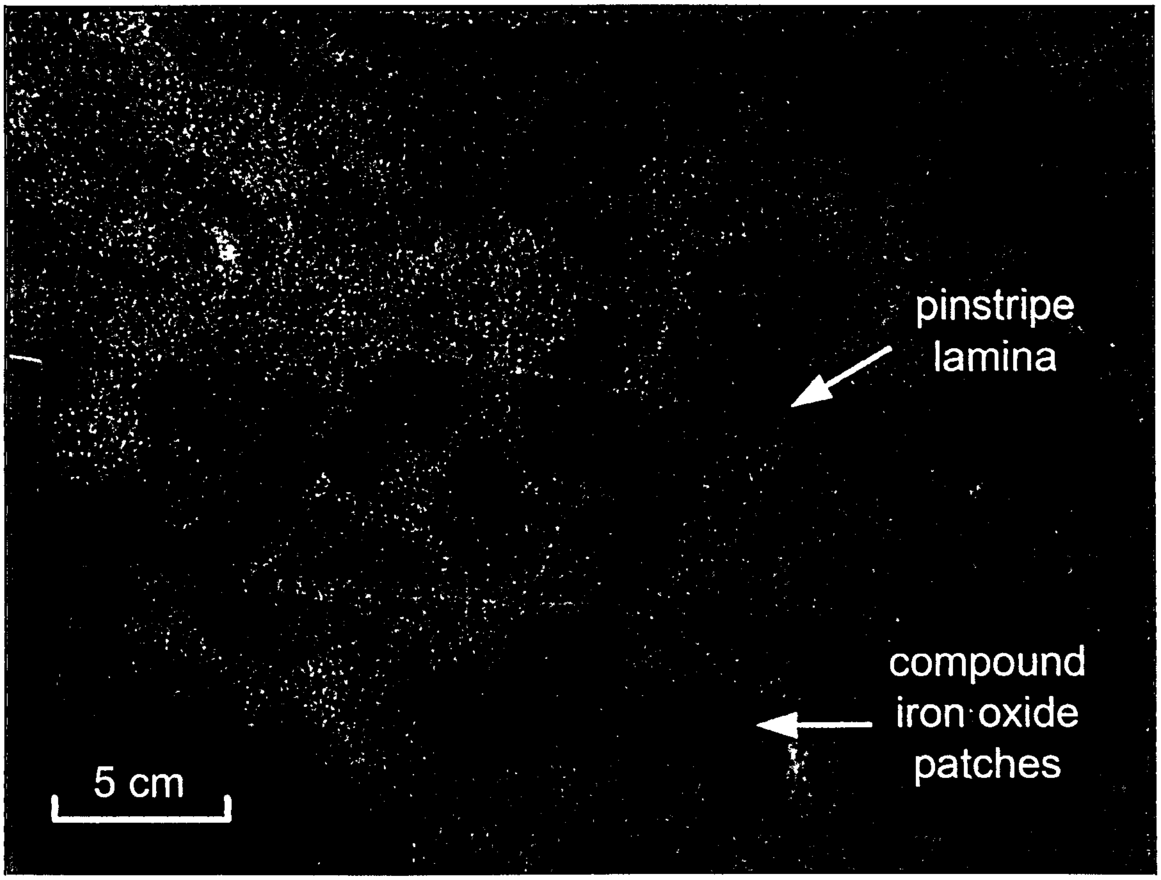

Figure 1.7. Patches of darker-colored iron oxide forming in grainflow strata. Finer-grained pinstripe laminae mark the boundary between successive grainflow deposits.

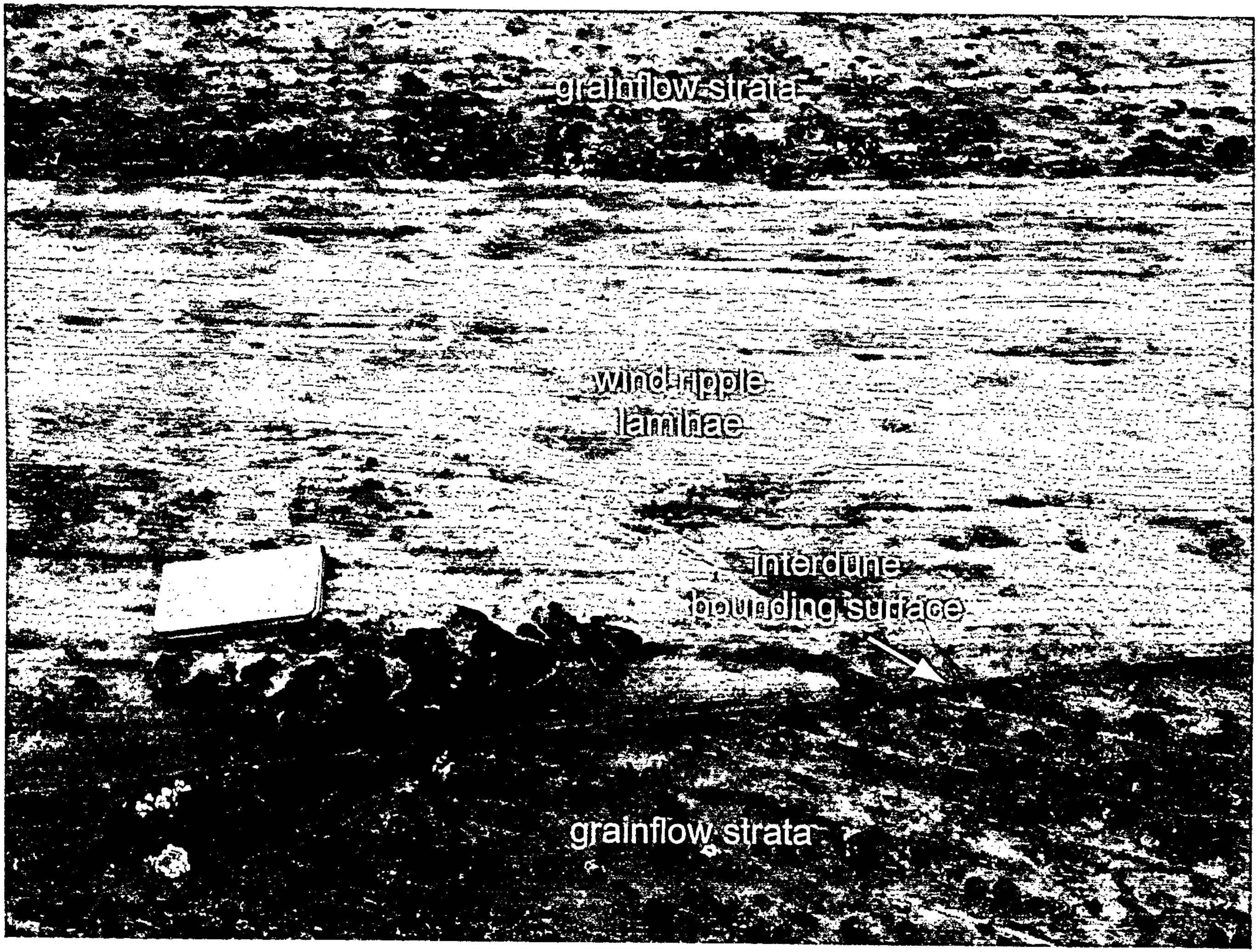

Figure 1.8
Preferential formation of iron oxide concretions in higher-permeability grainflow strata.

and possible inverse grading (Fig. 1.8; Schenk, 1983). Because wind ripple laminae are typically finer-grained and better sorted than grainflow deposits, their permeability is usually much lower (Net, 2003).

Chapter Summaries

Chapters in this paper focus on different aspects of diagenesis in the Navajo Sandstone of southwestern Utah. Chapter 1 defines six diagenetic coloration facies (including 12 subfacies) in the SW Utah area and characterizes the distribution of iron oxide in each. The spatial distribution of coloration facies in the Zion NP area (Fig. 1.1) is examined and compared with primary permeability patterns within the formation. Processes that may concentrate bleaching within the upper formation are also explored. Spatial relationships are used to estimate the relative timing of major diagenetic events in the region.

Chapter 2 focuses on spatial relationships between different styles of bleaching in the Snow Canyon SP area. Bleaching features are mapped and classified based upon their scale, geometry, and relative distance from the main reaction front. Horizontal and vertical successions of bleached features are compared and methods for spatial correlation are discussed. The relationship of diagenetic features to joints and faults are used to estimate the timing of bleaching. Comparisons are made between bleaching styles in the Snow Canyon SP and Zion NP areas.

Chapter 3 focuses on concentrated iron oxide cementation in the lower Navajo Sandstone. A hierarchal taxonomy is presented for classifying these features based upon relative iron oxide concentration and cementation style. The geometry and spatial extent of large-scale iron oxide horizons are evaluated and potential structural and hydrogeological controls on cementation are discussed. Timing of cementation is also evaluated based upon relationships to structural features. The impact of secondary iron oxide precipitation is evaluated and implications for reservoir architecture are explored. Similarities with analogous cementation features on Mars are discussed.

The appendices of this paper provide full data sets and additional images related to aspects of diagenetic alteration that are too specific to cover in the body of the paper. Information on the mineralogy and bulk chemical composition of the Kayenta and Temple Cap Formations (Fig. 1.1) is also provided. An accompanying 1:10,000 map (Plate 1) shows detailed relationships between diagenetic coloration facies in the Snow Canyon SP area.

References

Bowen, B.B., 2005, Sandstone bleaching and iron concretions: An index to fluid pathways and diagenetic history of the Jurassic Navajo Sandstone, Southern Utah [Ph.D. thesis]: Salt Lake City, University of Utah, 221. p.

Chan, M.A., Parry, W.T., and Bowman, J.R., 2000, Diagenetic hematite and manganese oxides and fault-related fluid flow in Jurassic sandstones southeastern Utah: American Association of Petroleum Geology Bulletin, v. 84, p. 1281–1310.

Chan, M.A., Beitler B., Parry W.T., Ormo, J., and Komatsu, G., 2004, A possible terrestrial analogue for hematite concretions on Mars: Nature, v. 429, p. 731–734.

Chan, M.A., Ormo, J., Park, A.J., Stich, M., Sousa-Egipsy, V., and Komatsu, G., 2007, Models of iron oxide concretion formation: Field, numerical, and laboratory comparisons: Geofluids v. 7, p. 356–368.

Clark, R.N., 1995, Reflectance spectra, *in* Ahrens, T.J., ed., Rock physics and phase relations, a handbook of physical constants: Washington, D.C., American Geophysical Union, p. 178-188.

Cornell, R.M., and Schwertmann, U., 2003, The iron oxides: Structure, properties, reactions, occurrences and uses: Germany, Wiley-VCH, Second Edition, 573 p.

Eichhubl, P., Taylor, W.L., Pollard, D.D. and Aydin, A., 2004, Paleo-fluid flow and deformation in the Aztec Sandstone at the Valley of Fire, Nevada – evidence for the coupling of hydrogeologic, diagenetic, and tectonic processes: Geological Society of America Bulletin, v. 116, p. 1120-1136.

Enghag, P., 2004, Encyclopedia of the elements: Germany, Wiley-VCH, 1243 p.

Fryberger, S.G. and Schenk, C.J., 1988, Pin stripe lamination – a distinctive feature of modern and ancient eolian sediments: Sedimentary Geology, v. 55, p. 1–15.

Kocurek, G., and Dott, R.H., 1981, Distinction and uses of stratification types in the interpretation of eolian sand: Journal of Sedimentary Petrology, v. 51, p. 579-595.

Kocurek, G., 1996, Desert aeolian systems, *in* Reading, H.G., ed., Sedimentary environments: Processes, facies and stratigraphy, Oxford, Blackwell, Third Edition, p. 125-153.

Lindquist, S.J., 1988, Practical characterization of eolian reservoirs for development: Nugget Sandstone, Utah-Wyoming thrust belt, *in* Kocurek, G., ed., Late Paleozoic and Mesozoic eolian deposits of the Western Interior of the United States: Sedimentary Geology, v. 56, p. 515-339.

Net, L.I, 2003, Diagenesis and reservoir quality of the Eolian Nugget / Navajo Sandstone (Early Jurassic), Utah and Wyoming [Ph.D. thesis]: University of Texas, Austin, 182 p.

Parry, W.T., Chan, M.A., and Beitler, B., 2004, Chemical bleaching indicates episodes of fluid flow in deformation bands in sandstone: American Association of Petroleum Geologists Bulletin, v. 88, p. 1–17.

Parry, W.T., Chän, M.A., and Nash, B.P., 2009, Diagenetic characteristics of the Navajo Sandstone in the Covenant oil field, central Utah thrust belt, American Association of Petroleum Geologists Bulletin, v. 93, p. 1031-1061.

Potter, S.L., 2009, Characterization of Navajo Sandstone hydrous ferric oxide concretions [M.S. thesis], Salt Lake City, University of Utah, 180 p.

Schenk, C.J., 1983. Textural and structural characteristics of some experimentally formed eolian strata, *in* Brookfield, M.E., and Ahlbrandt, T.S., eds., Eolian sediments and processes: Developments in Sedimentology, v. 38, Amsterdam, Elsevier, p. 41-49.

Schwertman, U., and Cornell, R.M., 2000, Iron Oxides in the laboratory: Preparation and characterization: New York, Wiley VCH, Second Edition, 188 p.

Stwertka, A., 2002, A guide to the elements: Oxford, Oxford University Press, Second Edition, 248 p.

Tucker, M.E., 1991, Sedimentary petrology – an introduction to the origin of sedimentary rocks: Oxford, Blackwell Scientific Publications, Second Edition, 260 p.

CHAPTER 2

DIAGENETIC COLORATION FACIES AND ALTERATION HISTORY OF THE JURASSIC NAVAJO SANDSTONE, ZION NATIONAL PARK AND VICINITY, ·SOUTHWESTERN UTAH

Reprinted with permission from
Utah Geological Association, Publication 38,
Geology and Geological Resources and Issues of Western Utah, p. 67-96.
Gregory B. Nielsen, Marjorie A. Chan, and Erich U. Petersen

Abstract

Coloration patterns in the Jurassic Navajo Sandstone of Zion National Park and vicinity are examined using a broad variety of geochemical, geospatial, petrographic, and bedform analysis techniques. Six diagenetic coloration facies (including 12 subfacies) are defined and characterized. Results indicate a prolonged and complex diagenetic history with variations in color resulting largely from changes in the concentration and distribution of iron oxides. In the northern Kolob Plateau, the Navajo Sandstone has a uniform red pigmentation (red primary facies) that formed during early diagenesis to produce the "primary" sandstone color. In contrast, Navajo Sandstone of main Zion Canyon displays "secondary" alteration features occurring in three distinct vertical coloration facies: brown (lower), pink (middle), and white (upper).

The white and pink facies in Zion Canyon are characterized by a combination of prevalent bleaching, areas of remnant "primary" sandstone, and small concretionary iron-enriched lenses. Bleaching is concentrated in the upper Navajo Sandstone where alteration occurred during middle diagenesis (deep burial). Widespread bleaching and alteration in Zion Canyon terminates abruptly in the central part of the park but narrow, well-defined, white bleached bands locally follow high-permeability beds northward for several kilometers into the red-colored Kolob Plateau (red/white facies). The brown facies is characterized by widespread dark iron oxide cement concentrations precipitated beneath a well-defined subhorizontal boundary. Isolated lenses of dense ironstone in overlying facies represent possible ancient conduits for transporting mobilized iron. Later episodes of limited iron oxide precipitation produced brightly colored cementation (multicolored facies) along some joints in the upper part of the formation.

The spatial distribution of alteration features at Zion National Park is related to permeability variations corresponding to stratigraphic shifts in eolian bedform morphology. Moving stratigraphically upward through the Navajo Sandstone, bedform changes here include increased foreset dip (from 18 to 22 degrees), a clockwise rotation of mean transport direction (from S to SW) and higher percent grainflow strata (from 17 to 25%). Increased prevalence of grainflow strata in the upper part of the formation likely facilitated bleaching fluids in this zone. These examples show the importance of primary textures in controlling fluid flow within an eolian reservoir system.

Introduction

As the 19th-century American geologist Clarence Dutton conducted a pioneering survey of the upper gorge of the Virgin River (now Zion National Park, Fig. 2.1), he marveled at the diverse coloration patterns, "The slopes, the widening ledges, the bosses of projecting rock, the naked, scanty soil, display colors which are truly amazing. . .(The towers) are white above, and change to a strong, rich red below" (Dutton, 1882, p. 57-59). Although these exposures have been the setting for decades of geologic research, relatively little previous work has specifically explored the diverse diagenetic coloration patterns in the Zion National Park (Zion NP) area. These coloration patterns are significant both as records of fluid-related alteration events as well as indicators of past and present permeability pathways within the sandstone. This study examines the mineralogy and spatial distribution of coloration features in order to better understand the nature and relative timing of events that produced them. It also correlates key diagenetic features observed in Zion NP with similar patterns recognized elsewhere in southwestern Utah.

A framework for investigating the diagenetic history of Zion NP has been established by previous investigations. Gregory (1950) attributes the major colors in Zion NP to different iron-bearing minerals and suggests the white color of the upper Navajo Sandstone indicates an absence of iron. In a widely used geologic map and guidebook to the park, Hamilton (1978, 1992) subdivides the Navajo Sandstone into three informal subunits: brown (lower), pink (middle), and white (upper). He attributes the white color of the upper Navajo Sandstone to the removal of cement by flowing

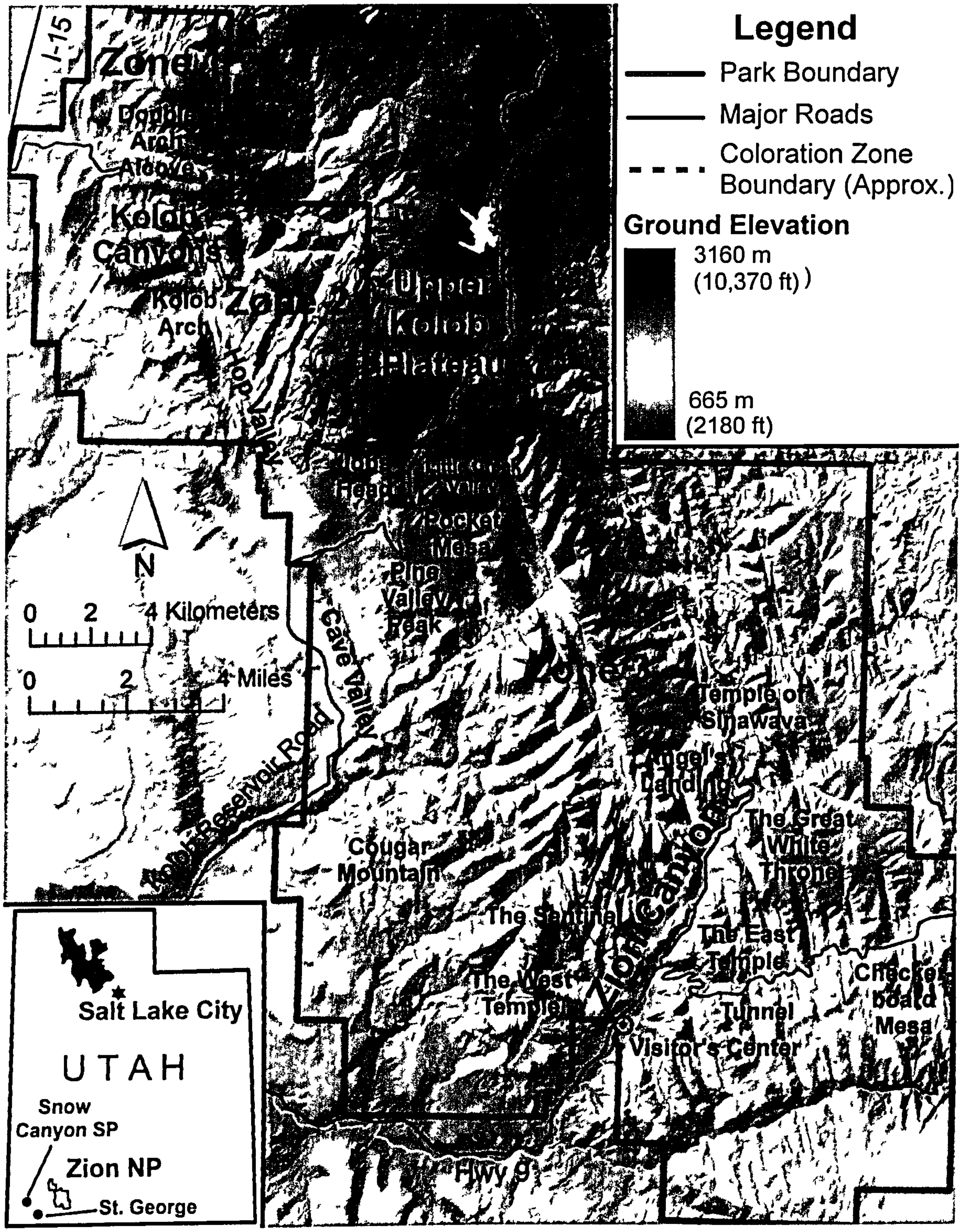

Figure 2.1
Map of Zion NP showing geographic zones and selected locations referred in this paper. Navajo Sandstone in each zone has a distinct appearance and is associated with different diagenetic coloration facies.

groundwater and brown color to a combination of hematite and limonite produced by the re-precipitation of previously dissolved iron. Biek et al. (2003) also attribute the light colors of the upper Navajo Sandstone to alterations in iron oxide mineralogy related to changes in the oxidation state, with particular relation to the dense ironstone features within the pink subunit of the park. Chapter 4 explores the origin of widespread concentrated iron oxide cementation features in the lower Navajo Sandstone of SW Utah (including Zion NP) and discuss the impact of this cementation on reservoir quality.

Similar coloration patterns to those in Zion NP have been studied elsewhere in the Navajo Sandstone and other formations (e.g., Chan et al., 2000; Net, 2003; Eichhubl et al., 2004; Beitler et al., 2005). Variations in sandstone color result from differences in mineralogy, cement distribution, crystal size, and other factors with iron oxide concentrations having a dominant effect (Cornell and Schwertmann, 2003; Net, 2003). Shortly after deposition, most of the Navajo Sandstone had an even reddish pigmentation produced by thin coats of iron oxide surrounding grains (Walker, 1979). Present-day variations in color (white, yellow, brown, etc.) result from later alteration by subsurface fluids, including both the chemical reduction and removal of iron ("bleaching") and the secondary precipitation of additional iron oxide cement ("enrichment"). These changes are often fabric selective (Fig. 2.2) and may be locally controlled by eolian stratification patterns (Lindquist, 1988; Net, 2003; Beitler et al., 2005). Relatively coarse and poorly sorted grainflow strata (Hunter, 1977; Kocurek and Dott, 1981) typically show the broadest diversity of colors as a result of high primary permeability (Net, 2003). In contrast, wind ripple strata (Hunter, 1977; Kocurek and Dott, 1981) and wet interdune deposits (Lancaster and Teller, 1988) have lower permeability and are more likely to

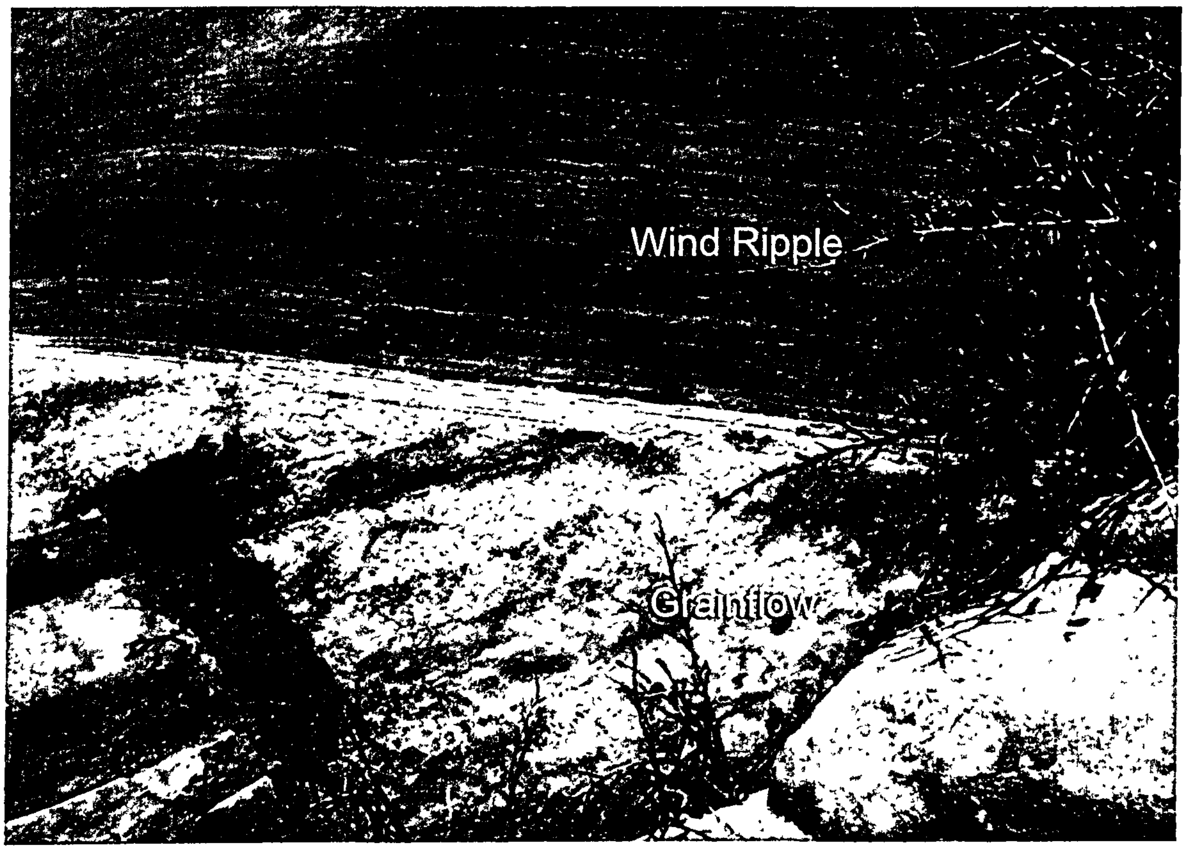

Figure 2.2.
Interdune bounding surface separating wind ripple and grainflow deposits. Note preferential bleaching of the coarser-grained, more permeable grainflow strata (length of ruler in lower left is 15 cm).

retain original red pigmentation. Eolian bounding surfaces generally separate sandstones of different permeabilities, and may be associated with sharp color contrasts (Fig. 2.2).

Geologic Setting

Jurassic Stratigraphy

The dominant cliff-forming unit in Zion NP area is the Navajo Sandstone (Fig. 2.3), which is a fine- to medium-grained sandstone with prominent, large-scale, eolian cross-bed sets and variable coloration. During the Early Jurassic, the Navajo sand sea produced deposits extending southward from Idaho and Wyoming to southern Arizona (Marzolf, 1988; Peterson, 1988, Blakey, 1994). The resulting eolian Navajo Sandstone unit attains its maximum thickness in the southwest Utah area where it locally exceeds 600 m (~2000 ft) (McKee, 1979; Biek et al., 2003). The Navajo Sandstone is underlain conformably by reddish-brown fluvial units of the Lower Jurassic Kayenta and Moenave Formations (Fig. 2.3). The top of the Navajo Sandstone is marked by the J-1 unconformity, a regionally extensive surface that marks a period of erosion that nearly leveled the top of the Navajo Sandstone (Pipiringos and O'Sullivan, 1978). Above the J-1 unconformity is the Middle Jurassic Temple Cap Formation that is divided into two members: the lower, Sinawava Member consists of reddish-brown sandstone and the upper, White Throne Member consists of multicolored, cross-bedded eolian sandstone (Peterson and Pipiringos, 1979; Biek et al., 2003). The top of the Temple Cap Formation is marked by the J-2 unconformity which represents a brief period of erosion preceding the invasion of a shallow sea from the northeast that deposited the marine limestone of the Carmel Formation (Brenner and Peterson, 2004).

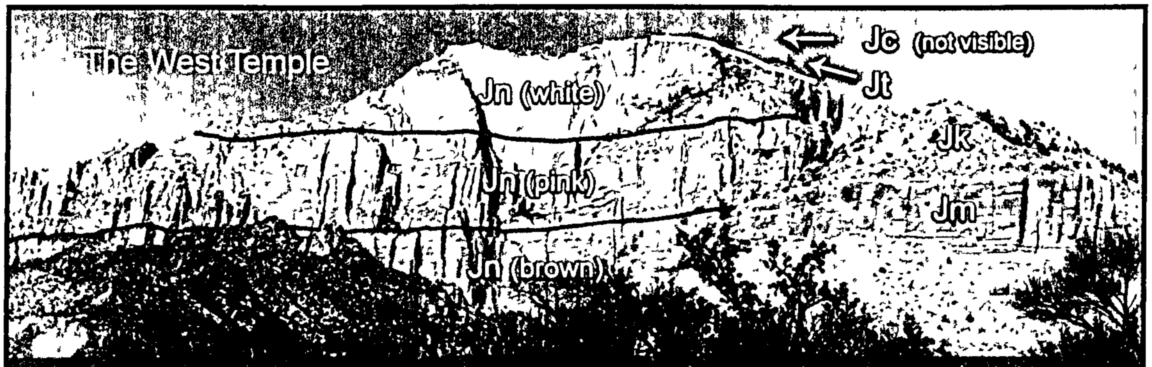

Generalized Jurassic Stratigraphy of Zion National Park, Utah

SYSTEM	SERIES	FORMATION	SYMBOL	APPROX. THICKNESS m (ft)	LITHOLOGY
JURASSIC	MIDDLE	Carmel Fm.	Jc	300 (850)	Pale yellow to gray marine limestone.
					J2 Unconformity
		Temple Cap Fm.	Jt	60 (200)	Fine-grained, reddish-brown sandstone and siltstone at base (Sinawava Mbr). Multicolored, eolian sandstone above (White Throne Mbr.).
					J1 Unconformity
	LOWER	Navajo Sandstone	Jn	610 (2000)	Fine- to medium-grained, cliff-forming, eolian sandstone with large-scale cross-bedding and well-developed joints. Divided into informal coloration subunits in the southern park. (white / pink / brown)
		Kayenta Fm.	Jk	180 (600)	Reddish-brown fluvial sandstone, siltstone, and mudstone. Lower members form slopes and upper member forms cliffs that merge with the base of the Navajo Sandstone.
		Moenave Fm.	Jm	150 (490)	Reddish-brown fluvial sandstone, siltstone, and mudstone with isolated thin lenses of conglomerate. Upper member forms prominent cliffs.

Figure 2.3
Generalized Jurassic stratigraphy of Zion NP in the main Zion Canyon area (Fig. 2.1: Zone 1). Top photo shows the West Temple from near the Visitor's Center looking west. The distant cliffs are approximately 1 km (0.6 mi) in front of the outcrops in the right of the photo. Stratigraphic column adapted from Biek et al. (2003) and Graham (2006).

Regional Tectonics

Tectonic activity in the vicinity of Zion NP is associated with two major events: the Sevier-Cordilleran orogeny and Basin and Range extension. Deformation began in the Middle Jurassic (soon after deposition of the Navajo Sandstone) when a low-relief back-bulge basin at the leading edge of the Sevier thrust system formed over much of Utah, allowing a shallow epicontinental sea to move across the area from the northeast (Stokes, 1986; Lawton, 1994; Willis, 1999; Biek et al., 2003). As the thrust system continued to migrate across the region, folds and thrust faults formed, climaxing in the Late Cretaceous (Willis, 1999). The Kanarra anticline and Taylor Creek thrust-fault zones in the Kolob Canyons area of Zion NP likely formed about 75 to 55 million years ago as part of this phase of deformation (Biek et al., 2003). The Kanarra anticline is co-linear with the Virgin anticline approximately 30 km (18 mi) to the southwest in the St. George, Utah area (Biek, 2003). Thrusting in southern Utah ended approximately 40 million years ago (Willis, 1999).

Major normal faults that cross-cut diagenetic features in the Zion NP area are associated with late Tertiary Basin and Range extension. Most estimates place the onset of movement along the Hurricane and Sevier faults (west and east of Zion NP) as occurring during the Miocene to early Pliocene (Biek et al., 2003; Lund et al., 2007; Lund et al., 2008). North-northwest trending joints in the park are either related to Basin and Range extension or to the earlier relaxation of compressional forces associated with the Sevier orogeny (Hamilton, 1992; Biek et al., 2003; Rogers et al., 2004).

Methods

Bulk Composition and Mineralogy

Rock colors were coded using the standardized Munsell rock color system (Rock-Color Chart Committee, 1991) and facies relationships were documented during extensive field reconnaissance. The mineralogy and diagenetic history of each facies was characterized in the lab using a combination of spectral, x-ray diffraction, petrographic, and mass spectrometer analysis. A portable analytical spectrometer was used to measure visible to short wave infrared reflectance spectroscopy for samples from various locations throughout Zion NP as well as other locations in the nearby St. George, Utah area (n=59). All samples were evaluated under artificial light across both visible and near infrared wavelengths. X-ray diffraction was performed on 25 powdered samples to further facilitate mineral identification (2θ = 5-35° at 2°/minute). Powdered specimens were mixed with water then agitated slightly to align the particles and improve the clay detection threshold (clay extraction by centrifuging was not performed). The relative abundance and distribution of kaolinite, illite, iron oxide, and other minerals was characterized using point count analysis on 15 representative thin sections (n=15,000 total points at 1 mm spacings), as well as qualitative analysis of 9 additional sections. Slides were partially stained with sodium cobalt nitrite to assist in feldspar identification. Inductively coupled plasma mass spectrometry (ICP-MS) was performed in a commercial laboratory on 30 samples (26 from the Navajo Sandstone, 2 from the Kayenta Formation and 2 from the Temple Cap Formation) to measure the average weight percent for major oxides and the abundance of selected trace elements (sample localities are listed in Appendix B).

Eolian Bedform Analysis

Bedding orientation and dominant stratification type were measured at 635 points within a variety of outcrops in the lower, middle, and upper Navajo Sandstone of Zion NP, as well as at Snow Canyon State Park (Snow Canyon SP) to the west (Fig. 2.1). Measurements were made at regularly spaced intervals in an oblique direction relative to bedding in order to maximize the variety of stratification types coded (grainflow, wind ripple, grainfall, etc. [Hunter, 1977]). Interdune data were excluded when calculating percent grainflow. Average foreset dip and mean dip direction were calculated using the GEOrient software of Holcombe (2009). In order to tentatively evaluate the potential of units overlying the Navajo Sandstone as a stratigraphic trap, gas permeability measurements were made on three surface plugs by a commercial laboratory.

Soxhlet Extraction and Fluid Inclusions Analyses

Soxhlet extraction isolates compounds from rock through repeated circulation of a distilled solvent. Soxhelt extraction of organics using methylene chloride solvent was performed by a commercial laboratory on eight Navajo Sandstone samples to determine if detectable traces of hydrocarbon were present. Six of these samples were bleached or otherwise diagenetically altered and the other two were samples with primary red coloration. Two additional samples from with known properties were also analyzed to serve as a control. Compounds extracted from the Navajo samples were analyzed using gas chromatography to determine if the signatures were consistent with degraded hydrocarbon. Hydrocarbon gas phase analysis (Wavrek et al., 2004) was performed by Petroleum Systems International on 16 variably altered samples (80 total analyses) from the St. George, Utah area in order to determine the isotopic composition and hydrocarbon signal strength of fluid inclusions. The location of petroleum inclusions within select samples was evaluated by analyzing thin sections using UV light.

Preliminary Characterization of Diagenetic Coloration Facies

Coloration in the Navajo Sandstone is highly variable as a result of diagenetic alteration. Navajo Sandstone of the Zion NP region (including the St. George, Utah area to the west [Fig. 2.1]) is divided into six major diagenetic coloration facies and subdivided into 12 subfacies based upon similarities in rock color and shared diagenetic features (Table 2.1). Each facies group consists of regional-scale (km+) areas of rock having similar visual and compositional characteristics, implying a distinct diagenetic origin. Subfacies are used to differentiate localized variations within parent facies. Symbols used to reference facies and subfacies in figures are listed in Table 2.1. These symbols consist of the formation abbreviation (e.g., Jn) followed by one or more letters that give the dominant color or colors of the facies (e.g., Jn-r for red primary facies, Jn-rw for the red/white transition facies). Generalized color names were used when naming facies and more precise Munsell color designations are given in Appendix A. This paper provides a preliminary characterization of each diagenetic facies with emphasis on iron oxides and other minerals that contribute to coloration. Diagenetic coloration facies and subfacies are described moving north to south through the park (from Zones 1 to 3 on Figs. 2.1 and 2.4). The petrographic and mineralogical characteristics of each coloration facies are given in Figs. 2.5 to 2.7.

Table 2.1.

Major diagenetic coloration facies and subfacies of the Navajo Sandstone for Zion NP and vicinity.

Diagenetic Facies	Symbol	Zion Zone (Fig. 1)	Stratigraphic Position (Thickness)	Subfacies	Characteristic Features	Zion	Snow Cny.
Red Primary	Jn-r	1	Entire Formation	-	Uniform reddish coloration with minimal alteration.	Y	Y
Red/White Intermixed	Jn-rw	2	Variable	-	Banded and interfingered zones of red and white sandstone.	Y	Y
Multicolored Local	Jn-m	3	Middle/ Upper (Localized)	Liesegang Banded	Brightly colored Liesegang-type bands, commonly near joints.	Y	Y
				Yellow/Orange Patchy	Bright yellow to red coloration patches, commonly near joints.	Y	Y
White Bleached	Jn-w		Upper (270 m / 880 ft)	Tan	Zone of tan alteration in upper bleached zone.	N	Y
				White Speckled	White with abundant brown specks (~1mm).	Y	N
				White	White, bleached sandstone, usually near the top of the formation.	Y	Y
				Yellow	Areas of yellowish alteration in white facies.	Y	Y
Pink Altered	Jn-p		Middle (165 m / 540 ft)	Uneven Red/Orange	Uneven pinkish coloration with areas of Fe-oxide enrichment and depletion.	Y	N
				Ferruginous Lens	Narrow "lenses" of dense brown to black ironstone in lower part of pink facies.	Y	N
Brown Ferruginous	Jn-b		Lower (165 m / 540 ft)	Overprinted White	White bleached sandstone overprinted with darker cementation features.	N	Y
				Overprinted Red	Reddish sandstone overprinted with darker cementation features (spots, concretions, etc).	Y	Y
				Green and Brown	Greenish sandstone with abundant brown spots.	Y	N
				Ironstone	Dense brown to black iron-enriched sandstone.	N	Y

Approximate unit thicknesses measured near the Great White Throne in main Zion Canyon. A list of corresponding Munsell colors for each coloration facies are given in Appendix A.

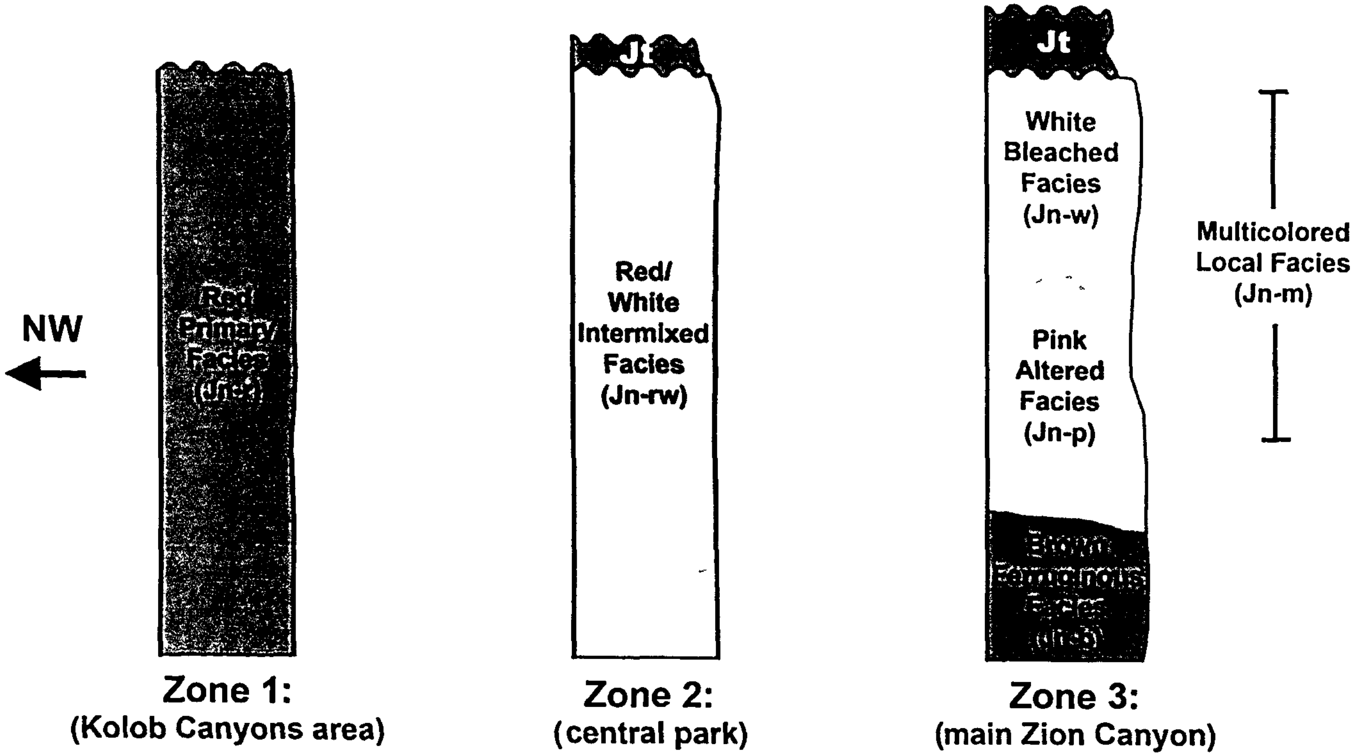

Figure 2.4
Spatial relationships among diagenetic coloration facies in different areas of Zion NP. Jn: Jurassic Navajo Sandstone, Jt: Temple Cap Formation.

Figure 2.5
Thin section micrographs (plane light) for representative Navajo Sandstone samples from different diagenetic facies at Zion NP (localities shown in Fig. 2.1). (A) *Primary red facies.* Thin, reddish-brown iron-oxide grain coats line individual grains to produce a uniform orangish-red color. Grain coats are missing along some interpenetrating grain contacts. Locality: Double Arch Alcove. (B) *Red/white intermixed facies.* Secondary iron-oxide cementation and partially removed grain coats produce uneven orangish coloration. Locality: Hop Valley. (C) *Brown ferruginous facies.* Iron oxide present as well-developed primary grain coats and as secondary pore-filling cement. The pore fill area corresponds to a dark cementation spot visible in outcrop. Locality: main Zion Canyon. (D) *Brown ferruginous facies (green and brown spotty subfacies).* Both calcite and green micaceous cement are locally abundant as secondary pore-filling cements. (E) *Pink altered facies.* Uneven iron oxide precipitation and removal produces patchy orangish-pink coloration. Locality: main Zion Canyon. (F) *Pink altered facies (ferruginous lens subfacies).* Dense iron oxide cementation locally produces dark-colored "ironstone." Locality: main Zion Canyon. (G) *White bleached facies (white speckled subfacies).* Missing iron oxide coats around grains result in a nearly white sandstone. Small concentrations of iron oxide produces visible brown "speckles" in outcrop. Locality: main Zion Canyon. (H) *White bleached facies (yellow subfacies).* Faint yellowish coats around grains produce yellowish-orange sandstone. Locality: main Zion Canyon. (I) *Multicolored local facies.* Secondary cementation in pore spaces and alteration of grain coats produces a red and yellow Liesegang-banded sandstone. Locality: main Zion Canyon.

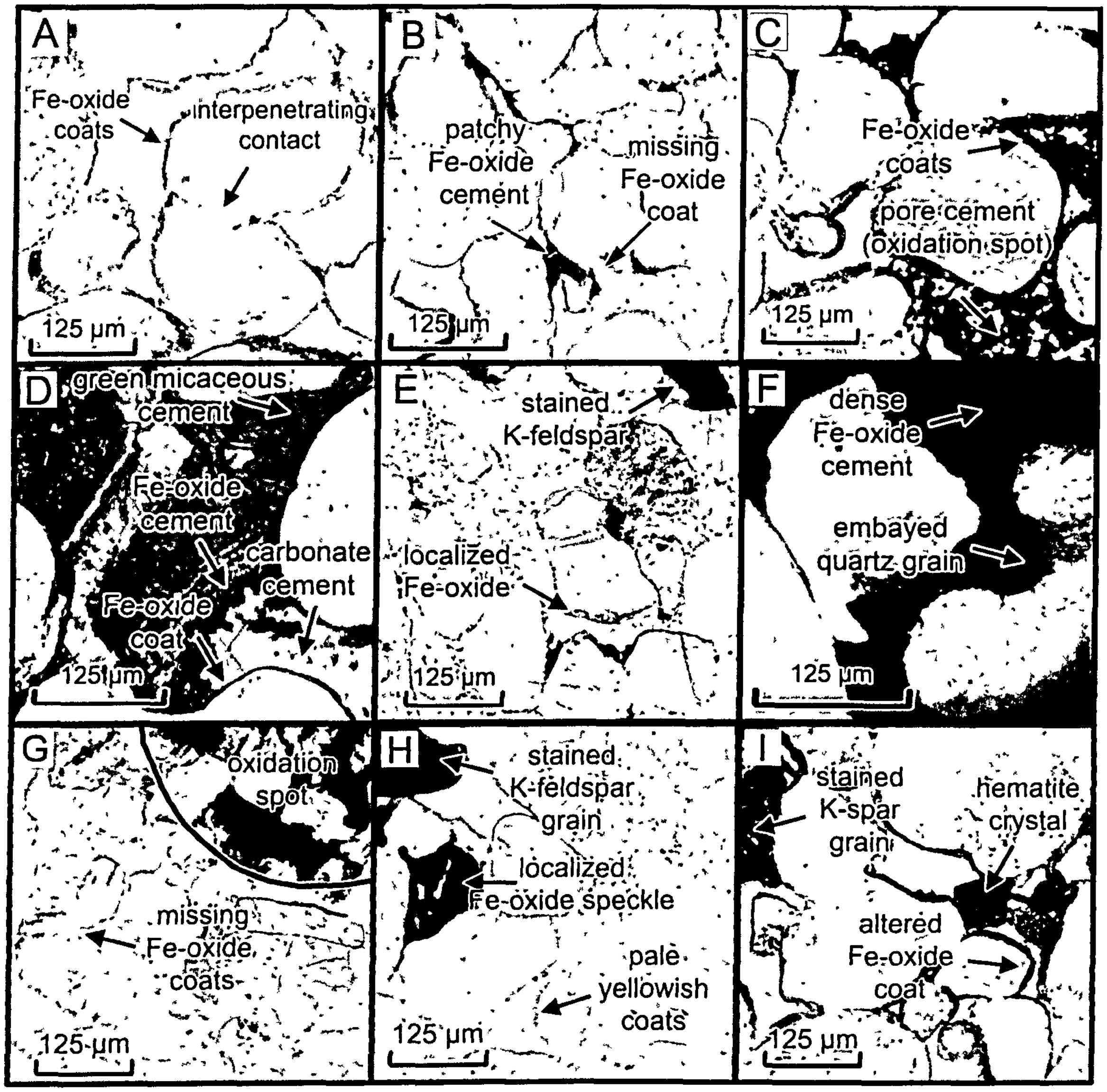
A
Fe-oxide coats
interpenetrating contact
125 μm
B
patchy Fe-oxide cement
missing Fe-oxide coat
125 μm
C
Fe-oxide coats
pore cement (oxidation spot)
125 μm
D
green micaceous cement
Fe-oxide cement
carbonate cement
Fe-oxide coat
125 μm
E
stained K-feldspar
localized Fe-oxide
125 μm
F
dense Fe-oxide cement
embayed quartz grain
125 μm
G
oxidation spot
missing Fe-oxide coats
125 μm
H
stained K-feldspar grain
localized Fe-oxide speckle
pale yellowish coats
125 μm
I
stained K-spar grain
hematite crystal
altered Fe-oxide coat
125 μm

Figure 2.6

Artificial light spectral reflectance for representative Navajo Sandstone samples from different diagenetic coloration facies at Zion NP. Strong absorption at near 0.9 μm in the uniform red and grayish brown samples is indicative of iron oxide. Hematite has narrower band at ~0.86 μm and goethite has wider band at ~0.93 μm (Cornell and Schwertmann, 2003; Bowen et al., 2007; Chapter 4). The band at 2.2 μm occurs in clay minerals with the doublet in uniform red sample indicating the mineral kaolinite. Prominent bands near 1.4 μm and 1.9 μm are characteristics of clays and other minerals that contain water or OH if only the 1.4 μm band is present (Clark, 1995). Absorption at approximately 2.3 μm commonly represents carbonate (Clark et al., 2007). Additional spectra available in Appendices E and F.

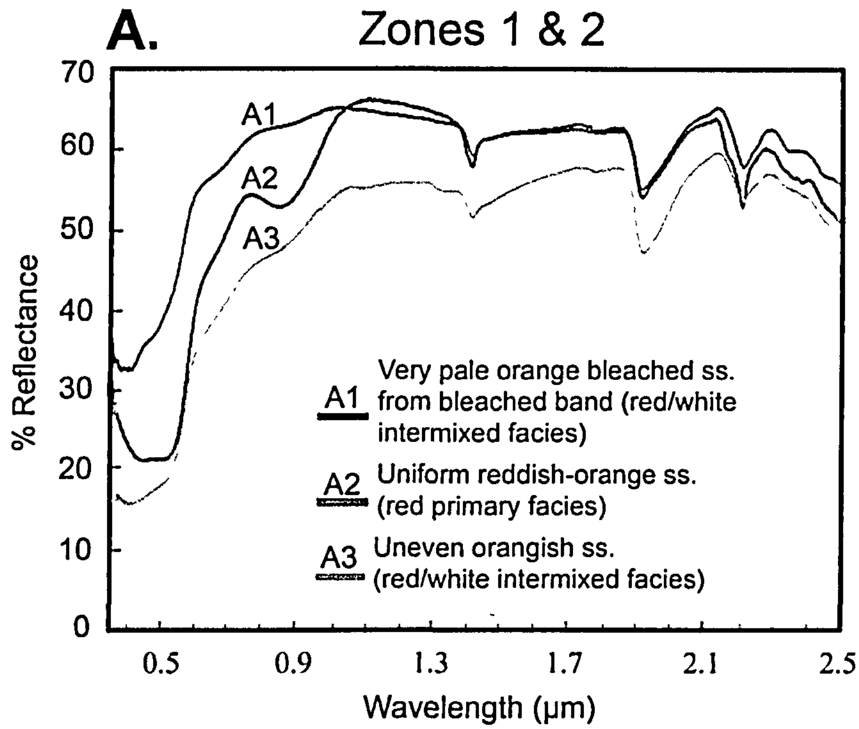
A.
Zones 1 & 2
70
60
50
40
30
20
10
0
% Reflectance
A1
A2
A3
Very pale orange bleached ss. from bleached band (red/white intermixed facies)
Uniform reddish-orange ss. (red primary facies)
Uneven orangish ss. (red/white intermixed facies)
0.5
0.9
1.3
1.7
2.1
2.5
Wavelength (μm)

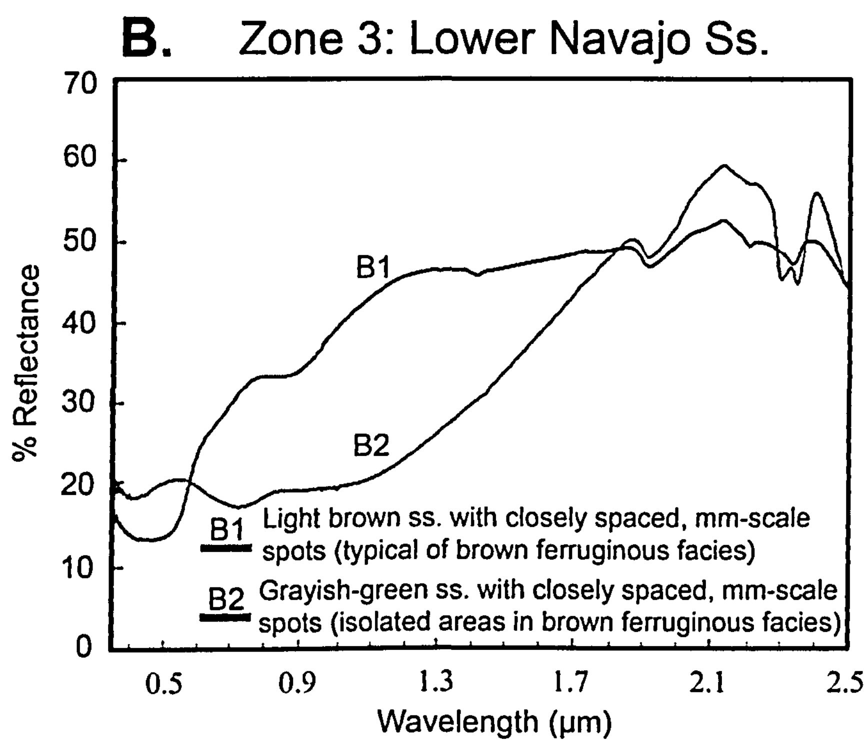
B.
Zone 3: Lower Navajo Ss.
70
60
50
40
30
20
10
0
% Reflectance
B1
B2
Light brown ss. with closely spaced, mm-scale spots (typical of brown ferruginous facies)
Grayish-green ss. with closely spaced, mm-scale spots (isolated areas in brown ferruginous facies)
0.5
0.9
1.3
1.7
2.1
2.5
Wavelength (μm)

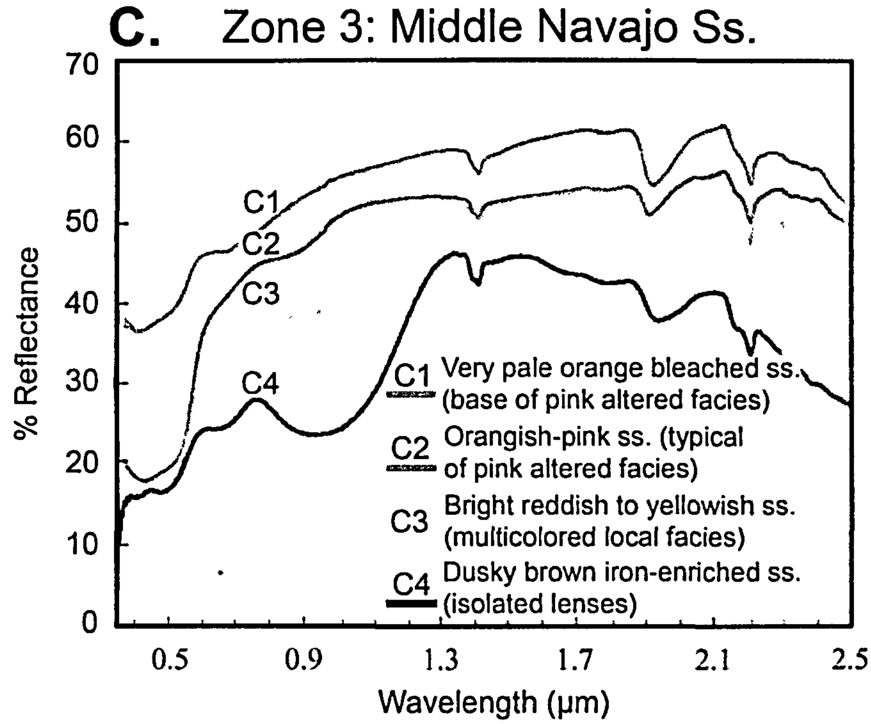

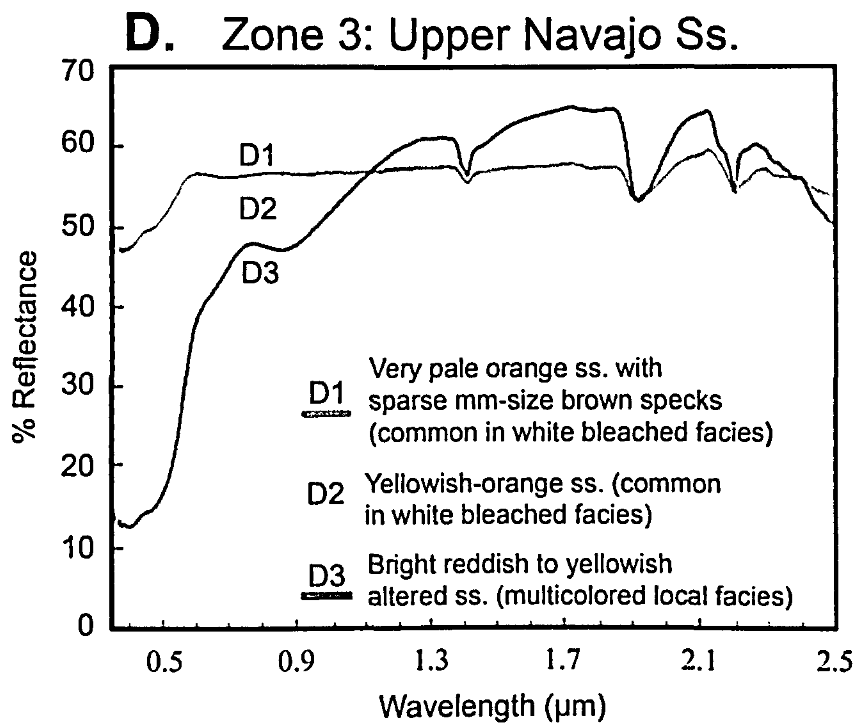

Figure 2.6 continued

Figure 2.7
X-ray diffraction (XRD) patterns for representative samples from different diagenetic coloration facies at Zion NP. Intensity patterns have been artificially offset in 200-unit increments in order to separate them visually. Strong two-theta peaks for selected minerals are indicated for each zone (wavelength to compute theta = 1.54Å[Cu]). Mineral identifications were made in conjunction with petrographic and other analyses and should be viewed as tentative where less than three matching peaks are present. Because clay extraction by centrifuging was not performed, kaolinite and illite concentration may fall below the detection threshold for this method (compare with point count results in Table 2.3). Iron oxide occurring as grain coats also falls below the detection threshold (but higher concentrations of iron oxide in pore spaces may be detected).

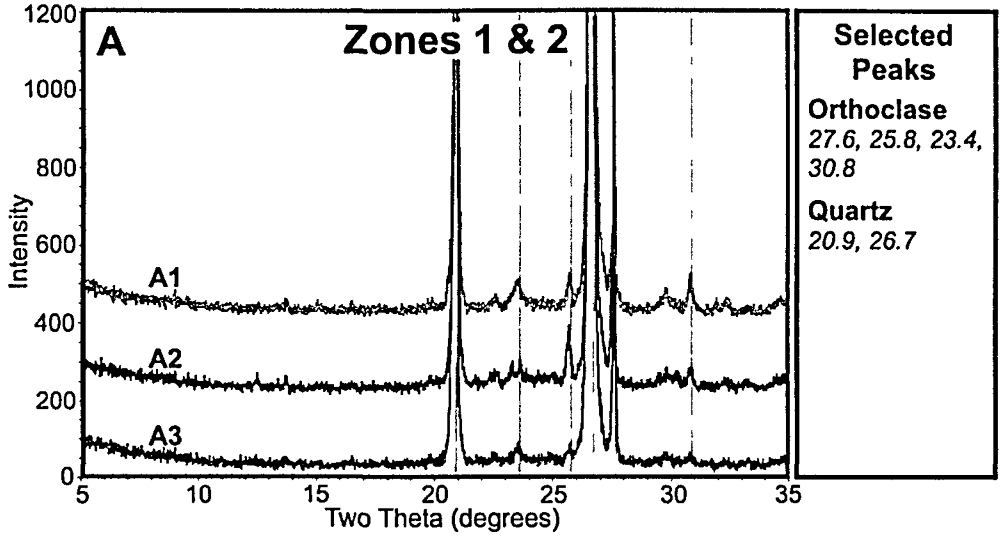

Samples

- A1 Very pale orange ss. from bleached band (red/white intermixed facies)
- A2 Uniform reddish-orange ss. (red primary facies)
- A3 Uneven orangish ss. (red/white intermixed facies)

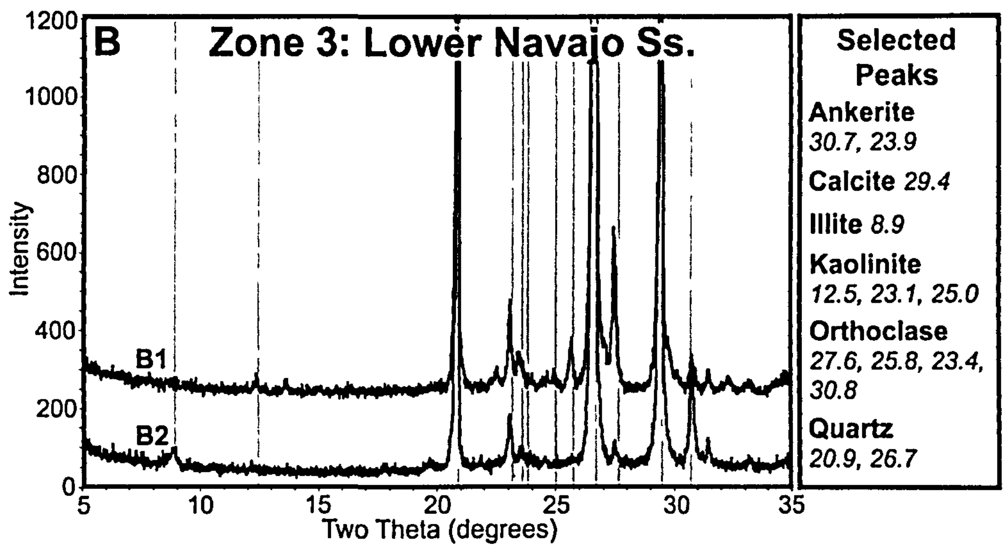

Samples

- B1 Light brown ss. with closely spaced, mm-scale brown spots (typical of brown ferruginous facies)
- B2 Grayish-green ss. with closely spaced, mm-scale brown spots (isolated areas of brown ferruginous facies)

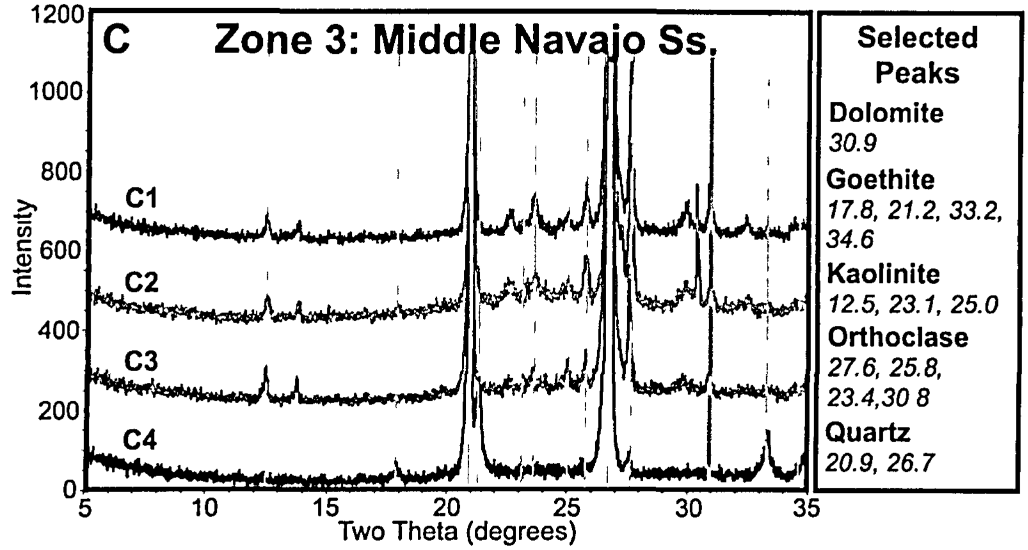

Samples

C1 Very pale orange bleached ss. (base of pink altered facies)

C2 Orangish-pink ss. (typical of pink altered facies)

C3 Bright reddish to yellowish altered ss. (multicolored local facies)

C4 Dusky brown, iron-enriched ss. (isolated lenses in pink altered facies)

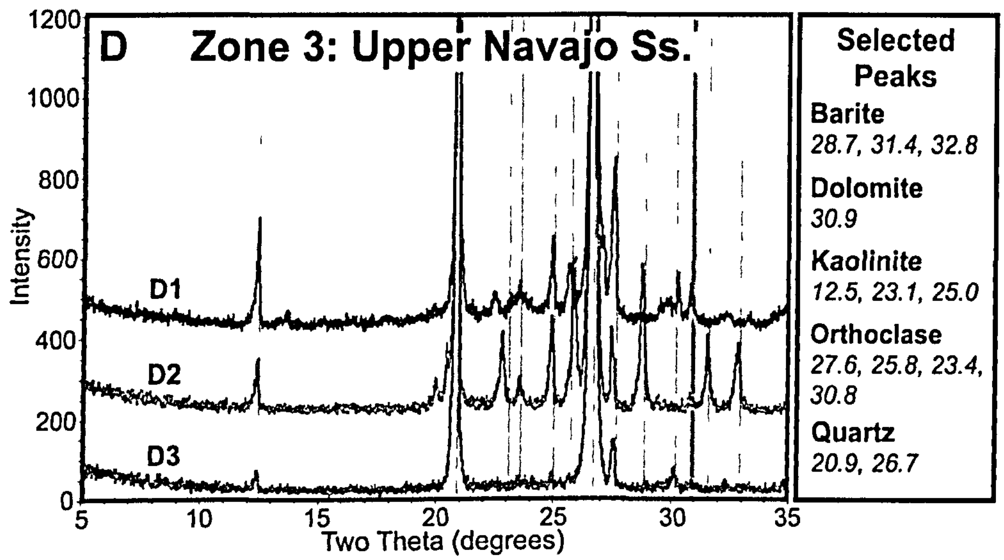

Samples

D1 Very pale orange ss. with mm-size brown specks (typical of white bleached facies)

D2 Pale yellowish-orange ss. (common in white bleached facies)

D3 Bright reddish to yellowish altered ss. (multicolored local facies)

Figure 2.7 continued

Red Primary Facies (Jn-r)

The term "primary" refers to sandstone interpreted as having retained its initial coloration produced shortly after deposition (Chapter 4). Evenly colored sandstone associated with the red primary facies occurs throughout the entire Navajo Sandstone section in Zone 1 (Fig. 2.1). Pigmentation is fairly uniform (Fig. 2.8A) with the exception of localized areas of minor discoloration. The red color is produced by evenly distributed grain coats that are visible in thin section (Fig. 2.5A). The actual amount of iron oxide present is small (~0.7%; Table 2.2) and commonly occurs in association with illite (Table 2.3; see also Parry et al., 2004). Spectral analysis indicates that hematite is the dominant iron oxide (Fig. 2.6A) and other cements are relatively uncommon (Table 2.3; Fig. 2.7A). The relatively low iron oxide concentration and dominance of hematite in this facies is consistent with uniform red-colored sandstone at other locations (Eichhubl et al., 2004; Beitler et al., 2005; Bowen et al., 2007).

Red/White Transition Facies (Jn-rw)

Uneven, orangish-red coloration and well-defined white "bleached bands" characterize the red/white intermixed facies (Fig. 2.8B). This is the dominant facies of Zone 2 in northern to central Zion NP (Fig. 2.1) and is comparable to partially bleached sandstones elsewhere in the region (Eichhubl et al., 2004; Seiler and Chan, 2007; Nielsen and Chan, 2009). Bleached bands are apparent features produced when narrow, sheet-like areas of bleached rock are exposed in cross-section within the 2-D plane of an outcrop (Nielsen and Chan, 2009). They are typically less than a few meters high but may extend laterally for kilometers. In the Hop Valley area of Zion NP (Fig. 2.1),

Figure 2.8
Characteristic diagenetic features of northern and central Zion NP (Fig. 1: Zones 1 and 2). (A) *Red primary facies*. Uniform red sandstone cliffs with surficial white and black streaks that extend downward from seeps (top is hidden in clouds). Locality: Kolob Canyons. (B) *Red/white intermixed facies*. Linear bleached bands follow interdune bounding surfaces in unevenly colored Navajo Sandstone to the middle right of image B. Evenly colored primary red cliffs are visible to the rear (north). Locality: Hop Valley. (C) *Red/white intermixed facies (detail)*. Lobe and cusp structure (Eichhubl et al., 2004) associated with white bleached bands indicates apparent paleofluid flow in a roughly northward direction. Locality: Hop Valley.

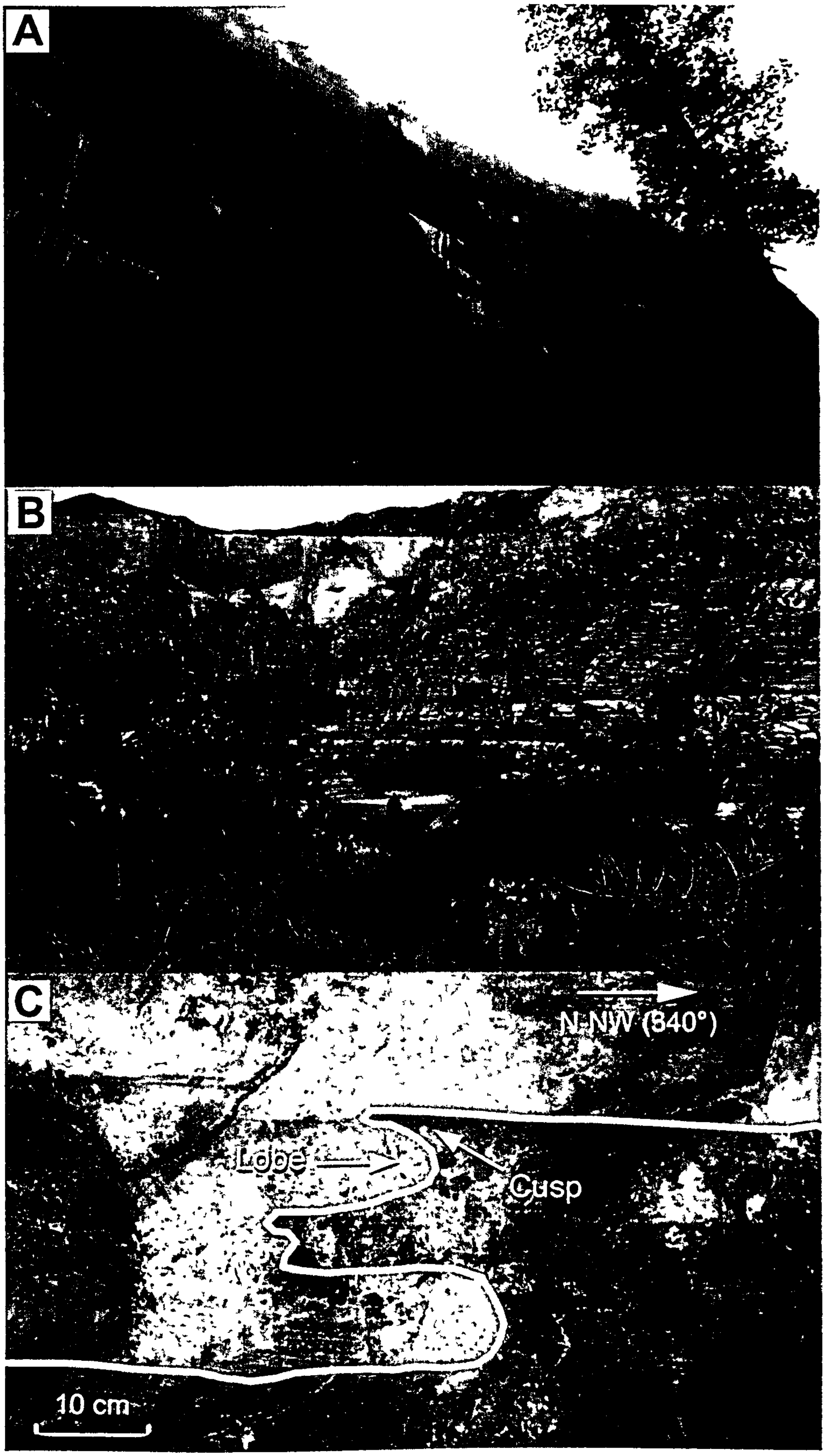
A
B
C
N-NW (340°)
Lobe
Cusp
10 cm

Table 2.2

Average abundance (ICP-MS weight % and standard error of the mean) of selected oxides for representative samples from each diagenetic facies in the Navajo Sandstone of Zion NP and vicinity.

Diagenetic Facies	Subfacies	n	SiO_2 %	Al_2O_3 %	Fe_2O_3 %	MnO %	MgO %	CaO %
Red Primary	-	2	94.95 (0.11)	2.03 (0.16)	0.68 (0.09)	< 0.01 (N/A)	0.07 (0.01)	0.04 (0.02)
Red/White Intermixed	(Unbleached)	2	96.08 (1.8)	1.85 (1.0)	0.84 (0.13)	0.01 (0.01)	0.07 (0.02)	0.02 (0.00)
	(Bleached)	2	93.99 (4.11)	1.54 (0.39)	1.23 (0.64)	0.01 (0.00)	0.04 (0.01)	0.12 (0.09)
Multicolored Local	Liesegang Banded	1	95.55	1.77	1.4	0.01	0.06	0.12
	Patchy	3	92.69 (1.06)	2.44 (0.32)	1.33 (0.52)	0.01 (0.01)	0.05 (0.01)	0.03 (0.01)
White Bleached	Tan	1	93.88	2.78	0.88	0.01	0.08	0.04
	White Speckled	1	94.36	2.27	1.24	0.01	0.07	0.04
	White	1	94.13	3.10	0.20	<0.01	0.06	0.02
	Yellow	2	94.43 (0.65)	1.95 (0.25)	0.57 (0.12)	<0.01 (0.00)	0.05 (0.05)	0.02 (0.01)
Pink Altered	Uneven Red/Orange	2	93.00 (0.76)	2.57 (0.35)	0.95 (0.23)	0.01 (0.01)	0.04 (0.01)	0.04 (0.01)
	Ferruginous Lens	1	82.57	1.27	13.22	0.05	0.09	0.04
Brown Ferruginous	Overprinted White	1	88.45	1.59	4.39	2.60	0.10	0.72
	Overprinted Red	5	88.24 (3.8)	3.23 (0.47)	1.32 (0.17)	0.07 (0.04)	0.10 (0.02)	2.32 (2.2)
	Green and Brown	1	73.12	0.57	1.54	0.09	0.69	12.38
	Ironstone	1	73.28	1.21	19.32	0.10	0.09	0.79
COMBINED		**26**	**90.75 (1.41)**	**2.23 (0.18)**	**2.36 (0.84)**	**0.13 (0.10)**	**0.09 (0.02)**	**1.01 (0.63)**

Values for the red/white intermixed facies include both unbleached and bleached samples. Full ICP-MS results (including trace element abundance and data for the Kayenta and Temple Cap Formations) are available in Appendix B.

Table 2.3

Mineral abundance (volume %) and porosity for representative samples from each diagenetic coloration facies.

Specimen Info				Grains %			Coats%			Cement%						Por. %
Facies	Subfacies	Locality	n	Qtz	Kfs	Oth	FeO	Ill	Oth	FeO	Kln	Ill	Qtz	Cbn	Oth	
Red Primary	-	Zion	1000	67.7	3.9	3.1	1.9	1.0	0	0.6	0.5	0.6	0	0	1.1	19.6
R/W Inter-mixed	(unbleached)	Zion	1000	71.1	2.3	5.0	1.7	0.9	0	0.5	0.1	0	0.1	0	0	18.3
	(bleached)	Zion	1000	68.3	9.8	2.8	0.5	1.0	0	0.6	0	0.3	1.4	0	0.1	15.2
Multi-colored Local	Liesegang Banded	Zion	1000	67.2	3.1	0.5	3.8	0.1	0	3.6	0.5	0.3	0.1	0	0.1	20.7
	Patchy	Zion	1000	68.8	5.5	1.9	2.2	0.1	0	1.0	0.2	0.3	0.2	0	0.1	19.7
White Bleached	Tan	Snow Cny	1000	69.0	3.2	1.4	0.8	1.7	0	0	0	0.3	4.1	0	0	19.5
	White Speckled	Zion	1000	67.7	11.3	2.7	0	0	0	0.2	0.5	0.3	0.4	0	0.1	16.8
	White	Snow Cny	1000	71.4	2.9	2.3	0	0.2	0	0	1.3	0.2	0.1	0	0	21.6
	Yellow	Zion	1000	68.5	4.3	2.6	0	1.9	0	0.5	2.8	0	0	0	0.4	19.0
Pink Altered	Uneven Red/Orange	Zion	1000	72.5	6.6	1.3	1.5	0.5	0	1.3	0.6	0	0.1	0	0.1	15.5
	Ferruginous Lens	Zion	1000	68.1	0.9	1.5	0.2	0	0	22.8	0	0	0	0	0	6.5
Brown Ferru-ginous	Overprinted White	Snow Cny	1000	64.3	3.1	1.5	0.2	0.1	0	12.9	0.1	0.3	0	2.3	6.2	9.0
	Overprinted Red	Zion	1000	65.8	1.5	0.9	3.1	0	0	11.4	0.4	0.2	0	0	0.1	16.6
	Green and Brown	Zion	1000	61.7	0.6	2.1	2.6	1.2	0.1	6.9	0	0.7	0.1	18.4	3.0	2.6
	Ironstone	Snow Cny	1000	67.6	-	2.1	2.2	0	0	12.7	0.2	0.2	0	1.5	0	13.5
Comb.	-	-	**15,000**	**68.0**	**4.2**	**2.1**	**1.4**	**0.6**	**0**	**5.0**	**0.5**	**0.2**	**0.4**	**1.5**	**0.7**	**15.6**

Mineral abundance from point count analysis. Qtz = quartz; Kfs = potassium feldspar; FeO = iron oxide; Ill = illite; Kln = kaolinite; Cbn = carbonate; oth = other; por. = porosity.

bleached bands are closely spaced (~1 to 15 m [3 - 50 ft]) and occur within northward tilted strata (Figs. 2.8B and 2.8C). Bands become progressively sparser and occur stratigraphically lower moving northward (partial discoloration follows the same tend). Only a few isolated bands are present near the northern boundary of Zone 2.

Uneven (mottled and patchy) coloration results from irregular distribution of iron oxide around grains (Fig. 2.5B). Bulk geochemical analysis (ICP-MS) indicates that the concentration of iron oxide in the orangish-red areas of this facies is similar to sandstone of both the red primary and pink altered facies (Table 2.2). Paradoxically, iron oxide concentrations within some white bleached bands in the Hop Valley area (Fig. 2.1) is higher than surrounding unbleached rock (Table 2.2). This is a result of small, mm-scale concentrations ("speckles") of iron oxide cement that are similar to those in the white speckled facies of main Zion Canyon (Table 2.1). In thin section, these iron oxide speckles appear as localized areas of pore-filling cement in an otherwise bleached matrix that lacks primary grain coats (similar to Fig. 2.5G). The spatial extent and cause of speckled cementation in Zion NP has not been determined. Bleached areas at nearby Snow Canyon SP (Fig. 2.1; Nielsen and Chan, 2009) lack these small speckles and have an iron oxide concentration that is lower than surrounding red rock.

Brown Ferruginous Facies (Jn-b)

The brown ferruginous facies is the lower of three vertically superimposed coloration belts in main Zion Canyon (Figs. 2.1 and 2.4 – Zone 3; Fig. 2.9A; Hamilton, 1978), as well as elsewhere in the southwest Utah region. Sandstone associated with this facies has a darker overall appearance than the red primary facies and is characterized by

Figure 2.9
Characteristic features of the brown ferruginous subfacies in main Zion Canyon (Fig. 1: Zone 3). (A) Three superimposed diagenetic facies are present in main Zion Canyon: brown ferriginous facies (Jn-b), pink altered facies (Jn-p) and white bleached facies (Jn-w). A narrow band of concentrated bleaching occurs along the base of the lower boundary of the pink altered facies. Surficial red streaking is visible over large areas of the uppermost white bleached facies. (B) Detail of boundary between brown ferruginous and pink altered facies showing spotty cementation below the boundary and an absence of spots above. (C) Local geometry of the brown/pink facies boundary. Boundary lobe (arrow) points in a roughly northward direction (apparent) and is flattened against the base of an interdune bounding surface. White rock above boundary is the bleached zone at the base of the pink altered facies.

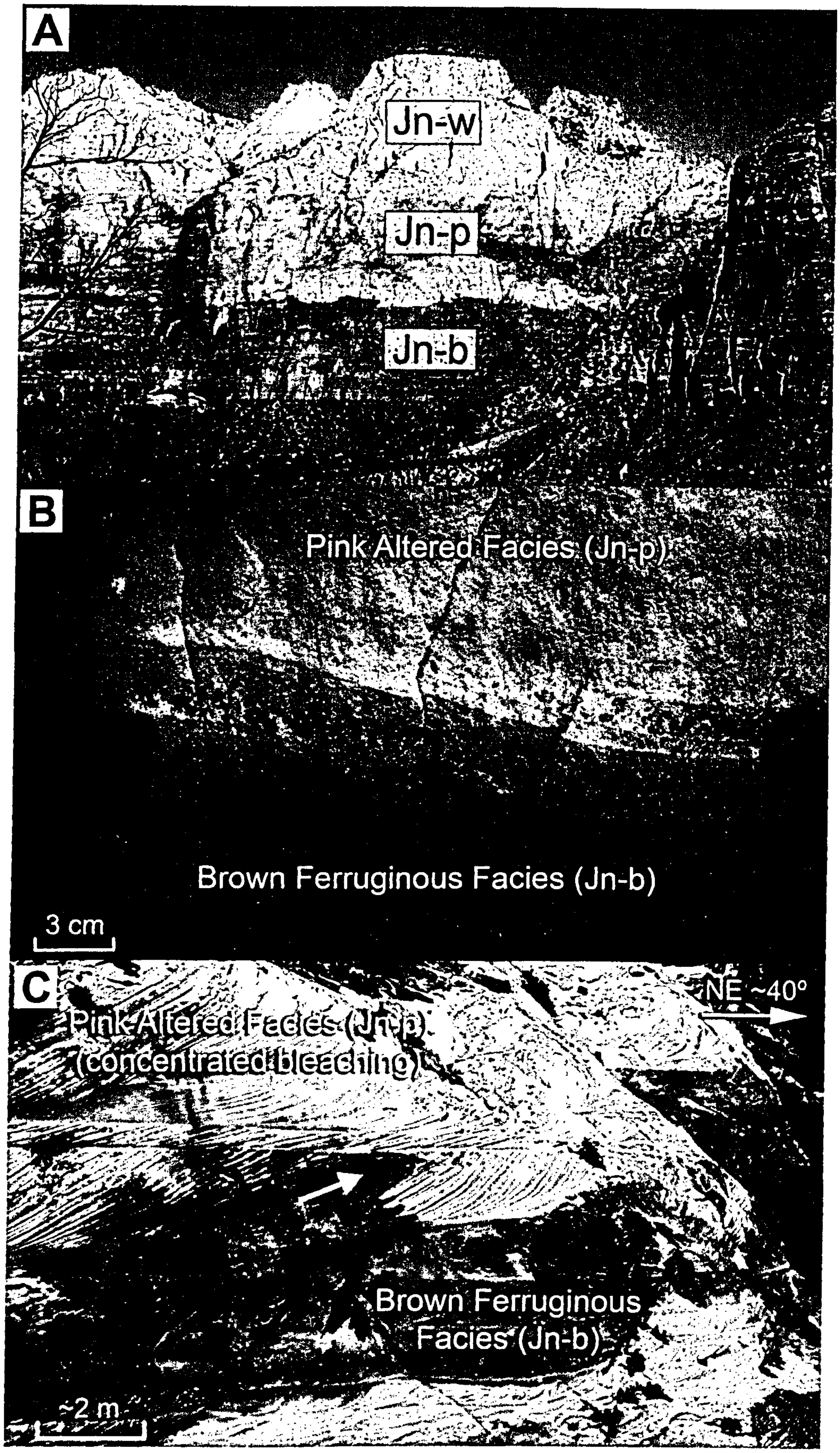
A
Jn-w
Jn-p
Jn-b
B
Pink Altered Facies (Jn-p)
Brown Ferruginous Facies (Jn-b)
3 cm
C
NE ~40°
Pink Altered Facies (Jn-p)
(concentrated bleaching)
Brown Ferruginous
Facies (Jn-b)
~2 m

extensive spotty cementation along a well-defined subhorizontal boundary in the Zion Canyon area (Figs. 2.9B-C). Grains commonly have remnant coats of reddish-brown iron oxide similar to the primary red sandstone of the northern park (Zone 1). The darker color is produced by secondary iron oxide which locally fills intergranular pores (Fig. 2.5C, Table 2.3) to give the sandstone a spotty appearance. Iron oxide concentration is highly variable but is generally a few percent or less for red sandstones overprinted with spotty cementation (Table 2.2). Calcite is locally abundant near the upper facies boundary (Figs. 2.6B, 2.7B) and illite may also be present (Table 2.3).

The brown ferruginous facies is subdivided into four subfacies based upon iron oxide concentration and the overall color of the rock. The overprinted white subfacies occurs locally in areas such as Snow Canyon SP where white bleached sandstone is recemented with secondary iron oxide, producing a white matrix with dark-colored spots and patches. In addition to reddish-brown iron oxides, black manganese oxides and carbonate cements occur locally in this facies (coded as "other cement" in Table 2.3). The overprinted red subfacies is characterized by remnant grain coats beneath secondary iron oxide cement (Fig. 2.5A). The green and brown subfacies is exposed in at least one area of Zion NP and is typified by grayish green and spotty brown cementation (Table 2.1). The green mineral has a micaceous appearance in thin section (Fig. 2.5D), moderate birefringence, and occurs in association with iron oxide, calcite, and illite cements (Figs. 2.6B and 2.7B). Although this mineral has not yet been definitively identified, the color, chemical composition, and reflectance spectroscopy suggest that it is an iron-bearing clay mineral, possibly a member of the smectite group (compare with McKinley et al., 2003; Net, 2003). The ironstone facies is characterized by dense, dark-colored sandstone with high concentrations of iron oxide cement (this facies occurs primarily in the Snow Canyon SP area [Nielsen and Chan, 2009]). Illite is rare or absent in this subfacies (Table 2.3).

Pink Altered Facies (Jn-p)

The pink altered facies is the middle of three vertically superimposed coloration belts in main Zion Canyon (Figs. 2.4, 2.9A). Navajo Sandstone of this facies is characterized by partial alteration of primary sandstone (both bleaching and secondary iron enrichment) and an uneven, orangish-pink pigmentation (uneven red/orange sufacies; Fig. 2.10A). The base of this facies is typically marked by a narrow zone (~10 to 25 m [30 - 80 ft]; Figs. 2.9A, 2.9C, 2.10A) of concentrated bleaching while the upper boundary is gradational in nature with intermixing of red and white coloration (Fig. 2.10B).

Several characteristics differentiate Navajo Sandstone of the pink alteration facies from primary sandstones of Zone 1. Iron oxide is unevenly distributed and grain coats are commonly partial or missing (Fig. 2.5E). Dolomite is common in some samples from the alteration facies (Fig. 2.7C) but was not detected in samples from the red primary facies. Preliminary data suggest that average iron oxide concentration in the uneven reddish-orange areas of the pink facies (0.95%) is similar to that of unbleached sandstone in the red/white intermixed facies (0.8%; Table 2.2). However, because of the diversity within these facies, a much larger sample size is required to verify this relationship.

Isolated lenses of dark reddish- or grayish-brown ironstone (Fig. 2.10C) occur locally in the pink middle facies, sometimes forming a protective cap over small buttes

Figure 2.10
Characteristic features of the pink altered facies in main Zion Canyon (Fig. 1.1: Zone 3). (A) Lower portion of the pink altered facies shows narrow zone of concentrated bleaching and a dark-colored ironstone lens. (B) Boundary between the pink altered and white bleached facies. Note the gradational nature of the transition with intermixed whitish and pinkish sandstone. A thin lens of dense, black ironstone forms a protective cap over narrow hoodoos (bedrock columns). (C) Detail of dense concretionary ironstone lens in the lower portion of the pink altered facies.

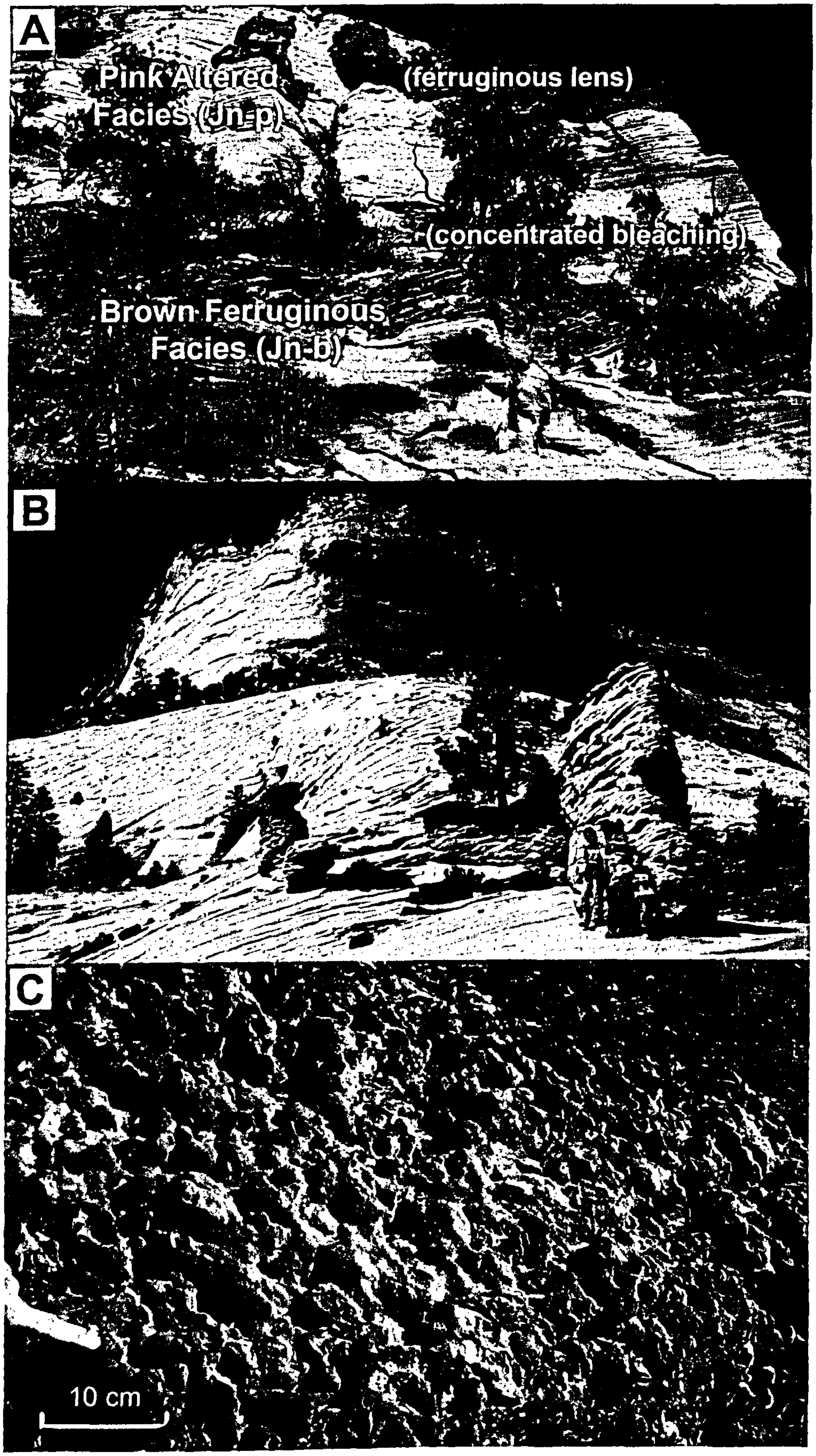
A
Pink Altered
Facies (Jn-p)
(ferruginous lens)
(concentrated bleaching)
Brown Ferruginous
Facies (Jn-b)
B
C
10 cm

and hoodoos (ferruginous lens subfacies; Figs. 2.10A-B). The dark color is produced by dense iron oxide (primarily goethite) cementation within pore spaces (Figs. 2.5F, 2.6C, and 2.7C; Table 2.3). ICP-MS results indicate high iron oxide concentrations, as well as relatively high concentrations of chromium and arsenic in some samples (Table 2.2). Although spatial distribution of arsenic and other trace elements at Zion NP was not evaluated, iron oxide cement has been suggested as a possible source for high arsenic levels in several groundwater wells in the St. George, Utah area (Fig. 2.1; Langley, 2006).

White Bleached Facies (Jn-w)

Approximately the upper third to half of the Navajo Sandstone in the southern part of Zion NP is nearly white in color (including areas of light yellow and tan). These areas of bleached rock define the white bleached facies (Figs. 2.9A and 2.11A).. The outer surface of this facies is locally stained by large red streaks that descend from the overlying brownish-red Sinawava Member of the Temple Cap Formation (Fig. 2.9A). Extensive (km-scale) areas of bleached sandstone are referred to as "zonal bleaching" (Nielsen and Chan, 2009) and are widespread throughout southern Utah, where they are commonly associated with structural uplifts (Beitler et al., 2003). The area of bleached sandstone that includes Zion NP continues to the east (Fig. 2.11B) and south of the park for 10s of km. The original westward extent of bleaching is unknown because erosion along the Hurricane Fault has removed the Navajo Sandstone across an approximately 20 km (12 mi) wide area immediately west of the park. Although widespread bleaching of the upper Navajo Sandstone does occur in the St. George, Utah area (Fig. 2.1; Utah and

Figure 2.11
Characteristic features of the white bleached facies, main Zion Canyon and vicinity (Fig. 1: Zone 3). (A) Nearly white sandstone is shown with areas of yellowish-orange alteration (yellow subfacies) and small (mm-scale) speckles that are common in many areas of the upper bleached zone. Locality: Zion Canyon (B) Lobe and cusp structures along the lower boundary of bleaching suggest paleoflow in a roughly southward direction. Locality: Elkheart Cliffs ~30 km (19 mi) east of Zion NP.

Chan, 2009), this zone of erosion prevents direct westward correlation. Bleaching tapers out to the north of main Zion Canyon near Jobs Head in the central park area (Fig. 2.1; Fig. 2.12). The nature of this exposed transition from bleached to unbleached rock is examined later is this paper.

Thin section micrographs of bleached Navajo Sandstone show that primary reddish iron oxide grain coats are largely missing (Fig. 2.5G). Despite these missing coats, the weight percentage of iron oxide is higher in some bleached samples (~1.2%) than in the primary red facies (~0.7% - Table 2.2) as a result of small, mm-size brownish speckles (speckled white subfacies; Figs. 2.5G, 2.11A) similar to those previously described in the Hop Valley area (Fig. 2.1: Zone 2). Concentration of iron oxide into these small specks has minimal visual impact on the overall white color of the rock. Because of the rugged terrain and limited access to most outcrops at Zion NP, the spatial extent of these speckles within the upper formation remains to be determined (they have not been observed in the white bleached zone of the upper Navajo Sandstone in the St. George, Utah area).

Detrital grains in the yellow subfacies (Table 2.1) of the white bleached facies have thin coats of a pale yellowish mineral (Fig. 2.5H) that has a high birefringence. These coats are petrographically and spectrally similar in illite (Fig. 2.6D), but may be colored by goethite (Cornell and Schwertmann, 2003) or other impurities. Barite ($BaSO_4$) is also present as indicated by strong XRD two-theta values (Fig. 2.7D) and a spike in the relative concentration of barium in ICP-MS data (Table 2.2). In addition, kaolinite cement and small specks of iron oxide occur within this subfacies (Table 2.3). Grains of the tan subfacies (present primarily in the Snow Canyon SP area) also have

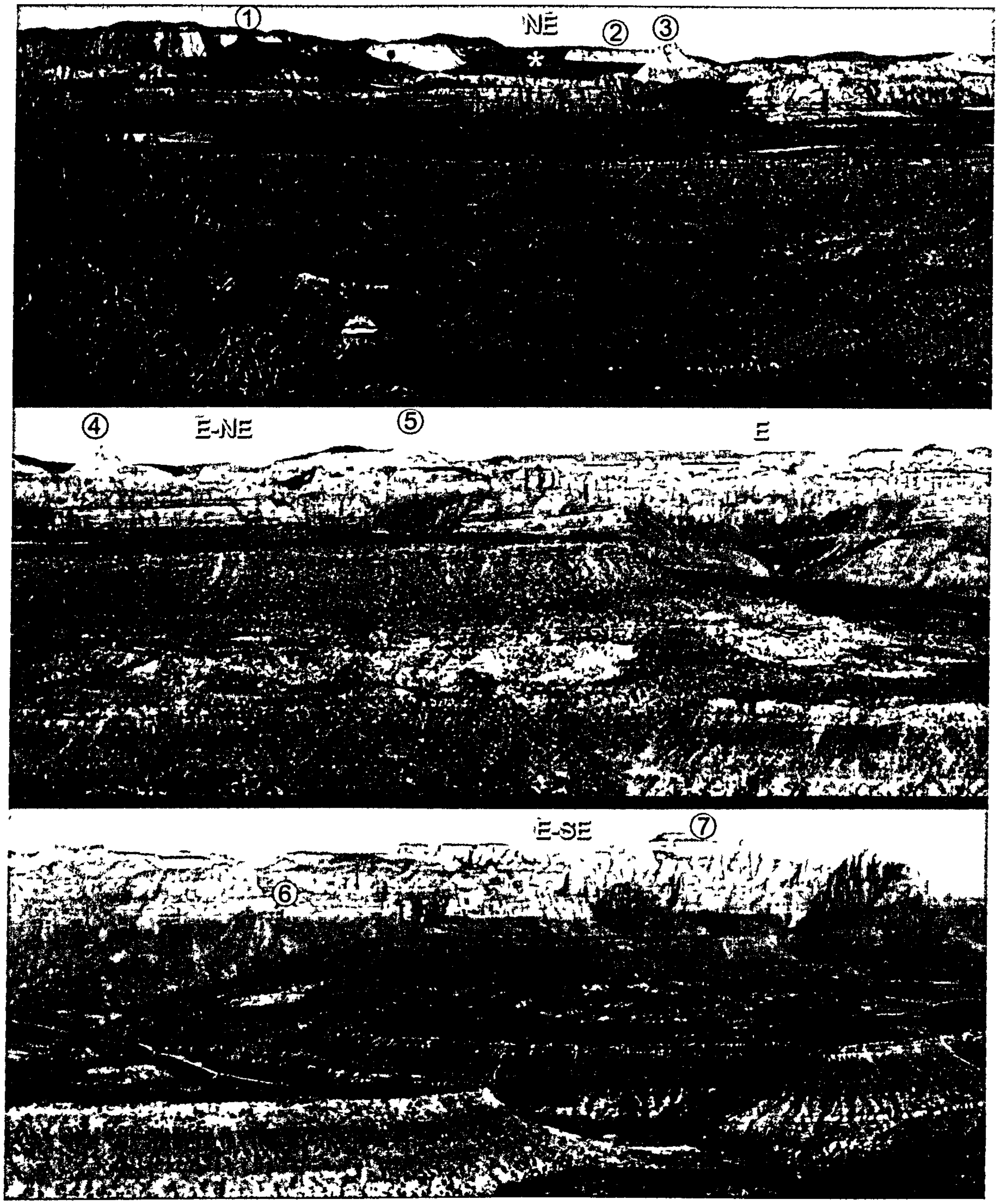

Figure 2.12
Composite panoramic image of Zion NP from Hurricane Mesa ~20 km (12 mi) west of main Zion Canyon. The top of the Navajo Sandstone is bleached in the southern end of the park until the Jobs Head transition (asterisk). Reference points: 1) Jobs Head, 2) Pocket Mesa, 3) Pine Valley Peak, 4) North Guardian Angel, 5) South Guardian Angel, 6) Cougar Mountain, and 7) The West Temple. Note that the depth of the bleached zone gradually increases moving south.

illite grain coats (sometimes partial or missing) as well as microcrystalline quartz cement (Table 2.3).

The identity of fluids that bleached the Navajo Sandstone is undetermined. Dissolved organic yields from solvent extraction on eight bleached and unbleached samples from the Navajo Sandstone are very low (avg. 0.012 mg/g), making it difficult to distinguish n-alkane peaks potentially produced by thermogenic hydrocarbon from that produced by environmental and/or human organic contaminants. Fluid inclusion and hydrocarbon gas phase analysis performed on 16 samples produced low to very low hydrocarbon signals (well below what would be expected within a hydrocarbon migration pathway; Appendix C). The strongest signals across samples were produced by methane gas. Where present, liquid hydrocarbon inclusions occur primarily within detrital quartz grains and not in surrounding cements (Fig. 2.13).

Multicolored Local Facies (Jn-m)

The multicolored local facies is characterized by brightly colored patches of yellow, orange, and red coloration (patchy subfacies) as well as millimeter-scale Liesegang-type coloration bands (Liesegang banded subfacies). This facies occurs locally in the upper Navajo Sandstone at Zion NP, commonly in association with closely-spaced, high-angle, N-NW-trending joints (Fig. 2.14). Similar localized coloration features are in the upper Navajo Sandstone of the Snow Canyon SP area (Nielsen and Chan, 2009) as well as in the Aztec Sandstone (a correlative equivalent of the Navajo Sandstone) at Valley of Fire State Park in Nevada (Eichhubl et al., 2004). Petrographic analysis indicates uneven distribution of iron oxide with secondary alteration of grain

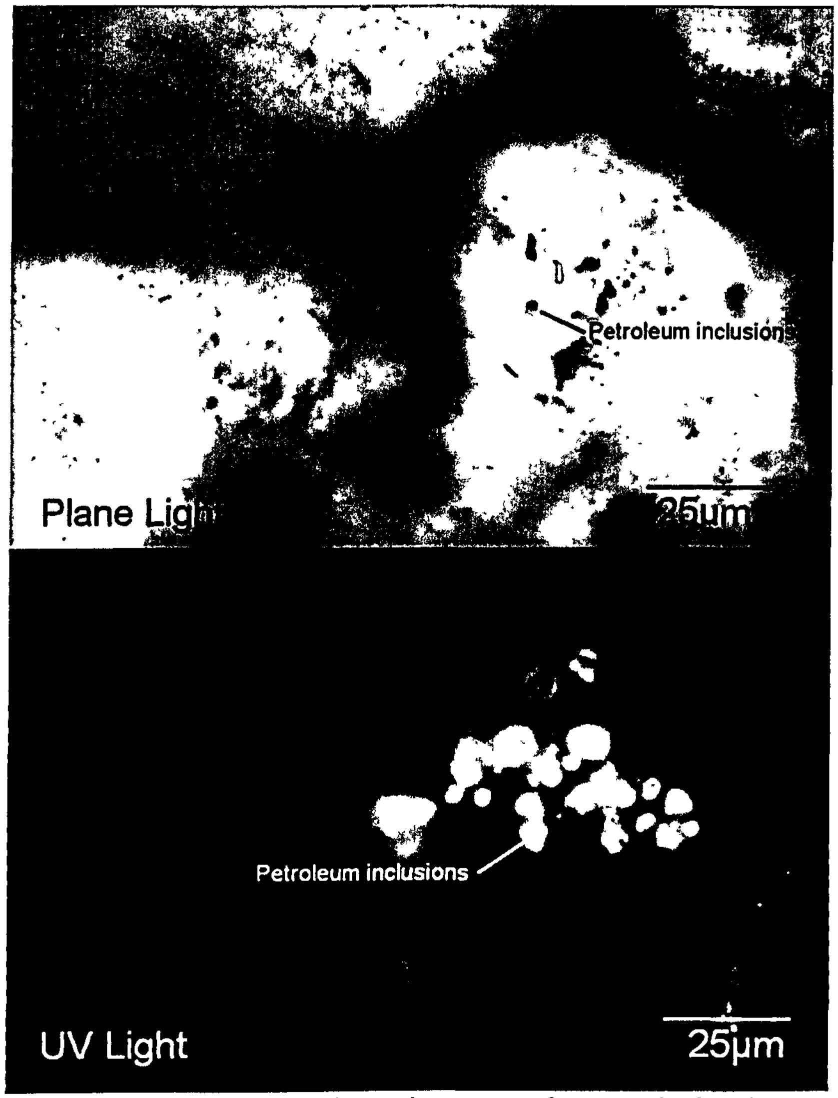

Figure 2.13. Fluid inclusion microscopy for Navajo Sandstone from the Snow Canyon SP area showing bright fluorescent liquid hydrocarbon inclusions within detrital quartz grains. Surrounding cements largely lack these inclusions. Image courtesy of David A.Wavrek, Petroleum Systems International, Inc.

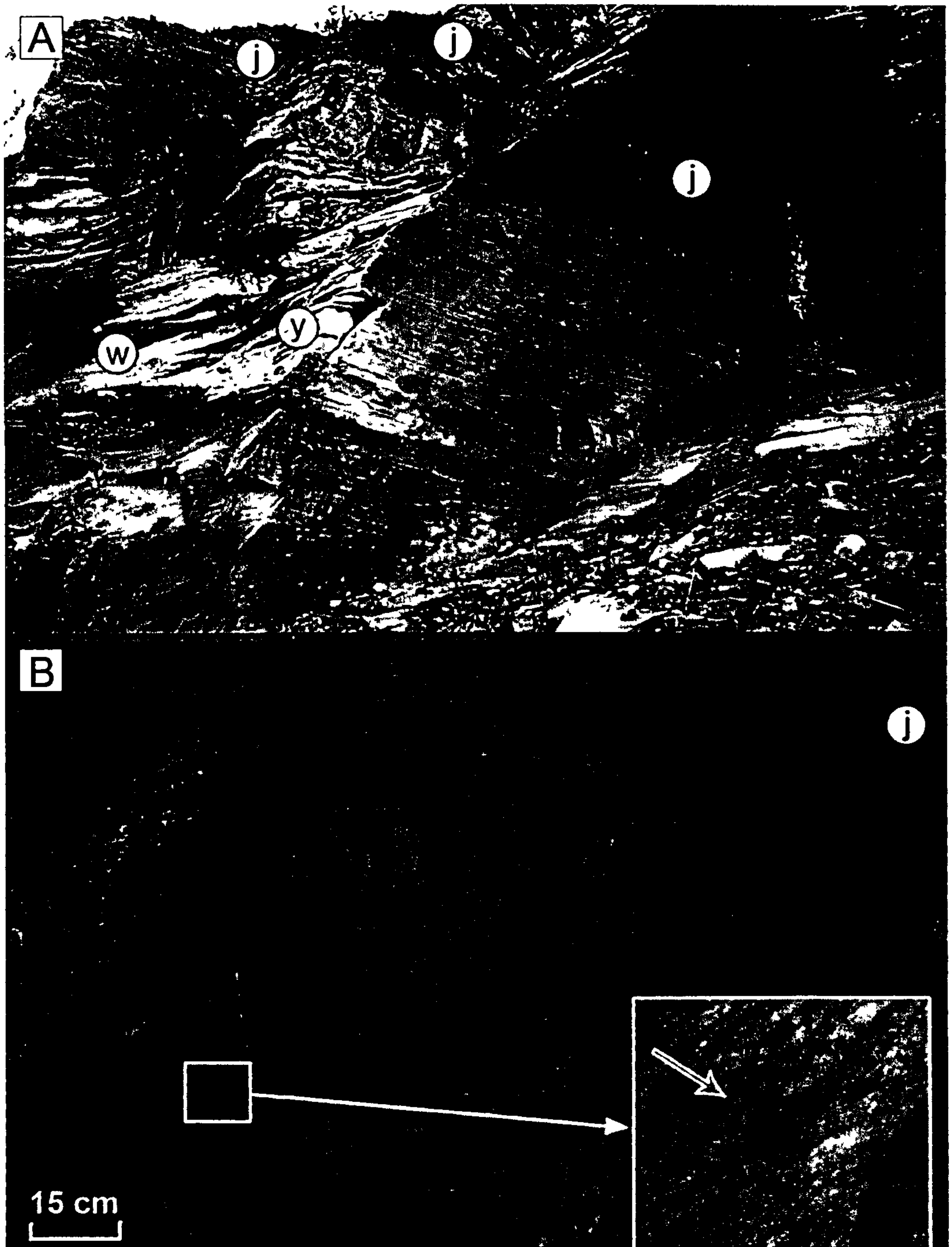

Figure 2.14.
Characteristic features of the multicolored local facies in main Zion Canyon (Fig. 1: Zone 3). (A) Closely spaced joints (j) have well-developed oxidation surfaces. Mean trend of joints in the immediate area is ~310°. Note that yellow coloration (y) appears to follow the joint in the foreground with sandstone becoming white (w) to the left. (B) Detail of well-developed Liesegang-type banding adjacent to a joint surface (j). Close examination shows band deflection around a small concretion (insert), likely indicating solute transport to the NE and toward the joint (see Eichhubl, 2004).

coats and localized pore-fill cementation (Fig. 2.5I). Joints in these areas typically have well-developed, brownish-black iron oxidation surfaces. Only a small amount of illite occurs in this facies.

Transition Between Bleached and Unbleached Sandstone

The transition between bleached Navajo Sandstone of southern Zion NP and reddish Navajo Sandstone of the northern park occurs between Pine Valley Peak and Jobs Head (Fig. 2.1, boundary between Zones 1 and 2; Fig. 2.12; Appendix D). Bedrock in this area is mostly hidden by basalts of the Lava Point flow (Biek et al., 2003) but available exposures show a remarkably subtle transition with bleached rock gradually darkening to an uneven reddish orange moving northward (Figs. 2.15 and 2.16). No other exposures of this transition were located in the park. The short distance (~ 2 km [1.2 mi]) over which the transition occurs suggests possible association with a fault or joint near Little Creek Valley (Fig. 2.16). However, evidence for structural control is lacking: the trend of the valley (NE) differs from that of the dominant joint system in the park (NNW) and the rim of the Navajo Sandstone displays minimal offset in the area.

Correlation Between Stratification Patterns and Bleaching

To test the hypothesis that alteration of the Navajo Sandstone may be related to primary sedimentary texture (Chan et al., 2000; Beitler et al., 2005), both bedding orientation and eolian stratification type (grainflow, wind-ripple, etc.) were measured at 635 points within various diagenetic coloration facies at Zion NP and Snow Canyon SP. Results indicate a change in both stratification type and cross-bed dip angle moving

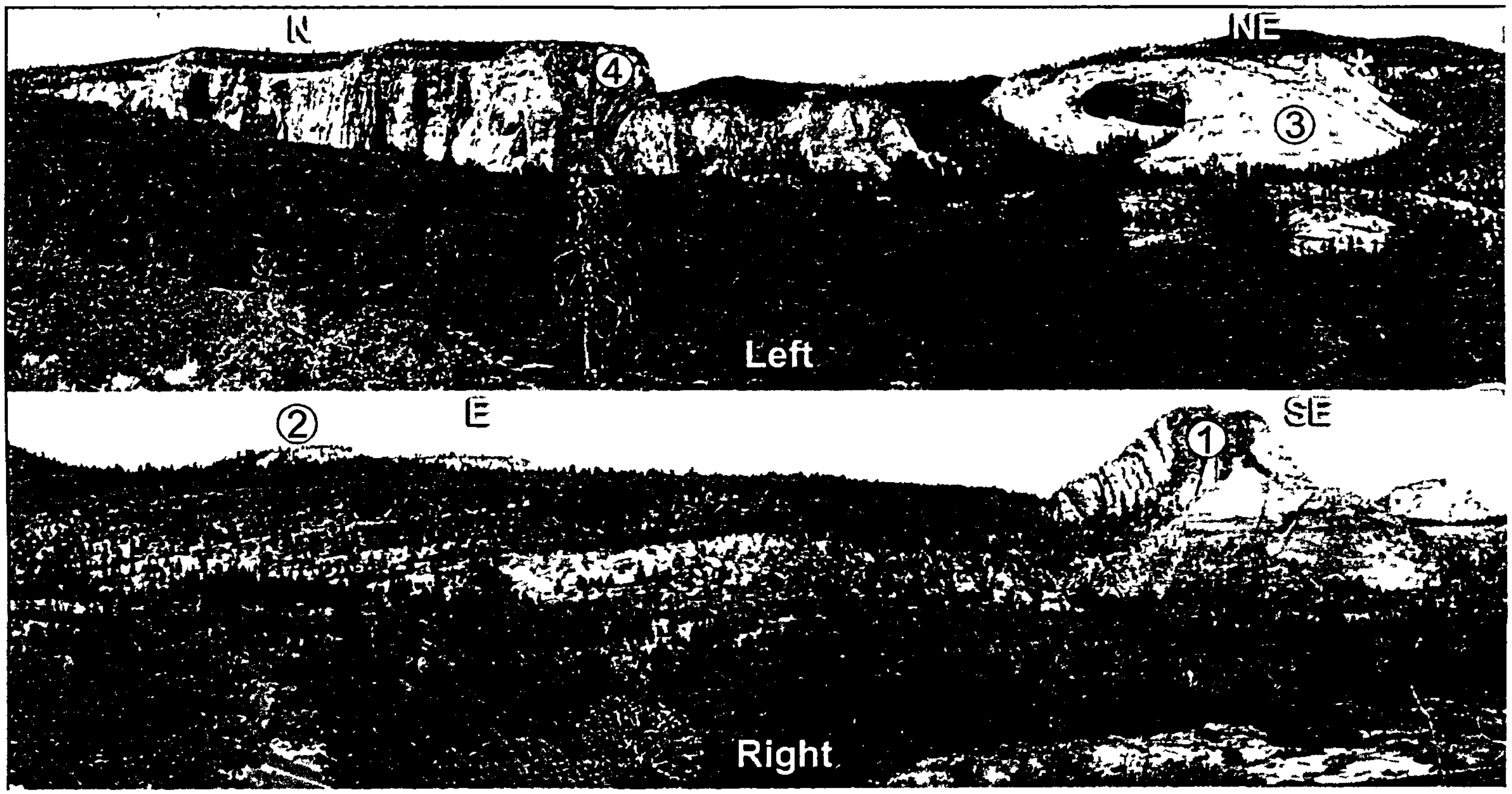

Figure 2.15
Split panorama showing the lateral transition zone between bleached white Navajo Sandstone in the southern park (Zone 3: white bleached facies) and unevenly colored reddish-orange sandstone in the central park (Zone 2: red/white intermixed facies). Marked locations: 1-Pine Valley Peak (bleached), 2-Pocket Mesa (bleached), 3-unnamed transitional outcrop (pale pink to white), and 4-Jobs Head (uneven reddish-orange). Asterisk indicates the location where Fig. 16 was taken. See also Appendix D.

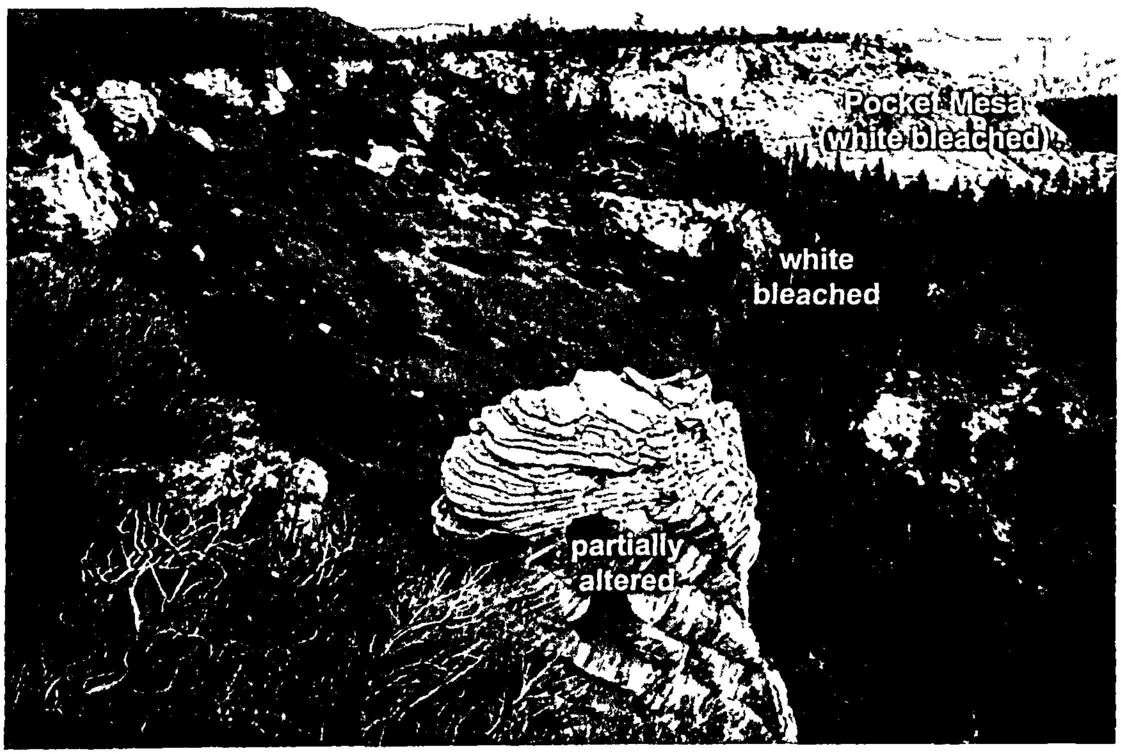

Figure 2.16
View looking south from on top of the transition outcrop in Fig. 15. Picture taken from point marked by asterisk looking south). White sandstone cliffs in the rear occur on the north side of Pocket Mesa and Little Creek Valley (Fig. 1) is directly in front of these cliffs.

upward through the formation as well as a shift in the dominant transport direction (Figs. 2.17 and 2.18). Bedforms in all three facies were likely oriented perpendicular to the dominant wind direction, as plotted foreset dip orientations (Fig. 2.17) have unimodal distributions that are bilaterally symmetrical (McKee, 1979, Rubin, 1987; Kocurek, 1991; Rubin, 2006). The broad range of dip directions throughout the formation (and tabular appearance of cross strata sets when viewed parallel to the mean orientation of foreset dip [SW]) implies a sinuous dune crest morphology, consistent with a southwestward migrating crescentic-ridge type dune system (McKee, 1979, Ahlbrandt and Fryberger, 1982; Kocurek, 1996). The brown ferruginous facies in the lower Navajo Sandstone of main Zion Canyon is characterized by moderate angle (average=18°) cross-bedding and a dominance of wind ripple/grainfall stratification (Fig. 2.17A). In contrast, the upper white facies is characterized by higher angle (average=22°) cross-bedding and a dominance of grainflow stratification. Dip angle and stratification type for the middle pink facies is intermediate between the other two. Differences in average dip between the pink and white facies are statistically significant (Table 2.4; <.05 level) whereas differences between the brown and pink facies are not (the smaller sample size makes statistical significance less likely). Differences between the brown and white facies show a very high level of significance. A similar pattern is observed at Snow Canyon SP between vertically superimposed red, white, and tan facies (Fig. 2.17B). These changes reflect an evolution in dune morphology over time, likely related to a transition from the margins to the center of an erg (Porter, 1986; Cox et al., 1994; Morse, 1994).

In addition to changes in stratification type and dip angle, a clockwise (or westward) shift in the dominant direction of sand transport (as indicated by the mean

Figure 2.17
Relationship between eolian bedform morphology and large-scale bleaching patterns in the Navajo Sandstone of Zion NP (A) and Snow Canyon SP (B). Foresets plotted as lines parallel to dip of the plane with the mean direction indicated by a red square and % grainflow based upon field classification of lithofacies. Prior to performing calculations the data were rotated to adjust for the tilt of the Navajo Sandstone in each area (Chapter 4; Nielsen and Chan, 2009). Rose diagram (C) shows combined foreset dip directions for both parks.

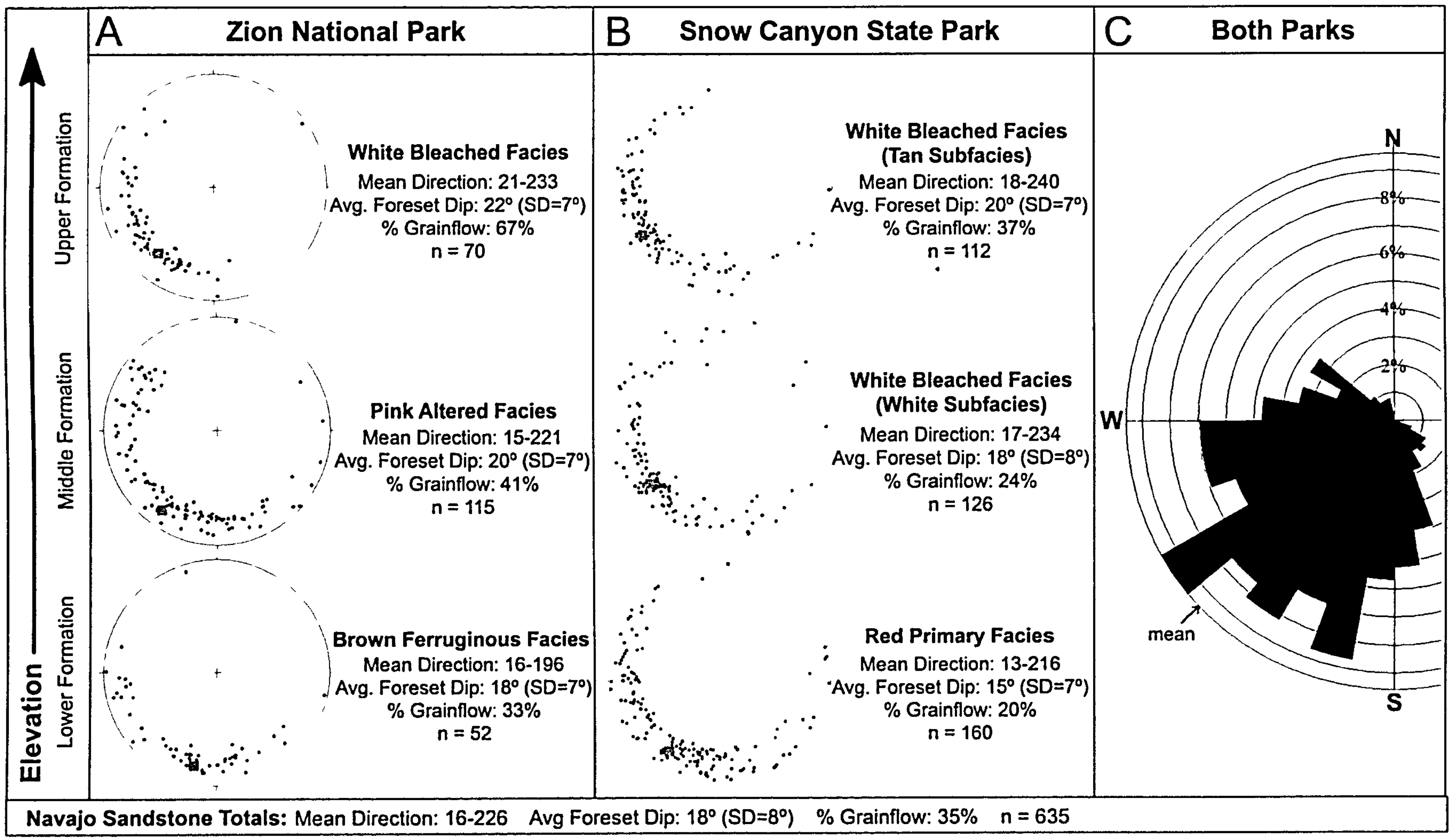

A Zion National Park
B Snow Canyon State Park
C Both Parks
Elevation
Upper Formation
Middle Formation
Lower Formation
White Bleached Facies
Mean Direction: 21-233
Avg. Foreset Dip: 22° (SD=7°)
% Grainflow: 67%
n = 70
Pink Altered Facies
Mean Direction: 15-221
Avg. Foreset Dip: 20° (SD=7°)
% Grainflow: 41%
n = 115
Brown Ferruginous Facies
Mean Direction: 16-196
Avg. Foreset Dip: 18° (SD=7°)
% Grainflow: 33%
n = 52
White Bleached Facies
(Tan Subfacies)
Mean Direction: 18-240
Avg. Foreset Dip: 20° (SD=7°)
% Grainflow: 37%
n = 112
White Bleached Facies
(White Subfacies)
Mean Direction: 17-234
Avg. Foreset Dip: 18° (SD=8°)
% Grainflow: 24%
n = 126
Red Primary Facies
Mean Direction: 13-216
Avg. Foreset Dip: 15° (SD=7°)
% Grainflow: 20%
n = 160
N
W
S
8%
6%
4%
2%
mean
Navajo Sandstone Totals: Mean Direction: 16-226 Avg Foreset Dip: 18° (SD=8°) % Grainflow: 35% n = 635

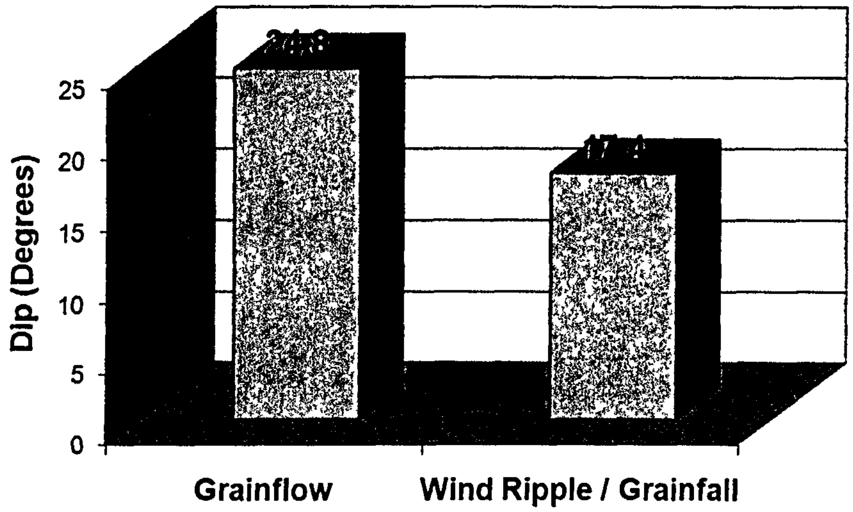

Figure 2.18. Average dip of eolian foresets by stratification type in the Navajo Sandstone (n=499).

Table 2.4

Combined sample size and statistical significance (2-tailed t test) for differences in eolian foreset dip between different diagenetic coloration facies.

Location	**Facies 1**	**Facies 2**	**Combined Sample Size**	**Significance (p)**	**< 0.05**
Zion	Brown (lower)	Pink (middle)	167	2.1×10^{-1}	N
	Brown (lower)	White (upper)	122	2.2×10^{-4}	Y
	Pink (middle)	White (upper)	185	1.5×10^{-2}	Y
Snow Canyon	Red (lower)	White (middle)	287	1.6×10^{-4}	Y
	Red (lower)	Tan (upper)	271	8.2×10^{-7}	Y
	White (middle)	Tan (upper)	236	6.2×10^{-2}	N
Combined	All Lower (not bleached)	All Upper (bleached)	635	4.1×10^{-7}	Y

Brown = brown ferruginous facies; red = red primary facies; pink = pink altered facies; white = white bleached facies; tan = tan subfacies.

foreset orientation) is also observed moving stratigraphically upward through the Navajo Sandstone (Fig. 2.17). The trend may reflect a larger pattern of clockwise rotation in crossbedding resultants for other sandstone members of the Glen Canyon Group: the Lower Jurassic Kayenta Formation, Lower Jurassic Navajo Sandstone, and Middle Jurassic Page Sandstone (Peterson, 1988 – his figure 14; Parrish and Peterson, 1988). A strong relationship exists between stratification type and foreset dip angle (Fig. 2.18). This reflects the dynamics of dune systems with flows typically originating near the dune brink to blanket the relatively steep slipface, whereas wind ripples are most commonly preserved at the base of a dune where the dip angle is shallow (Hunter, 1977). Corey et al. (2005) report an average foreset dip angle of 24° for grainflow stratification in the Navajo Sandstone (compare with the 23.9° average dip calculated here) and show that this is consistent with the angle of repose for sand after accounting for vertical compaction.

Discussion

Concentration of Bleaching in the Upper Navajo Sandstone

Bleaching in Zion NP and vicinity is commonly concentrated within broad zones at the top of the Navajo Sandstone (white bleached facies). The position of this widespread bleaching in the upper formation can potentially be explained by either permeability relationships or fluid buoyancy.

Permeability Relationships

Bleaching in the Navajo Sandstone preferentially follows high permeability strata (e.g., grainflow deposits) and tends to concentrate along boundaries between high and low permeability zones such as interdune bounding surfaces (Lindquist, 1988; Net, 2003; Beitler et al., 2005; Nielsen and Chan, 2009). The impact of local permeability variations on bleaching is observed in the boundary area between the white bleached and pink altered facies where intermixed colors correspond to variations in primary sedimentary texture (Fig. 2.10B). In a similar manner, large-scale bleaching patterns in Zion NP and vicinity may also be controlled by primary stratification. Grainflow strata typically have a larger average grain size and higher primary porosity/permeability than grainfall or wind ripple strata (Lindquist, 1988; Net, 2003). Because of this, an upward trend of increasing grainflow stratification in the Navajo Sandstone (Fig. 2.17) implies an upward increase in primary permeability. Although spatial correlation between bleaching and sedimentary texture does not necessitate a causal connection, it is reasonable to assume that migrating fluids would tend to concentrate within higher permeability zones in the upper part of the formation.

The inclination of eolian interdune bounding surfaces (i.e. first-order surfaces [Kocurek, 1988; Kocurek, 1996]) may also influence fluid migration. The accumulation of sand in an eolian system implies that these surfaces must climb in the direction of net sand transport (Kocurek, 1996). Because these inclined interdune surfaces are often high-contrast permeability boundaries, fluids moving laterally in the direction of surface climb (southwest in Zion NP; Fig. 2.17) would tend to follow a path upward along these boundaries toward the top of the formation (e.g., Nielsen and Chan, 2009). In contrast, fluids moving in the opposite direction (SE in Zion NP; Fig. 2.8B-C) would be focused downward toward lower permeability strata and flow may be inhibited. More research is needed to evaluate the potential impact of these inclined bounding surfaces on large-scale fluid migration.

Concentration of bleached rock within the upper Navajo Sandstone may also be related to permeability barriers that overlie the formation. In the Zion NP area these include the lower, Sinawava Member of the Temple Cap Formation and overlying limestone of the Carmel Formation (Fig. 2.3; Appendix E). Although bleaching patterns in the upper, White Throne Member of the Temple Cap Formation are similar to those of the Navajo Sandstone (Fig. 2.19), measured permeability of the underlying Sinawava Member is relatively low (14 mD), suggesting that the lower boundary of the Temple Cap Formation acts as a barrier to fluid transmission. Attempts to directly measure the permeability of the Carmel Formation were unsuccessful due to fracturing produced by the plug cutting process; however, measured porosity is low (3.9%) and the micritic composition and uniform structure of this formation indicate it is likely an effective hydraulic cap in areas where it is unfractured. This tentative result is consistent with studies that characterize the Carmel Formation as a hydraulic barrier at other locations (e.g., Allis et al., 2001; Truini and Macy, 2005; Parry et al., 2007). Just as bleaching patterns on an outcrop scale indicate preferential permeability pathways (Fig. 2.2), on a regional scale the high-contrast permeability boundary between the upper Navajo Sandstone and overlying formations represents a probable pathway for fluid migration.

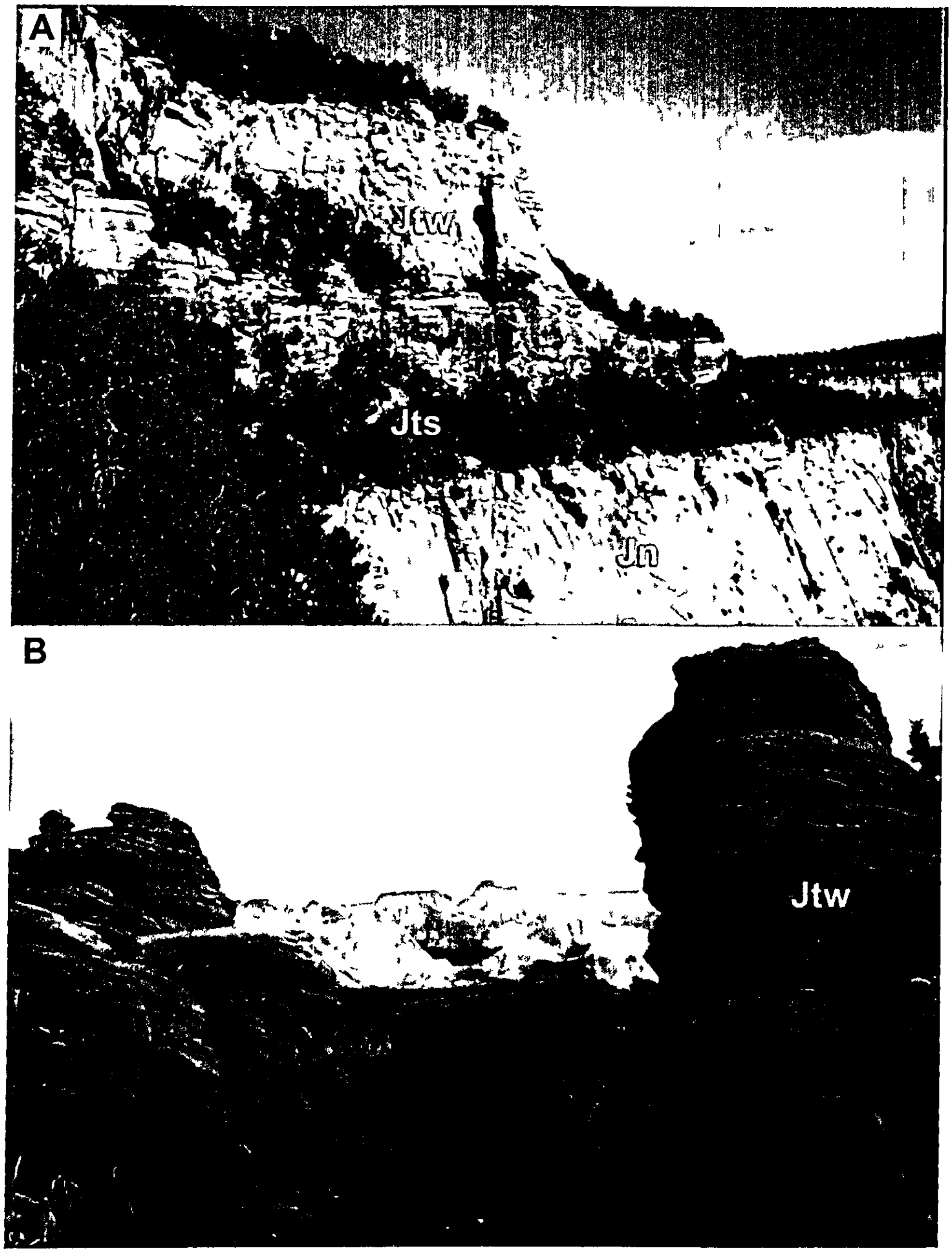

Figure 2.19
Bleaching of the Temple Cap Formation in Zion NP. (A) Temple Cap Formation in main Zion Canyon near the Great White Throne (Fig. 1: Zone 3). Jn = Jurassic Navajo Sandstone, Jts = Temple Cap Sinawava Member; Jtw = Temple Cap White Throne Member. Note the red streaks descending downward over the Navajo Sandstone from the Sinawava Member and the light orangish color of the White Throne Member. (B) Reddish brown rocks of the White Throne Member of the Temple Cap Formation (Jtw) in the Jobs Head area of central Zion NP (Fig. 1: Zone 2). Note the eolian bounding surface on the outcrop to the right. The pink altered facies and white bleached facies of main Zion Canyon are visible in the distance.

Fluid Buoyancy

Buoyancy of a fluid increases as its density decreases relative to surrounding fluids. Fluid density is influenced by several factors including fluid type (hydrocarbon is more buoyant than water), concentration of dissolved solids (e.g., fresh water is more buoyant than saline water), and temperature (warmer formation waters may be buoyant). The accumulation of buoyant reducing fluids beneath the lower permeability rocks that cap the Navajo Sandstone has been suggested as a possible explanation for the concentration of bleaching near the top of the formation. For example, Garden et al. (2001) attribute bleaching along the crest of the Moab anticline in southeastern Utah to the concentration of hydrocarbons that migrated upward through fractures and faults in the higher density, water-saturated sandstone. Identification of the bleaching fluid as a hydrocarbon is based upon bitumen-filled fractures as well a close correspondence with the established timing for hydrocarbon maturation and migration in the Moab area. Beitler et al. (2003) show that the spatial patterns of bleached Navajo Sandstone in Utah correlate with Laramide uplifts in the region, and also suggest fluid buoyancy as a possible control. Although concentration of bleached rock beneath low-permeability units in the upper Navajo Sandstone at Zion NP suggests that the fluids may have been buoyant, the identity of these fluids has not been determined, and the relative importance of fluid properties and sedimentary textures in controlling the location of alteration warrants further study.

Diagenetic History of the Navajo Sandstone in the Zion National Park Area

Multiple episodes of subsurface fluid movement on both regional and local scales contributed to the distinctive color variations at Zion NP. These are discussed in approximate relative time order and grouped according to three diagenetic stages: early diagenesis, middle diagenesis, and late diagenesis (Table 2.5).

Early Diagenesis

Early diagenesis involves the compaction of sediment shortly after deposition and initial cementation of grains. During this stage elevated pressure and temperature associated with overlying sediment are not yet significant factors in producing mineralogical changes and pore water chemistry is similar to the depositional environment in which it originated (Tucker, 1991). Diagenetic events likely associated with this stage of alteration include precipitation of thin, iron oxide grain coatings and precipitation of initial pore cements.

Iron oxide grain coats. Thin iron oxide grain coats (Fig. 2.5A) that characterize sandstone in Zone 1 represent a very early diagenetic episode, the remnants of which can be observed in the other alteration zones and facies in the Zion NP area. This diagenetic episode was dominated by oxidation-reduction reactions and established the primary reddish-orange color of the rock (Dapples, 1979; Walker, 1979; Tucker, 1991; Eichhubl et al., 2004; Beitler et al., 2005). Hematite and its precursor ferrihydrates typically form under oxidizing (moderate to high Eh) conditions with potential sources of iron being

Table 2.5

Correlation and estimated timing of major diagenetic events in the SW Utah area.

Diagenetic Stage	**Estimated Timing**	**Major Alteration Events**
Early (deposition to early burial)	Early to Middle(?) Jurassic	• Formation of oxide grain coats that characterize the red primary facies.
Middle (deep burial)	Late Jurassic to early Tertiary(?)	• Widespread bleaching of the upper Navajo Sandstone. to form the white bleached facies, red/white intermixed facies and pink altered facies. • Precipitation of spotty Fe oxide cements to form the brown ferruginous facies.
Late (uplift and exhumation)	Middle Tertiary to Quaternary(?)	• Secondary mineralization along joints in upper Navajo Sandstone to form the multicolored local facies.
Recent	Quaternary to Recent	• Surficial streaking of the upper Navajo Sandstone. • Formation of thin iron/manganese oxide films ("desert varnish") on exposed sandstone surfaces.

detrital clay particles or the in situ breakdown of iron-bearing silicate minerals such as hornblende and biotite (Kessler, 1978; Walker, 1979; Tucker, 1991). A relative lack of hematite along some interpenetrating grain contacts in sandstone from the primary red facies suggests that precipitation of hematite occurred within buried sediment (perhaps through the impregnation of preexisting clay grain coats [Tucker, 1991; Willis, 1992; Net, 2003]). The uniform color and even distribution of grain coats suggests an early burial origin, before the original permeability of the formation was substantially reduced by compaction and precipitation of other cements. These conditions are consistent with an Early to Middle Jurassic setting (Table 2.5).

Pore cements. The precipitation of cement in pore spaces within the Navajo Sandstone occurred during multiple diagenetic stages, but cementation likely began during early diagenesis (Larsen and Chilingar, 1983; Tucker, 1991). Though relatively rare, quartz overgrowths may occur below secondary iron oxide cement, suggesting a relatively early diagenetic origin. Calcite can also be an early diagenetic mineral (Tucker, 1991; Beitler et al., 2005), but appears to be most commonly associated with secondary cementation of the brown ferruginous facies in the Zion NP region (Table 2.3). Kaolinite forms in neutral to low pH fluids with low ratios of K^+ from products generally contributed through the weathering of feldspar and other relatively unstable aluminum silicates (Tucker, 1991). Although kaolinite can precipitate in different diagenetic stages including early burial (Baker and Golding, 1992), its association with bleached facies at Zion NP suggests a later diagenetic origin (compare with Beitler et al., 2005). Illite generally forms under more alkaline conditions through the alteration of precursor minerals (feldspar, kaolinite, etc.) and is typically favored by higher temperature and greater burial depth (Tucker, 1991; Net, 2003; Parry et al., 2004; Beitler et al., 2005). Although illite at Zion NP is commonly associated with early hematite grain coats (red primary facies), it is typically absent where precipitation of dense iron oxide cement has occurred (ferruginous lens and ironstone subfacies; Table 2.3). Pore cement relationships at Zion NP are complex and further study using larger sample sizes is warranted to fully characterize each diagenetic coloration facies.

Deformation bands. Davis (1999) interprets noncataclastic deformation bands (mm- to cm-scale bands of crushed and altered rock) in the uppermost 10 to 15 m (33 to 50 ft) of the Navajo SS in the Zion NP area as an early diagenetic feature produced by volume reduction during early compaction of the formation (Middle Jurassic). Although the present study did not evaluate the relative timing of deformation band formation, variations in band color between diagenetic facies provides a possible future avenue for better understanding when and how they formed (see Parry et al., 2004).

Middle Diagenesis

Middle diagenesis involves deeper burial, increasing pressure and temperature, and the modification of pore water chemistry to the point that it is no longer similar to its original environment (Tucker, 1991). In addition to the continued development of pore cements, at least two important alteration episodes are assigned to this diagenetic stage at Zion NP: widespread bleaching and secondary iron oxide cementation.

Chemical bleaching. The dissolution of iron oxide grain coats in the white facies implies chemically reducing conditions. This is because iron, in hematite, occurs in its Fe^{3+} state which is relatively insoluble in pure water and typically must be reduced to its more soluble ferrous Fe^{2+} state before transport can occur (Chan et al., 2000). Although the identity of bleaching fluids in the southwest Utah area remains to be determined, compounds such as hydrocarbons, methane, organic acids, and hydrogen sulfide have been suggested as natural reactants that, in combination with water, could act as effective reduction and transport agents (Shebl and Surdam, 1996; Chan et al., 2000). Dissolution and transport may also be facilitated by complexation and biotically-mediated processes (Cornell and Shwertmann, 2003). Chemical reactions that produce bleaching progress toward a state of local equilibrium with time and it is the exchange of components through advective transport and diffusion that allows the alteration process to continue (Lake et al., 2002). Mass balance calculations using ICP-MS data for a first approximation indicate that transforming 1 m^3 (1.3 yd^3) of red primary sandstone to white bleached sandstone requires that 9.34 kg (20.59 lbs) of iron oxide be mobilized and removed in a reaction that consumes 472 g (1.04 lbs) of H^+ from solution. Bleaching of the upper formation therefore required sustained migration of fluid and would be unlikely to occur within a static reservoir (see Parry et al., 2004). Chemical conditions within bleached zones of the Navajo Sandstone have likely also changed with time. The presence of barite in yellowish areas of the white bleached facies as well small iron oxide specks within bleached zones indicate subsequent cementation under oxidizing conditions after bleaching (reduced conditions) had removed most or all of the original iron oxide grain coats from the rock.

The white bleached facies of main Zion Canyon (Figs. 2.11 and 2.12) represents chemical reduction within the middle of a large fluid alteration zone where flow paths converge beneath the Temple Cap and Carmel Formations to produce a high-probability migration pathway. Because permeability is related to the rate of fluid flow through a material (Selley, 1998), the mobilization and removal of most iron oxide from even the lowest permeability bedforms of this facies implies large-scale sustained fluid transport over a long time period. In contrast, bleached bands and areas of partial discoloration in the red/white and pink altered facies (Figs. 2.8 and 2.9A) represent areas where laterally migrating bleaching fluids have locally infiltrated into unaltered rock along high permeability bedsets (see Nielsen and Chan, 2009). Bleaching dominates the upper part of the Navajo Sandstone in the southern park area (Zone 3), and is restricted to localized bands in the middle part of the park (Zone 2), but is rarely present in the northern part of the park (Zone 1). Despite the apparent simplicity of this trend, actual field relationships are complex and may indicate multiple episodes of alteration. For example, bleaching in southern part of the park (Zone 3) occurs primarily in the upper formation whereas well-defined bleaching bands in Zone 2 occur primarily in the lower to middle formation with no noticeable correlation between these features in the Jobs Head area.

The gradational nature of the transition between bleached and unbleached rock at Jobs Head (Fig. 2.15) and lack of obvious structural or stratigraphic control along this boundary suggest it represents a lateral geochemical gradient, possibly controlled by the availability of reactants. Sandstone of the red/white intermixed facies in the central park is similar in appearance and composition (Table 2.2) to that of the pink altered facies in main Zion Canyon. This suggests these two facies may represent a continuation of the same diagenetic zone with pigmentation becoming progressively more even moving northward toward the Kolob Canyons area (Figs. 2.4 and 2.8B).

The timing of widespread bleaching of the upper Navajo Sandstone in the Zion NP region is uncertain. Bleached rock is offset by the Sevier fault (Fig. 2.11B), which is likely Miocene to early Pliocene in age (Lund et al., 2008), and which provides an upper limit for when bleaching could have occurred. Boundaries between bleached and unbleached Navajo Sandstone in the Snow Canyon SP area to the west are cross-cut by large-scale lineaments postulated to correspond to Sevier-age thrusting (Willis and Higgins, 1996), suggesting that bleaching preceded the development of these features during the Late Cretaceous to early Tertiary (see Nielsen and Chan, 2009).

Spatial relationships between bleaching and iron oxide enrichment may further constrain timing. The red/white intermixed facies in the middle Navajo Sandstone and the brown ferruginous facies in the lower formation locally overlap in areas of Snow Canyon SP to produce white sandstone that has been overprinted with brown and black cementation features (overprinted white subfacies). This overprinting suggests that large-scale bleaching either preceded or was coincident with the concentrated iron oxide cementation phase in these areas (Chapter 4), but it is unknown whether this relationship also applies to Zion NP. At least some localized bleaching at Zion NP seems to have occurred after secondary iron oxide cementation, as indicated by the narrow zone of concentrated bleaching at the base of the pink middle facies which follows the top of the lower-permeability iron enrichment zone. In Fig. 2.5C, note that grain coats remain intact below the enrichment boundary, suggesting that concentrated iron oxide cementation impeded the subsequent migration of bleaching fluids.

Iron oxide enrichment. Concentrated iron oxide cementation features associated with multiple generations of iron oxide cement (Fig. 2.5C) are common in the lower

Navajo Sandstone of southwestern Utah. Two distinctive iron oxide enrichment facies are present in Zion NP. The brown ferruginous facies in the lower Navajo Sandstone has many features in common with iron oxide precipitation features in outcrops of the St. George, Utah area to the west (Fig. 2.1), and may share a similar genetic origin (see detailed discussion in Chapter 4). In contrast, the ferruginous lens subfacies (pink altered facies) was only noted in main Zion Canyon where narrow "lenses" of dense ironstone occur a short distance (10's of m) above the main iron oxide enrichment zone in the lower formation. It is possible that these lenses may serve as conduits for transporting mobilized iron that has concentrated in the lower formation. However, the iron oxide mineralogy of these facies differs (Fig. 2.6) and a direct spatial connection has not been observed.

All three diagenetic facies in main Zion Canyon are cut by deep N-NW trending vertical joints that are likely middle to late Tertiary in age (Biek et al., 2003). Thus, widespread iron oxide cementation must have occurred prior to this period. Although timing is poorly constrained, relationships between the geometry of the upper cementation boundary and structural folding in the Snow Canyon SP area tentatively suggest that, like bleaching, concentrated iron oxide precipitation in that area preceded (or perhaps was coincident with) Sevier-age deformation (Table 2.5; Chapter 4). The applicability of this timing relationship to Zion NP remains to be determined.

Late Diagenesis

Late diagenesis involves alteration that is associated with uplift and exhumation. At Zion NP, many joints in the upper Navajo Sandstone have heavily mineralized surfaces, providing evidence of localized fluid migration that is likely middle Tertiary in age or younger (Hamilton, 1992; Biek et al., 2003; Rogers et al., 2004). In places these fluids appear to have diffused outward from joints to form brightly colored "haloes" associated with the multicolored local facies (Fig. 2.14; compare with Eichhubl et al., 2004). Because some of these joints cut downward through underlying bleached and iron oxide-enriched facies, the brightly colored mineralization must be the more recent event. Surficial red streaks on canyon walls near the top of the Navajo Sandstone are very late diagenetic features that form as iron is transported downward from the overlying Sinawava Member of the Temple Cap Formation (Fig. 2.17; Hamilton, 1992). These streaks are also a reminder that diagenetic processes are ongoing in the Zion NP area. As noted by Fillmore (2000): "Zion is, and will always be a masterwork in process."

Conclusions

Distinctive coloration patterns in the Jurassic Navajo Sandstone of Zion National Park and the surrounding area record a complex diagenetic history involving multiple episodes of alteration. Six diagenetic coloration facies (including 12 subfacies) are defined and characterized in order to better understand the nature and relative timing of diagenetic events in the region. Detailed geochemical, geospatial, petrographic, and bedform analysis indicates that:

1. Color variations in the Navajo Sandstone at Zion NP are produced by a complex diagenetic history involving multiple episodes of fluid-related alteration with distinctive diagenetic events occurring during early, middle, and late diagenesis.

2. Each of three zones at Zion NP displays a different style of diagenetic alteration. The northern part of the park (Zone 1) is characterized by evenly colored reddish sandstone (red primary facies). The central part of the park (Zone 2) is characterized by reddish sandstone with localized white bleached bands (red/white intermixed facies). The southern part of the park (Zone 3), including main Zion Canyon, is subdivided into three vertically superimposed diagenetic facies: brown ferruginous (lower), pink altered (middle), and white bleached (upper). Brightly colored alteration occurs locally near joints in the middle to upper formation (multicolored local facies).
3. Bleaching (removal of iron cement from sandstone) preferentially follows high permeability strata (e.g., grainflow deposits), tends to concentrate along boundaries between high and low permeability zones, and is most prevalent along the top of the Navajo Sandstone. Mass balance relationships indicate that exchange of components during bleaching requires large volumes of fluid and therefore a sustained advective transport process is implied.
4. Eolian bedform analysis indicates that foreset dip becomes steeper, grainflow strata become more common, and mean transport direction shifts in a clockwise direction (from 196° to 233°) moving upward through the Navajo Sandstone. This increase in grainflow stratification implies an upward increase in primary permeability that may partially explain the concentration of bleaching in the upper formation. Other factors that may play a role include upward migration of fluids along inclined interdune bounding surfaces, fluid buoyancy, and relatively

impermeable rocks that overlie the Navajo Sandstone (the Temple Cap and Carmel Formations).

5. A narrow (~10 to 25 m [35 - 80 ft]) zone of concentrated bleaching at the base of the pink altered facies indicates that reduction of permeability related to formation of the brown ferruginous facies was sufficient to impede the subsequent migration of bleaching fluids.

In summary, diverse coloration patterns at Zion NP provide a history of changing geochemical conditions and allow the relative timing of major Mesozoic to Recent diagenetic events to be reconstructed. Relationships between primary sedimentary texture and fluid flow have important implications for analyzing the migration of groundwater, hydrocarbons, and other fluids in similar eolian reservoirs worldwide.

Acknowledgements

This study was funded by the Utah Geological Survey (UGS) under the "Characterization of Utah's Natural Gas Reservoirs and Potential New Reserves" initiative. Tom Chidsey, Craig Morgan, Rick Allis, and others at the UGS provided support and feedback on the project. We thank Leslie Courtright, Museum Curator at Zion National Park as well as other park staff for their assistance. Finally, we gratefully acknowledge David Wavrek of Petroleum Systems International, Inc. who assisted in evaluating liquid hydrocarbon and gas inclusions.

References

Ahlbrandt, T.S., and Fryberger, S.G., 1982, Introduction to eolian deposits, *in* Scholle, P.A., and Spearing, D., eds., Sandstone depositional environments: Tulsa, Oklahoma, American Association of Petroleum Geologists, p. 11-47.

Allis, R., White, S., Chidsey, T., Gwynn, W., Morgan, C., Adams, M., Moore, J., 2001., Natural CO2 reservoirs on the Colorado Plateau and Southern Rocky Mountains: Candidates for CO2 sequestration, *in* Proceedings of the First National Conference on Carbon Sequestration, Washington DC, May 2001: U.S. Department of Energy–National Energy Technology Laboratory, p. 19. <http://geology.utah.gov/emp/co2sequest/pdf/ reservoirs.pdf> [accessed 7/21/205]

Baker, J.C., and Golding, S.D., 1992, Occurrence and paleohydrological significance of authigenic kaolinite in the Aldebaran Sandstone, Denison Trough, Queensland, Australia: Clays and Clay Minerals, v. 40, p. 273-279.

Beitler, B., Parry, W.T., and Chan, M.A., 2003, Bleaching of Jurassic Navajo Sandstone on Colorado Plateau Laramide highs: Evidence of exhumed hydrocarbon supergiants?: Geology, v. 31, p. 1041–1044.

Beitler, B., Parry, W.T., and Chan, M.A., 2005, Fingerprints of fluid flow – chemical diagenetic history of the Jurassic Navajo Sandstone, Southern Utah, U.S.A.: Journal of Sedimentary Research, v. 75, p. 547-561.

Biek, R.F., 2003, Geology of Quail Creek State Park, Utah, *in* Sprinkel, D.A., Chidsey, T.C., Jr., and Anderson, P.B., eds., Geology of Utah's parks and monuments: Utah Geological Association Publication 28, p. 465-477.

Biek, R.F., Willis, G.C., Hylland, M.D., and Doelling, H.H., 2003, Geology of Zion National Park, Utah, *in* Sprinkel, D.A., Chidsey, T.C., and Anderson, P.B., eds., Geology of Utah's parks and monuments: Utah Geological Association Publication 28, p. 107-135.

Blakey, R.C., 1994, Paleogeographic and tectonic controls on some Lower and Middle Jurassic erg deposits, Colorado Plateau, *in*, Caputo, M.V., Peterson, J.A., and Franczyk, K.J., eds., Mesozoic systems of the Rocky Mountain region: Denver, Colorado, Rocky Mountain Section of the Society for Sedimentary Geology, p. 273-298.

Bowen, B.B., Martini, B.A., Chan, M.A., and Parry, W.T., 2007, Reflectance spectroscopic mapping of fluid flow pathways in the Jurassic Navajo Sandstone: American Association of Petroleum Geologists Bulletin, v. 91, p. 173-190.

Brenner, R.L., and Peterson, J.A., 1994, Jurassic sedimentary history of the northern portion of the Western Interior Seaway, USA, *in*, Caputo, M.V., Peterson, J.A., and Franczyk, K.J., eds., Mesozoic systems of the Rocky Mountain region, USA: Denver, Colorado, Rocky Mountain Section of the Society for Sedimentary Geology, p. 217-232.

Chan, M.A., Parry, W.T., and Bowman, J.R., 2000, Diagenetic hematite and manganese oxides and fault-related fluid flow in Jurassic sandstones southeastern Utah: American Association of Petroleum Geologists Bulletin, v. 84, p. 1281-1310.

Clark, R.N., 1995, Reflectance spectra, *in* Ahrens, T.J., ed., Rock physics and phase relations, a handbook of physical constants: Washington, D.C., American Geophysical Union, p. 178-188.

Clark, R.N., Swayze, G.A., Wise, R., Livo, E., Hoefen, T., Kokaly, R., and Sutley, S.J., 2007, U.S. Geological Survey digital spectral library splib06a: U.S. Geological Survey, Digital Data Series 231. <http://speclab.cr.usgs.gov/spectral-lib.html> [accessed 8/30/2007]

Corey, M.A., Simonson, B.M., and Loope, D.B., 2005, Physical compaction as a cause of reduced cross-bed dip angle in the Navajo Sandstone: Geological Society of America Abstracts with Programs, v. 37, p. 254.

Cornell, R.M., and Schwertmann, U., 2003, The iron oxides: Structure, properties, reactions, occurrences and uses: New York, Wiley-VCH, Second Edition, 664 p.

Cox, D.L., Lindquist, S.J., Bargas, C.L., Havholm, K.G. and Srivastava, R.M., 1994, Integrated modeling for optimum management of a giant gas condensate reservoir, Jurassic eolian Nugget Sandstone, Anschutz Ranch east field, Utah overthrust (U.S.A.), *in* Yarus, J.M. and Chambers, R.L., eds., Stochastic modeling and geostatistics: Principles, methods, and case studies: American Association of Petroleum Geologists Computer Applications in Geology 3, p. 287-321.

Dapples, 1979, Diagenesis of sandstones, *in* Larsen, G. and Chilingar, G.V., eds., Diagenesis in sediments and sedimentary rocks: New York, Elsevier Scientific Publishing Company, p. 31-97.

Davis, G.H., 1999, Structural geology of the Colorado Plateau region of southern Utah with special emphasis on deformation bands: Geological Society of America Special Paper 342, 167 p.

Dutton, C.E., 1882, Tertiary History of the Grand Cañon District: U.S. Geological Survey Monograph 2, 264 p.

Eichhubl, P., Taylor, W.L., Pollard, D.D., and Aydin, A., 2004, Paleo-fluid flow and deformation in the Aztec Sandstone at the Valley of Fire, Nevada – evidence for the coupling of hydrogeologic, diagenetic, and tectonic processes: Geological Society of America Bulletin, v. 116, p. 1120-1136.

Fillmore, R., 2000, The geology of the parks, monuments and wildlands of southern Utah: Salt Lake City, University of Utah Press, 268 p.

Garden, I.R., Guscott, S.C., Burley, S.D., Foxford, K.A., Walsh, J.J., and Marshall, J., 2001, An exhumed palaeo-hydrocarbon migration fairway in a faulted carrier system, Entrada Sandstone of SE Utah, USA: Geofluids, v. 1, p. 195-213.

Graham, J., 2006, Geologic resource evaluation report: U.S. National Park Service NPS D-259: Online, <http://www2.nature.nps.gov/geology/inventory/publications/reports/zion_gre_rpt_view.pdf> [accessed 6/27/2006].

Gregory, H.E., 1950, Geology and geography of the Zion Park region, Utah and Arizona: U.S. Geological Survey Professional Paper 220, 200 p.

Hamilton, W.L., 1978 (revised 1987), Geologic map of Zion National Park, Utah: Springdale, Utah, Zion Natural History Association, scale 1:31,680.

Hamilton, W.L., 1992, The sculpturing of Zion: Springdale, Utah, Zion Natural History Association, 132 p.

Holcombe, R., 2009, GEOrient software. <www.holcombe.net.au>

Hunter, R.E., 1977, Basic types of stratification in small eolian dunes: Sedimentology, v. 24, p. 361-387.

Kessler, L.G., 1978, Diagenetic sequence in ancient sandstones deposited under desert climatic conditions: Journal of the Geological Society of London, v. 135, p. 41-49.

Kocurek, G., 1991, Interpretation of ancient eolian sand dunes: Annual Review of Earth and Planetary Sciences, v. 19, p. 43-75.

Kocurek, G., 1996, Desert aeolian systems, *in* Reading, H.G., ed., Sedimentary environments: Processes, facies and stratigraphy: Oxford, Blackwell, Third Edition, p. 125-153.

Kocurek, G., and Dott, R.H., 1981, Distinction and uses of stratification types in the interpretation of eolian sand: Journal of Sedimentary Petrology, v. 51, p. 579-595.

Kocurek, G., 1988, First-order and super bounding surfaces in eolian sequences – bounding surfaces revisited: Sedimentary Geology, v. 56, p. 193-206.

Lake, L.W., Bryant, S.L., and Araque-Martinez, A.N., 2002, Geochemistry and fluid flow: New York, Elsevier, 226 p.

Lancaster, N., and Teller, J.T., 1988, Interdune deposits of the Namib Sand Sea: Sedimentary Geology, v. 55, p. 91-107.

Langley, T., 2006, Characterization of cements in Moki marbles as possible source of arsenic in groundwater, Washington County, Utah: Geological Society of America Abstracts with Programs, v. 38, p. 37.

Lawton, T.F., 1994, Tectonic setting of Mesozoic sedimentary basins, Rocky Mountain region, United States, *in*, Caputo, M.V., Peterson, J.A., and Franczyk, K.J., eds., Mesozoic systems of the Rocky Mountain region, Rocky Mountain Section of the Society for Sedimentary Geology, Denver, Colorado, p. 1-26.

Lindquist, S.J., 1988, Practical characterization of eolian reservoirs for development: Nugget Sandstone, Utah-Wyoming thrust belt: Sedimentary Geology, v. 56, p. 315-339.

Lund, W.R., Hozik, M.J., and Hatfield, S.J., 2007, Paleoseismic investigation and long-term slip history of the Hurricane fault in southwestern Utah: Utah Geological Survey Special Study 119, 81 p.

Lund, W.R., Knudsen, T.R., and Vice, G.S., 2008, Paleoseismic reconnaissance of the Sevier fault, Kane and Garfield Counties, Utah: Utah Geological Survey Special Study 119, 31 p.

Marzolf, J.E., 1988, Controls on late Paleozoic and early Mesozoic eolian deposition of the western United States, *in* Kocurek, G., ed., Late Paleozoic and Mesozoic eolian deposits of the western interior of the United States: Sedimentary Geology, v. 56, p. 167-191.

McKee, E.D., 1979, Ancient sandstones considered to be eolian, *in* McKee, E.D., ed., A study of global sand seas: U.S. Geological Survey Professional Paper 1052, p. 187-238.

McKinley, J.M., Worden, R.H., and Ruffell, A.H., 2003, Smectite in sandstones: A review of the controls on occurrence and behaviour during diagenesis, *in* Worden, R.H., and Morad, S. eds., Clay mineral cements in sandstones: International Association of Sedimentologists Special Publication, v. 34, p.109-128.

Morse, D.G., 1994, Siliciclastic reservoir rocks, *in* Magoon, L.B., and Dow, W.G. ed., The petroleum system – from source to trap: American Association of Petroleum Geologists Memoir, v. 60, p. 121-139.

Net, L.I, 2003, Diagenesis and reservoir quality of the Eolian Nugget / Navajo Sandstone (Early Jurassic), Utah and Wyoming [Ph.D. thesis]: Austin, University of Texas, 182 p.

Nielsen, G.B., and Chan, M.A., 2009, Mapping and correlation of diagenetic coloration facies, Jurassic Navajo Sandstone, Snow Canyon State Park, Southwestern Utah *in* Tripp, B., Krahulec, K., and Jordan, J.L., eds., Geology and geologic resources and issues of western Utah: Utah Geological Association Publication 38, p. 97-123.

Parry, W.T., Chan, M.A., and Beitler, B., 2004, Chemical bleaching indicates episodes of fluid flow in deformation bands in sandstone: American Association of Petroleum Geologists Bulletin, v. 88, p. 1-17.

Parry, W.T., Forster, C.B., Evans, J.P., Bowen, B., and Chan, M.A., 2007, Geochemistry of CO_2 sequestration in the Jurassic Navajo Sandstone, Colorado Plateau, Utah. Environmental Geosciences, v. 14, p. 91–109

Parrish, J.T., and Peterson, F., 1988, Wind directions predicted from global circulation models and wind directions determined from eolian sandstones of the western United States – a comparison: Sedimentary Geology, v. 56, p. 261-282.

Peterson, F., 1988, Pennsylvanian to Jurassic eolian transportation systems in the western United States: Sedimentary Geology, v. 56, p. 207-260

Peterson, F., and Pipiringos, G.N., 1979, Stratigraphic relations of the Navajo Sandstone to Middle Jurassic formations, southern Utah and northern Arizona: U.S. Geological Survey Professional Paper 1035-B, 43 p.

Pipiringos, G.N., and O'Sullivan, R.G., 1978, Principle unconformities in Triassic and Jurassic rocks, western interior U.S.A., preliminary report: U.S. Geological Survey Professional Paper 1035-A, 29 p.

Porter, M.L., 1986, Sedimentary record of erg migration: Geology, v. 14, p. 497-500.

Rock-Color Chart Committee, 1991, Rock color charts: Boulder, Colorado, Geological Society of America, 10 p.

Rogers, C.M., Myers, D.A., and Engelder, T., 2004, Kinematic implications of joint zones and isolated joints in the Navajo Sandstone at Zion National Park, Utah – Evidence for Cordilleran relaxation: Tectonics, v. 23., TC1007, 16 p.

Rubin, D.M., 1987, Cross-bedding, bedforms, and paleocurrents: Tulsa, Oklahoma, Society of Economic Paleontologists and Mineralogists, Concepts in Sedimentology and Paleontology, v. 1, 187 p.

Rubin, D.M., 2006, U.S. Geological Survey bedform sedimentology site, <http://walrus.wr.usgs.gov/seds> [accessed 3/28/2009]

Seiler, W.M. and Chan, M.A., 2007, Coloration and diagenetic history of Jurassic Navajo Sandstone at Coyote Buttes, Vermilion Cliffs National Monument, Arizona: Geological Society of America Abstracts with Programs, v. 39, p. 562.

Selley, R.C., 1998, Elements of petroleum geology, New York, Academic Press, Second Edition, 470 p.

Shebl, M.A. and Surdam, R.C., 1996, Redox reactions in hydrocarbon clastic reservoirs: Experimental validation of this mechanism for porosity enhancement: Chemical Geology, v. 132, p. 103-117.

Stokes, W.L., 1986, Geology of Utah: Salt Lake City, Utah Museum of Natural History Occassional Paper 6, 280 p.

Truini, M. and Macy, J.P., 2005, Lithology and thickness of the Carmel Formation as related to leakage between the D and N aquifers, Black Mesa, Arizona. U.S. Geological Survey Report 2005-5187. 8 p.

Tucker, M.E., 1991, Sedimentary petrology – an introduction to the origin of sedimentary rocks: Oxford, Blackwell Scientific Publications, Second Edition, 260 p.

Walker, T.R., 1979, Red color in dune sand, *in* McKee, E.D., ed., A study of global sand seas: U.S. Geological Survey Professional Paper 1052, p. 61-68.

Wavrek, D.A., Coleman, D., Pelphrey, S., Hall, D., Tobey, M., and Jarvie, D.M., 2004, Got gas? Innovative technologies for evaluating complex reservoir zones: American Association of Petroleum Geologists Bulletin, v. 13, p.145.

Willis, G.C., 1999, The Utah thrust system – an overview, *in* Spangler, L.E., and Allen, J.J., editors, Geology of Northern Utah and Vicinity: Utah Geological Association Publication 27, p. 1-9.

Willis, G.C., and Higgins, J.M., 1996, Interim geologic map of the Santa Clara quadrangle, Washington Co., Utah: Utah Geological Survey Open-File Report 339, scale 1:24,000.

Wilson, M.D., 1992, Inherited grain-rimming clays in sandstones from eolian and shelf environments: Their origin and control on reservoir properties, *in* Houseknecht, D.W. and Pittman, E.D., eds., Origin, diagenesis, and petrophysics of clay minerals in sandstones: Society for Sedimentary Geology Special Publication No. 47, p. 209-255.

CHAPTER 3

MAPPING AND CORRRELATION OF DIAGENETIC COLORATION FACIES, JURASSIC NAVAJO SANDSTONE, SNOW CANYON STATE PARK, SOUTHWESTERN UTAH

Reprinted with permission from
Utah Geological Association, 2009, Publication 38,
Geology and Geological Resources and Issues of Western Utah, p. 97-123.
Gregory B. Nielsen and Marjorie A. Chan

Abstract

Exceptional exposures of diagenetic alteration at Snow Canyon State Park, Utah are valuable analogs for characterizing the Navajo Sandstone and other subsurface reservoirs worldwide. Mapping of six diagenetic coloration facies/subfacies was completed at a 1:10,000 scale and covers a total area of ~60 km^2. Measured stratigraphic sections further define the spatial relationships between facies. A compiled taxonomy relates bleaching type to the duration of alteration and relative distance from the main bleached zone.

The various diagenetic coloration facies at Snow Canyon were produced along or near a spatially extensive chemical reaction front boundary (or "redox transition zone"). These facies document the complex lateral transition between red-colored "primary" rock in the southern park (enriched in iron oxide) and yellow to white colored "bleached" rock

in the northern park (depleted in iron oxide). Subsequent precipitation of dense iron oxide produced brown to black coloration that "overprints" other facies in the lower Navajo Sandstone. Geospatial relationships indicate a complex diagenetic history with distinct episodes of bleaching and iron oxide precipitation influenced by local eolian stratification features. Paleofluid migration associated with bleaching was likely toward the south or southwest. Structural relationships tentatively suggest that bleaching preceded the development of Sevier-age (Late Cretaceous to early Tertiary) deformation features.

Spatial correlation of diagenetic facies involves both horizontal and vertical components. Horizontal migration of bleaching fluids within higher permeability eolian strata produces well-defined bands of white, bleached sandstone that extend for several kilometers into unbleached red sandstone. A variety of bleaching geometries may be roughly indicative of relative distance from the main bleached zone. The order of succession for bleaching features in vertical section often mirrors lateral transitions observed in the field. For example, the upper bleached zone at Snow Canyon typically overlies an intermixed red/white zone with bleaching becoming less prevalent moving stratigraphically downward. Factors that may contribute to this pattern include changes in primary bedding fabric and the vertical superimposition of horizontally contiguous coloration facies (loosely akin to sedimentary facies relationships of Walther's law). Repetition and complexity in the architecture of diagenetic facies along the reaction front boundary result from multifaceted interaction between sedimentary, structural, and diagenetic processes.

Introduction

The purpose of this study is to analyze exceptional exposures of diagenetic alteration in the Jurassic Navajo Sandstone of southwestern Utah in order to gain a better understanding of how iron is mobilized, transported, and precipitated in the subsurface. Primary goals of the study are to map diagenetic coloration facies, show geospatial relationships, and establish the relative timing of major diagenetic events. The Navajo Sandstone and its correlative equivalent the Nugget Sandstone of northern Utah are important hydrocarbon reservoirs being actively studied in an effort to locate new reserves. An important application of this study is to better characterize this reservoir system with applications to eolian reservoirs worldwide.

Snow Canyon State Park (Snow Canyon SP) in southwestern Utah (Fig. 3.1) was named after Erastus Snow, a prominent Utah settler of the 1800s (Alder and Brooks, 1996). It could have just as easily been named for the bright white sandstone cliffs that dominate the northern end of the park. These bleached sandstones cut southward into the native red rock like advancing fingers of frost, producing a dramatic color contrast (Fig. 3.2). The visual effect is heightened by the common presence of brown and black iron-cemented sandstone (ironstone) that caps local knobs and litters the ground as large blocks. Sandstone color is commonly related to the composition and distribution of iron oxide cement, with increased concentration resulting in progressively darker-colored sandstone (Chapter 4; Cornell and Schwertmann, 2003). Bleaching occurs as primary (early) iron oxide that is commonly present as sand grain coatings is mobilized and removed from sandstone by secondary processes such as interaction with reducing fluids (Chan et al., 2000; Beitler et al., 2003; Parry et al., 2004). Abrupt changes in color (like

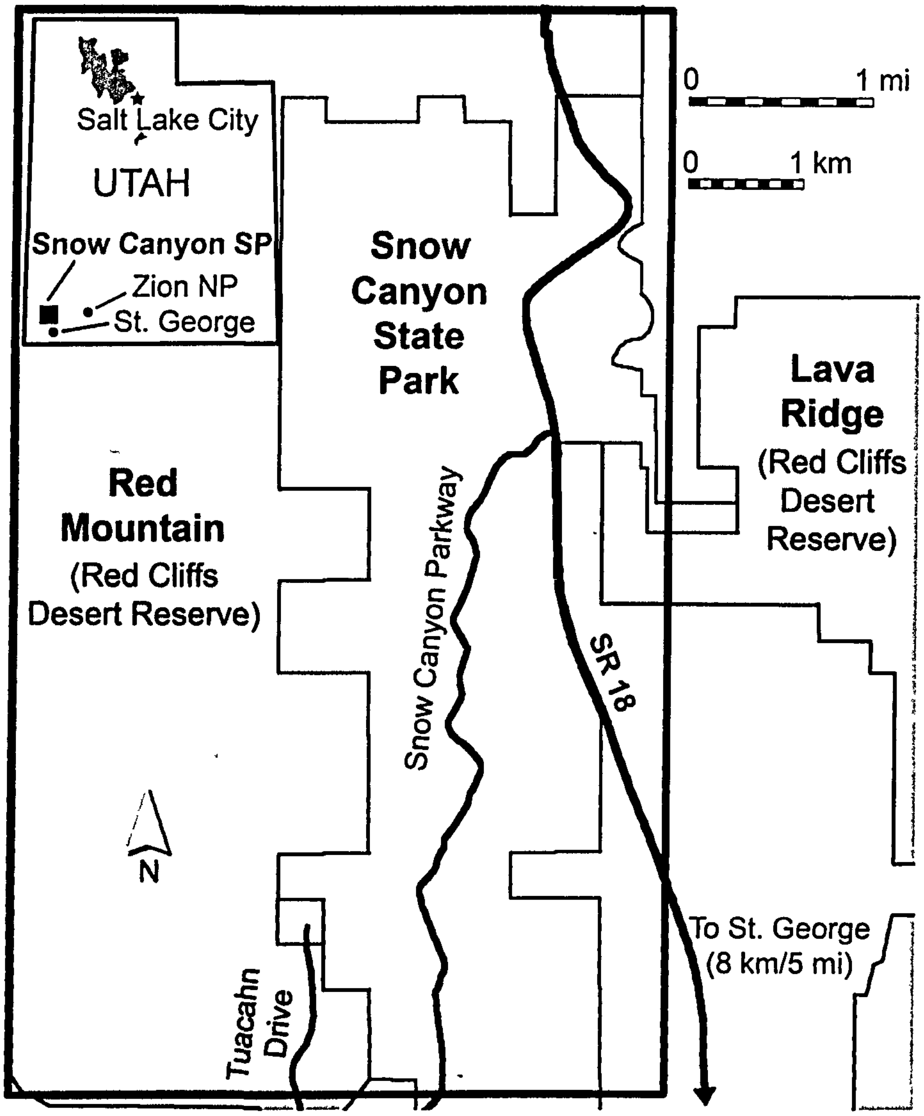

Fig. 3.1
Location of Snow Canyon SP and the Red Cliffs Desert Reserve, approximately 8 km (5 mi) north of St. George, Utah. The study area is indicated with a red boundary.

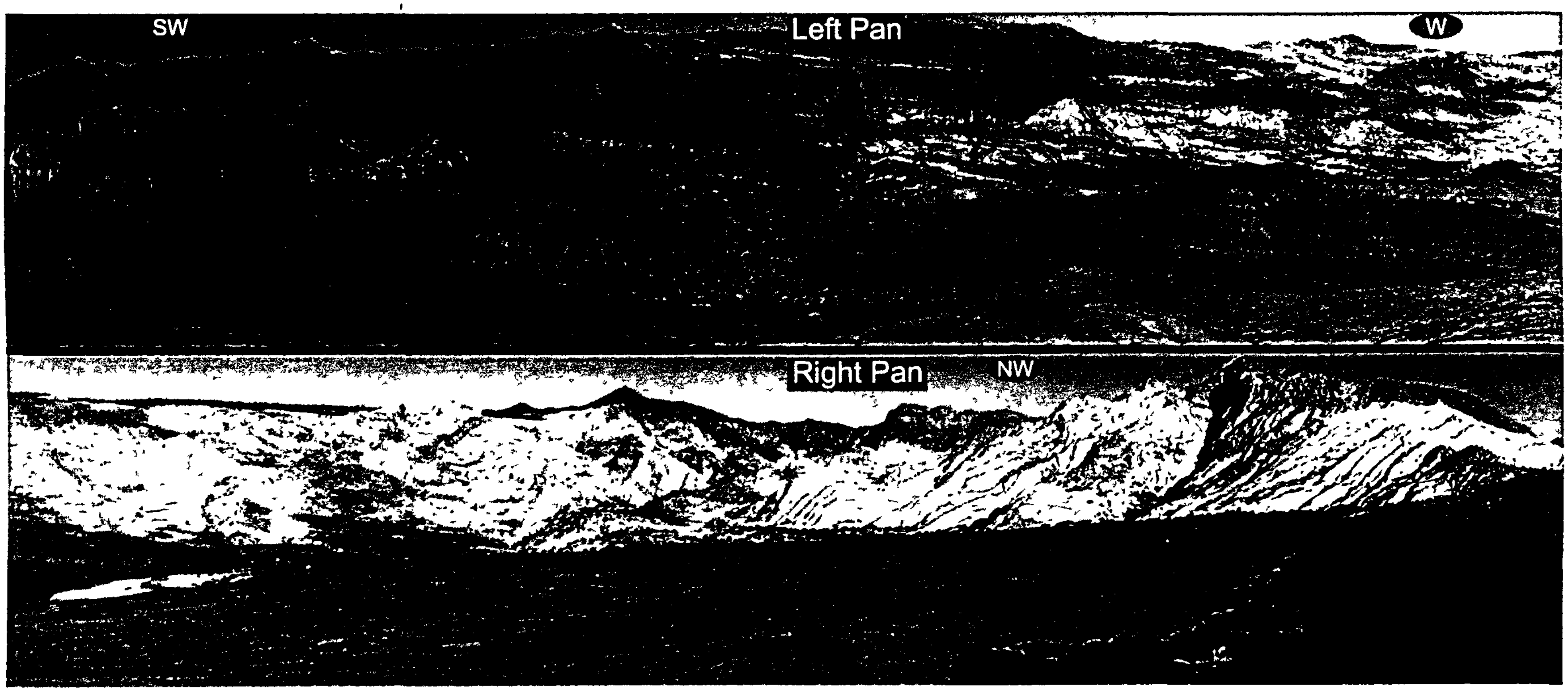

Figure 3.2.
Composite panoramic image looking west toward Red Mountain from the Snow Canyon Overlook (Fig. 4). With the exception of dark-colored basalts in the foreground, all outcrops in the image are Navajo Sandstone. The interfingered red/white zone is a reaction front boundary separating red, relatively unaltered sandstone to the south (upper image) and white, bleached sandstone to the north (lower image).

those at Snow Canyon SP) reflect changing diagenetic conditions and provide a record of paleo-fluid movement within the reservoir system (e.g., Eichhubl et al., 2004; Parry et al., 2004; and Beitler et al., 2005).

White-colored Navajo Sandstone at Snow Canyon SP is part of a much larger expanse of bleached rock that extends across much of southern Utah (Beitler et al., 2003). Snow Canyon SP and the surrounding Red Cliffs Desert Reserve (Fig. 3.1) comprise a unique locality where extensive exposures of the transition between primary red and beached white sandstone are clearly visible and a broad variety of facies relationships are observed. Previous chemical and petrographic analyses of diagenetic facies in the Navajo Sandstone of southern Utah indicate a complex diagenetic history with multiple stages of fluid alteration (Beitler et al., 2005; Nielsen et al., 2009). Mapping of diagenetic units in the Jurassic Aztec Sandstone of southern Nevada (a correlative equivalent of the Navajo Sandstone) shows a close relationship between diagenetic alteration patterns and local structural deformation features (Eichhubl et al., 2004). Nielsen et al. (2009) document the diagenetic history of the Navajo Sandstone in the St. George, Utah area (including both Zion National Park [Zion NP, Fig. 3.1] and Snow Canyon SP) and define six major diagenetic coloration facies (subdivided into 12 subfacies) within the local formation. The diversity of diagenetic and structural features at Snow Canyon SP provides an opportunity to characterize spatial relationships between these facies and evaluate the complex fluid-rock interactions that occur along the margin of a subsurface (now exhumed) bleached zone.

Geologic Setting

Basin History

With the exception of relatively young Quaternary basalts, all of the rocks within the study area are Early to Middle Jurassic in age. These Mesozoic sedimentary units were deposited in the Utah/Idaho trough, a large flexural subsidence basin that occupied the western interior of the United States during the middle Mesozoic (Blakey et al., 1988; Lawton, 1994; Peterson, 1994; Bjerrum and Dorsey, 1995). During the Early Jurassic, the southwest Utah area was occupied by streams that flowed roughly westward from the Uncompahgre Uplift area of the Ancestral Rocky Mountains (Stokes, 1986; Luttrell, 1993; Riggs and Blakey, 1993). Channels, floodplain, distal playa, and short-lived lake deposits from this river system produced the Kayenta Formation that is exposed in the southern end of Snow Canyon SP (Peterson, 1994; Higgins, 2003).

As plate tectonic motions carried the region northward into a drier latitudinal zone and volcanic highlands developed to the west (likely producing a rain shadow), the area transitioned first into sandy salt flats (a sabkha environment) and later into a broad, windswept desert (Kocurek and Dott, 1983; Marzolf, 1988; Parrish, 1993; Peterson, 1994; Biek et al., 2003). Large, southward-migrating coastal and inland dunes blanketed the region with thick sand to form the Navajo Sandstone (e.g., McKee, 1979; Blakey et al., 1988; Sansom, 1992; Blakey, 1994). Deposition of the Navajo was followed during the Middle Jurassic by transitional sabka/evaporite and eolian conditions (Temple Cap Formation) and later by the invasion of an epicontinental sea from the northeast, producing the marine deposits of the Carmel Formation (Blakey et al., 1983; Blakey et al., 1988; Lawton, 1994; Peterson, 1994).

Regional Tectonics

Subsequent to deposition, rocks of the Snow Canyon SP area have undergone multiple episodes of tectonism beginning with compressional deformation and followed by extensional fracturing. Compressional deformation in the Navajo Sandstone during the late Mesozoic to early Tertiary is evidenced by linear zones of crushing and shear offset (deformation band shear zones) as well as regional folding and tilting of strata (Cook, 1960; Lageson and Schmitt, 1994; Willis and Higgins, 1996; Hurlow, 1998; Davis, 1999). Structural tilt of the Snow Canyon SP area is associated with the northeast-dipping limb of the St. George syncline (Higgins and Willis, 1995; Hurlow, 1998; Higgins, 2003). Both the St. George syncline and the Virgin anticline immediately to the southeast are postulated to have formed during the Sevier orogeny as a result of minor thrust detachment in underlying strata (Biek, 2003; Higgins, 2003). Sevier-age deformation climaxed in the Late Cretaceous and ended in the early Tertiary [Willis, 1999])

Extensional deformation in the Navajo Sandstone is evidenced by numerous closely-spaced, high-angle joints and local normal faults. Most joints in the region are associated with either the relaxation of compressional forces at the end of the Sevier orogeny (Early Tertiary) or the subsequent development of extensional forces in the eastern Basin and Range Physiographic Province (Miocene to Holocene) (Biek et al., 2003a; Rogers et al., 2004). Joint formation may also be influenced by a reduction in confining pressure associated with the erosion of overlying strata (Willis and Higgins, 1996). Large normal faults in the area (e.g., Hurricane fault) are associated with Basin and Range extension (Davis, 1999; Lund et al., 2007).

Tertiary and Quaternary Volcanism

A number of intrusive and extrusive volcanic events have occurred in conjunction with Basin and Range extension in the Snow Canyon area. During the middle to late Tertiary, several large laccoliths were emplaced in the southern Utah region. The Pine Valley Mountains approximately 24 km (15 mi) northeast of Snow Canyon are part of this system of intrusions and have been dated to ~20 to 22 Ma (McKee et al., 1995; Hintze, 2005). Recent Quaternary basalt flows occur as cap ridges to the east of Snow Canyon SP and down-canyon flows within the park. Three flow events are documented in Snow Canyon: the Lava Ridge flow (1.41 ± 0.01 Ma), the Snow Canyon Overlook flow (1.16 ± 0.03 Ma), and the Santa Clara flow (20,000 to 10,000 years ago) (Higgins, 2003).

Methods

Study Area

The study area for this project (Fig. 3.1) includes most of Snow Canyon SP as well as parts of the surrounding Red Cliffs Desert Reserve. Mapping builds on the general geologic map of Willis and Higgins (1996), with detailed focus on diagenetic facies, and structural features related to fluid alteration patterns. Mapped units correspond to the diagenetic coloration facies and subfacies defined by Nielsen et al. (2009).

Mapping and Field Reconnaissance

Diagenetic coloration facies were mapped at a 1:10,000 scale using orthorectified, one-meter (three-ft) color aerial photography from the National Agricultural Imagery

Program (NAIP). A digital base map was generated using 10-m- (33-ft-) resolution values from the National Elevation Dataset (NED) and key points were georeferenced using a survey-grade global positioning satellite (GPS) receiver. Outcrops were mapped in the field as well as from aerial photos and spatial relationships were analyzed using geographic information system (GIS) software. The map was then refined using 2000+ digital photographs taken at locations throughout the study area. Finally, the map was extensively field checked and the location of key features and outcrops were indexed using a GPS receiver. A combination of field measurements and plotted GIS points were used to calculate the average orientation and thickness of major stratigraphic units and diagenetic facies.

Stratigraphic Sections

Stratigraphic sections were measured approximately 2 km (1.2 mi) apart at the southern, middle, and northern ends of the study area. The locations of these sections were chosen to illustrate both lateral and vertical relationships between diagenetic facies. In areas where the terrain was steep or impassible, apparent thickness measurements were made at oblique angles to strike and then converted trigonometrically to true thickness utilizing distance measurements.

Results

The area mapped for this project is dominated by the Navajo Sandstone but also includes parts of the underlying Kayenta Formation as well as the overlying Temple Cap and Carmel Formations. A simplified stratigraphic column showing Jurassic units in the

Snow Canyon SP area is shown in Fig. 3.3. Diagenetic coloration facies were mapped only for the Navajo Sandstone.

Mapped Stratigraphic and Structural Features

The overall structure of the Snow Canyon area is fairly uniform with beds dipping gently to the northeast. Calculations in this paper use the mean dip of the Kayenta and Carmel Formations (strike 328°, dip 06° NE) as an estimate for the local dip of the Navajo Sandstone because it does not have a consistent internal surface that can be used as an orientation datum and the upper part of the formation is missing in much of the southern field area. This dip value is consistent with other estimates of regional dip for the west limb of the St. George syncline (Higgins, 2003).

Navajo Sandstone

The Navajo Sandstone is the primary cliff-forming unit in the Snow Canyon SP area (Fig. 3.3). It is a fine- to medium-grained sandstone characterized by large-scale eolian bedsets with laterally extensive bounding surfaces and high-density jointing. The base of the Navajo Sandstone is an approximately 55-m- (180-ft-) thick, planar-bedded sandstone with small-scale deformation structures and evaporite clasts that are interpreted as sabka deposits (Sansom, 1992). Calculations from field data indicate total unit thickness in the study area is ~ 670 m (2200 ft), making it one of the thickest documented Navajo Sandstone localities. The color of the Navajo Sandstone varies widely from reds, yellows, and whites to dark browns and blacks depending upon the diagenetic history of a particular location. For the purposes of this paper, general color names are used for the

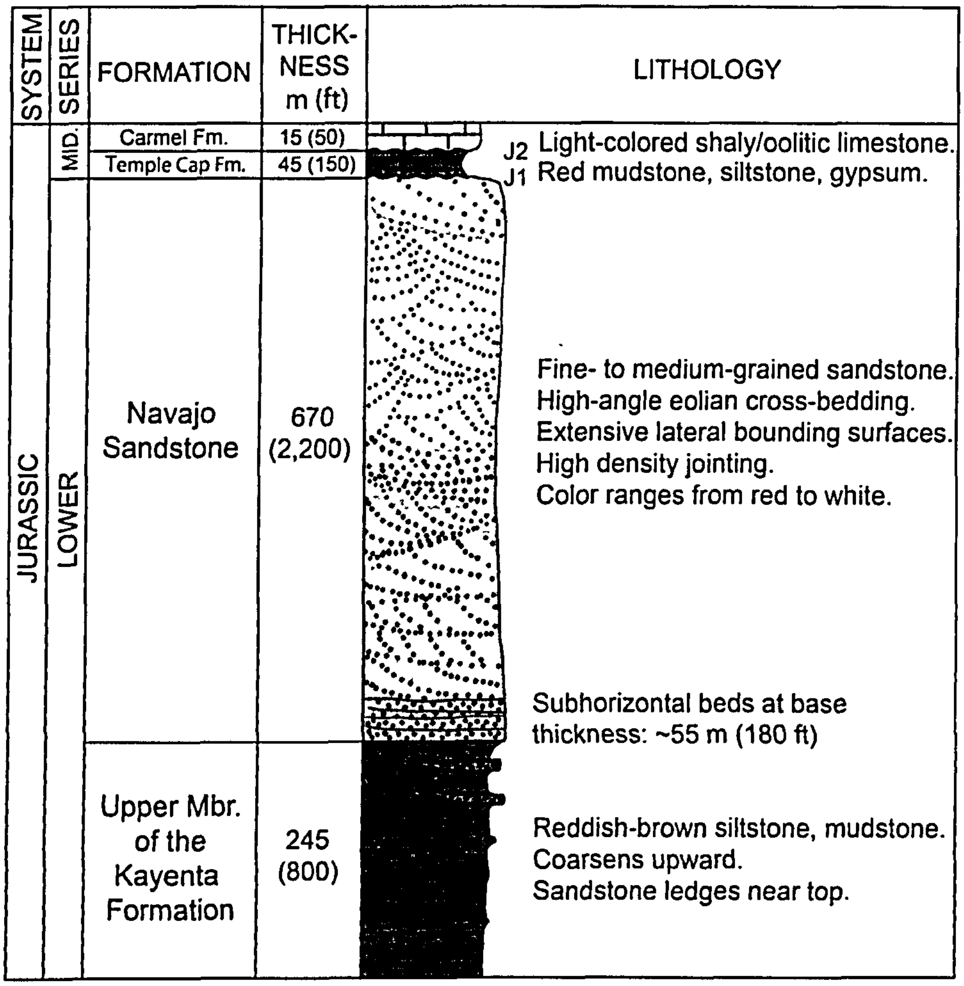

Figure 3.3. Simplified stratigraphic column showing the relationship between Lower to Middle Jurassic units exposed in the Snow Canyon SP area. J1 and J2 indicate major Jurassic unconformities. Modified after Higgins (2003) using thickness calculations and outcrop descriptions from this study.

sandstone coloration, but the specific Munsell rock color chart names are summarized in Nielsen et al. (2009). The morphology and average orientation of foresets indicates deposition by a southwestward-migrating eolian dune system (see Kocurek and Dott, 1983; Peterson, 1988; Nielsen et al., 2009). Well-defined bands of white, bleached sandstone locally follow interdune bounding surfaces (Kocurek, 1988; Kocurek, 1996) that are laterally traceable for large distances and climb gradually in the direction of foreset dip (SW).

Kayenta Formation

The Navajo Sandstone is underlain conformably by the upper member of the Lower Jurassic Kayenta Formation (Figs. 3.3 and 3.4). This formation consists of reddish-brown siltstones and mudstones with localized areas of bleaching, including pale greenish-yellow iron reduction spots (Appendix E). Narrow, light-colored mudstone beds near the base of the unit have been interpreted as short-lived lake deposits (Hintze, 2005). The unit gradually coarsens upward and two prominent sandstone ledges occur near the top. Following the work of Willis and Higgins (1996), the Kayenta-Navajo boundary is placed on top of the highest mudstone and at the base of the massive, cliff-forming sandstones. The measured dip of this formation is approximately 7° NE.

Temple Cap Formation

The Middle Jurassic Temple Cap Formation disconformably overlies the Navajo Sandstone (Fig. 3.3). It is mostly covered by alluvium but a few small exposures in the northeast corner of the study area (just north of the mapped area) are characterized by

Figure 3.4
Simplified geologic map of Jurassic stratigraphic units and corresponding diagenetic facies in the Snow Canyon SP area. A full-scale 1:10,000 version of this map is available in Nielsen and Chan (2010) and as Color Plate A. Numbers refer to locations referenced in this paper.

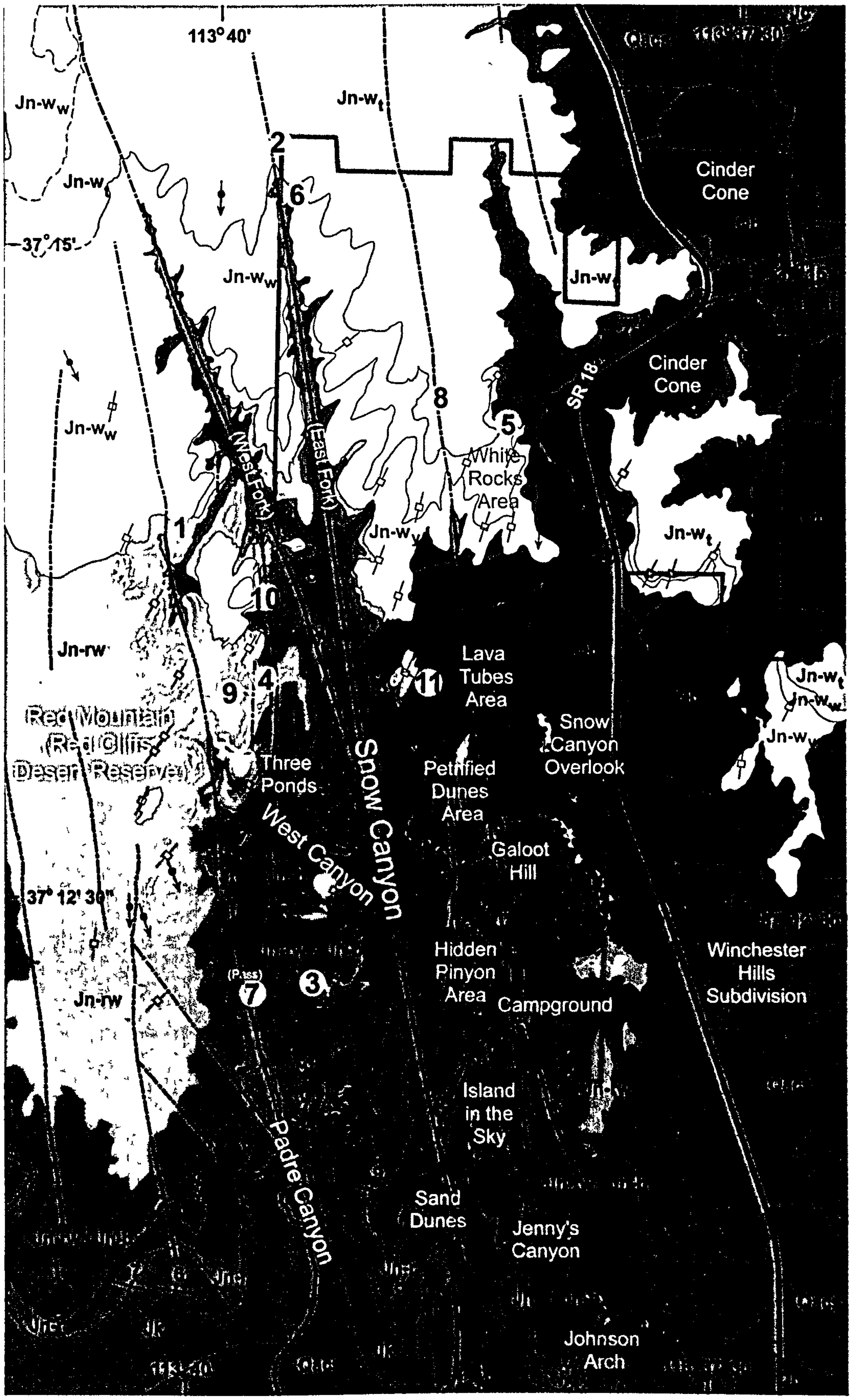
113°40'
Jn-ww
Jn-wt
Jn-wt
37°15'
2
6
Jn-ww
Jn-wt
Cinder Cone
Cinder Cone
SR 18
8
5
White Rocks Area
Jn-ww
(West Fork)
(East Fork)
1
Jn-wv
Jn-wt
10
Jn-rw
Lava Tubes Area
11
9
4
Red Mountain (Red Cliffs Desert Reserve)
Snow Canyon Overlook
Jn-wt
Jn-ww
Jn-wv
Three Ponds
Snow Canyon
Petrified Dunes Area
West Canyon
Galoot Hill
37° 12' 30"
Hidden Pinyon Area
Campground
Winchester Hills Subdivision
(Pass)
7
3
Jn-rw
Island in the Sky
Padre Canyon
Sand Dunes
Jenny's Canyon
Johnson Arch

EXPLANATION

QUATERNARY

Qacs	Quaternary Alluvium, Colluvium, Sand
Qb	Quaternary Basalts

unconformity

JURASSIC

Jc	Carmel Formation

unconformity?

Jtc	Temple Cap Formation (not exposed in mapped area)

unconformity

Navajo Sandstone

White Bleached Facies

$Jn\text{-}w_t$	Tan Subfacies
$Jn\text{-}w_w$	White Subfacies
$Jn\text{-}w_y$	Yellow Subfacies

Red/White Intermixed Facies

Jn-rw

Red Primary Facies

Jn-r

Brown Ferruginous Facies

Jn-b

Jk	Kayenta Formation (Upper Member)

0 0.5 1.0

Miles

0 1.0 2.0

Kilometers

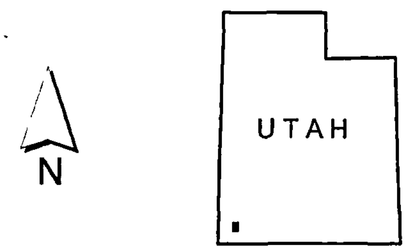

Map Symbols

- Contact
- 6 — Strike and Dip of Bedding
- Strike of Vertical or Subvertical Joint
- Lineament (used for large, widely spaced joints)
- Eolian Paleocurrent (arrow points in direction of flow, uncorrected for regional dip)
- State Park Boundary
- State Highway
- Local Road
- Small Road/Subdivision

brown mudstones with lenses of yellowish brown evaporite minerals. Thickness of this unit was estimated at ~30 to 50 m (100-150 ft). The base of the Temple Cap Formation is marked by the J-1 regional unconformity and the top is marked by the J-2 regional unconformity (Pipiringos and O'Sullivan, 1978). Analysis of associated volcanic ash beds places the age of the J-2 unconformity between 169 and 168 Ma (Kowallis et al., 2001).

Carmel Formation

The Carmel Formation overlies the J-2 regional unconformity and is exposed in the NE corner of the study area (Figs. 3.3 and 3.4). This formation is a thin-bedded, oolitic, and shaly limestone with a pale yellowish-gray color. Prominent white to orangish pink evaporite beds occur near the base of the unit and are locally deformed. The measured dip of beds in this formation is approximately 6° NE.

Quaternary Basalts

Quaternary basalt flows in the Snow Canyon SP area are mapped and described by other authors (Willis and Higgins, 1996; Higgins, 2003). As part of this project the extent of these flows is mapped (and symbolized with a darker gray to distinguish them from other Quaternary deposits) but they are not differentiated (Fig. 3.4).

Joints and Deformation Bands

Previous researchers mapped and described two sets of prominent linear features visible in aerial photographs of the Snow Canyon SP area (Willis and Higgins, 1996;

Hurlow, 1998). Because these features are important to interpreting diagenetic facies relationships, they were also partly mapped and examined as part of this study. Consistent with Willis and Higgins' (1996) earlier work, the larger, more widely spaced linear features were mapped using lineament symbols whereas the smaller, more densely spaced local joints were mapped using joint symbols. The largest set of lineaments at Snow Canyon SP has a dominantly N-NW trend and relatively wide spacing (Fig. 3.4). Snow Canyon formed along one of these major lineaments and both Padre Canyon and West Canyon formed along another to the west (Figs. 3.4 and 3.5). Some lineaments are locally associated with deformation band shear zones (Mollema and Antonellini, 1996; Davis, 1999; Eichhubl et al., 2004; Myers and Aydin, 2004; Parry et al., 2004) that weather differentially out of the surrounding rock to form narrow (meter-scale) ridges (Fig. 3.6). The second set of prominent linear features at Snow Canyon SP is closely spaced joints that trend roughly to the northeast (Fig. 3.7; Hurlow 1998). Because of the close spacing, only the overall trend of these joints was mapped, with the frequency of symbols roughly reflecting the relative density of fracturing.

Mapped Diagenetic Coloration Facies (Navajo Sandstone)

Key characteristics of mapped diagenetic coloration facies within the Snow Canyon SP area are shown in Fig. 3.8 and summarized in Table 3.1 (the multicolored local facies is described but not mapped because of its limited spatial extent). The white bleached facies is subdivided into three subfacies: yellow, white, and tan. For brevity, facies are sometimes referred to using only their unique color name. Symbols used to reference each coloration facies includes an abbreviation of the formation age and name

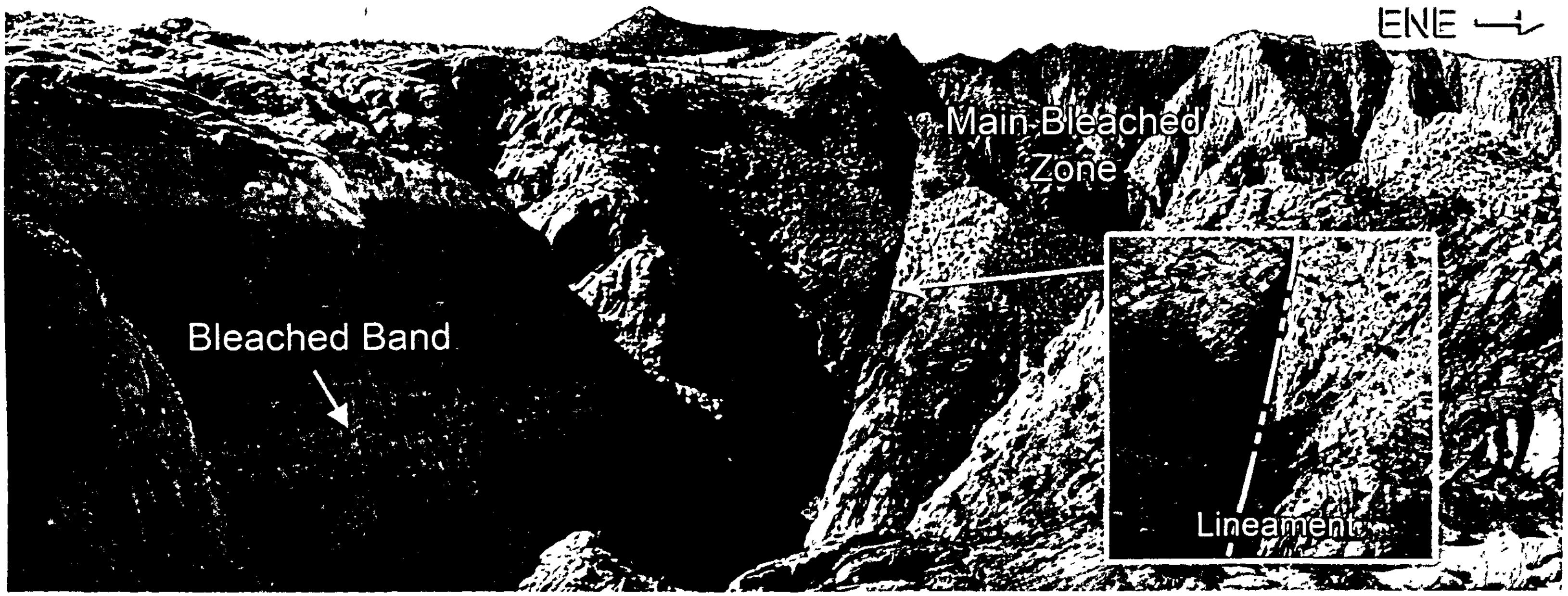

Figure 3.5
Composite panoramic image of the Padre Canyon lineament where it intersects the lower boundary of the main bleached zone northwest of Three Ponds (Fig. 4, location 1). The lineament appears to crosscut the main bleached boundary as well as bleached bands in the lower formation without visible offset offset of these features (insert). In aerial photos, the composite bleached band in the lower left of the image (labeled) continues northeastward until it appears to intersect with the main bleached zone (intersection point not shown).

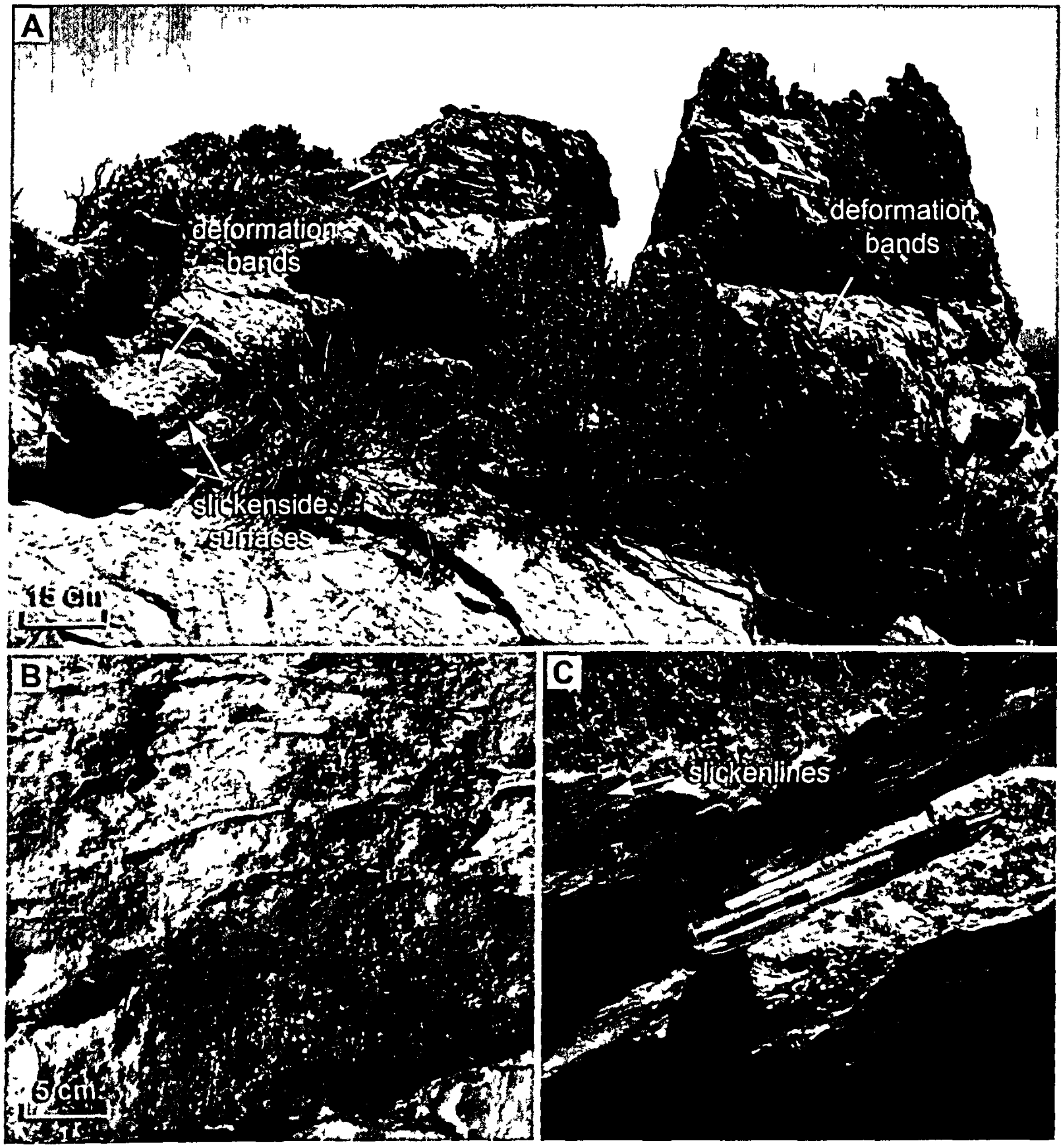

Figure 3.6
Deformation band shear zones at Snow Canyon SP. (A) Protruding outcrop produced by differential weathering of a deformation band shear zone at the head of main Snow Canyon (Fig. 4, location 2 [tan subunit]). Image looks south toward the main canyon. (B) Detail of deformation bands just northeast of image A. (C) Detail of slickenside surfaces visible in image A. Polished and striated surfaces are indicative of movement along a fault plane. Strike of the surface is 320° (parallel to the main canyon). The slickenlines are roughly horizontal and dip gently to the south.

Figure 3.7
Aerial photograph shows closely-spaced, northeast-trending joints to the northeast of Padre Canyon (Fig. 3.4, location 3). The red/white intermixed facies dominates the image. Note that joints cross-cut bleached boundaries in the Navajo Sandstone. Image source: National Agricultural Imagery Program (NAIP).

Figure 3.8
Panoramic image of central Snow Canyon SP from location 4 (Fig. 3.4) looking east. Vertical superposition of each of the six mapped Navajo diagenetic facies/subfacies (table 1) is shown. Both the contrast and saturation of the images have been increased to make subtle variations in color visible. Units shown from bottom to top: brown ferruginous facies (Jn-b), red primary facies (Jn-r), red/white intermixed facies (Jn-rw), and three subfacies of the white bleached facies (yellow [Jn-w_y], white [Jn-w_w], and tan [Jn-y_t]).

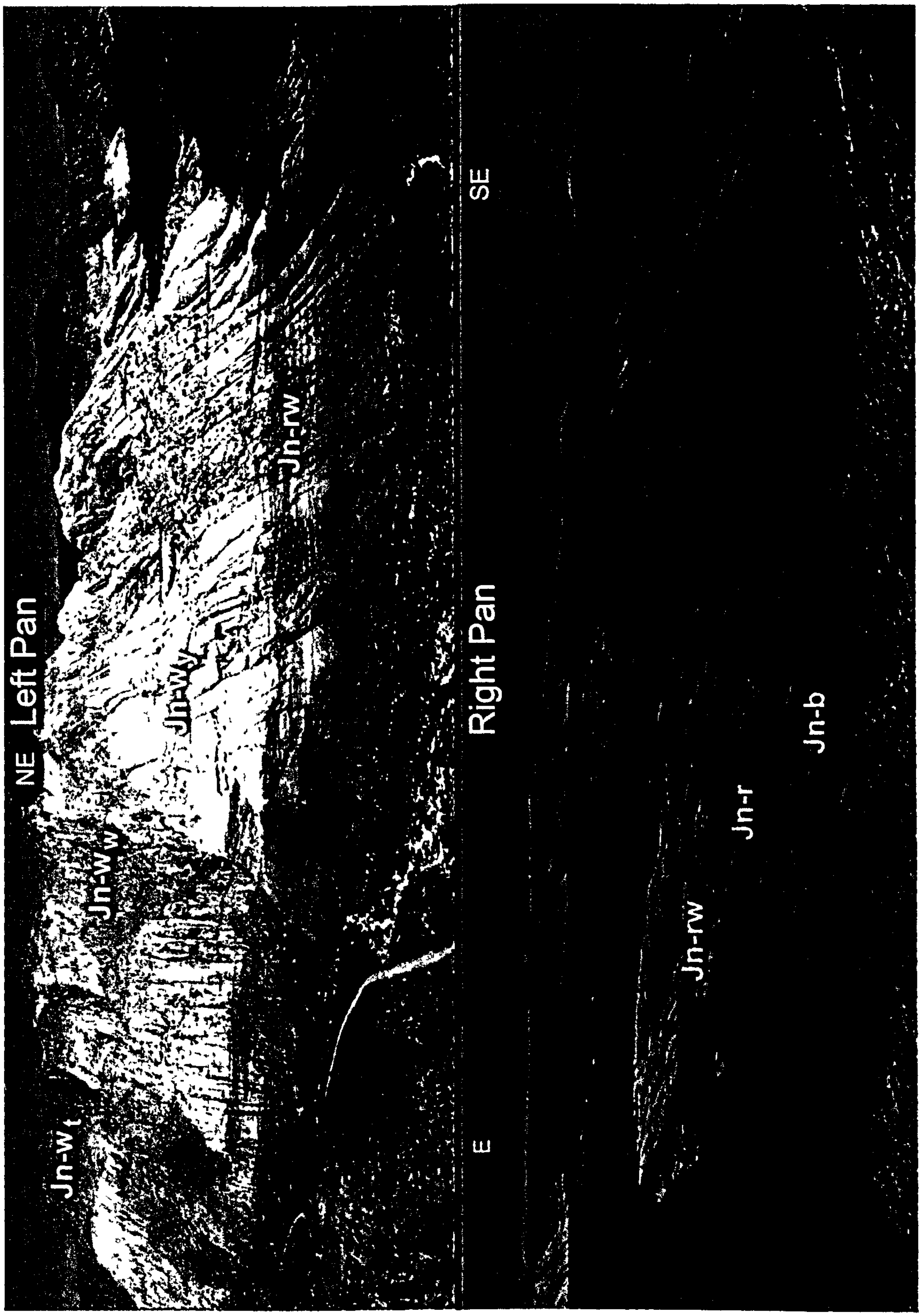

NE
Left Pan
SE
Jn-wt
Jn-ww
Jn-wy
Jn-rw
E
Right Pan
Jn-rw
Jn-r
Jn-b

Table 3.1.

Visual characteristics of major diagenetic facies and subfacies of the Navajo Sandstone at Snow Canyon SP and the surrounding area. Facies names and symbols from Nielsen and others (2009).

Facies	Subfacies	Symbol	Stratigraphic Position	Characteristic Features
Multicolored Local		Jn-m	Middle/Upper	• Brightly colored Liesegang-type bands and coloration patches (not mapped).
White Bleached	Tan	Jn-w$_t$	Uppermost	• Blocky, weathered appearance. • Silica-cemented deformation band shear zones.
	White	Jn-w$_w$	Middle to Upper	• Uniform white coloration. • Shallow polygonal fracturing.
	Yellow	Jn-w$_y$	Middle	• Irregular areas of intermixed yellow and white coloration.
Red/White Intermixed		Jn-rw	Middle	• Banded and interfingered zones of red and white sandstone. • Mottled appearance (uneven coloration).
Red Primary		Jn-r	Lower to Middle	• Even and pervasive reddish coloration.
Brown Ferruginous		Jn-b	Lower	• Dark-colored iron oxide cementation that overprints other facies (concentrated along upper boundary of facies). • Concretions, ironstone slabs, etc. • Liesegang-type bands in area immediately below boundary.

(e.g., "Jn" for the Jurassic Navajo Sandstone) followed by a dash and an abbreviation of the facies name (e.g., "Jn-w" for the white bleached facies). Abbreviations for subfacies are designated using subscripts (e.g., "Jn-w_y" for the yellow subfacies of the white bleached facies). The visual characteristics and spatial occurrence of each facies are briefly described below (a detailed analysis of the mineralogic and geochemical characteristics of these facies is presented in Nielsen et al., 2009 and Appendix F).

Red Primary Facies (Jn-r)

This facies is characterized by sandstone with an even and pervasive red pigmentation that does not have features associated with secondary alteration by fluids (Fig. 3.9). This uniform red color is typically produced by thin hematite grain coats on the detrital grains that are visible in thin section (see Walker, 1979; Beitler et al., 2005; Nielsen et al., 2009). In the southern areas of the park this facies is commonly overprinted by the brown ferruginous facies.

Red/White Intermixed Facies (Jn-rw)

The red/white intermixed facies occurs where sandstone of the red primary facies has been partially altered by reducing fluids (Fig. 3.9). It is distinguished from the red primary facies by uneven reddish coloration and partial bleaching in well-defined bands. The red-white intermixed facies occurs directly above the red primary zone (Fig. 3.9) as well as within a broad lateral transition zone in central Snow Canyon SP (Fig. 3.2). The lower boundary of the facies is defined as the first occurrence of bleached rock and the upper facies boundary is defined by the last occurrence of red rock. Boundaries of

Figure 3.9

Vertical facies transition in central Snow Canyon SP (true color). Symbols: red primary facies (Jn-r), red/white transition facies (Jn-rw), and yellow subfacies (Jn-w_y). Areas of intermixed yellow and white (Jn-w_y) are generally restricted to the lower white facies at Snow Canyon SP.

mapped areas of isolated bleaching within the red/white facies (Fig. 3.4) are approximate due to complex gradational transitions between bleached and unbleached rock.

White Bleached Facies (Jn-w)

The white bleached facies is a large zone of light colored rock in which primary grain coats have been almost entirely removed (compare with Chan et al., 2000; Beitler et al., 2005; Nielsen et al., 2009). This facies is restricted to the upper part of the Navajo Sandstone in the northern park (Figs. 3.2 and 3.4). Although rare, small "erratic patches" of remnant red rock may occur in the lower unit. The white bleached facies is subdivided into three vertically superimposed units: the yellow, white, and tan subfacies (boundaries between these subfacies are commonly gradational or poorly defined).

Yellow subfacies (Jn-w_y): The yellow subfacies is a zone of intermixed pale yellow and white rock that occurs in the lower part of the white facies in some areas of the park (Fig. 3.9). Where present at Snow Canyon, this facies typically occurs adjacent to the boundary with the red/white intermixed facies.

White subfacies (Jn-w_w): The white subfacies is a zone in the middle of the white bleached facies at Snow Canyon that lacks pigmentation and is characterized by an absence of iron oxide grain coats in thin section (Fig. 3.10). Shallow polygonal cracking is common in some areas of this subfacies, producing a checkerboard appearance.

Tan subfacies (Jn-w_t): The tan subfacies in the upper white bleached facies at Snow Canyon has a blocky, fractured appearance and frequently produces colluvium slopes (Fig. 3.10). The boundary between the white and tan subfacies is typically well

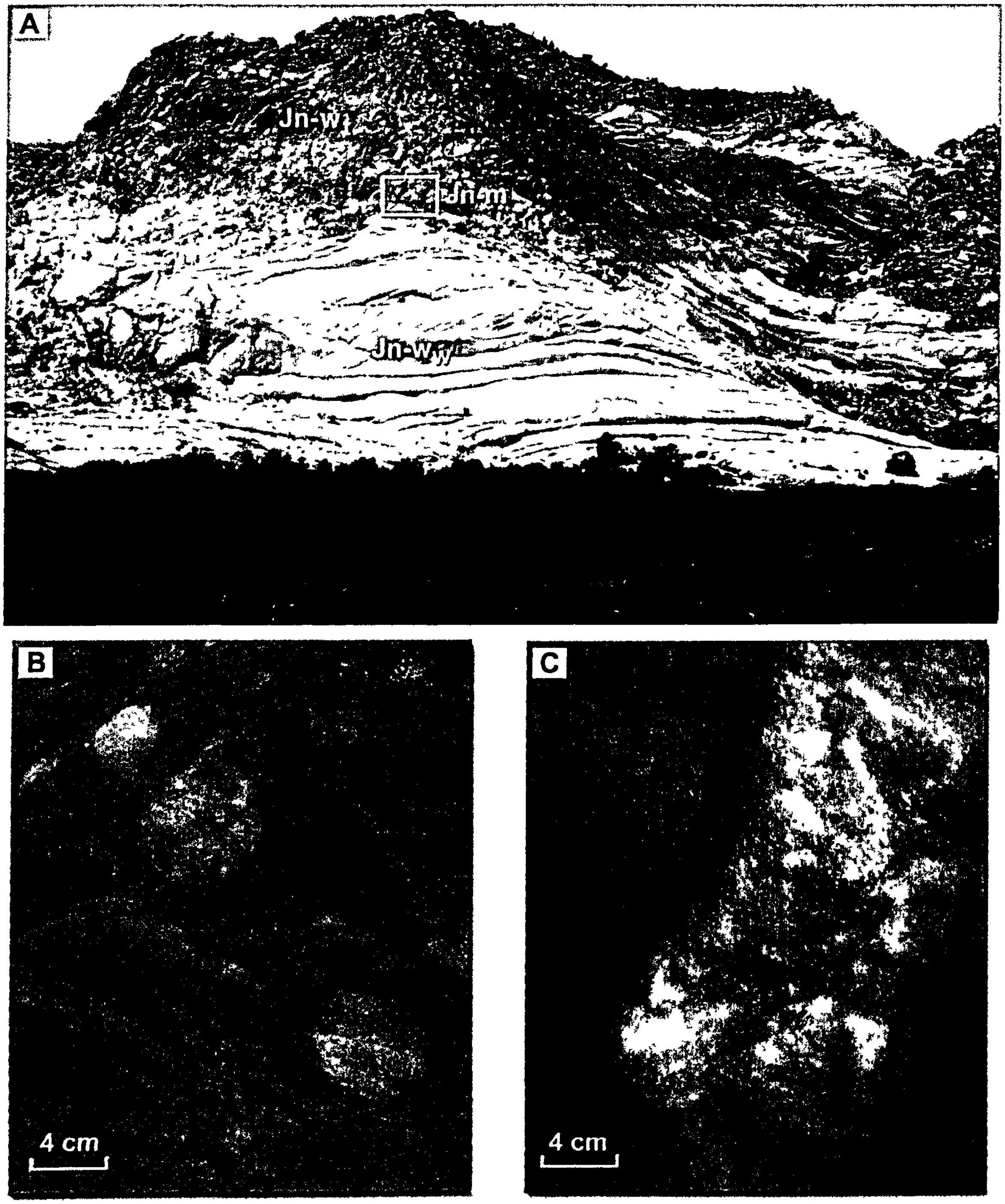

Figure 3.10
Diagenetic facies of the upper Navajo Sandstone in northern Snow Canyon SP. (A) Boundary between the white subfacies (lower) and tan subfacies (upper) in the White Rocks area (Fig. 3.4, location 5). The white subfacies (Jn-w_w) has clearly defined eolian bedforms and well-developed bounding surfaces. In contrast, the tan subfacies (Jn-w_t) has a blocky, fractured appearance and eolian strata are poorly defined. Brightly colored cementation of the multicolored local facies (Jn-m) occurs near the base of the tan subfacies (white box). (B and C) Detail of brightly colored, patchy, red and yellow cementation associated with the multicolored local facies.

defined, approximating a homoclinal surface (dip 290/04-05N from GIS measurements). This boundary corresponds to a regional, eolian bounding surface in some areas.

Multicolored Local Facies (Jn-m)

Bright secondary yellow to orange coloration occurs near joints in localized areas of the upper Navajo Sandstone (Figs. 3.10 and 3.11). At Snow Canyon this alteration commonly occurs within the tan subfacies and is most pronounced along the lower subfacies boundary (Fig. 3.10A). The occurrence of the tan and multicolored facies in areas of Snow Canyon SP appears to be related to prevalent vertical joints as well as larger-scale cross-bedding in the upper formation (Fig. 3.11; Nielsen et al., 2009). Because of its localized occurrence, this facies is described but was not mapped.

Brown Ferruginous Facies (Jn-b)

The brown ferruginous facies is discussed last because it lacks a unique spatial zone and instead overlaps with other facies in the lower portions of the formation (stratigraphically in the lower third, Fig. 3.4). It is characterized by areas of concentrated iron oxide cementation that apparently "overprint" other diagenetic facies (see discussion of subfacies produced by overprinting in Nielsen et al., 2009). The upper boundary of the brown ferruginous facies is locally well-defined and characterized by a broad variety of unique cementation features including oxidations spots, concretions, Liesegang-type bands (millimeters-scale), and ironstone slabs (Fig. 3.12; Chapter 4). On a regional (km+) scale, this upper boundary forms a subhorizontal, gently undulating surface that dips at an oblique angle to the base of the red/white intermixed facies (Figs. 3.13 and

Figure 3.11
Brightly colored secondary coloration (multicolored local facies) occurs in close proximity to vertical joint surfaces (arrow) in the tan subfacies near the Navajo Sandstone rim (Fig. 3.4, location 6). Note the large-scale cross-bedding in the upper part of the formation.

Figure 3.12
Dark-colored ironstone slabs occur along the upper boundary of the brown ferruginous facies (Hidden Pinyon area, Fig. 3.4). The continuation of this boundary is visible as a dark-colored boundary that overprints the red/white intermixed facies in cliffs to the west (background of the photo). Distance to the cliffs is approximately 0.5 km (0.3 mi).

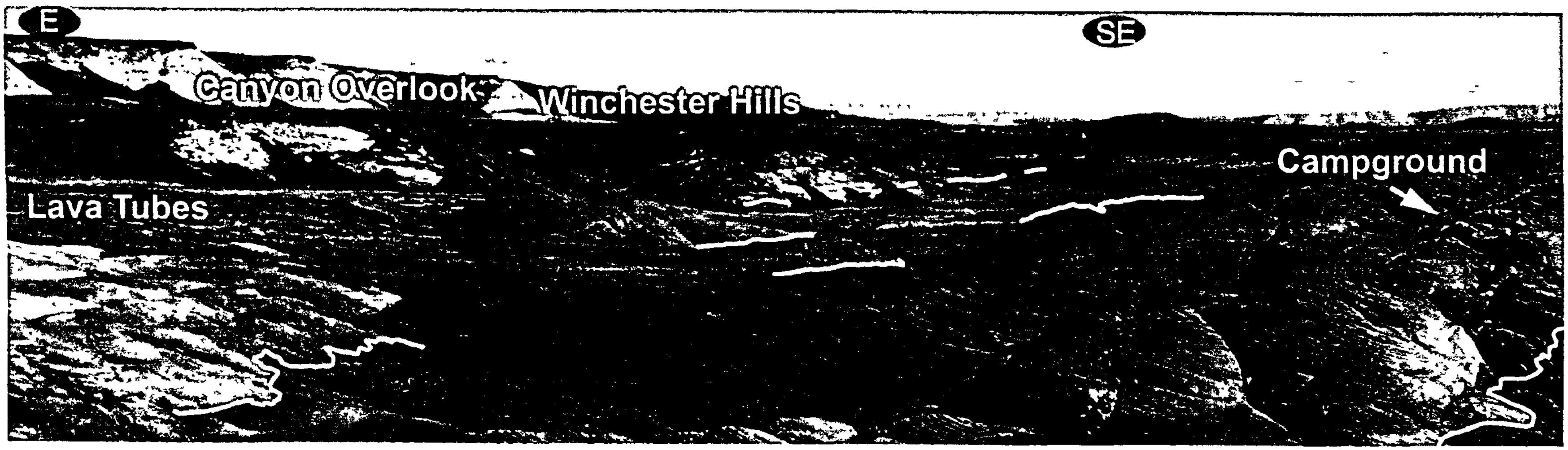

Figure 3.13
Perspective-corrected panoramic image of Snow Canyon looking southeast from location 4 (Fig. 3.4). The subhorizontal upper boundary of the brown ferruginous facies is traced in white.

3.14). Because of this, the brown ferruginous facies overprints the red/white facies in the southern park (Fig. 3.12) and occurs below this facies in the central park (Fig. 3.8). The calculated trend for the upper boundary of the brown ferruginous facies (n = 67 reference points) is strike 334°, dip 6° northeast, very similar to the estimated trend for structural tilt of the Navajo Sandstone (strike 328°, dip 06° NE). For a detailed geochemical and geospatial analysis of the brown ferruginous facies see Chapter 4.

Transition Between Bleached and Unbleached Sandstone

The transition from unbleached to bleached sandstone at Snow Canyon SP generally follows the same sequential pattern in both horizontal and vertical section. In horizontal transitions, unbleached red sandstone in the southern park (red primary facies) transitions to partially bleached sandstone in the middle park (red/white intermixed facies) and completely bleached sandstone in the northern park (white bleached facies) (see Figs. 3.2 and 3.14). Vertical transitions typically mirror this sequence, with the red primary facies in the lowest stratigraphic position, red/white intermixed facies in the middle, and white bleached facies in the highest stratigraphic position (see Figs. 3.9 and 15). The lower boundary of the white bleached facies in the northern park dips non-uniformly to the northeast and has a calculated trend (strike 324°, dip 08° northeast) that is also similar to the overall structural tilt of the Navajo Sandstone (strike 328°, dip 06° northeast), although the boundary locally deviates substantially from its trend surface. The significance of these spatial relationships to estimating the timing and direction of bleaching fluid migration are discussed below.

Figure 3.14
Spatial distribution of the mapped diagenetic facies/subfacies in the Snow Canyon area. Image created by draping mapped unit boundaries (Fig. 3.4) onto a computer-generated oblique view of the area. Grayish zone on top of Red Mountain represents soil cover where bleaching patterns are not visible. A larger, undivided version of this figure is available in Nielsen and Chan (2010).

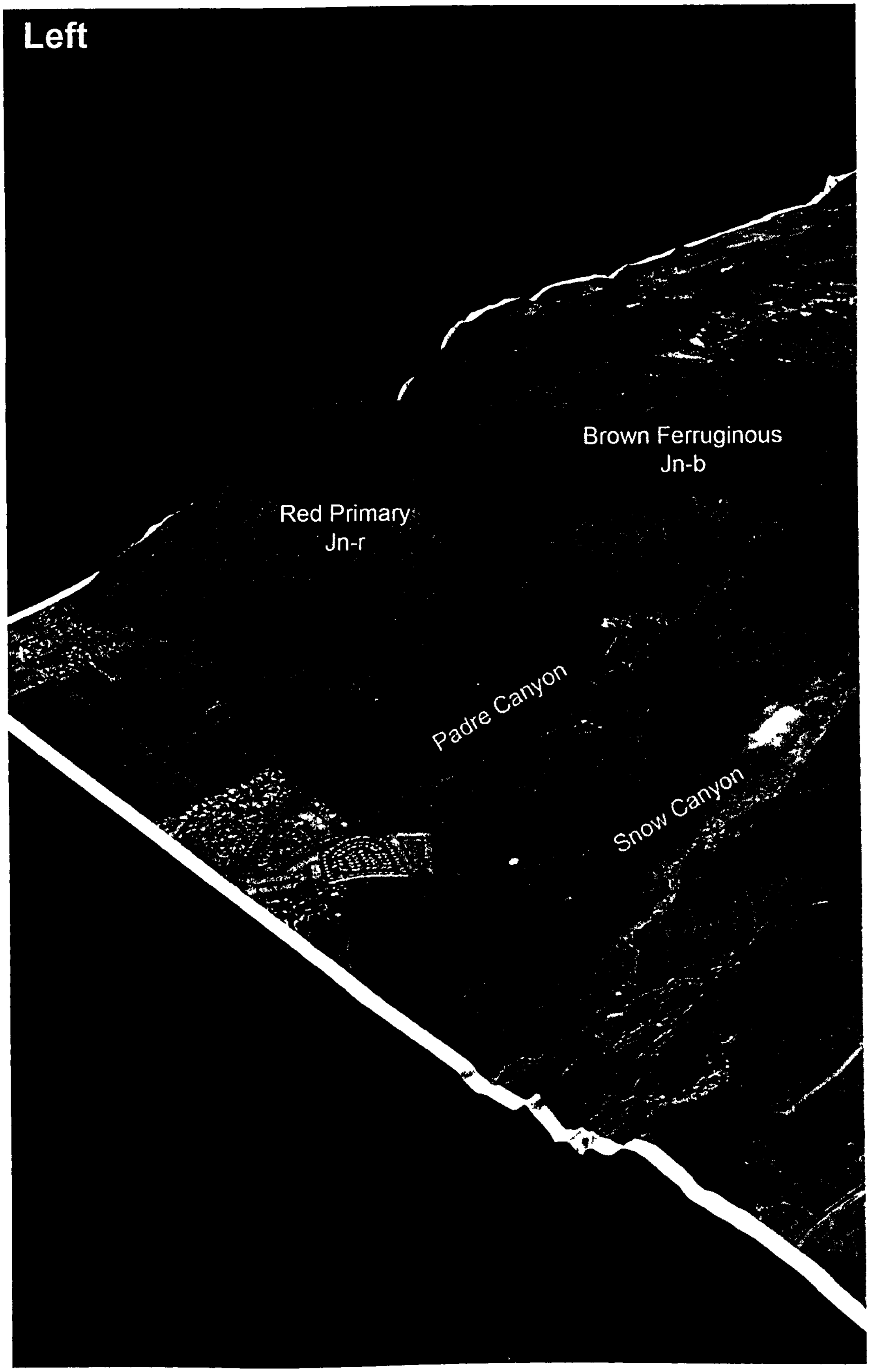

Left
Brown Ferruginous
Jn-b
Red Primary
Jn-r
Padre Canyon
Snow Canyon

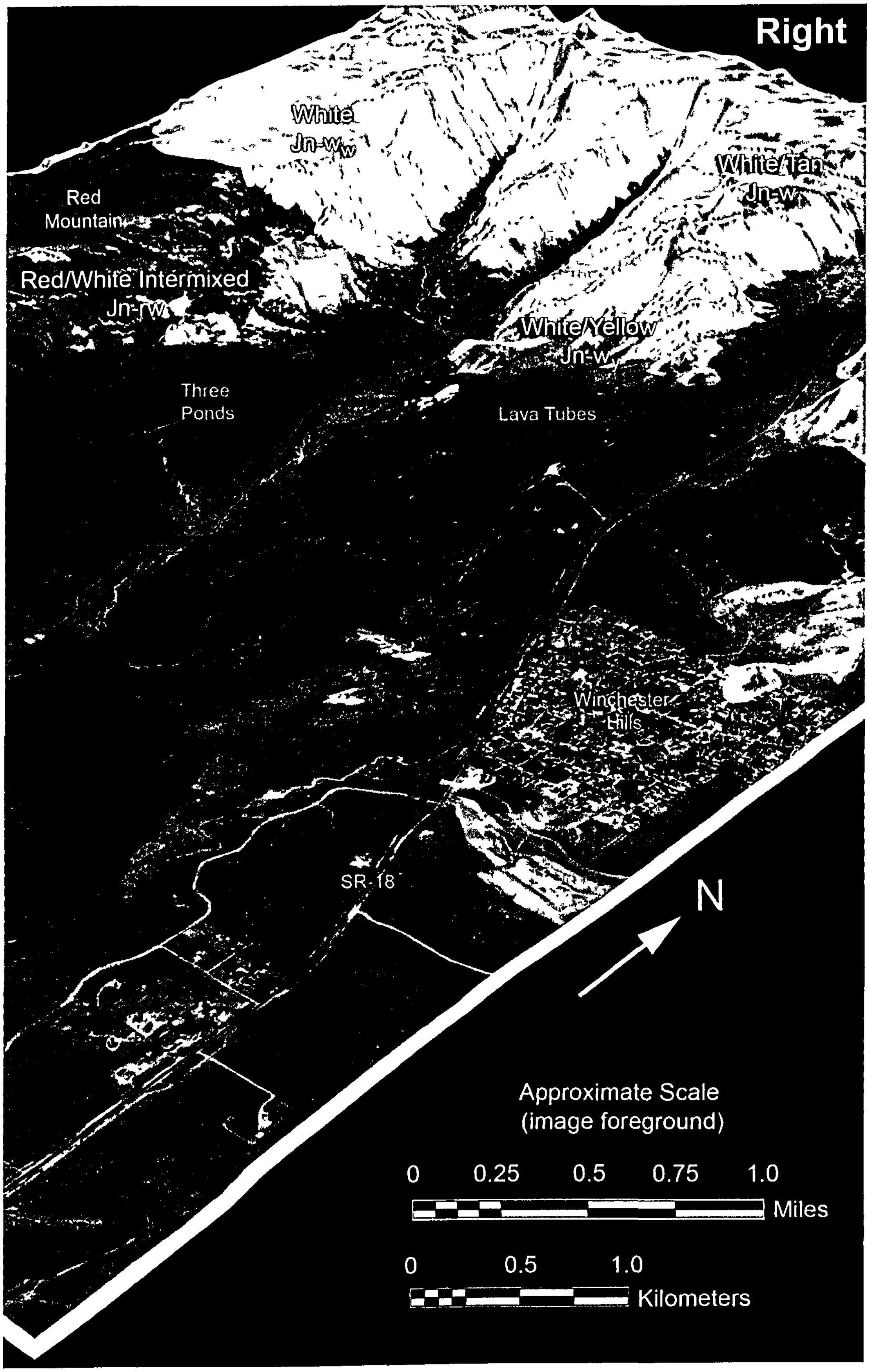
Right
White
Jn-w_w
White/Tan
Jn-w
Red
Mountain
Red/White Intermixed
Jn-rw
White/Yellow
Jn-w_y
Three
Ponds
Lava Tubes
Winchester
Hills
SR-18
N
Approximate Scale
(image foreground)
0 0.25 0.5 0.75 1.0
Miles
0 0.5 1.0
Kilometers

Figure 3.15
Measured stratigraphic sections show vertical relationships between diagenetic facies at locations in the southern, central, and northern areas of Snow Canyon SP (Fig. 3.4, locations 7, 4, and 5). Secondary iron oxide cement (brown ferruginous facies) locally overprints other facies in the southern park while bleached sandstone (white bleached facies) dominates the northern park.

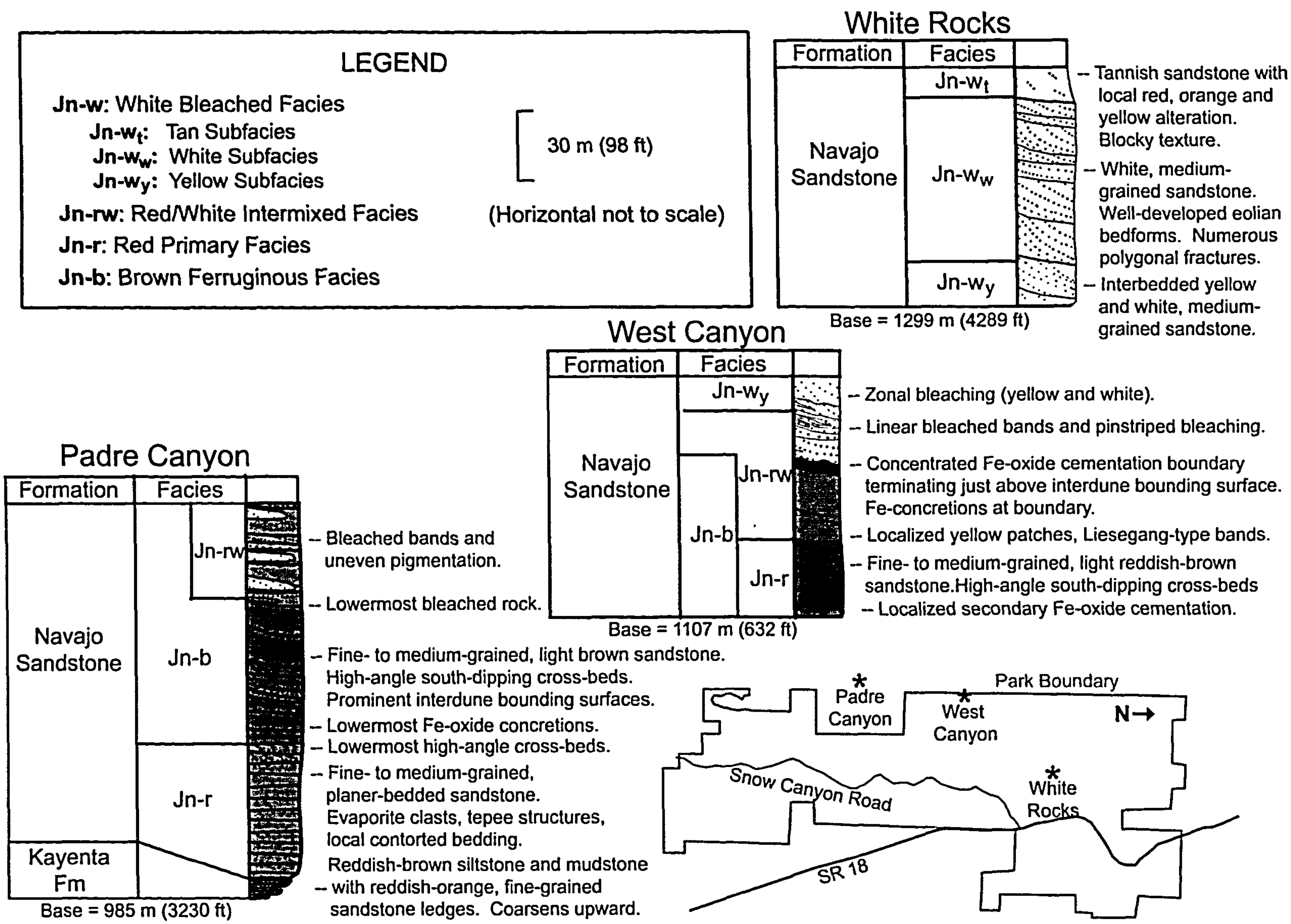

LEGEND
Jn-w: White Bleached Facies
Jn-wt: Tan Subfacies
Jn-ww: White Subfacies
Jn-wy: Yellow Subfacies
Jn-rw: Red/White Intermixed Facies
Jn-r: Red Primary Facies
Jn-b: Brown Ferruginous Facies
30 m (98 ft)
(Horizontal not to scale)
White Rocks
Formation
Facies
Navajo Sandstone
Jn-wt
Jn-ww
Jn-wy
Base = 1299 m (4289 ft)
-- Tannish sandstone with local red, orange and yellow alteration. Blocky texture.
-- White, medium-grained sandstone. Well-developed eolian bedforms. Numerous polygonal fractures.
-- Interbedded yellow and white, medium-grained sandstone.
West Canyon
Formation
Facies
Navajo Sandstone
Jn-wy
Jn-rw
Jn-b
Jn-r
Base = 1107 m (632 ft)
-- Zonal bleaching (yellow and white).
-- Linear bleached bands and pinstriped bleaching.
-- Concentrated Fe-oxide cementation boundary terminating just above interdune bounding surface. Fe-concretions at boundary.
-- Localized yellow patches, Liesegang-type bands.
-- Fine- to medium-grained, light reddish-brown sandstone.High-angle south-dipping cross-beds
-- Localized secondary Fe-oxide cementation.
Padre Canyon
Formation
Facies
Navajo Sandstone
Jn-rw
Jn-b
Jn-r
Kayenta Fm
Base = 985 m (3230 ft)
-- Bleached bands and uneven pigmentation.
-- Lowermost bleached rock.
-- Fine- to medium-grained, light brown sandstone. High-angle south-dipping cross-beds. Prominent interdune bounding surfaces.
-- Lowermost Fe-oxide concretions.
-- Lowermost high-angle cross-beds.
-- Fine- to medium-grained, planer-bedded sandstone. Evaporite clasts, tepee structures, local contorted bedding.
-- Reddish-brown siltstone and mudstone with reddish-orange, fine-grained sandstone ledges. Coarsens upward.
Padre Canyon
West Canyon
Park Boundary
N→
Snow Canyon Road
White Rocks
SR 18

Discussion

Horizontal Facies Relationships

The dominance of white bleached rock in the northern area of Snow Canyon SP, and its relative absence in the southern park, is attributed to a combination of three factors: structural tilt, slope of the canyon floor, and a horizontal shift in bleaching styles related to the lateral migration of fluids. Structural tilt along the St. George syncline rotated Navajo Sandstone of the southwestern park upward relative to Navajo Sandstone in the northeastern park and much of the upper formation (more than 400 m [1300 ft] in some areas) has been removed by erosion in the southwestern park area. A close correspondence between the regional dip of the Navajo Sandstone and the dip of the lower boundary of the white bleached facies suggests that bleaching may have preceded structural deformation, with bleached areas also tilted northeastward along the syncline. If this interpretation is correct, then the relative lack of bleached rock in the southwestern park may be principally attributed to removal of the uppermost formation where bleaching is typically most prevalent (see Fig. 3.15). The slope of the canyon floor accentuates this visual (exposed) transition, dropping more than 150 m feet [500 ft] from the northern park (where only the upper, bleached Navajo Sandstone is exposed) to the south park entrance (dominated by red coloration of the lower formation).

Another factor that likely contributes to the color transition at Snow Canyon SP is a horizontal change in bleaching styles related to the lateral migration of paleofluids. The lower boundary of the white bleached facies deviates locally from its trend surface (Fig. 3.16) and is steeply inclined along its southwestern margin, with local dip of the boundary exceeding 50° in some areas (e.g., location 10 in Fig. 3.4). Some bleached

Figure 3.16
Composite panoramic image shows the lower boundary of the white bleached facies (A) which dips nonuniformly to the northeast. Photo taken from Fig. 3.4, location 8. Numbers refer to figures that detail bleaching relationships adjacent to the main boundary (1 = Fig. 3.5; 2 = Fig. 3.17). (B) Calculated trend surface for the lower boundary of the white bleached facies (strike 324°, dip 08° NE). Plotted elevation points are shown in red (n=238). Maximum positive deviation from the trend surface is 115 m, maximum negative deviation is 118 m, and the standard error of the estimate is 56 m. Eastward dip of the boundary locally exceeds 50° in some areas near location 1.


A
Jn-rw
Jn-wy
Jn-wy
Jn-rw
1
2
SSE
B
1
2
SSE

bands (Fig. 3.5) in the southern park can be traced northward to where they interconnect with the white bleached facies along steeply dipping areas of the boundary (Fig. 3.17A). In other cases, interconnection of bleached bands to the main bleached zone can only be inferred, as the point of potential convergence commonly occurs above or below the present topographic surface (e.g., Fig. 3.5). Assuming that most bleached bands do interconnect with the main bleached zone, a regular horizontal succession of bleaching types can be demarcated (Fig. 3.18), with "zonal bleaching" (a regional [km-scale] area of completely bleached rock) in the northern park transitioning southward into "interfingered bleaching" (a broad [m- to km-scale] area of interpenetrating bleached and unbleached rock that locally cut across permeability boundaries) and "bleached bands" (narrow [m-scale] zones of bleached rock that follow high permeability eolian bedsets and may extend laterally for kilometers [Fig. 3.2]). Although individual bleached bands can be difficult to trace in two-dimensional outcrop, the broad lateral extent of these features implies sustained horizontal migration of chemically reducing fluids (see discussion of bleaching processes in Parry et al., 2004; Beitler et al., 2005; Nielsen et al., 2009).

Vertical Facies Relationships

The vertical succession of bleaching types in the Navajo Sandstone at Snow Canyon SP commonly mirrors the horizontal transition described above. Unbleached red rock in the lowermost Navajo Sandstone typically transitions upward into an area of localized bleaching (interfingered or bleached bands) and then into completely bleached sandstone (Figs. 3.9 and 3.19). Preliminary observations suggest at least two factors that

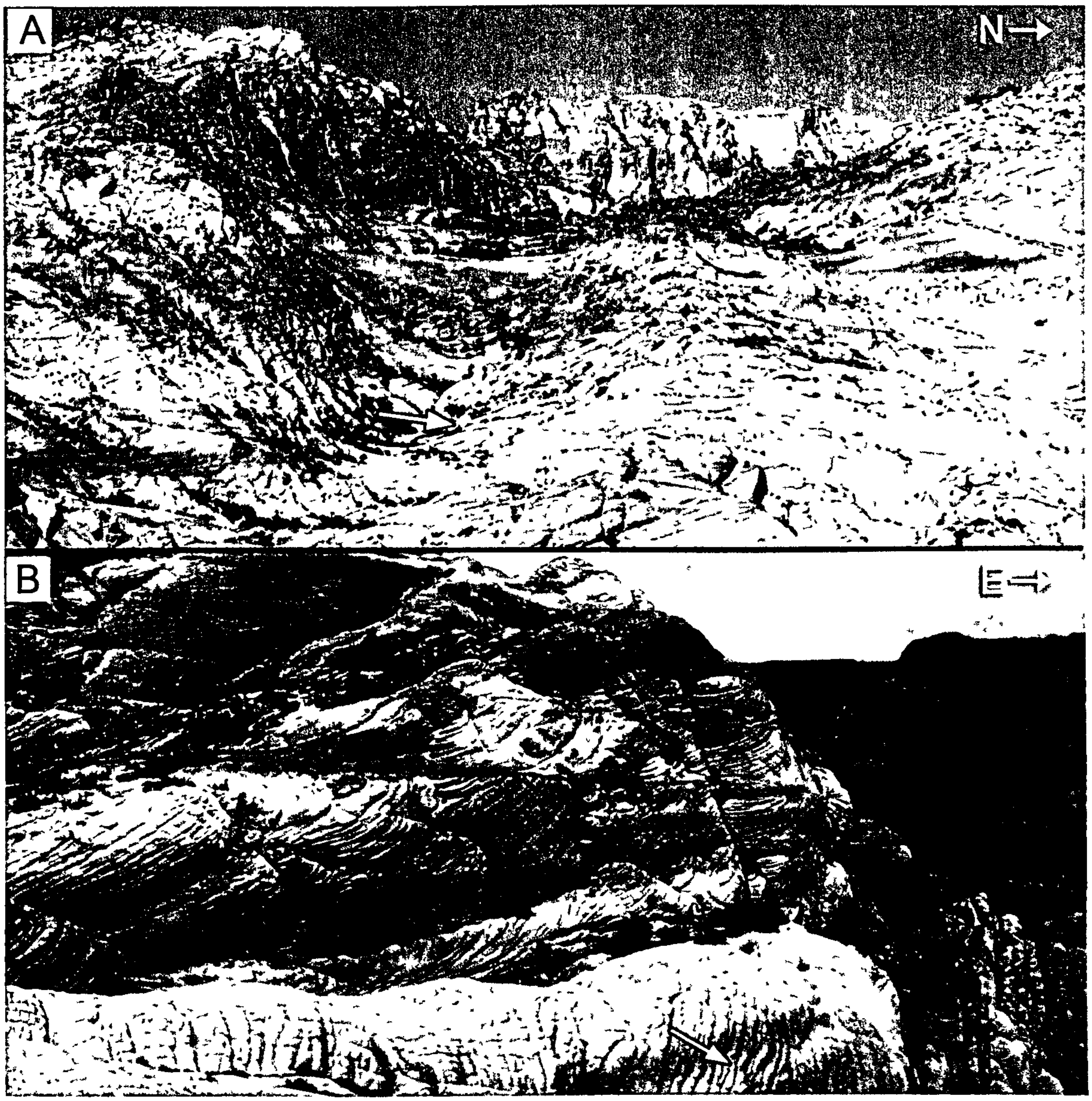

Figure 3.17
Bleaching relationships within the red/white intermixed facies (Fig. 3.4, location 9). (A) Bleached bands from the red/white intermixed facies appear to connect to the white bleached facies in some areas (arrow). (B) Brightly colored alteration in the central park may have been produced by a combination of partial bleaching (red/white intermixed facies) and subsequent secondary cementation (multicolored local facies). Arrow points to bright yellowish coloration (note person for scale).

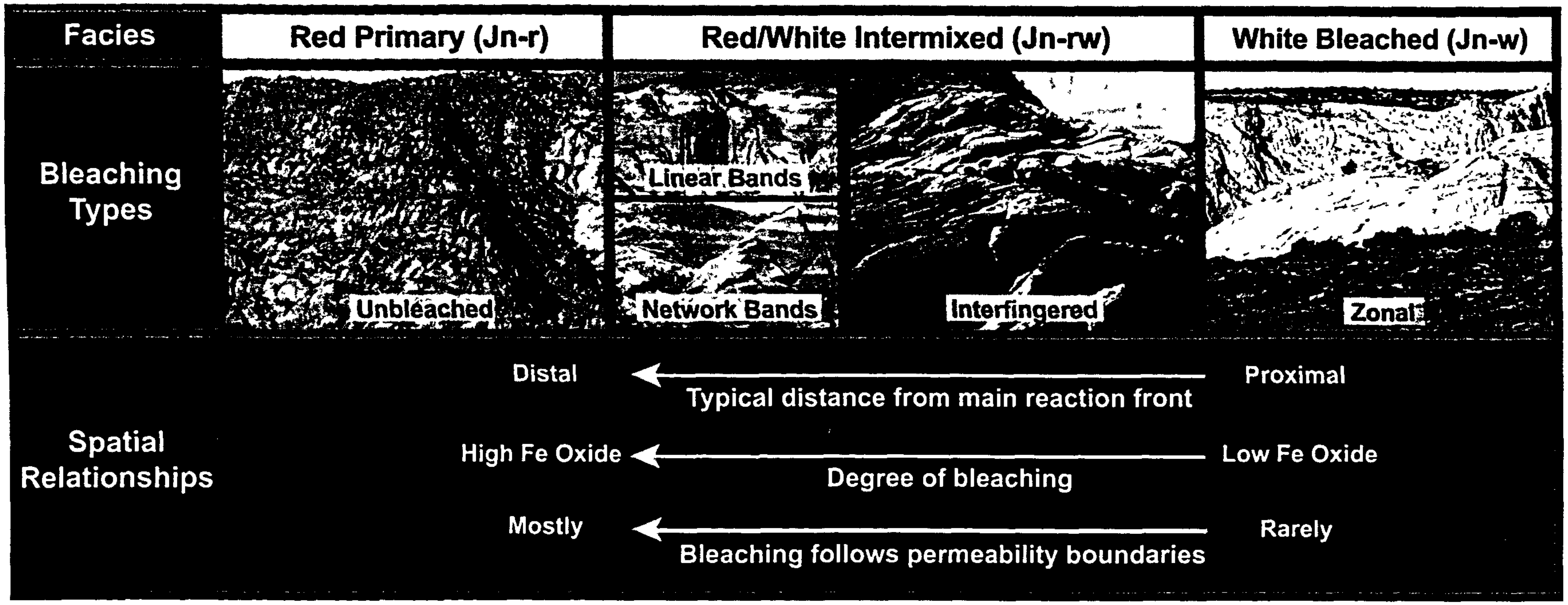

Figure 3.18
Typical horizontal relationships and associated bleaching styles for major diagenetic facies at Snow Canyon SP.

Figure 3.19
Vertically superimposed bleached features at Snow Canyon SP. (A) Upward succession of bleached bands near Three Ponds (Fig. 3.4): Isolated bleaching (1), bleached bands (2), network bleached bands (3), and zonal bleaching (4). The upper boundary of the brown ferruginous facies cross-cuts the red/white transition facies at this location (arrow). (B) Upward succession of interfingered bleaching features in the central part of the park (Fig. 3.4, location 11): red primary sandstone (5), bleached fingers (6), remnant red sandstone (7), and completely bleached rock (8). The upper boundary of the brown ferruginous facies occurs below the red/white facies (arrow) at this location. (C) Step-like succession of stacked, trough-shaped bleached features (9-11) in the central park (Fig. 3.4, location 10). (D) Large, red-colored "erratic patch" in the bleached zone at Winchester Hills (Fig. 3.4) appears isolated but likely represents a three-dimensional finger of primary rock that has been truncated and exposed by erosion.

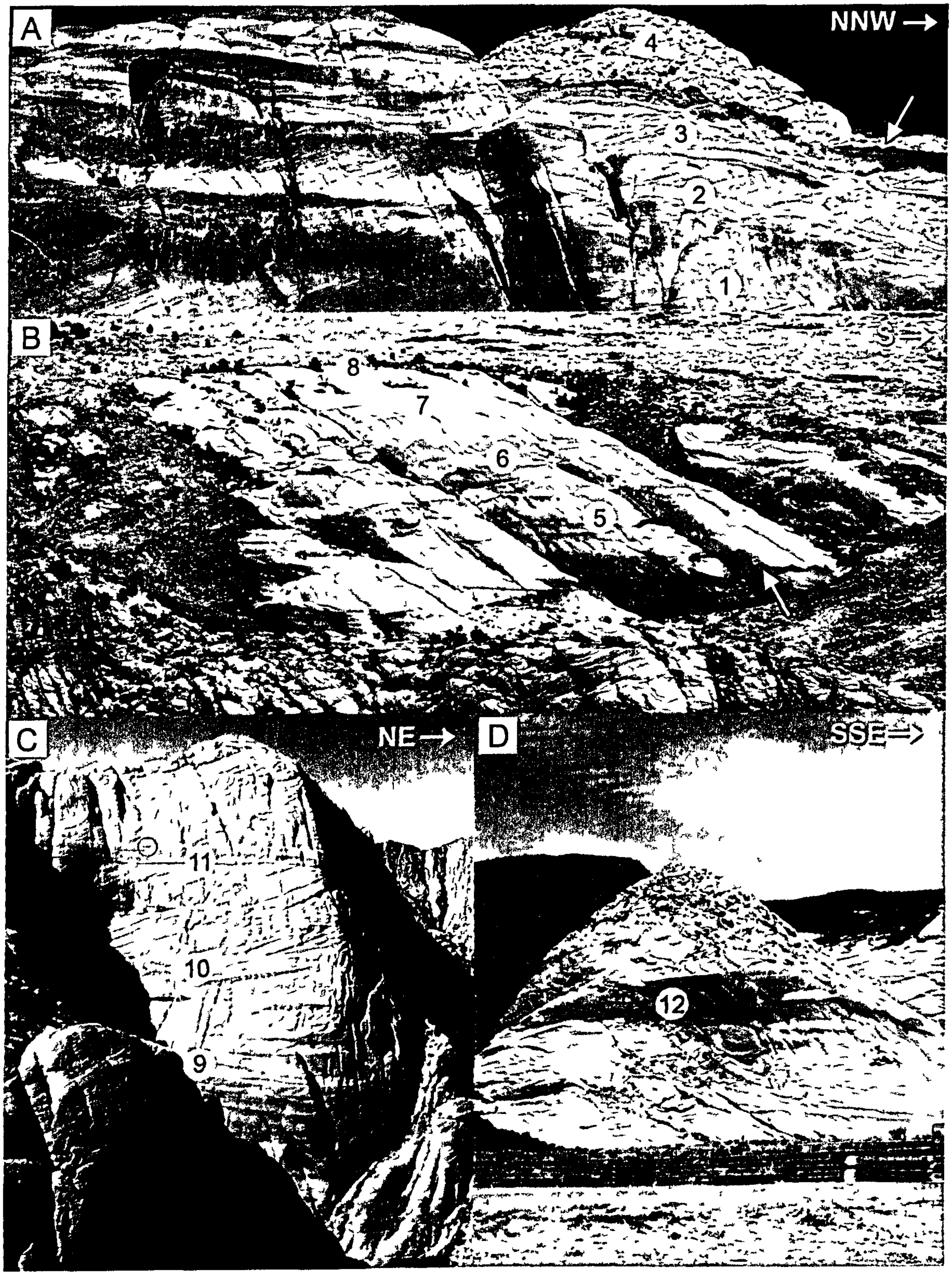
A
NNW →
4
3
2
1
B
S →
8
7
6
5
C
NE →
11
10
9
D
SSE ⇒
12

may contribute to this pattern: changes in primary bedding fabric and the vertical superimposition of laterally contiguous facies.

Changes in primary bedding fabric may influence bleaching when they are associated with variations in permeability. Grainflow strata typically have higher permeability than other eolian bedding types (Lindquist, 1988; Net, 2003), and bleaching fluids may preferentially follow these high permeability zones (see Nielsen et al., 2009, their Fig. 3.2). Nielsen et al. (2009) show that the prevalence of grainflow stratification in the Navajo Sandstone at Snow Canyon SP (as well as Zion NP) increases moving stratigraphically upward within the formation. This upward trend, perhaps in combination with other factors such as fluid buoyancy and the relative impermeability of strata that overly the Navajo Sandstone, may contribute to the preferential concentration of bleached rock in the upper part of the formation and localization of bleaching in the middle part of the formation (see discussion in Nielsen et al., 2009).

Assuming that most bands and fingers of bleached rock within the red/white intermixed facies of the central park are interconnected with the main bleached zone in the northern park, the common presence of similar bleaching features immediately below the main bleached boundary (Fig. 3.19) suggests the possibility that laterally adjacent diagenetic facies at Snow Canyon SP can be superimposed in vertical section. This is loosely akin to the spatial relationships of Walther's Law, where sedimentary facies that lie conformably on top of one another in vertical section are implied to have been produced by the oblique climb of laterally adjacent depositional environments (Fig. 3.20A; Middleton, 1973). In a similar manner, bands of bleached rock that occur beneath the main bleached zone in vertical section at Snow Canyon SP may represent alteration

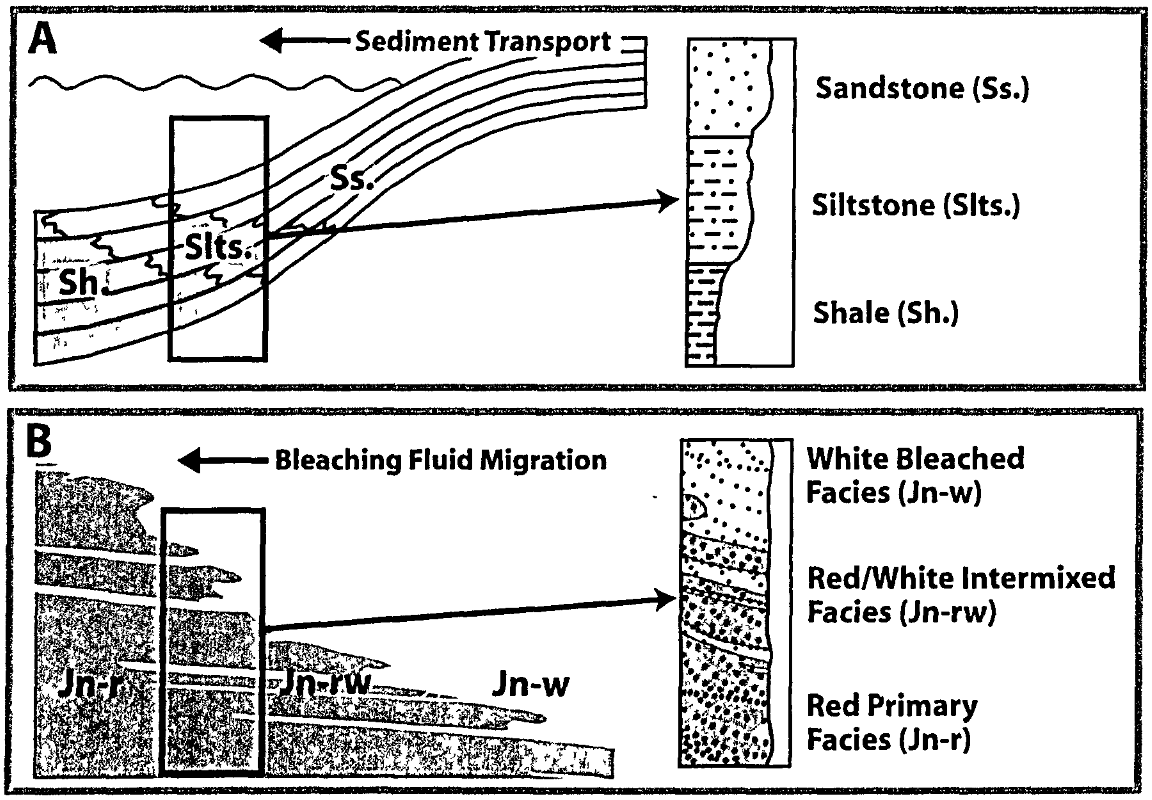

Figure 3.20
Diagrams compare the superimposition of laterally adjacent facies in both sedimentary and diagenetic settings. (A) Progradation of marginal marine sediments causes sedimentary facies to occur on top of one another in vertical section (this relationship is referred to as Walther's Law). (B) Proposed model for the superimposition of diagenetic facies along an inclined diagenetic reaction front boundary. Note the similar sequence of facies and bleaching features that occurs in both horizontal and vertical section (red primary facies, red/white intermixed facies, and then white bleached facies). Vertical transitions in bleaching style can also result from other processes (e.g., changes in primary bedding fabric, etc.).

that occurred some horizontal distance (10's of m to km) away from the main reaction front (Fig. 3.20B). This relationship is exemplified where the lower boundary of the bleached white facies climbs steeply and completely bleached rock from above the boundary overlies bleached bands that likely interconnect horizontally with the same boundary at a point farther to the north (e.g., Fig., 3.5). Although some parallels with Walther's Law may exist (Fig. 20), there are clearly fundamental differences between diagenetic and sedimentary facies. Whereas sedimentary facies are deposited sequentially from bottom to top, diagenetic facies may overlap in both time (bleaching may occur at different stratigraphic positions simultaneously) and space (bleached features can represent the cumulative product of multiple episodes of alteration). Because of these complexities, the relative importance of sedimentary and diagenetic processes in producing the apparent repetition of facies at Snow Canyon SP still warrants further study.

Direction of Bleaching Fluid Migration

Areas of white rock in the Navajo Sandstone of Snow Canyon SP are interpreted as primary red rock that has subsequently been "bleached" by geochemical processes. The interpretation of red as the primary or earliest sandstone color is based mainly on the spatial distribution of bleaching within the formation. White sandstone in the southern park occurs mostly within high-permeability pathways such as bedsets dominated by grainflow strata (medium-grained sandstone), whereas lower permeability wind ripple strata (fine- to very fine-grained sandstone) are commonly red (see example in Nielsen et al., 2009, Fig. 3.2). It is unlikely that iron-bearing fluids would precipitate iron oxide within these low-permeability strata without cementation also occurring within the higher permeability zones. In fact, concentrated cementation within the brown ferruginous facies commonly follows such high permeability features (Chapter 4). It is therefore most probable that the iron oxide grain coats that produce reddish coloration were originally ubiquitous throughout the Navajo Sandstone at Snow Canyon SP and areas of white rock were produced during a later diagenetic stage, probably through contact with chemically reducing fluids (Chan et al., 2000; Parry et al., 2004; Eichhubl et al., 2004; Beitler et al., 2005). Thus, the red/white intermixed facies at Snow Canyon SP likely represents a complex and extensive reaction front between chemically oxidizing and reducing zones in the subsurface (Beitler et al., 2005). The origin and nature of paleofluids that produced bleaching at Snow Canyon SP is presently unknown (only one location has been found thus far where bleaching fluids may have locally migrated upward along a joint or fault at Snow Canyon SP and the vertical extent of migration is unknown).

Although the primary direction of bleaching fluid migration has not been precisely determined, several observations suggest it was toward the south or southwest, likely migrating upward along gently inclined eolian interdune bounding surfaces. First, most bleached bands appear to originate near the boundary of the main bleached zone in the central park and extend southward (Fig. 3.17A). Local areas of bleached rock that cannot be traced directly northward to the main bleached zone may have originated more to the northeast where the Navajo Sandstone has been removed by the down-cutting of main Snow Canyon. Second, bleached bands most commonly terminate in a roughly southward direction (Fig. 3.21A). Although apparent bleaching band terminations are not always a reliable indicator of the extent of bleaching when viewed in two dimensions,

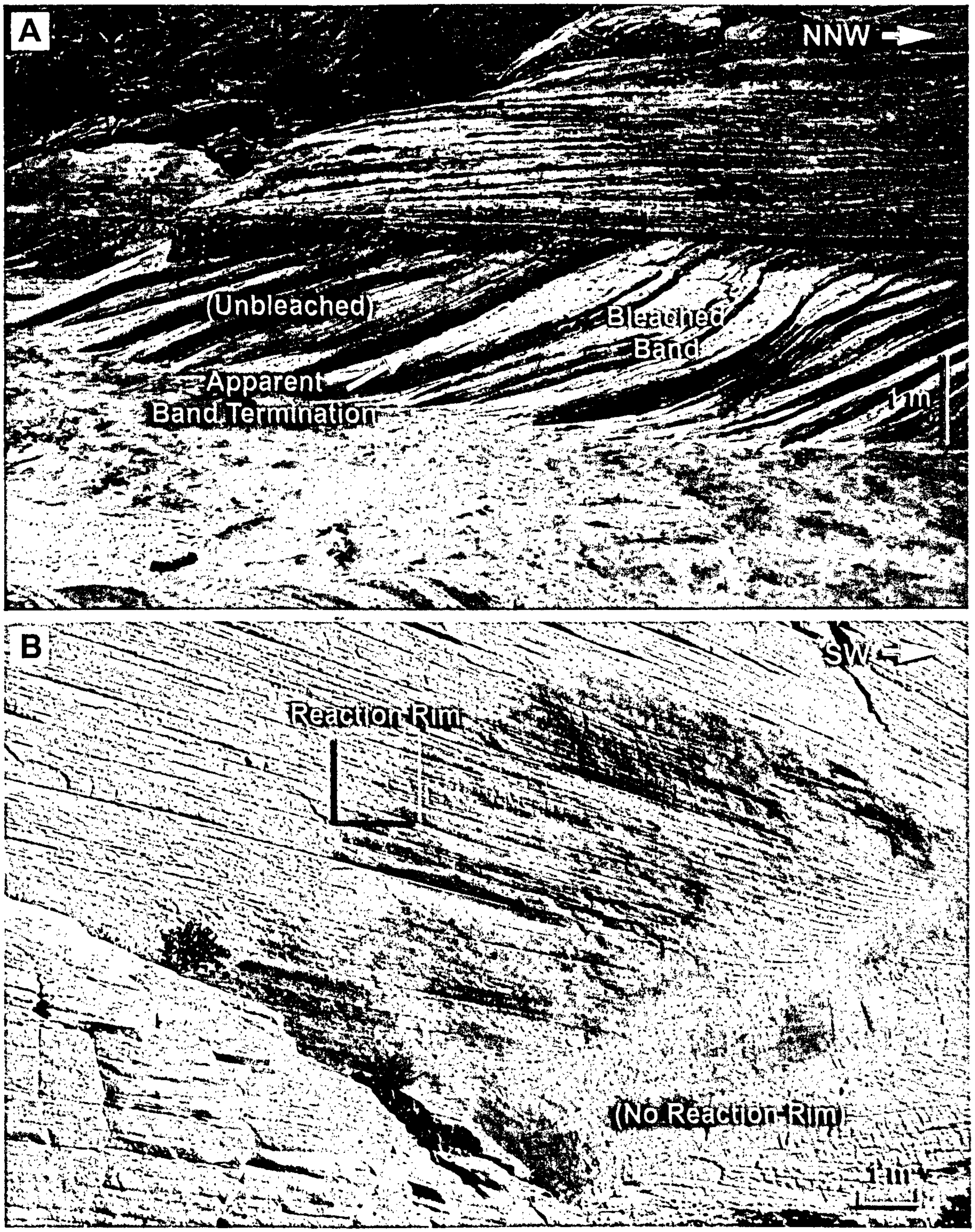

Figure 3.21
Apparent bleached band termination (A) near West Canyon (Fig. 3.4). The main bleached zone is to the right. (B) Narrow "infiltration rim" (width ~20 to 30 cm [8 to 12 in]) of transitional orange rock (boxed) occurs along the boundary between bleached and unbleached sandstone (Fig. 3.4, location 11; Fig. 3.17B). The main bleached zone is to the left.

preliminary three-dimensional analysis of these features using GIS software and field examination of outcrops also suggests that fluids generally penetrated to the southwest. Third, "reaction rims" (light-colored transitional boundaries between bleached and unbleached rock) are typically best developed along the south-facing edges of bleached fingers of rock at Snow Canyon (Fig. 3.21B). The use of reaction rims as a paleofluid flow direction indicators should be viewed as tentative because they were not systematically studied and it is unknown whether they are produced at the time of original bleaching or by subsequent fluid alteration events.

Relative Timing of Bleaching

Spatial relationships between structural features and bleached rock provide clues about the possible timing of bleaching in the Snow Canyon SP area. Bands of bleached rock are cross-cut by high-density vertical joints (Fig. 3.7), indicating that bleaching occurred prior to Basin and Range extension (middle Tertiary). In addition, the boundary between bleached rock in the upper Navajo Sandstone and primary red rock in the lower Navajo Sandstone is cross-cut by the Padre Canyon lineament (Figs. 3.4 and 3.5). This lineament parallels the Snow Canyon lineament (Fig. 3.4) which is observed to be associated with shear (or cataclastic) deformation bands (Mollema and Antonellini, 1996; Davis, 1999) and striated slickenside surfaces that indicate lateral, subhorizontal offset (Fig. 3.6C). Because the formation of shear bands reduces sandstone permeability by up to several orders of magnitude once they have progressed past their initial dilation stage (Antonellini and Aydin, 1994; Davis, 1999; Parry et al., 2004), deformation band shear zones that have not been breached by joints generally act as barriers to fluid transmission (Hurlow, 1998; Eichhubl et al., 2004; Tindall, 2006). It is presently unknown whether the Padre Canyon lineament is an impedance boundary or a fluid conduit. However, in either case, the lack of noticeable change in bleaching patterns moving across this feature (Fig. 3.5) implies that bleaching preceded development of the lineament.

The similarity in trend between the lower boundary of bleaching and the regional tilt of strata at Snow Canyon SP suggests that bleaching also preceded formation of the St. George syncline. Both the lineament and syncline are postulated to be Sevier-age features (Willis and Higgins, 1996), implying that bleaching preceded the development of deformation features in the region, likely during the Late Cretaceous to early Tertiary. This is consistent with timing estimates for the precipitation of concentrated iron oxide cement (brown ferruginous facies), which appears to locally overprint bleached rock (e.g., Fig. 3.22), and may have also preceded structural deformation (see Chapter 4). The estimated timing of bleaching at Snow Canyon SP is somewhat earlier than timing estimates for other bleached areas in the surrounding region (Beitler et al., 2003; Eichhubl et al., 2004). Variations in the timing and nature of diagenetic alteration between these localities (see discussion below) may be a function of local tectonics, different fluids, reservoir partitions, and other factors. The proposed timing of widespread bleaching at Snow Canyon SP remains tentative because the ages of structural features are poorly constrained and good exposures of cross-cutting relationships are rare.

Figure 3.22
Apparent overprinting of the red/white intermixed facies by the upper boundary of the brown ferruginous facies (left arrow) near Three Ponds (Fig. 4.4). Concentrated iron oxide cementation along the upper boundary of the brown ferruginous facies appears to have slightly darkened the underlying red and white sandstone. The boundary dips to the northeast and also occurs below the base of bleaching in the central part of the park (right arrow).

Diagenetic Architecture of the "Redox Transition Zone"

The red/white facies in the central park forms a laterally extensive transition zone between bleached and unbleached facies. This zone includes a variety of bleached features that provide information on the duration of the bleaching process and relative distance from the main reaction front boundary. These features are described in order of size from subtle variations visible only in outcrop to larger-scale features visible in aerial photographs. Minor alteration by fluids typically results in sandstone with a mottled appearance (Fig. 3.23A). In cases where fluids preferentially follow mm-scale laminae, pin-striped alteration can occur (Fig. 3.23B). As chemical reduction continues, local areas of sandstone may be bleached white whereas surrounding rock remains relatively unaltered. These bleached areas typically correspond to high permeability zones related to primary sandstone fabric. In the Navajo Sandstone, the highest permeability is typically within laterally extensive cross-bed sets that are dominated by grainflow stratification. These bedsets have a sheet-like geometry, and when bleached they have a banded appearance in outcrop (Fig. 3.24). Because bands in a given outcrop are viewed in two dimensions only, apparent terminations (Fig. 3.21A) may not indicate the actual extent of bleaching, but instead typically occur where the margin of a bleached rock moves out of the plane of view in an outcrop.

It is postulated that with continued chemical reduction, progressively lower permeability sandstone is altered, producing an increasingly complex network of interconnected bleaching features, with the final result being light-colored sandstone in which nearly all of the previously precipitated iron oxide grain coats were removed (white bleached facies). Because fluid flow rates through low permeability laminae such

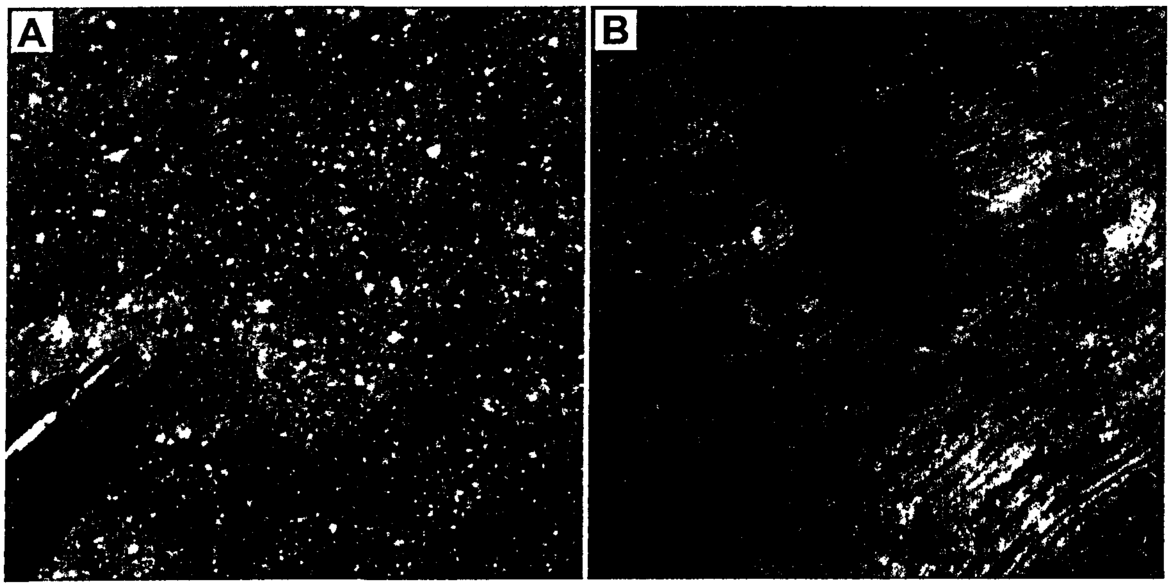

Figure 3.23
Small-scale features produced by minor alteration of primary sandstone. (A) "Mottled discoloration." (B) "Pinstripe alteration."

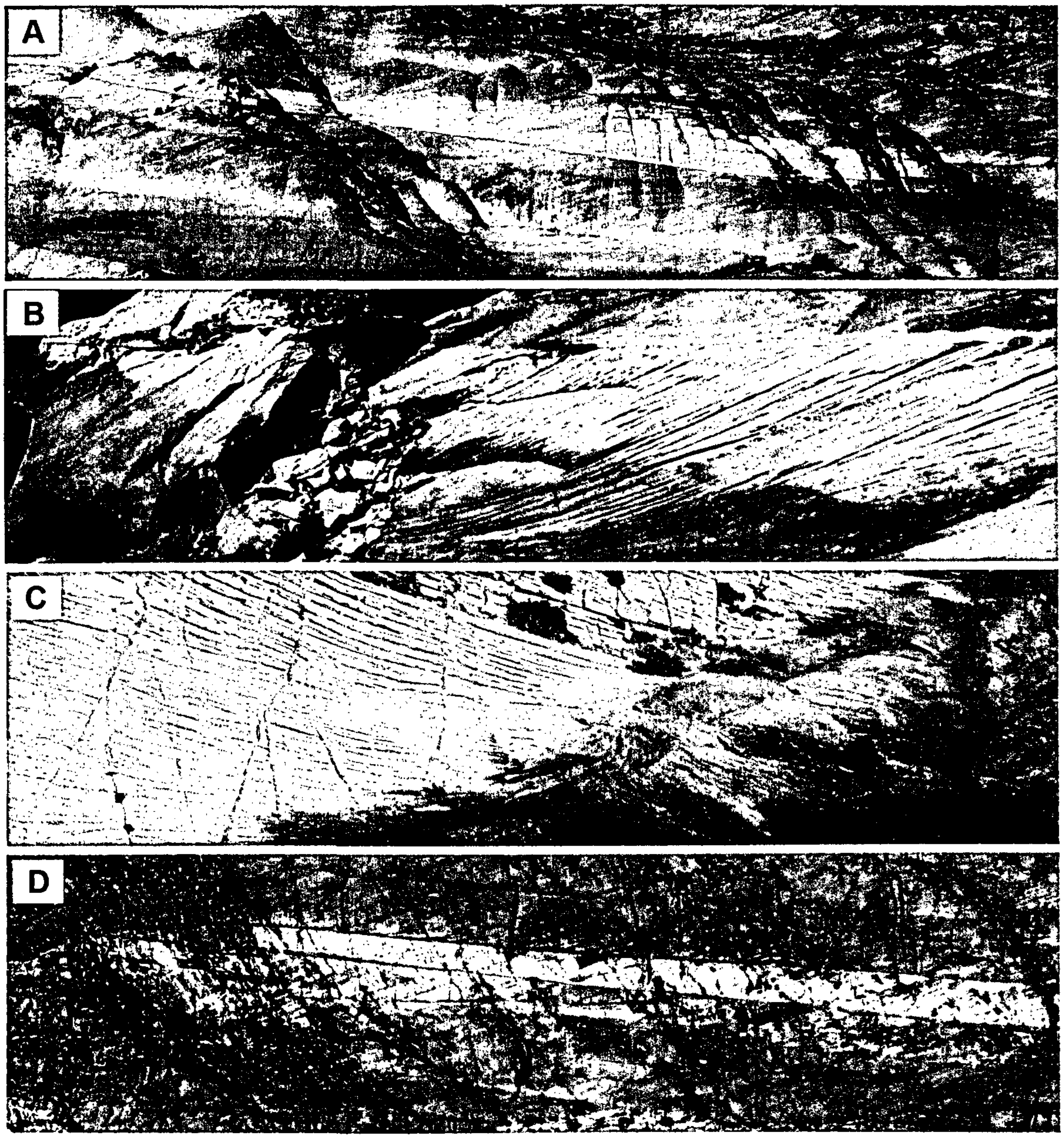

Figure 3.24
Bleached band geometries in eolian sandstone reflect permeability patterns within the cross-bed sets as well as the direction of fluid flow relative to foreset dip. (A) "basal bleached band," (B) "apical bleached band," (C) "zigzag bleached band," and (D) "constricted bleached band."

as wind ripple strata are low, and the reduction and removal of iron oxide requires large volumes of fluid (Parry et al., 2004; Nielsen et al., 2009), the complete bleaching of both high and low permeability strata over an entire km-scale zone implies a sustained chemical reduction process (Nielsen et al., 2009). Although evidence of previous bleaching stages is erased within large bleached zones, horizontal and vertical bleaching patterns along the margins provide clues about the earlier alteration processes that likely occurred. It is the presence of these marginal bleaching patterns at Snow Canyon that make it an excellent outcrop analog for understanding how sedimentary fabric impacts the early migration of hydrocarbons or other fluids through carrier beds in a reservoir system.

Regional Comparisons of Bleached Facies

Bleaching of the upper Navajo Sandstone in Snow Canyon SP and the surrounding area marks the westernmost extent of exposed zonal bleaching in the state of Utah mapped by Beitler et al. (2003, Fig. 3.4). However, outcrops of the white bleached facies do extend eastward for about 30 km (18 mi) through the Red Cliffs Desert Reserve to near the Hurricane fault and may correlate with bleaching in the Zion NP area (erosion associated with the fault prevents direct correlation). In comparison with the sharply defined boundaries between bleached and unbleached rock at Snow Canyon SP, boundaries at Zion NP tend to be more gradational in nature and nearly horizontal (Nielsen et al., 2009, Fig. 3.9A). Well-defined bleached bands like those that dominate the southern part of Snow Canyon SP are uncommon in the main canyon area of Zion NP but do occur locally in the northern park. One possible explanation for these differences is that Snow Canyon SP may represent the margin of a regional bleached zone (where bleaching fluids penetrate laterally outward into unbleached rock), whereas main Zion Canyon may represent the interior of a bleached zone (where iron oxide has been completely removed from both high and low permeability facies by sustained fluid alteration).

Comparisons can also be made between bleached units at Snow Canyon SP and those mapped by Eichhubl et al. (2004) in the Jurassic Aztec Sandstone of Valley of Fire SP (110 km [70 mi] to the southwest). Similar to Snow Canyon, the horizontal color transition at Valley of Fire SP results largely from the regional dip of bedding (~22 NE), with red-colored sandstone occupying the lowest stratigraphic position. However, white, completely bleached rock is comparatively rare at Valley of Fire SP, being restricted to narrow (< 50 m [164 ft]), subhorizontal zones that are typically surrounded by other facies (Eichhubl et al., 2004, their Fig. 3.6). Uniform, red-colored sandstone near the top of the formation at Valley of Fire SP lacks a parallel in the Snow Canyon area. Coloration units at Valley of Fire SP are commonly offset by faults and other features (Eichhubl et al., 2004, Fig. 3.5) and the influence of structural controls is more pronounced than at Snow Canyon SP. These comparisons underscore the complex nature of diagenetic processes and show the importance of mapping and other spatial analysis techniques in accurately interpreting diagenetic features.

Conclusions

Detailed mapping and analysis of diagenetic alteration patterns in the Navajo Sandstone in the Snow Canyon SP area indicate complex interactions between sedimentary, structural, and diagenetic processes. Specific conclusions of this study include the following:

1. Diagenetic coloration facies and subfacies at Snow Canyon SP are spatially extensive, mappable, and represent at least four distinct episodes of alteration: formation of primary grain coats (primary red facies), localized bleaching and removal of primary grain coats (white bleached facies), precipitation of dark-colored iron oxides in the lower formation (brown ferruginous facies), and precipitation of brightly colored secondary iron oxide near joints in the upper formation (multicolored local facies).
2. The dominance of bleached rock in the northern area of Snow Canyon SP, and its relative absence in the southern park, is attributed to a combination of three factors: structural tilt, slope of the canyon floor, and a horizontal shift in bleaching types produced by the lateral migration of fluids. Diagenetic facies successions in vertical outcrop parallel those that occur horizontally.
3. Overprinting of partially bleached rock by the upper boundary of the brown ferruginous facies indicates that bleaching either preceded or was coincident with concentrated iron oxide cementation.
4. Spatial relationships with structural features (joints, deformation band shear zones, folds, etc.) tentatively suggest that bleaching preceded the development of deformation features during the Late Cretaceous to early Tertiary (Sevier orogeny).

In summary, well-exposed diagenetic coloration patterns and facies of the Navajo Sandstone have significant geologic implications for understanding the processes of iron oxide bleaching and transport in the subsurface. The Navajo Sandstone is both an important reservoir and aquifer unit and comprises a valuable diagenetic model for other porous sandstones units of the Western Interior.

Acknowledgements

This study was funded by the Utah Geological Survey under the "Characterization of Utah's Natural Gas Reservoirs and Potential New Reserves" initiative. We are grateful for this funding as well as the helpful assistance of Tom Chidsey, Craig Morgan, and others at the Utah Geological Survey with the project. We are also grateful to Kristin Comella and the other staff and volunteers at Snow Canyon State Park who provided research access and gave advice on how to best access specific field areas.

References

Alder, D.D., and Brooks, K.F., 1996, A history of Washington County: from isolation to destination: Salt Lake City, Utah, Utah State Historical Society, 418 p.

Antonellini, M.A., and Aydin, A., 1994, Effect of faulting on fluid flow in porous sandstones: Petrophysical properties: American Association of Petroleum Geologists Bulletin, v. 78, p. 355– 377.

Beitler, B., Parry, W.T., and Chan, M.A., 2003, Bleaching of Jurassic Navajo Sandstone on Colorado Plateau Laramide highs: Evidence of exhumed hydrocarbon supergiants?: Geology, v. 31, p. 1041–1044.

Beitler, B., Parry, W.T., and Chan, M.A., 2005, Fingerprints of fluid flow – chemical diagenetic history of the Jurassic Navajo Sandstone, southern Utah, U.S.A.: Journal of Sedimentary Research, v. 75, 547-561.

Biek, R.F., 2003, Geology of Quail Creek State Park, Utah, *in* Sprinkel, D.A., Chidsey, T.C., Jr., and Anderson, P.B., eds., Geology of Utah's Parks and Monuments: Utah Geological Association Publication 28, p. 465-477.

Biek, R.F., Willis, G.C., Hylland, M.D., and Doelling, H.H., 2003, Geology of Zion National Park, Utah, *in* Sprinkel, D.A., Chidsey, T.C., Jr., and Anderson, P.B., eds., Geology of Utah's Parks and Monuments: Utah Geological Association Publication 28, p. 107-135.

Bjerrum, C.J., and Dorsey R.J., 1995, Tectonic controls on deposition of Middle Jurassic strata in a retroarc foreland basin, Utah-Idaho trough, western interior, United States: Tectonics, v.14, p. 962-978.

Blakey, R.C., Peterson, F., Caputo, M.V., Geesaman, R.C., and Voorhees, B.J., 1983, Paleogeography of Middle Jurassic continental, shoreline, and shallow marine sedimentation, southern Utah, *in* Reynolds, M.W., and Dolly, E.D., eds., Mesozoic Paleogeography of West-Central United States: Rocky Mountain Section, Society of Economic Paleontologists and Mineralogists, Rocky Mountain Paleogeography Symposium 2, p. 77-100.

Blakey, R.C., Peterson, F., and Kocurek, G., 1988, Synthesis of Late Paleozoic and Mesozoic eolian deposits of the western interior of the United States, *in* Kocurek, Gary, eds., Late Paleozoic and Mesozoic eolian deposits of the Western Interior of the United States: Sedimentary Geology, v. 56, p. 3-125.

Blakey, R.C., 1994, Paleogeographic and tectonic controls on some Lower and Middle Jurassic erg deposits, Colorado Plateau, *in*, Caputo, M.V., Peterson, J.A., and Franczyk, K.J., eds., Mesozoic systems of the Rocky Mountain region, USA: Denver, Colorado, Rocky Mountain Section of the Society for Sedimentary Geology, p. 273-298.

Chan, M.A., Parry, W.T., and Bowman, J.R., 2000, Diagenetic hematite and manganese oxides and fault-related fluid flow in Jurassic sandstones southeastern Utah: American Association of Petroleum Geologists Bulletin, v. 84, p. 1281-1310.

Cook, E.F., 1960, Geologic atlas of Utah—Washington County: Utah Geological and Mineralogical Survey Bulletin 70, scale 1:125,000, 119 p.text.

Cornell, R.M., and Schwertmann, U., 2003, The iron oxides - structure, properties, reactions, occurrences and uses – 2nd edition: Weinheim, Germany, Wiley-VCH, 573 p.

Davis, G.H., 1999, Structural geology of the Colorado Plateau region of southern Utah with special emphasis on deformation bands: Geological Society of America Special Paper 342, 167 p.

Eichhubl, P., Taylor, W.L., Pollard, D.D., and Aydin, A., 2004, Paleo-fluid flow and deformation in the Aztec Sandstone at the Valley of Fire, Nevada –evidence for the coupling of hydrogeologic, diagenetic, and tectonic processes: Geological Society of America Bulletin, v. 16, no. 9, p. 1120-1136.

Higgins, J.M., 2003, Geology of Snow Canyon State Park, Utah, *in* Sprinkel, D.A., Chidsey, T.C., Jr. and Anderson, P.B., eds., Geology of Utah's parks and monuments: Utah Geological Association Publication 28, p. 479-494.

Hintze, L.F., 2005, Utah's spectacular geology – How it came to be: Provo, Utah, Brigham Young University Press, 203 p.

Hurlow, H.A., 1998, The geology of the central Virgin River Basin, southwestern Utah, and its relation to ground-water conditions: Utah Geological Survey, Water Resources Bulletin 26, 53 p., 6 plates.

Kocurek, G., 1988, First-order and super bounding surfaces in eolian sequences – Bounding surfaces revisited: Sedimentary Geology, v. 56, p. 193-206.

Kocurek, G., 1996, Desert aeolian systems, *in* Reading, H.G., ed., Sedimentary environments – processes, facies and stratigraphy: Blackwell, Oxford, Third Edition, p. 125-153.

Kocurek, G., and Dott, R.H., Jr., 1983, Jurassic paleogeography and paleoclimate of the central and south Rocky Mountains region, *in* Reynolds, M.W., and Dolly, E.D., eds., Mesozoic paleogeography of west-central United States: Rocky Mountain Section, Society of Economic Paleontologists and Mineralogists, Rocky Mountain Paleogeography Symposium 2, p. 101-116.

Kowallis, B.J., Christiansen, E.H., Deino, A.L., Zhang, C., and Everett, B.H., 2001, The record of Middle Jurassic volcanism in the Carmel and Temple Cap Formations of southwestern Utah: Geological Society of America Bulletin, v. 113, no. 3, p. 373-387.

Lageson, D.R., and Schmitt, J.G., 1994, The Sevier orogenic belt of the western United States: recent advances in understanding its structural and sedimentologic framework, *in*, Caputo, M.V., Peterson, J.A., and Franczyk, K.J., eds., Mesozoic systems of the Rocky Mountain region, USA: Denver, Colorado, Rocky Mountain Section of the Society for Sedimentary Geology, p. 27-64.

Lawton, T.F., 1994, Tectonic setting of Mesozoic sedimentary basins, Rocky Mountain region, United States, *in*, Caputo, M.V., Peterson, J.A., and Franczyk, K.J., eds., Mesozoic systems of the Rocky Mountain region, USA: Denver, Colorado, Rocky Mountain Section of the Society for Sedimentary Geology, p. 1-26.

Lindquist, S.J., 1988, Practical characterization of eolian reservoirs for development: Nugget Sandstone, Utah-Wyoming thrust belt: Sedimentary Geology, v. 56, p. 315-339.

Lund, W.R., Hozik, M.J., and Hatfield, S.J., 2007, Paleoseismic investigation and long-term slip history of the Hurricane fault in southwestern Utah: Utah Geological Survey Special Study 119, 81 p.

Luttrell, P.R., 1993, Basinwide sedimentation and the continuum of paleoflow in an ancient river system; Kayenta Formation (Lower Jurassic), central portion Colorado Plateau: Sedimentary Geology, v. 85, p. 411-434.

Marzolf, J.E., 1988, Controls on late Paleozoic and early Mesozoic eolian deposition of the western United States: Sedimentary Geology, v. 56, p. 167-191.

McKee, E.H., Blank, H.R., and Rowley, P.D., 1995, Potassium-argon ages of Tertiary igneous rocks in the eastern Bull Valley Mountains and Pine Valley Mountains, southwestern Utah, *in* Maldonado, F. and Nealey, L.D., eds., Geologic studies in the Basin and Range-Colorado Plateau transition in southeastern Nevada, southwestern Utah, and northwestern Arizona: U.S. Geological Survey Bulletin 2153, p. 241-252.

Middleton, G.V., 1973, Johannes Walther's Law of the correlation of facies: Geological Society of America Bulletin, v. 84, p. 979-988.

McKee, E.D., 1979, Ancient sandstones considered to be eolian, *in* McKee, E.D., ed., A study of global sand seas: U.S. Geological Survey Professional Paper 1052, p. 187-238.

Mollema, P.N., and Antonellini, M.A., 1996, Compaction bands: A structural analog for anti- mode I cracks in aeolian sandstone: Tectonophysics, v. 267, p. 209–228.

Myers, R.D., and Aydin, A., 2004, The evolution of faults formed by shearing across joint zones in sandstone: Journal of Structural Geology, v. 26, p. 947–966.

Net, L.I, 2003, Diagenesis and reservoir quality of the Eolian Nugget / Navajo Sandstone (Early Jurassic), Utah and Wyoming [Ph.D. thesis]: Austin, University of Texas, 182 p.

Nielsen, G.B., Chan, M.A., and Petersen, E.U., 2009, Diagenetic coloration facies and alteration history of the Jurassic Navajo Sandstone, Zion National Park and vicinity, southwestern Utah *in* Tripp, B.T., Krahulec, K, and Jordan, J.L., editors, Geology and geologic resources and issues of western Utah, Utah Geological Association Publication 38, p. 67-96.

Nielsen, G.B., and Chan, M.A., 2010, Geologic map and coloration facies of the Jurassic Navajo Sandstone, Snow Canyon State Park and areas of Red Cliffs Desert Reserve, Washington County, Utah: Utah Geological Survey Open-File Report 561, scale 1:10,000, 17 p. text.

Parry, W.T., Chan, M.A., and Beitler, B., 2004, Chemical bleaching indicates episodes of fluid flow in deformation bands in sandstone: American Association of Petroleum Geologists Bulletin, v. 88, p. 1-17.

Parrish, J.T., 1993, Mesozoic climates of the Colorado Plateau, *in* Morales, M., ed., Aspects of Mesozoic geology and paleontology of the Colorado Plateau, Museum of Northern Arizona Bulletin 59, p. 1-11.

Peterson, F., 1988, Pennsylvanian to Jurassic eolian transportation systems in the western United States, *in* Kocurek, G., ed., Late Paleozoic and Mesozoic eolian deposits of the Western Interior of the United States: Sedimentary Geology, v. 56, p. 207-260

Peterson, F., 1994, Sand dunes, sabkhas, streams, and shallow seas: Jurassic paleogeography in the southern part of the Western Interior basin, *in* Caputo, M.V., Peterson, J.A., and Franczyk, K.J., eds., Mesozoic systems of the Rocky Mountain region, USA: Denver, Colorado, Rocky Mountain Section of the Society for Sedimentary Geology, p. 233-272.

Pipiringos, G.N., and O'Sullivan, R.G., 1978, Principle unconformities in Triassic and Jurassic rocks, western interior U.S.A., preliminary report: U.S. Geological Survey Professional Paper 1035-A, 29 p.

Riggs, N.R., and Blakey, R.C., 1993, Early and Middle Jurassic paleogeography and volcanology of Arizona and adjacent areas, *in* Dunne, G.C., and McDougall, K.A., eds., Mesozoic paleogeography of the western United States–II: Tulsa, Oklahoma, Society for Sedimentary Geology, p. 347-373.

Rogers, C.M., Myers, D.A., and Engelder, Terry, 2004, Kinematic implications of joint zones and isolated joints in the Navajo Sandstone at Zion National Park, Utah – evidence for Cordilleran relaxation: Tectonics, v. 23., no. 1, 16 p.

Sansom, P.J., 1992, Sedimentology of the Navajo Sandstone, southern Utah, USA [Ph.D. thesis]: England, Department of Earth Sciences at Wolfson College, 291 p.

Stokes, W.L., 1986, Geology of Utah: Salt Lake City, Utah Museum of Natural History Occasional Paper 6, 280 p.

Tindall, S.E., 2006, Jointed deformation bands may not compartmentalize reservoirs: American Association of Petroleum Geologists Bulletin, v. 90, p. 177-192.

Walker, T.R., 1979, Red color in dune sand, *in* McKee, E.D., ed., A study of global sand seas: U.S. Geological Survey Professional Paper 1052, p. 61-68.

Willis, G.C., 1999, The Utah thrust system – an overview, *in* Spangler, L.E., and Allen, J.J., eds., Geology of northern Utah and vicinity: Utah Geological Association Publication 27, p. 1-9.

Willis, G.C., and Higgins, J.M., 1996, Interim geologic map of the Santa Clara quadrangle, Washington Co., Utah: Utah Geological Survey Open-File Report 339, scale 1:24,000, 87 p. text.

CHAPTER 4

CONCENTRATED IRON-OXIDE HORIZONS IN THE JURASSIC NAVAJO SANDSTONE, SOUTHWESTERN UTAH: PRECIPITATION MECHANISMS AND IMPACT ON RESERVOIR QUALITY

Abstract

Dense concentrations of concretionary iron oxide cement (up to 30% by weight) precipitated as discontinuous subhorizontal horizons along the top of a regionally extensive (more than 150 km^2) iron enrichment zone in the lower part of the Jurassic Navajo Sandstone of the southwest Utah region. Petrographic analysis indicates that pore-filling iron oxide cements overprinted primary hematite grain coats. Relationships with structural features indicate that concentrated cementation preceded the regional development of joints during Basin and Range extension. The broad lateral extent and local diagenetic features associated with the boundary suggest that most precipitation occurred along a regionally extensive reaction front between vertically superimposed reducing and oxic zones in the subsurface.

Iron-oxide cemented sandstones are classified by cement type and iron oxide concentration. Growth of cementation features (concretions, bands, etc.) is dependent upon iron supply, host rock texture, favorable nucleation, and other conditions. With

sustained precipitation, amalgamation of small-scale (mm-cm+) features forms medium-scale (m+) sheets that may coalesce to disrupt reservoir continuity. Precipitation locally follows previously high-permeability bedding features such as grainflow deposits that, upon cementation, become barriers to subsequent fluid flow ("permeability inversion"). The net result is discontinuous vertical permeability, ranging from 1000 mD+ for sparsely cemented sandstones to less than 1 mD for very dense "ironstones." These precipitation features have implications for interpreting mass transport processes in porous reservoir rocks. They may also be relevant to understanding groundwater fluctuation on Mars, where concretionary hematite cement occurs in sulfate-rich sediments.

Introduction

The effects of iron chemistry dominate the visual landscape of southwestern Utah, producing not only the well-known red rock scenery but also a variety of cementation features such as iron oxide concretions and cemented sheet geometries. Iron oxide cementation in the Jurassic Navajo Sandstone of the St. George, Utah area (Fig. 4.1) is widespread and commonly concentrates along discontinuous subhorizontal spatial horizons in the lower portion of the formation. Willis and Higgins (1996) suggest that these laterally extensive horizons may be related to an ancient water table, but this potential relationship remains to be established. Regional-scale concentrated iron oxide deposits have important implications for fluid flow pathways in this important aquifer and reservoir unit. This study examines these iron oxide deposits to: 1) determine the spatial extent of concentrated cementation, 2) characterize the diagenetic features present,

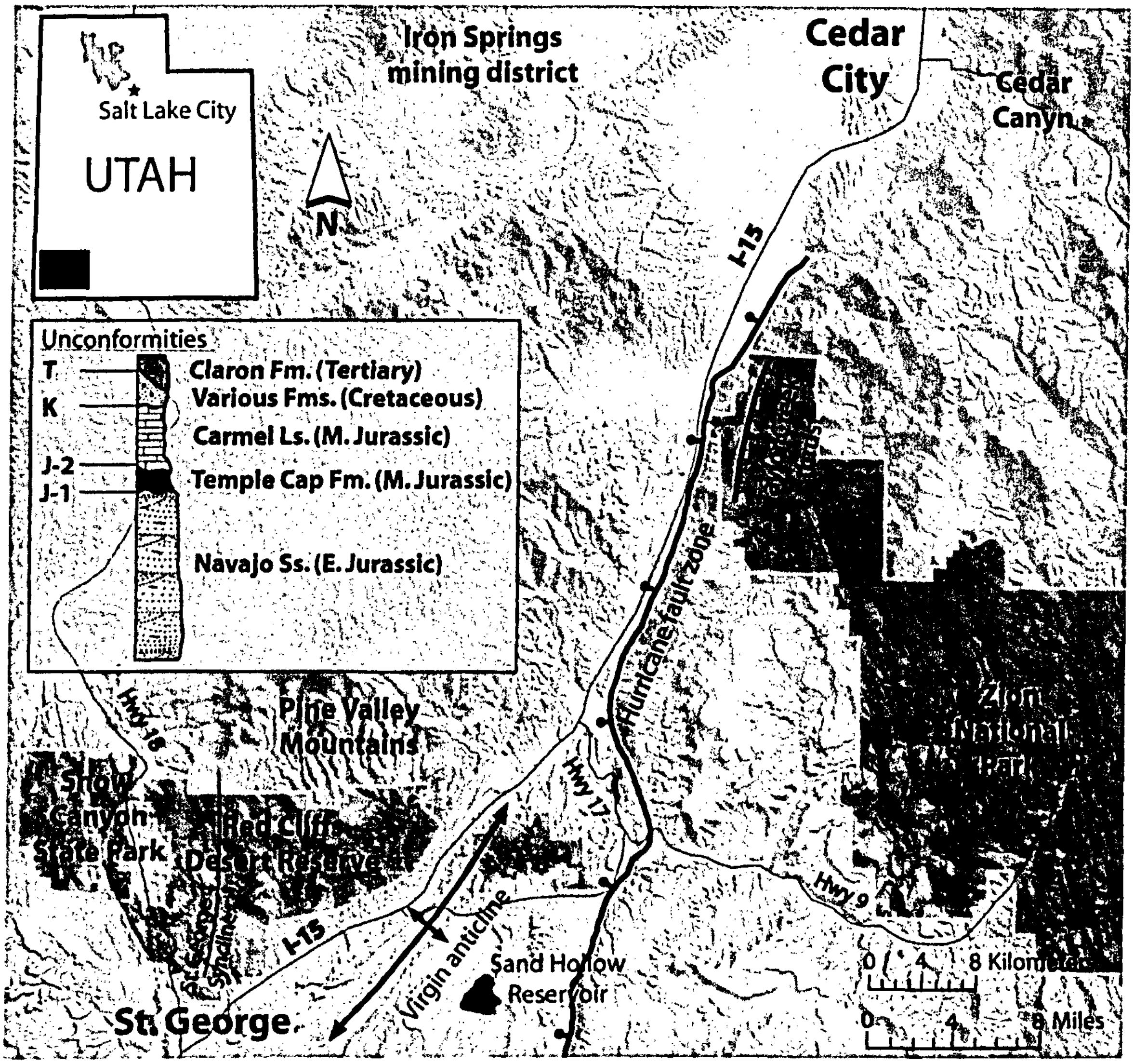

Figure 4.1
Location of study area in southwestern Utah showing selected structural features. Simplified stratigraphic column shows geological formations and regional unconformities that overly the Navajo Sandstone. Background image from the U.S. Geological Survey National Elevation Dataset (NED).

3) investigate geochemical mechanisms that produced cementation, and 4) evaluate the impact of concentrated cementation on reservoir quality.

Iron oxide and hydroxide cementation in the Navajo Sandstone is dominated by hematite (α-Fe_2O_3) and goethite (α-FeOOH), both of which are thermodynamically stable reaction series end-members (Cornell and Schwertmann, 2003). Resulting sandstones display colors in the longer wavelengths of the visible spectrum (red, yellow, brown, etc) with variations in hue produced by multiple factors including iron oxide concentration, crystal size and distribution, and isomorphic substitution of other metals into the lattice structure (Schwertman and Cornell, 2000). Where original iron oxide cement has been removed by secondary chemical processes, the resulting sandstone is commonly referred to as "bleached" (e.g., Lindquist, 1988; Chan et al., 2000; Parry et al., 2004; Beitler et. al., 2005). Diagenetic features associated with iron oxide cementation range from mm-scale spots, cm-scale concretions, and m+-scale sheets (Chan et al., 2000; Nielsen and Chan, 2009). In contrast to previous studies that explored these features on a microscopic and outcrop scales in southcentral and southeastern Utah (e.g., Chan et al., 2000; Chan et al., 2004; Potter, 2009), this study examines patterns of concentrated cementation on a regional scale over an ~1000 km^2 area in southwestern Utah.

Concentrated iron oxide cementation commonly occurs along subsurface chemical reaction fronts where oxidizing and reducing zones interact (Beitler et al., 2005). Precipitation of diagenetic hematite/goethite is documented within a broad variety of ancient and modern settings including springs (Britch et al., 2007), streams (Furniss et. al, 1999), lakes (Bowen et al., 2008), swamps (Yap, 1997), caves (Hill Polyak, 2005), subterranean estuaries (Spiteri et al., 2005; Charette and Sholkovitz, 2002), and perched aquifers (Zhang and Karathanasis, 1997). In some cases, concentrated cementation is interpreted as having occurred near the water table or capillary fringe (Breit, 2001; Temgoua et al., 2005; Widdowson, 2007). Hematitic horizons can also occur in soils as iron released by weathering is oxidized, producing iron-rich ferricrete (Cornell and Schwertmann, 2003; D'Amore et al., 2004). In addition to these terrestrial settings, abundant small hematite spherules have recently been discovered on the surface of Mars, and iron oxide concretions in the Navajo Sandstone are proposed as a terrestrial analog for these features (Christensen et al., 2001; Chan et al., 2004; Squyres et al., 2004; Chan et al., 2007; Golden et al., 2007).

The abundance, variety, and broad spatial distribution of iron oxide features in the St. George, Utah area make it an excellent location for evaluating both the mechanisms that produce cementation and its impact on reservoir quality. Precipitation of authigenic hematite and other cements locally reduces bedrock permeability and creates textural heterogeneities that can alter the architecture of a reservoir (Chapin, 1998; Net, 2003). As iron oxide cementation progresses, fluid migration pathways associated with primary depositional fabric can be modified and/or secondary pathways can be created. The location of present migration pathways can be difficult to predict as a result of the complex interaction between diagenetic, stratigraphic, and structural features (Lindquist, 1988). Because the Navajo Sandstone is an important reservoir system being actively explored for new hydrocarbon reserves (Moulton and Pinnell, 2005; Chidsey et al., 2007; Parry et al., 2009), the impact of extensive iron oxide cementation on reservoir permeability is an important consideration of this study.

Geologic Setting

The Navajo Sandstone of southwest Utah is a 600+ m thick succession of fine to medium-grained quartz arenite that displays prominent large-scale eolian cross-bed sets and a variety of coloration patterns produced by multiple episodes of diagenetic alteration. Because the study area occurs along the transition zone between the Basin and Range Province and Colorado Plateau, the Navajo Sandstone incorporates structural characteristics of both regions. Deformation reflects both regional compression associated with the Cretaceous to early Tertiary Sevier thrust system as well as Tertiary to Holocene Basin and Range extension (Davis, 1999; Willis, 1999; Biek, 2003; Biek et al., 2003; Higgins, 2003; Rogers et al., 2004; Lund et al., 2008). Features attributed to Sevier-age thrusting include the Taylor Creek thrust-fault zone in Zion National Park (Zion NP) and the St. George syncline near Snow Canyon State Park (Snow Canyon SP; Fig. 4.1). Features related to Basin and Range extension include the Hurricane fault (Fig. 4.1) and pervasive NW to NE trending vertical joints. Late Cenozoic downcutting by the Virgin River and its tributaries in southwest Utah has produced a network of canyons which provide three-dimensional exposures of the Jurassic Navajo Sandstone and associated Mesozoic strata.

Methods

Characterization of Iron Oxide Cements

Samples were collected throughout the study area (Fig. 4.1) and represent a broad diversity of iron oxide cementation features. Average weight percent for iron oxide cement and associated trace elements was measured using inductively coupled plasma mass spectrometry (ICP-MS) performed by a commercial laboratory (n=24). Hematite and goethite were differentiated based upon variability in the 0.85 to 0.95 μm range of continuum removed reflectance spectra (n=48) measured in the lab under artificial light conditions using a handheld analytical spectrometer (Hunt and Ashley, 1979; Clark and Roush, 1984; Morris et al., 1985; Cornell and Schwertmann, 2003; Bowen et al., 2007). Mass balance relationships were calculated using a combination of ICP-MS and porosity/permeability data (described below). Computerized geochemical modeling was performed using PHREEQC Interactive software developed by the U.S. Geological Survey (Parkhurst and Appelo, 1999).

The volume and spatial distribution of iron oxide cement around grains and within pore spaces was evaluated using point count analysis of 16 variably altered samples (1000 counts per thin section). Because cement coatings around grains are much narrower than the width of a standard thin section (~30 μm), the apparent thickness of grain coats varies substantially depending upon the angle at which they are sliced by the section. If oblique cuts are left uncorrected, this can result in an overestimate of cement volume (Halley, 1978). In order to reduce this error, point counts were made under high magnification (shallow depth of field) while focusing only on the upper surface of the sections.

Survey of Iron Oxide Cementation Features

Concentrated iron oxide horizons were identified in aerial photographs then traced in the field. Over 1000 georeferenced digital photographs were taken to document diagenetic characteristics associated with these horizons. Rock colors were coded from field samples using the standardized Munsell rock color system (Rock-Color Chart Committee, 1991). This system specifies colors based upon three dimensions: hue, value (brightness), and chroma (saturation). Trend surfaces for stratigraphic and structural boundaries were calculated using ESRI ArcMap. Data points were plotted (n=1494) using one meter color aerial photography from the National Agricultural Imagery Program (NAIP) and 10 m resolution elevation data from the National Elevation Dataset (NED). Prediction surfaces were calculated using geostatistical interpolation (ordinary kriging).

Porosity/Permeability Analysis

The impact of concentrated iron oxide cementation on sandstone permeability was evaluated by measuring the gas permeability of 32 surface plugs (2.5 cm diameter). Analysis was performed using a dual porosimeter/permeameter by a commercial laboratory. The orientation of each plug relative to bedding (parallel or perpendicular) was recorded as well as the dominant eolian stratification type (grainflow, wind ripple, etc. [Hunter, 1977; Kocurek and Dott, 1981]). In addition, ambient porosity, dry bulk density, and grain density were also measured/calculated for each plug by the same lab.

Results

Iron Oxide Concentration and Rock Color

Comparison of ICP-MS results with coded sandstone colors indicates that iron oxide concentration is loosely correlated with Munsell value (or "lightness"), with increasing cementation producing progressively darker colors (Table 4.1). Nomenclature

Table 4.1

Typical Munsell colors (Rock-Color Chart Committee, 1991)
for iron-enriched sandstones (n=24).

Class		Iron Oxide (defined range)	Munsell Colors (typical range)		
			Hue	Value (lightness)	Chroma (saturation)
Sandstone[1]		<0.5%	YR	6-8	2-6
Ferruginous Sandstone		0.5 – 9%	YR, R	4-6	4-6
Ironstone	sparse	10 – 14%	YR, R	2-4	2-6
	dense	≥15%	YR, R, N	1-2	1-2

Corresponding geochemistry in Table 2. Iron oxide concentration shows a close correspondence with Munsell "value" (lightness), but not with "hue" and "chroma." [1]The "sandstone" class includes both rock that lacks evidence of previous iron oxide cementation and "bleached" rock where original iron oxide grain coats have been removed by subsequent diagenesis.

used in this paper divides sandstones into three classes based upon overall iron concentration (Table 4.1). The unmodified term "sandstone" is used for rock with a very low iron oxide concentration (defined here as < 0.5%) and a white or pale color (high Munsell lightness). "Bleached sandstone" is used in cases where iron oxide was originally present, but has been subsequently removed by chemical processes (typical of the Navajo Sandstone). "Ferruginous sandstone" refers to rock with moderate iron oxide concentration (0.5 to 9%), resulting in intermediate Munsell lightness and a broad variety of colors (red, orange, yellow, etc.). The term "ironstone" is used in the geological literature for dark-colored sedimentary rock that is heavily cemented with iron oxide, usually defined as having concentrations > 15% (e.g., James, 1966; Kimberley, 1994). However, this strict definition has limited utility for field work in the Navajo Sandstone, where some dark, heavily ferruginized sandstones have iron oxide concentrations that fall below this value. This paper refers to sandstone with 10-14% iron oxide as "sparse ironstone" (typically dark brown) and sandstone with 15%+ iron oxide as "dense ironstone" (typically gray or black). "Ferricrete" is a setting-specific term that is generally reserved for iron-rich horizons that occur in soil or regolith (e.g., Wright et al., 1992; Phillips, 2000).

"Primary" and "Secondary" Ferruginous Sandstones

Iron oxide cementation of the Navajo Sandstone can be divided into two principle textural types: primary and secondary. "Primary" cementation is associated with thin coats (~10 μm) of reddish hematite cement that uniformly surround grains (Figs. 4.2 and 4.3). The even distribution of relatively small amounts of iron oxide

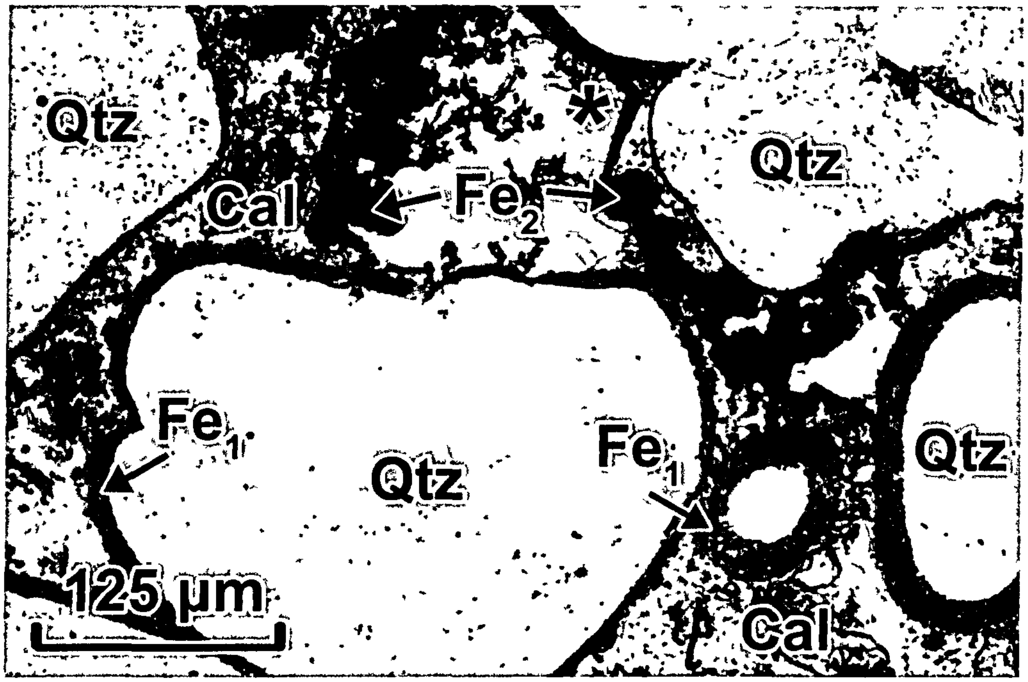

Figure 4.2.
Thin section micrograph shows quartz grains (Qtz) cemented with calcite (Cal) and multiple generations of iron oxide cement. Primary iron oxide (Fe_1) forms a uniform, thin, red-colored coat around grains and lies beneath other cements. Apparent variations in grain coat thickness result primarily from grain coats intersecting the thin section plane at different angles. Secondary iron oxide (Fe_2) occurs mainly as dark-colored, blocky masses within pore spaces. Asterisk marks a rhombohedral calcite crystal.

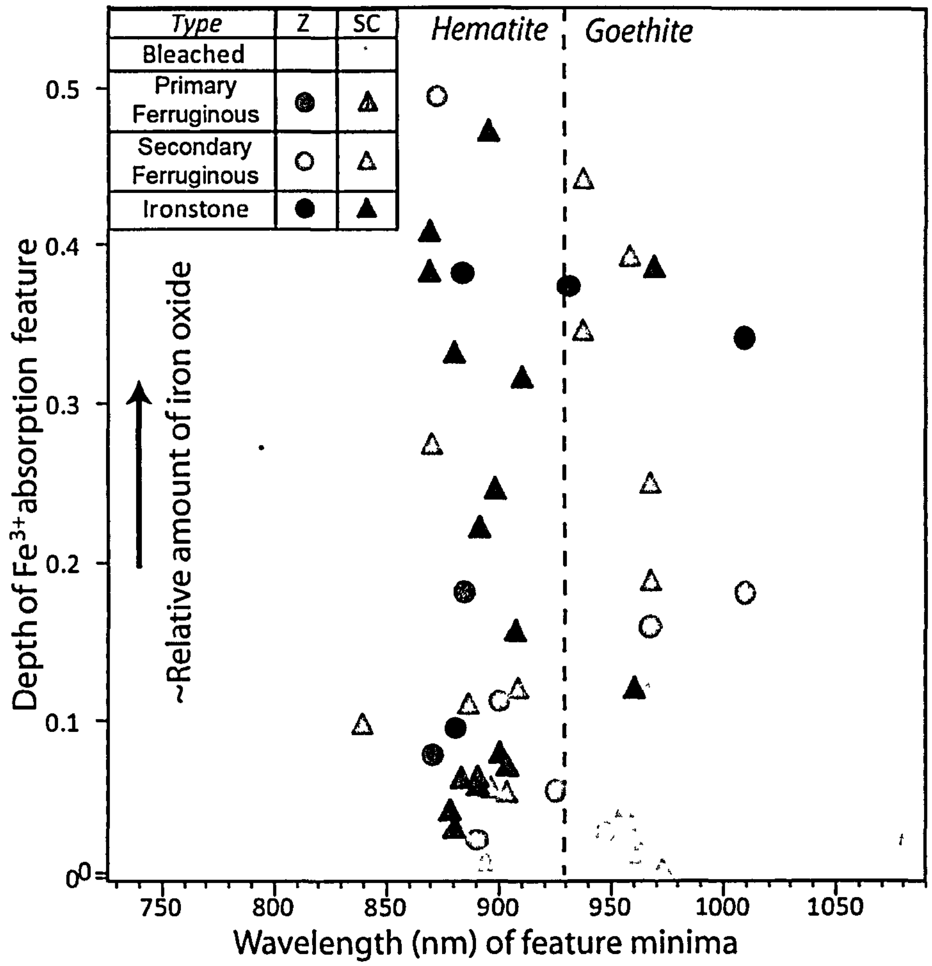

Figure 4.3.
Hematite and goethite mineralogy of different iron-enriched sandstones based upon absorption depth and wavelength of feature minima (n=48). Compare with Bowen et al. (2007). Approximate division line between minerals based upon analysis of samples with known mineralogy (confirmed with XRD) from the U.S. Geological Survey spectral library (Clark et al., 2007)

(~0.6% by weight [Table 4.2]) results in sandstone with a uniform, reddish pigmentation. Primary grain coats in the Navajo Sandstone are interpreted as early diagenetic features, having either a syndepositional or early burial origin (Walker, 1975; Dapples, 1979; Walker, 1979; Turner, 1980; Tucker, 1991; Weibel, 1998; Eichhubl et al., 2004; Beitler et al., 2005). "Secondary" cementation is indicated by precipitation of irregular areas of iron oxide that fill intergranular pore spaces and may replace or modify earlier generations of cement (Fig. 4.2). Secondary sandstones are characterized by uneven pigmentation and have a broad variety of colors and appearances depending upon the size, shape, mineralogy, and distribution of iron oxide crystals (Cornell and Schwertmann, 2003; Fig. 4.3).

The concentration of iron oxide in secondary sandstones is highly variable, reflecting spatial variations in cement distribution (Table 4.2), overprinting of different types of iron oxide cement (Fig. 4.2), and isomorphous substitution of trace elements (Cornell and Schwertmann, 2003). Where multiple generations of cement are present, secondary iron oxide features (concretions, etc.) commonly occur within either a red-colored matrix ("overprinted ferruginous sandstone") or a white-colored, bleached matrix ("replaced ferriginous sandstone"). In some cases, both limited bleaching and localized secondary cementation may occur in the same sample ("mixed ferruginous sandstone"). In contrast to primary red sandstones (dominated by hematite grain coatings), the composition of secondary ferruginous sandstones and ironstones in southwestern Utah ranges from dominantly hematite to mostly goethite (Fig. 4.3).

Table 4.2

Concentration and distribution of Fe_2O_3 and adsorbed trace elements in the Navajo Sandstone of southwest Utah.

Class		n		Iron Oxide					Selected Trace Elements - Avg. PPM (SE_m)					
		ICP-MS	Point Count	Mean Weight % (SE_m)	Mean Spatial %			Mean Dispersion Ratio[2]	As	Co	Ni	U	V	Zn
					Rims	Pore Fill	Total							
Sandstone[1]		5	2 x 1000	0.4 (0.05)	0.2	0.7	0.9	2.7	6 (4)	<1 (N/A)	<20 (N/A)	0.2 (0.05)	<5 (N/A)	<30 (N/A)
Ferruginous Sandstone	Primary Red	3	2 x 1000	0.6 (0.06)	3.0	2.4	5.4	8.1	<5 (N/A)	1 (1)	<20 (N/A)	0.3 (0.01)	<5 (N/A)	<30 (N/A)
	Secondary ("Overprinted")	8	7 x 1000	1.6 (0.2)	2.3	9.9	12.2	9.1	13 (8)	2 (0.4)	<20 (N/A)	0.7 (0.2)	8 (2)	<30 (N/A)
	Secondary ("Replaced")	2	2 x 1000	2.8 (1.6)	0.3	8.4	8.7	2.3	71 (71)	35 (33)	30 (30)	1.7 (1.1)	22 (15)	85 (85)
	Secondary ("Mixed")	3	1 x 1000	1.2 (0.3)	4.3	2.5	6.8	4.5	<5 (N/A)	1 (0.7)	<20 (N/A)	0.3 (0.1)	6 (3)	<30 (N/A)
	Combined	*16*	*12 x 1000*	*1.5 (0.2)*	*2.2*	*7.8*	*10.0*	*7.4*	*16 (9)*	*6 (4)*	*<20 (N/A)*	*0.7 (0.2)*	*8 (2)*	*12 (11)*
Iron-stone	Sparse	1	1 x 1000	13.2 (N/A)	0.1	22.9	23.0	1.7	266 (N/A)	10 (N/A)	30 (N/A)	11.4 (N/A)	38 (N/A)	60 (N/A)
	Dense	2	1 x 1000	24.6 (5.3)	0.0	41.7	41.7	1.4	117 (90)	85 (52)	100 (10)	1.0 (0.07)	57 (14)	325 (95)
ALL		**24**	**16,000**	**3.7 (1.8)**	**1.7**	**10.0**	**11.7**	**6.1**	**33 (18)**	**11 (8)**	**12 (8)**	**1.0 (0.6)**	**12 (4)**	**38 (25)**

Trace elements with a less than symbol (<) have concentrations that fall below the detection limit indicated. SE_m = standard error of the mean. [1]Samples of the "sandstone" class in this study include white and yellow bleached facies. Average Fe_2O_3 concentration for completely white sandstone is ~0.2%. [2]Dispersion ratio for Fe_2O_3 is the average weight % divided by the average spatial % for paired ICP-MS/point count samples.

Characterization of the Iron Oxide Enrichment Zone

Secondary iron oxide cementation features occur primarily within an enrichment zone encompassing approximately the lower third of the Navajo Sandstone ("brown ferruginous facies" in Nielsen et al., 2009). This zone is characterized by prevalent surficial darkening and localized areas of dense iron oxide cement. Concentrated cementation is most common near the upper boundary of this zone, where it locally forms well-defined horizons marked by spotty brown cement, upward-tapering concretions, and/or dark ironstone (Fig. 4.4). These discontinuous cementation horizons typically cut across primary bedding fabric (Fig. 4.5; Willis and Higgins, 1996), with lobe-shaped areas of the boundary commonly oriented upward and to the north (Fig. 4.4A). The degree of cementation ranges from m-scale sheets of dense ironstone to places where iron oxide enrichment is poorly demarcated or absent.

Because of its relatively undisturbed strata and excellent bedrock exposures, the Zion NP area is an excellent locality for characterizing the geometry of the upper boundary of the iron enrichment zone. The trend surface for the top of the Navajo Sandstone in the Zion NP area was calculated from GIS point measurements throughout the park (Fig. 4.6). A map of deviation from trend (Fig. 4.7A) shows that the top of the Navajo Sandstone is relatively uniform and flat in the southern park area and corresponds well to its trend surface. Structural dip (338/1.8 NE) was calculated using point measurements from this undisturbed area and depths for the upper boundary of the iron enrichment zone are reported relative to this surface (Fig. 4.7B). Total vertical change for the boundary within a ~100 km^2 area at Zion NP is approximately 166 m with steepest inclinations of ~2°. The calculated trend is 345/2.1 NE, varying only slightly

Figure 4.4
Concentrated iron oxide horizons in the Navajo Sandstone of southwestern Utah. (A) Well-defined horizon that has been sectioned along a joint to reveal both its internal and external structures. Lobe-shaped boundary points slightly upward and to the north, Snow Canyon SP. (B) Loose concretions (1) weathering from a cementation horizon (2) to form a surface lag deposit, Snow Canyon, SP. Arrows point to the trace of the same boundary cross-cutting the bleached zone on a cliff 1.7 km (1 mi) away. (C & D) Concentrated iron oxide horizons have similar characteristics in the Navajo Sandstone of Zion NP (C) and Snow Canyon State Park (D).

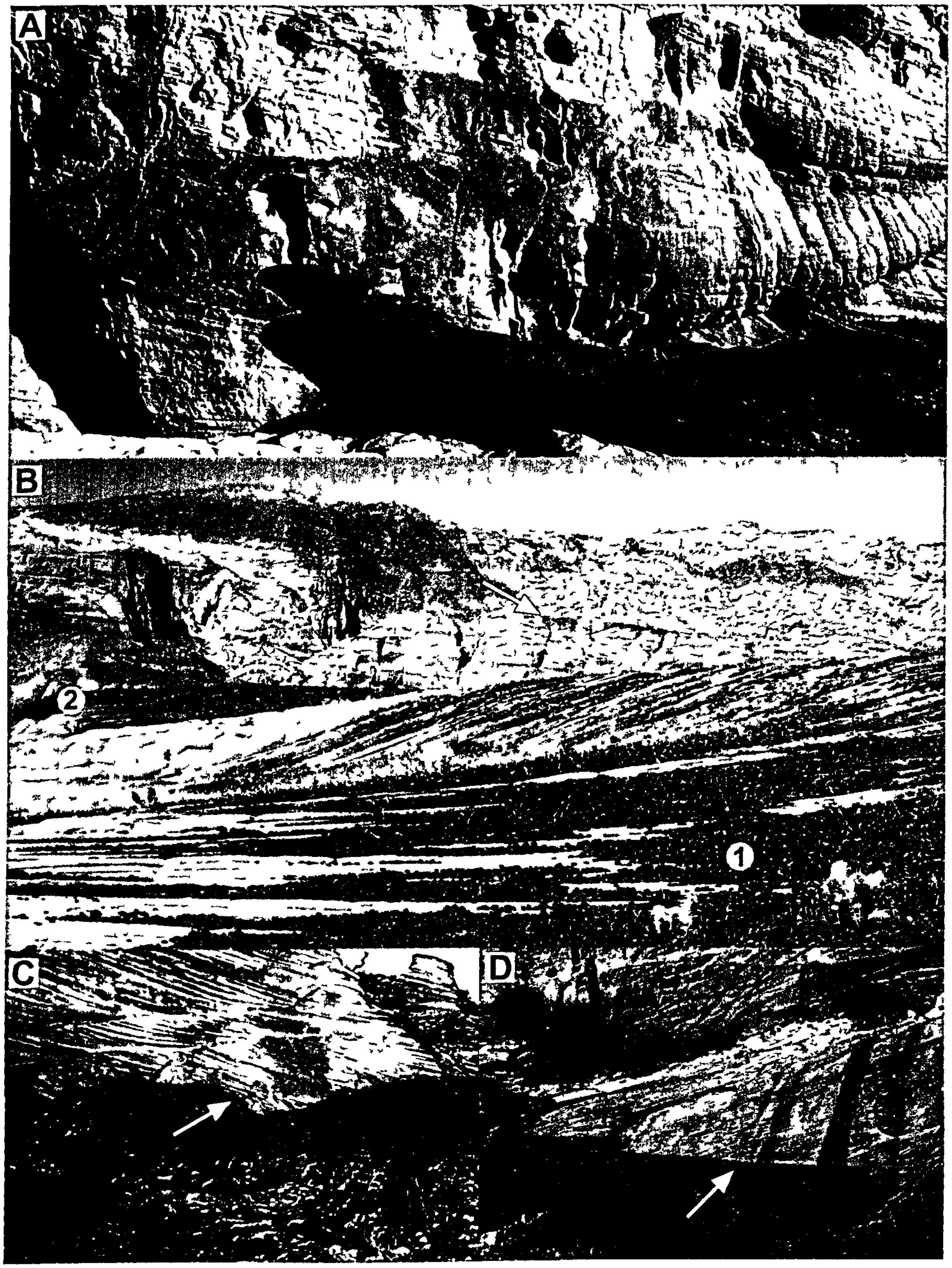
A
B
2
1
C
D

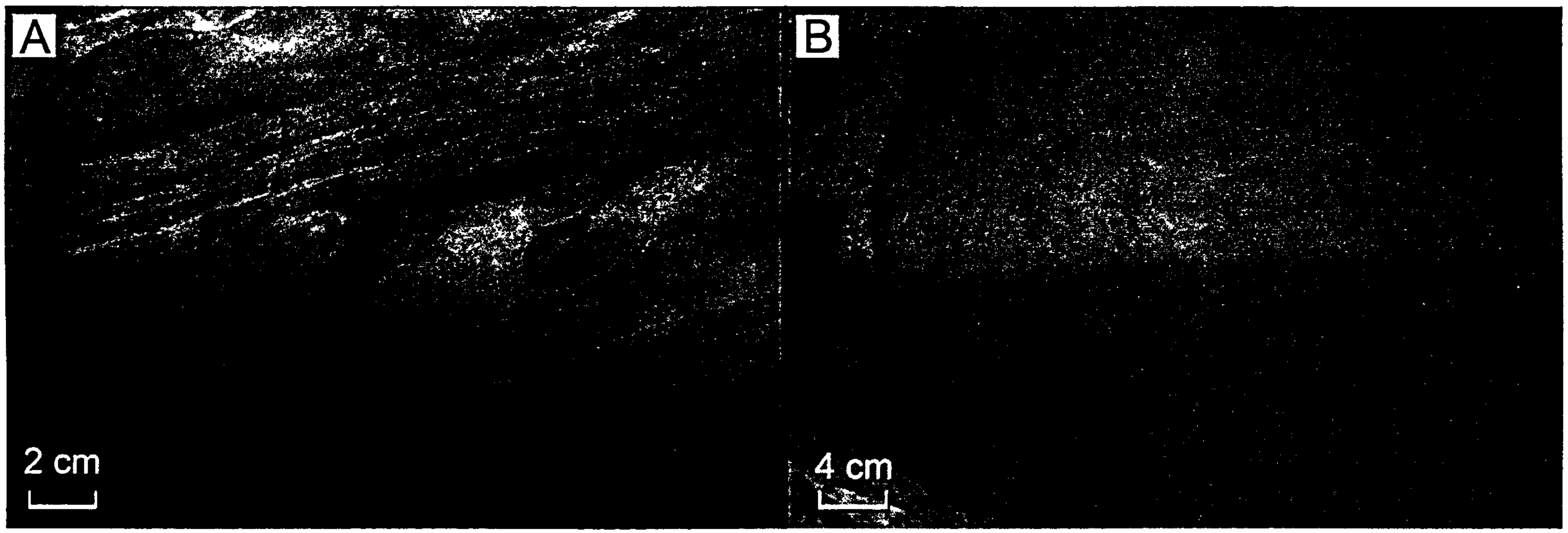

Figure 4.5
Diffuse to spotty cementation along concentrated iron oxide horizons cuts across primary bedding fabric at (A) Zion NP and (B) Red Cliffs Desert Reserve.

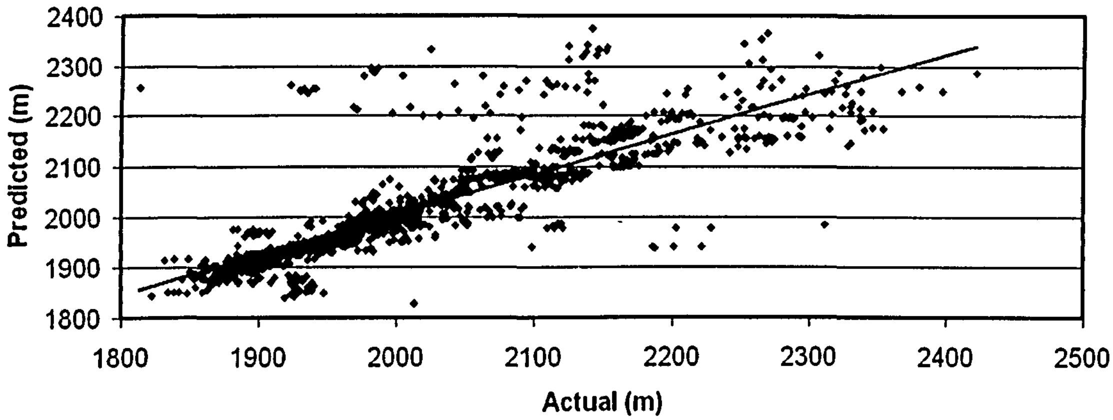

Figure 4.6.
Predicted vs. actual elevation for the top of the Navajo Sandstone in Zion NP using a trend surface oriented at 336.3/1.8 NE (n=1272; standard error of the estimate [SE_{est}] = 65 m). Best fit occurs between ~1830-2010 m (~6000-6600 ft). Most deviations from trend are associated with structural deformation in the northern part of the park (Fig. 4.1). Calculated using ESRI ArcMap.

Figure 4.7
Spatial relationship between the top of the Navajo Sandstone and the upper boundary of the iron oxide enrichment zone at Zion NP. (A) Deviation of the top of the Navajo Sandstone from its calculated trend of 336.3/1.8 NE (contour interval = 10 m; see Fig. 4.6). Uncontoured area in the west and south represents locations where the top of the Navajo Sandstone has been removed by erosion. Deviations from trend in the northern park correspond to deformational features associated with the Sevier orogeny and Basin and Range Extension (Biek et al., 2003). Reference features: 1-Zion Canyon; 2-Taylor Creek thrust zone; 3-Bear Trap Canyon fault. (B) Depth of the upper boundary of the iron enrichment zone (where exposed) relative to the trend surface for the top of the Navajo Sandstone (n=156; SE_{est} = 16 m). Smoothed using neighborhood averaging (circular radius = 500 m).

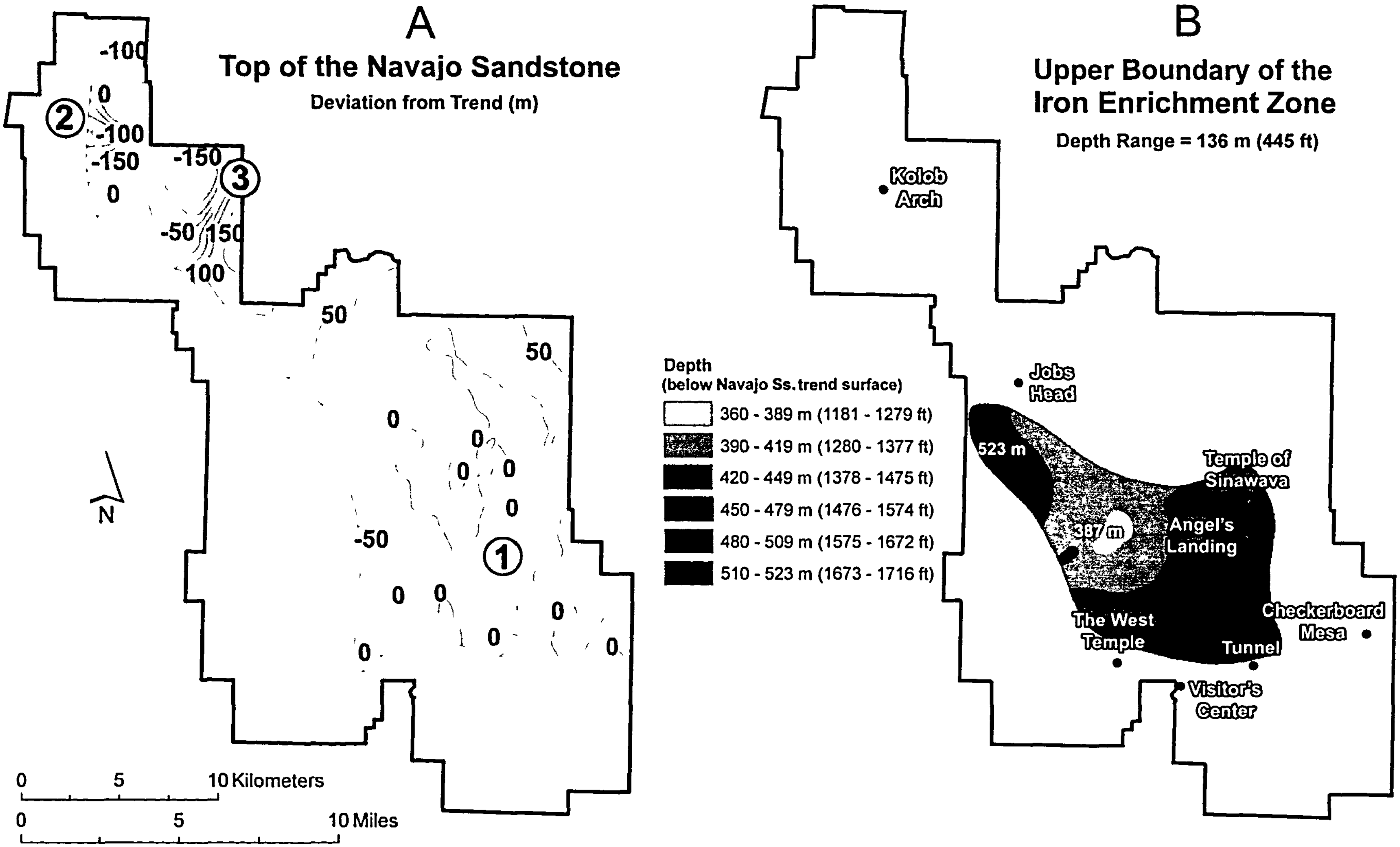
A
Top of the Navajo Sandstone
Deviation from Trend (m)
-100
0
-100
-150
0
-150
150
-50
100
50
50
0
0
0
0
0
-50
0
0
0
0
0
0
1
2
3
N
0 5 10 Kilometers
0 5 10 Miles
B
Upper Boundary of the
Iron Enrichment Zone
Depth Range = 136 m (445 ft)
Kolob Arch
Jobs Head
523 m
387 m
Temple of Sinawava
Angel's Landing
The West Temple
Checkerboard Mesa
Tunnel
Visitor's Center
Depth
(below Navajo Ss. trend surface)
360 - 389 m (1181 - 1279 ft)
390 - 419 m (1280 - 1377 ft)
420 - 449 m (1378 - 1475 ft)
450 - 479 m (1476 - 1574 ft)
480 - 509 m (1575 - 1672 ft)
510 - 523 m (1673 - 1716 ft)

from that of the Navajo Sandstone. These results indicate that the upper boundary of the iron enrichment zone in the Zion NP area is best characterized as a roughly planer (but gently undulating), subhorizontal surface.

Spatial Extent of Concentrated Iron Oxide Cementation

Concentrated iron oxide cementation features occur in many areas of southwestern Utah, including Zion National Park, Snow Canyon State Park and the Red Cliffs Desert Reserve (Fig. 4.1). Concentrated iron oxide horizons that locally mark the upper boundary of the iron enrichment zone are locally discontinuous, and erosion commonly prevents direct correlation. However, shared features suggest they were produced by similar processes, and in many cases may even represent different exposures of the same regional-scale reaction surface. Concentrated iron oxide cementation features are best developed at Snow Canyon SP, where a distinct upper iron enrichment zone boundary can be traced through much of the park. Similar features occur locally in areas of the Red Cliffs Desert Reserve to the west and east. Between the Red Cliffs Reserve and Zion NP (Fig. 4.1), the Navajo Sandstone has been removed by erosion due to uplift along the Hurricane Fault (Lund et al., 2008). However, many similarities between iron oxide cementation features at Zion NP and Snow Canyon SP area suggest that the iron enrichment zones at these two locations may be genetically related:

1. The iron enrichment zones at both locations extend from roughly the lowest cross-bedded eolian deposits in the Navajo Sandstone to a subhorizontal boundary further up in the formation. In both cases secondary cementation is sporadic and subtle in the lower formation and best defined near the upper boundary. Elevation

of this boundary varies at different localities in southwestern Utah (as a result of offset along the Hurricane fault and other structures), but its position is consistently in the lower part of the Navajo Sandstone.

2. Concentrated iron oxide cementation at both locations has a similar appearance, with cementation becoming more pronounced towards the upper boundary of the iron enrichment zone (Figs. 4.4, 4.5). At both locations the enrichment boundary cuts dune foresets and interdune (bounding) surfaces at oblique angles (Fig. 4.5; Willis and Higgins, 1996). Preliminary observations of the boundary at both locations commonly show lobate projections, both upward and northward (e.g., Figs. 4.4A; Fig. 2.4C).

3. Both iron enrichment zones can be traced over large areas (50+ km^2 each), although cementation is discontinuous in some places. The upper boundaries of both zones are roughly homoclinal and nearly parallel to the top of the Navajo Sandstone (Table 4.3). Rotating the boundaries to remove present tilt of the Navajo Sandstone (~2° at Zion NP and ~6° at Snow Canyon SP) restores both surfaces to a near horizontal orientation.

Other areas of southwestern Utah also display councentrated iron oxide cementation features that may have originated in a similar way to those at Snow Canyon SP and Zion NP. For example, the Sand Hollow Reservoir area to the south (Fig. 4.1) has numerous small (<3 cm diameter), loose concretions and angular ironstone cobbles that form surficial lag deposits similar to those produced near the iron enrichment boundary at Snow Canyon (Fig. 4.4B). Farther to the north, a poorly-cemented, steeply tilted (026/63 E) iron oxide horizon in the lower Navajo Sandstone of Cedar Canyon

Table 4.3

Comparison of strike and dip for calculated trend surfaces at Snow Canyon SP and Zion NP (~70 km / 45 mi to the east [Fig. 4.1]).

Locality	**Calculated Trend: Upper Boundary of the Iron Enrichment Zone**	**Calculated Trend: Top of the Navajo Sandstone**
Zion National Park, Utah	345 / 2.1 NE	338 / 1.8 NE
Snow Canyon State Park, Utah	334 / 5.6 NE	328 / 6.2 NE

Trends calculated using ESRI ArcMap from points plotted along each boundary (n=1494 total points). Navajo Sandstone trend at Snow Canyon SP is an estimate based upon averaged field measurements of the underlying Kayenta and overlying Carmel Formations.

(Fig. 4.1) is also oriented roughly parallel to the structural tilt of the Navajo Sandstone, and may have been produced by similar processes. A conservative estimate for the combined spatial extent of the concentrated cementation zone in the Snow Canyon SP, Red Cliffs Desert Reserve, and Zion NP areas is 150+ km^2 (58+ mi^2). Total extent may be much larger, but is difficult to determine due to discontinuous cementation and areas where the Navajo Sandstone is missing or not exposed.

Impact of Iron Oxide Cementation on Permeability

Gas permeability measurements from surface plugs vary considerably (<1 mD to >2000 mD), with average values that are highest for white bleached sandstones, intermediate for ferruginous sandstones and lowest for dense ironstones (Table 4.4). Very large standard errors for bleached and ferruginous sandstones reflect variations in grain size, bedding fabric (grain flow, wind ripple, etc.), and the variable presence of iron oxides and other pore-filling cements (authigenic clays, quartz, calcite, etc.). These heterogeneities in primary and secondary fabric result in highest permeability parallel to bedding (Table 4.5). The average permeability for primary ferruginous sandstones (mostly grain coats) in this study is similar to that of bleached white sandstones (898 and 820 mD respectively; both have high standard errors). Thin section analysis indicates that iron oxide in these primary ferruginous sandstone samples occurs as thin coats around grains but does not bridge or fill pore spaces. The precipitation of relatively small concentrations of secondary iron oxide within pore spaces can markedly reduce permeability. Grain density remains relatively constant across samples as a result of high quartz content relative to other constituents (Table 4.4).

Table 4.4

Density, porosity, and permeability for different classes of iron-enriched Navajo Sandstone (Table 4.2).

Property	Bleached Sandstone	Ferruginous Sandstone	Ironstone	ALL
n-plugs	7	20	5	32
n-sampled sites	7	14	4	25
Dry Bulk Density (g/cm^3)	1.95	2.03	2.23	2.04
Grain Density (g/cm^3)	2.63	2.63	2.75	2.65
Ambient Porosity (%)	25.7 (MD=26.7; SE_m=2.0)	22.8 (MD=23.3; SE_m=1.4)	19.0 (MD=20.9; SE_m=3.1)	23.0 (MD=23.4; SE_m=1.1)
Gas Permeability (mD)	820 (MD=958; SE_m=222)	494 (MD=317; SE_m=190)	9 (MD=8; SE_m=4)	508 (MD=248; SE_m=131)

Measured from surface plugs using a laboratory gas permeameter. Paired parallel/perpendicular plugs from the same site were averaged prior to performing calculations. MD = median; SE_m = standard error of the mean.

Table 4.5

Porosity and permeability of Navajo Sandstone samples measured at different axial directions relative to bedding (n=14 paired parallel/perpendicular plugs).

Property	Parallel to Bedding	Perpendicular to Bedding
Ambient Porosity (%)	23.6 (MD=24.1; SE_m=1.6)	21.7 (MD=25.4; SE_m=3.0)
Gas Permeability (mD)	888 (MD=908; SE_m=310)	704 (MD=181; SE_m=405)

Discussion

Progressive Cementation of Iron Oxide Features

Iron-enriched sandstones are classified based upon their iron oxide concentration and the dominant style of cementation (Fig. 4.8; Table 4.1). Cementation is a progressive process with resulting precipitation features controlled by the complex interaction of depositional fabric, fluid properties, and time. Early cementation produces basic features such as Liesegang bands and small oxidation spots (Figs. 4.8I-J). Continued growth of cementation features is dependent upon many factors including reactant supply, favorable nucleation, and solution chemistry (pH, Eh, etc.; Chan et al., 2007; Golden et al., 2007). Where iron supply is abundant and other conditions are favorable, continued cementation results in more concentrated features such as iron oxide concretions and dark-colored bands or patches (Figs. 4.8K-M). With sustained precipitation, amalgamation of these localized features forms medium-scale (m+) sheets that act as barriers to subsequent fluid flow (Figs. 4.8F-G). Dense ironstones in Snow Canyon SP and surrounding areas commonly show remnant diagenetic structures that are indicative of these earlier phases of cementation (Figs. 4.9A-D).

Precipitation Pathways

In contrast to primary red sandstones (dominated by hematitic grain coatings), the composition of secondary ferruginous sandstones and ironstones in SW Utah ranges from dominantly hematite to mostly goethite (Fig. 4.3). The precipitation pathways for iron oxides depend upon oxidation rate, pH, temperature, and the presence of foreign

Figure 4.8.
Classification of iron-enriched sandstones based on iron oxide concentration and dominant cementation style. Iron oxide textural subclasses (primary, secondary, etc.) are defined in this report. For a discussion of layered vs. solid concretions see Potter, 2009.
[1]The designation "sandstone" includes both rock that lacks evidence of previous iron oxide cementation and "bleached" rock where original iron oxide grain coats have been removed by subsequent diagenesis (all light-colored samples in the present study are bleached).

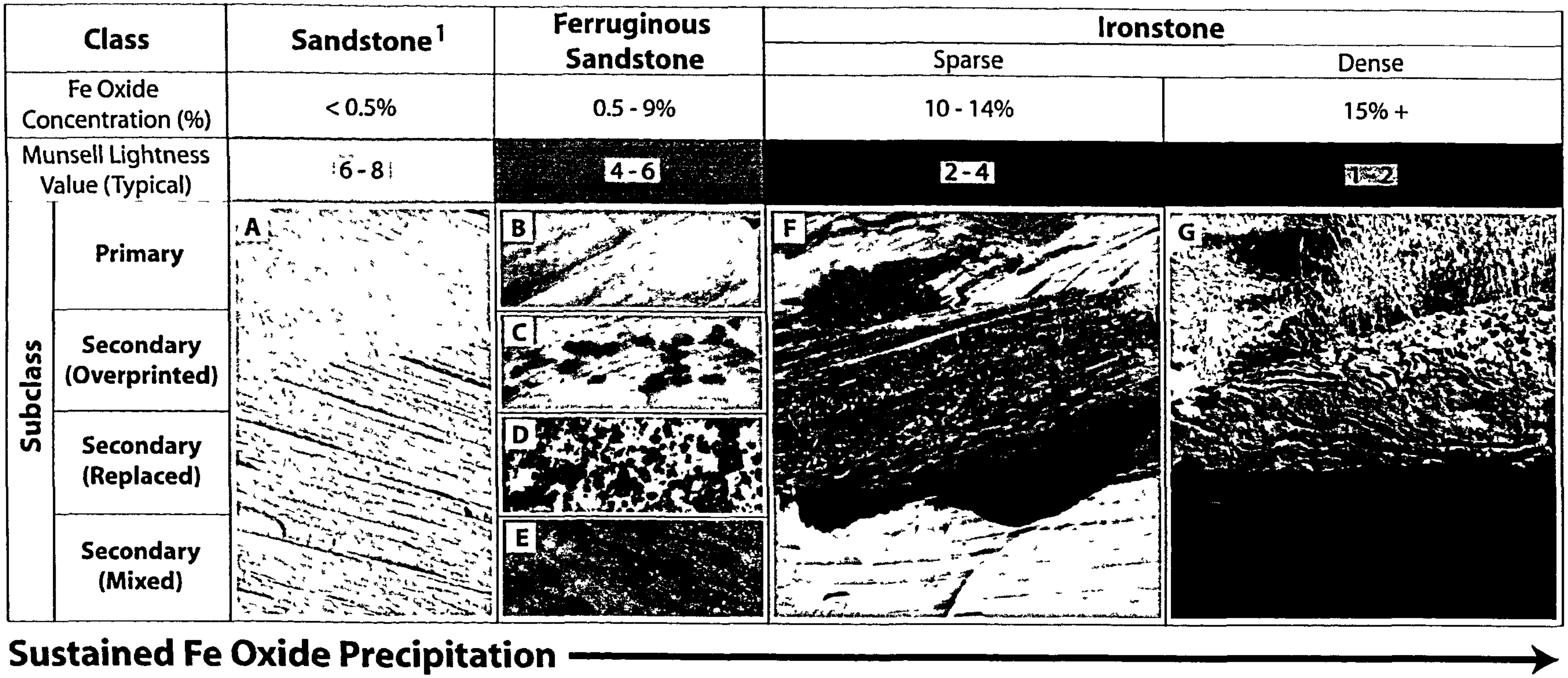

Descriptive terms for iron oxide distribution in ferruginous sandstones & ironstones.

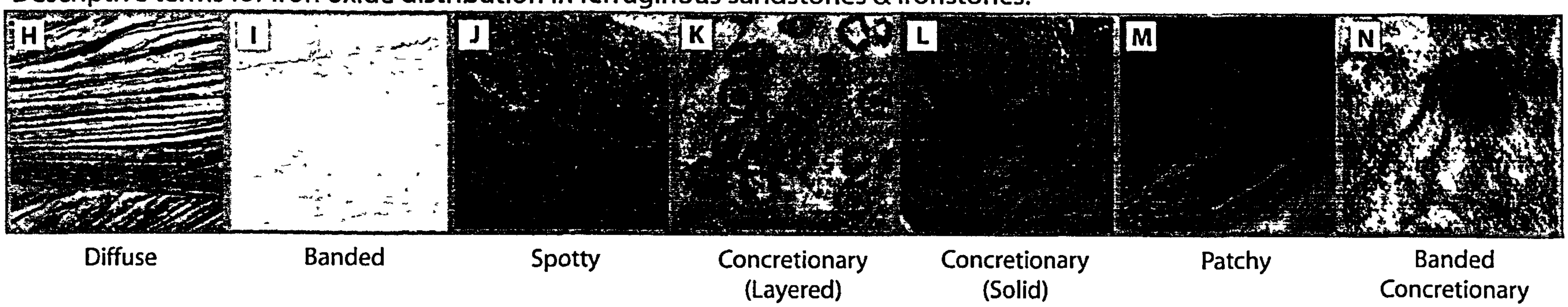

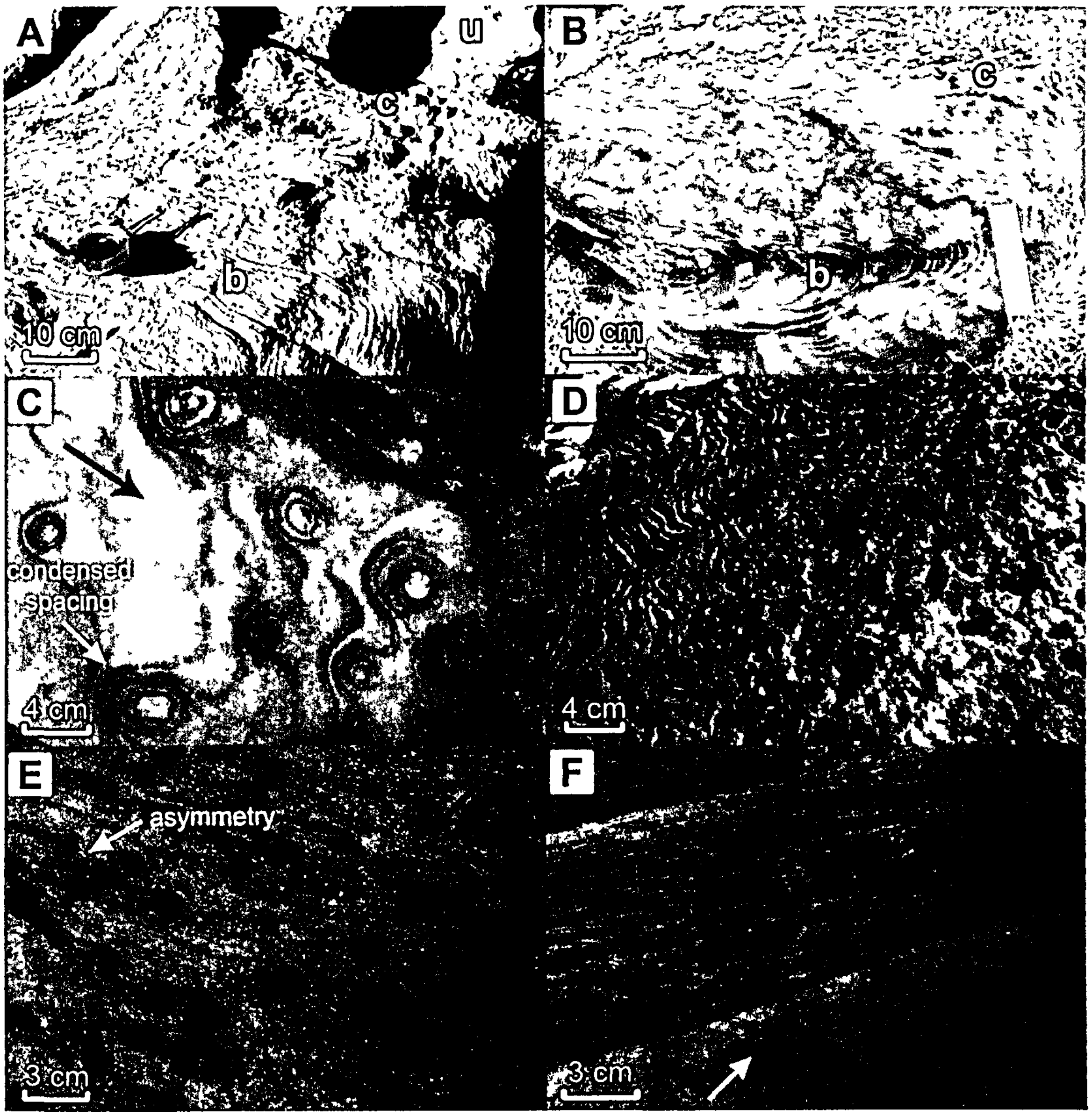

Figure 4.9
Relationships between Liesegang-type bands and iron oxide concretions near the upper boundary of the iron enrichment zone. (A-B) Paired images (ferruginous sandstone and ironstone) show the typical progression of diagenetic features with sustained iron oxide precipitation. Where present, Liesegang-bands (b) typically occur below the main reaction front boundary, concretions (c) along the boundary, and unaltered sandstone (u) in front of the boundary. Lobe-shaped (or "roll-front") type geometries are typically convex in the direction of solute migration (Drevor, 1982). (C-E) Condensed spacings and asymmetries in contorted Liesegang bands (blue arrows indicate inferred direction of reactant diffusion). (F) Concretions follow higher permeability strata while Liesegang bands (arrow) pass across the permeability boundary.

compounds in the system (Drevor, 1982; Kandori et al., 2000; Cornell and Schwertmann, 2003). Geothite typically precipitates directly from Fe^{2+} solution through oxidation and hydrolysis reactions, while hematite can follow a broader variety of pathways including the dehydroxilation and thermal transformation of ferrihydrite, goethite and other iron hydroxides precursors (Cornell and Schwertmann, 2003). Formation of goethite is favored by higher temperatures, high or low pH, and high Al activity (Schwertmann and Taylor, 1989; Cornell and Schwertmann, 2003; Eichhubl et al, 2004). In some cases bacteria and other organisms may also play a substantial role in mediating precipitation (Konhauser, 1997; Cornell and Schwertmann, 2003; Bowen et al., 2008). Solute supply, spacing of nuclei, and grain size are important factors in controlling the size and spatial distribution of cementation features (Chan et al., 2007; Barge et al., 2008).

Limiting Reactants

The formation of concentrated iron oxide horizons requires the transport of large quantities of dissolved iron to the reaction front boundary. Mass balance relationships were calculated for the direct precipitation of hematite from Fe^{2+} solution ($2Fe^{2+} + 0.5O_2 + 2H_2O \rightarrow Fe_2O_3 + 4H^+$), based upon ICP-MS and dry bulk density data. These calculations indicate that primary ferruginous sandstones (avg. wt% Fe_2O_3 = 0.64%) have an average iron oxide content of 12.7 kg/m^3. Converting to secondary ferruginous sandstone (avg. wt% Fe_2O_3 = 1.5%) requires the addition of 18.1 kg of iron oxide cement per m^3 of rock. If formation fluids have a relatively high initial Fe^{2+} concentration of 5 mg/L, the dissolved iron equivalent for 2.5 x 10^6 L (~2500 m^3) of fluid is required to produce each m^3 of secondary ferruginous sandstone. Local areas of dense ironstone may require the iron equivalent for 10-20 times this much fluid.

In addition to iron, oxygen is also a potential limiting reactant for the precipitation of iron oxide in subsurface settings. Mass balance relationships for the precipitation of hematite from Fe^{2+} solution (using the chemical parameters above) indicate that the precipitation of 1 m^3 of secondary ferruginous sandstone consumes 18.2 kg of dissolved O_2. The saturated dissolved oxygen concentration for pure water is calculated to be 8.3 mg/L at 25°C at 1 atm pressure. Actual concentrations in the subsurface are typically much lower due to contact with organic matter and other reductants (Kehew, 2001). Even at saturated concentration, producing 1 m^3 of secondary ferruginous sandstone requires the dissolved oxygen equivalent of ~2.2×10^6 L (~2,200 m^3) of water. Thus, concentrated iron oxide cementation necessitates replenishment of both iron and oxygen through mass transport processes.

Reactant Transport

The common occurrence of Liesegang-type bands in dense ironstone cements near the upper boundary of the enrichment zone (Figs. 4.9A-B) has implications for reactant transport. Liesegang bands are rhythmic cementation patterns postulated to be produced by either pulses of discontinuous supersaturation during nucleation or subsequent competitive regrowth of crystals (Ostwald, 1897; Ortoleva et al., 1987; Chernavskiia et al, 1991; Chan et al., 2000; Müller and Ross, 2003). Similar bands replicated in a laboratory setting develop in situ and are commonly produced by introducing ions into a gel which precludes advective transport (George and Varghese, 2002). Precipitation occurs as reactants diffuse outward, with bands oriented parallel to the direction of reactant transport (Müller and Ross, 2003). Liesegang-type bands associated with concentrated iron oxide horizons in the Navajo Sandstone commonly occur just below the main cementation boundary and are oriented roughly parallel to it (Fig. 4.9A). Assuming that these sandstone bands also form through diffusion, this orientation indicates that reactant transport near the boundary occurred in a direction more or less perpendicular to the main reaction front.

Relationships between Liesegang-type bands and other sandstone features provide additional insights into reactant transport. Where bands occur together with iron oxide concretions, they may display asymmetries and condensed spacings that record the local direction of solute transport (Figs. 4.9C-E; compare with Eichhubl et al., 2004, Fig. 5G). Another characteristic of Liesegang-type bands is that they typically pass across primary permeability boundaries such as interdune surfaces (Fig. 4.9F). In contrast, concretionary iron oxide cements commonly terminate along these boundaries (Fig. 4.9F). The mechanics of this phenomenon were not evaluated but may reflect the dominance of diffusive transport in fine-grained rocks with low hydraulic conductivity (Krumbein and Monk, 1942; Boving and Grathwohl, 2001).

The time required for the diffusion of ions is proportional to the square of the diffusion distance and inversely proportional to the effective diffusion coefficient and (Rice, 1985; Fetter, 1999; Appelo and Postma, 2006). Diffusion coefficients for the transport of molecules and ions through free solution are very small (typically on the order of 10^{-5} cm^2/sec or smaller [Fetter, 1999]). As a result, diffusion over even modest distances requires long time periods. For example, estimates using the approximation equation for diffusion (Appelo and Postma, 2006, p. 92) indicate that more than 2000 years would be required for 68% of Fe^{2+} cations in solution to diffuse across a distance of 10 m (based upon a diffusion coefficient for Fe^{2+} of 7.19 x 10^{-6} cm^2/yr in water at 25°C [Fetter, 1999]). Effective diffusion would be substantially slower through a porous rock such as sandstone because cations must follow longer flowpaths around grains (Fetter, 1999). These very slow transport rates (especially over large distances) suggest that diffusion was most important in transporting reactants near the main reaction front boundary and larger-scale advective transport processes were required in order to move the necessary quantities of iron and oxygen to the lower part of the Navajo Sandstone.

Potential Sources of Iron

In considering potential sources of iron for secondary cementation, the question arises as to whether the iron could come from nearby igneous sources or whether it was removed from bleached white areas of the Navajo Sandstone. Both of these possibilities is explored in the discussion below.

Iron from igneous sources. The Pine Valley laccolith (Pine Valley Mountains in Fig. 4.1) is a mid-Tertiary (~20 M.A.) calc-alkaline pluton that is the southernmost of a series of SW-trending intrusions. Related intrusions ~40 km to the north in the Iron Springs mining district (Fig. 4.1) produced the largest iron deposits in the western United States (Barker, 1995; McKee et al., 1995; Wray and Pedersen, 2009). In many places the margins of these intrusions have closely-spaced joints that are surrounded by light-colored rock that extends outward from the joint surface for up to ~1 m (Barker, 1995). These bleached margins (or "selvages") are areas where hydrothermal alteration replaced ferromagnesium minerals. This produced iron that later precipitated in joints and as strata-bound ore bodies in the adjacent Carmel Formation (Barker, 1995). Magmatic intrusions also facilitate the circulation of meteoric fluids and provide a possible mechanism for iron transport (Hanson, 1996).

Iron oxide horizons in the Navajo Sandstone locally occur in close proximity (within 5 km) to exposures of the Pine Valley laccolith. However, this laccolith is floored by Paleocene-Oligocene sedimentary rocks, placing it stratigraphically (as well as structurally) higher than the Navajo Sandstone in the St. George, Utah area (Hacker et al., 2002). The Tertiary-age rocks surrounding the Pine Valley laccolith lack iron deposits related to the intrusion (Barker, 1995). In the Iron Springs mining district, localized bleached rock and ore bodies occur primarily adjacent to the intrusion. However, bleaching and iron oxide cementation in the Navajo Sandstone occur on broad, regional scale, extending for 100's of km^2 in the study area. Although an extraformational source of iron related to Tertiary-age magmatism remains a possibility (perhaps related to hydrothermal fluids from the deeper subsurface), direct association with the Pine Valley laccolith seems unlikely.

Late Tertiary to Quaternary age basalts that form caprocks in the St. George Utah area (Hamblin, 1987) are another potential source of iron. However, lavas that produced these basalts likely erupted along the same joint system that cross-cuts the iron enrichment boundary (Higgins, 2003), indicating that iron oxide cementation occurred prior to volcanism. In addition, well-developed iron oxide cementation features in the Navajo Sandstone occur many kilometers away from the nearest basalt flows (e.g., the main canyon of Zion NP).

Iron removed from bleached zones. Locally derived, reduced iron from original red sandstones that are now white-colored "bleached" areas in the upper part of the Navajo Sandstone is also a possible source of iron for secondary cementation (Fig. 4.8A; Chan et al., 2008; Beitler et al., 2005). Most concentrated iron oxide horizons in SW Utah occur in close proximity to large zones of bleached rock in the upper formation (Nielsen and Chan, 2009; Nielsen et al., 2009). Iron oxide horizons occur below bleached rock in most of the study areas, but these two features locally overlap in the Snow Canyon SP area (Nielsen and Chan, 2009). Where overlap occurs, secondary iron oxide features locally overprint bleached rock to produce white sandstone with brown and black spots ("replaced ferruginous sandstone"; Fig. 4.8D). These spotty overprinted sandstones suggest that the onset of widespread bleaching either proceeded, or was coincident with the major iron enrichment phase at Snow Canyon SP, and iron removed from bleached rock is therefore a potential local source of iron in that area. It is unknown whether the same timing relationship also applies to the Zion NP area because most concentrated iron oxide cementation there is located well below the main bleached zone and spatial overlap is not observed (Nielsen et al., 2009).

Timing and Depth of Iron Oxide Precipitation

Diagenetic and structural relationships provide clues about the relative timing of concentrated iron oxide precipitation. Secondary iron oxide cements overprint primary grain coats in some areas (e.g., Figs. 4.2, 4.8C) and therefore represent a later stage of diagenesis. In addition, secondary iron oxide cements also overprint bleached white rock in the Snow Canyon SP area (see above). Bleaching is favored by reducing chemical conditions that are most likely to occur at depth. Both the J-1 and J-2 unconformities that overlie the Navajo Sandstone (see Fig. 4.1) seem to have acted as subsurface barriers to the migration of bleaching fluids (Nielsen et al., 2009). These unconformities are middle Jurassic (Bajocian) in age and dating of volcanic ash beds places the J-2 unconformity at 169 to 186 Ma (Kowallis et al., 2001). Consequently, this represents the earliest interval during which bleaching (or by inference secondary iron oxide cementation) could have occurred.

Additional clues about the timing of secondary iron oxide cementation are provided by relationships to topographic and structural features. Exposures of the upper boundary of the iron enrichment zone occur on opposite sides of canyon walls more than 300 m (1000 ft) above the canyon floor in at Zion NP and in areas of Snow Canyon SP. This indicates that cement precipitation predates the later stages of the canyon cutting. In addition, the cementation boundary is cross-cut by high-angle joints (Fig. 4.4A) that developed as Sevier-age compression transitioned to Basin and Range extension, likely during the middle to late Tertiary (Biek et al., 2003; Higgins, 2003; Rogers et al., 2004). The geometry and location of the boundary remains unchanged where it intersects these joints (Fig. 4.4A), whereas fluid-related alteration that occurs after joint formation is typically refocused and/or refracted along the fracture surface (e.g., Eichhubl et al., 2004). This relationship indicates that concentrated iron oxide horizons in southwest Utah formed prior to Basin and Range extension.

Some evidence suggests that secondary iron oxide cementation may also predate (or perhaps have been coincident with) Sevier-age deformation, but this remains tentative. The upper boundary of the secondary cementation zone in the Snow Canyon

SP area dips gently toward the northeast, corresponding well to the regional tilt of strata along the west limb of the St. George syncline (Table 4.3; Fig. 4.1; Hurlow, 1998). This syncline is interpreted to be a Sevier-age feature (Higgins, 2003). In addition, the upper boundary of the iron enrichment zone is cross-cut by major structural lineaments in the Snow Canyon SP area that are also postulated to be Sevier-age features (Willis and Higgins, 1996; Higgins, 2003). It is difficult to tell if the boundary is offset along these lineaments because they have shear deformation that is nearly horizontal and are associated with zones of highly fractured rock (Nielsen et al., 2009). Because the ages of both the syncline and lineaments are poorly constrained and cross-cutting relationships are difficult to interpret, the precise timing of secondary iron oxide cementation has not been determined. The best timing estimate at present is middle Mesozoic (after development of the J-2 unconformity) to middle Cenozoic (prior to Basin and Range extension).

Closely related to the question of timing is the depth at which concentrated iron oxide cementation occurred. The location of the upper boundary of the iron enrichment zone varies at different locations but is typically 300 to 400 m (1000 to 1300 ft) below the top of the Navajo Sandstone (Nielsen et al., 2009). Assuming that the iron enrichment phase occurred after burial of the formation and prior to canyon cutting (see above), this represents the minimum depth of cement precipitation below the paleo land surface. The actual depth of precipitation may have been substantially greater, but is difficult to constrain because timing estimates are tentative and overlying Mesozoic strata contain several regional unconformities where overlying strata have been removed by erosion (Fig. 4.1; Pipiringos and O'Sullivan, 1978; Hurlow, 1998; Biek et al., 2003).

Precipitation Mechanisms

Any viable model for the formation of concentrated iron oxide horizons in the Navajo Sandstone should meet at least three criteria. *First,* it should provide a geochemically viable mechanism for producing iron oxide precipitation and replenishing key reactants. *Second,* it should explain the geometry of the cementation horizons, including their shape, orientation, lateral extent. *Third,* the location of the reaction front should remain stable for sufficient periods of time to concentrate dense precipitates along well-defined horizons. A variety of potential settings for iron oxide precipitation are evaluated using these criteria.

Precipitation in a Saturated Groundwater Setting

Much of the shallow subsurface is saturated with groundwater. The potential for iron oxide precipitation in this setting has been explored by previous researchers (see overview in subsequent section), and is herein evaluated for the Navajo Sandstone. Some general constraints on fluid paleochemistry can be established from comparisons with modern fluids in the Navajo Sandstone aquifer of the St. George, Utah area (Table 4.6). Modern meteoric water in the shallow phreatic zone has an average pH of ~7.6 and a relatively low salinity (Table 4.6). Redox conditions vary widely within a shallow aquifer, but would likely have been mildly to moderately oxidizing (Fairbridge, 1979; Barcelona et al., 1989; Selley et al., 1998). Under these conditions, dissolved iron concentrations would be low (Back and Barnes, 1965). For example, concentration of dissolved iron in modern springs near the base of the Navajo Sandstone in the Zion NP area is ~0.01 mg/L (~10 parts per billion). This indicates that little iron oxide reduction

Table 4.6

Hydrologic data for the modern Navajo Sandstone aquifer in the St. George, Utah area.

	Well Depth (m)	Water Level Below Land Surface (m)	Historic Water Table Fluctuation (m)	pH	Temp (°C)	Dissolved Solute Concentration (ppm)						
						Ca^{2+}	Mg^{2+}	Na^{+}	K^{+}	HCO_3^-	SO_4^{2-}	Cl^-
Min.	30	7	0.4	6.6	11.0	17	1	5	1	54	11	4
Max.	341	230	24.9	8.3	43.5	114	38	350	29	260	462	430
Mean	186	66	7.7	7.6	20.2	62	16	51	5	172	114	48

Compiled from raw data in Wilkowske et al., 1998 (n=45 wells). Water table fluctuation based on 1011 measurements from 9 different wells over time periods of up to 63 years. Annual fluctuations are typically on the order of a few meters or less.

(and sandstone bleaching) is presently occurring (Utah Geological Survey, 2009). More acidic and reducing conditions that favor iron oxide solubility are typical of deeper formation waters. These conditions can also occur in shallower settings where buoyant fluids have moved upward or where groundwater was in contact with reducing agents (Selley, 1997; Chan et al., 2000; Kehew, 2001; Parry et al.,, 2004).

Interaction between superimposed fluid zones. The subhorizontal orientation of concentrated iron oxide horizons in the Navajo Sandstone indicates interaction between vertically superimposed fluid zones having differing chemistries. One possibility is that the precipitation of ferric (Fe^{3+}) oxides in southwestern Utah occurred as deeper, reduced fluids containing high concentrations of ferrous iron (Fe^{2+}) interacted with relatively shallow, oxygen-rich meteoric waters (Fig. 4.10; Chan et al., 2000; Eichhubl, 2004; Hill and Polyak, 2005). Potential reactant transport mechanisms in a saturated groundwater setting include flow related to changes in hydraulic head, convection produced by differences in temperature and/or salinity, and (on a more restricted scale) diffusion related to induced geochemical gradients (Fairbridge, 1979; Wood Hewett, 1984; Wolfe and Chilingarian,1988; Dominico, 1990; Boving Grathwohl, 2001; Hill Polyak, 2005).

Mixing of formation water with shallower meteoric water was modeled using PHREEQC Interactive (USGS; Parkhurst and Appelo, 1999). Within the Navajo Sandstone today, ferrous iron concentrations for formation water are commonly less than a few ppm but may locally exceed 10 mg/L (Hood and Patterson, 1984; Spangler et al., 1996; Chidsey et al., 2007). The formation water selected for modeling occurs at ~140 m

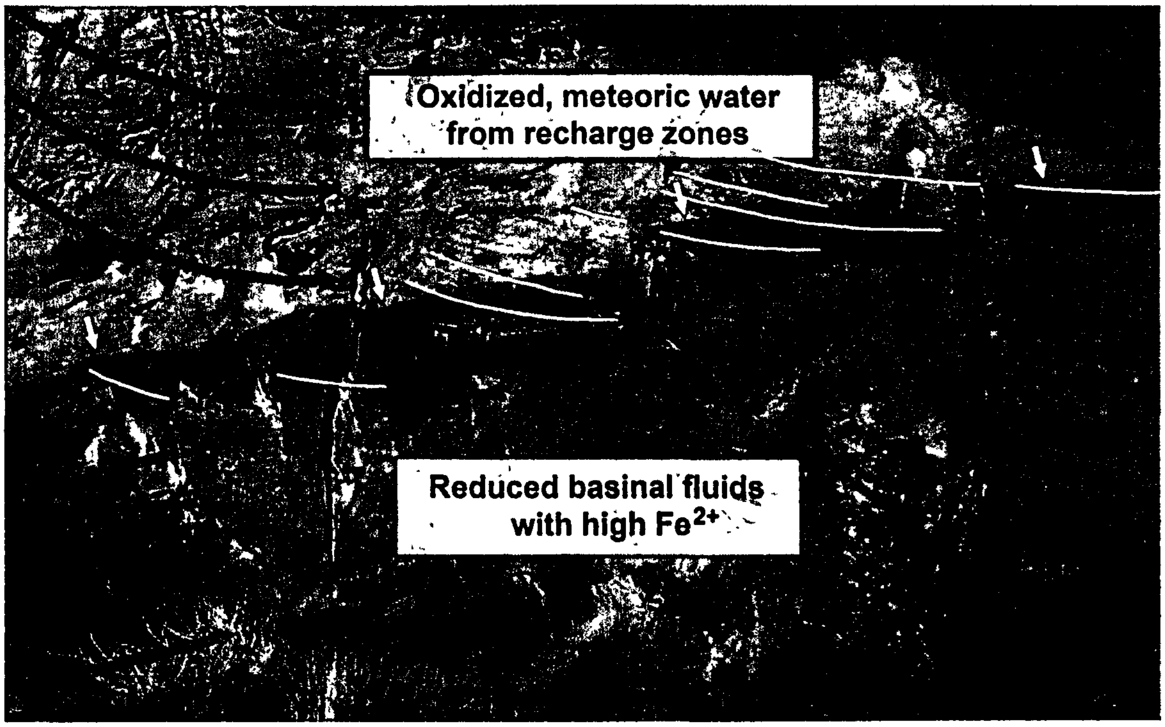

Figure 4.10
One model for the precipitation of iron oxide along a concentrated cementation horizon in the Navajo Sandstone. Meteoric water descending from recharge zones is O_2-rich and has a relatively high redox potential (Eh). Precipitation occurs as meteoric water mixes with reduced basinal fluids that have high concentrations of ferrous (Fe^{2+}) iron (e.g., $2Fe^{2+} + 3H_2O + \frac{1}{2} O_2 \rightarrow 2FeOOH_{\text{goethite}} + 4H^+$). Acid ($H^+$) that is generated by the reaction dissolves illite rims (see Nielsen et al., 2009, Table 3) and/or diffuses away from the reaction front (Beitler et al., 2005). The subhorizontal reaction front boundary (small arrows) cross-cuts eolian bedding fabric (white lines mark prominent foresets).

depth within the Navajo Sandstone of central Utah and is a saline fluid having a pH of 6.1 and a ferrous iron concentration of 5 mg/L (Hood and Patterson, 1984; solute concentrations: 120 mg/L Cl^-, 2500 mg/L Na^+,320 mg/L Ca^{2+}, 5600 mg/L SO_4^{2-}, 4.4 mg/L K^+, 280 mg/L Mg^{2+}). Mixing was simulated at a 50:50 ratio with meteoric water having the average composition in Table 4.6. A redox potential (Eh) of -0.2 V (slightly reducing) was used for formation water and 0.4 V (moderately oxidizing) for meteoric water (Pirson, 1983; Selley, 1998). Temperature was kept constant at 25°C. Mixing results in a nearly neutral solution (pH=7.3; Eh=0.2) that is oversaturated with respect to both hematite (SI = 10.7) and goethite (SI = 4.3) and could have theoretically produced iron oxide cementation.

Oxygen availability and cementation depth. The subhorizontal orientation, undulating shape, and broad lateral extent of iron oxide horizons in the Navajo Sandstone are similar to the geometry of a water table (Fig. 4.7B; Table 4.3; Willis and Higgins, 1996). The elevation of a water table in an unconfined aquifer generally follows overlying topography in a subdued fashion to form a rising and falling surface that may extend laterally for 100's of square kilometers (Jeppson et al., 1968; Dominico, 1990; Robson and Banta, 1995; Price, 1998; Heilweil et al, 2000; Weight, 2008). The dissolved oxygen concentration below the water table (in the water-saturated phreatic zone) typically diminishes with depth, transitioning downward into lower pH/Eh conditions. Although the depth of a water table below the land surface can vary widely (ranging from zero to hundreds of meters), it is commonly on the order of a few tens of meters (Mazor, 2004). In contrast, concentrated iron oxide horizons in the Navajo Sandstone occur hundreds of meters below the top of the formation, and may have precipitated at even greater depths (see above). The precipitation of iron oxide at these depths presents difficulties for explaining how dissolved oxygen was transported to (and replenished in) the deep subsurface.

Availability of dissolved oxygen in the phreatic zone is a function of multiple factors, including depth of the water table, organic content of the sediment, hydraulic conductivity, and proximity to recharge areas (Back and Barnes, 1965; Pirson, 1983; Barcelona et al., 1989; Malard and Hervant, 1999; Kehew, 2001). Relatively deep dissolved oxygen is expected in the Navajo Sandstone as a result of its low organic content, high overall permeability, and pervasive fracturing. The mean depth of the modern water table (below the land surface) in the Navajo Sandstone of the St. George basin is 66 m (216 ft; Table 4.6). Small, meter-scale fluctuations in water table level occur seasonally (Table 4.6), but average elevation over long time periods is controlled by climatic and tectonic processes. Analysis of nine Navajo Sandstone wells in southwestern Utah shows that the average dissolved oxygen concentration of groundwater is 7.7 mg/L at an average well screen depth of 136 m (445 ft) below the land surface (Wilkowske et al., 1998; Heilweil, 2009, written comm.).

Two wells in the Snow Canyon SP area have particular relevance to the question of how dissolved oxygen is replenished at depth. These wells have an average oxygen concentration of 11.6 mg/L at 147 m (483 ft) depth below the land surface and 58 m (189 ft) below the average water table level. They occur near a heavily fractured area and it is postulated that high dissolved oxygen levels may result from gas bubbles that become trapped as water table rises quickly during periods of heavy recharge (Heilweil, 2009, written comm.). These data highlight the important role of groundwater recharge and advection in transporting oxygen into the deeper subsurface. It may be significant that the best developed iron oxide horizons in southwestern Utah occur in the vicinity of Snow Canyon SP, where canyon cutting follows large structural lineaments that may have had an early dilation stage (Antonellini and Aydin, 1994; Willis and Higgins, 1996; Hurlow, 1998; Parry et al., 2004; Nielsen and Chan, 2009).

Alternative Settings for Iron Oxide Precipitation

Although much of the subsurface is saturated with groundwater, interaction between reducing and oxidizing conditions also occurs within other subterraneous environments. The potential for the development of concentrated iron oxide horizons in either the vadose (aerated) zone or a hydrocarbon reservoir system are discussed below.

Precipitation in the vadose zone. Pore spaces in the vadose zone contain a variable ratio of air and fluid. Water that surrounds grains in this zone can become enriched in iron through the breakdown of interstitial clays and other iron-bearing minerals (Turner, 1980). Dissolved oxygen concentrations are commonly high and ferrous iron that is released through weathering in shallow sediments is quickly immobilized to form ferric oxides (Cornell and Schwertmann, 2003). Under these conditions, precipitated iron oxide is typically distributed evenly within the sediment, producing uniform coloration (Cornell and Schwertmann, 2003). Where concentrated iron oxide horizons do occur in the shallow subsurface (e.g., soil ferricretes), they commonly form under saturated or near-saturated conditions where biotic reduction locally outpaces oxygen diffusion and iron can be effectively mobilized (Callebaut, 1982; Cornell and Schwertmann, 2003).

Precipitation in a hydrocarbon reservoir system. Bleaching of the Navajo Sandstone indicates that reducing conditions once dominated the upper part of the formation. Both hydrocarbons and oil field brines tend to be strongly reducing (Selley, 1998), and contact with these agents is a potential means for producing widespread bleaching (Shumacher, 1996; Chan et al., 2000; Garden et al., 2001; Parry et al., 2004; Beitler et al., 2005; Parry, 2009). The relatively flat and laterally continuous shape of iron oxide horizons is similar in some ways to the geometry of an oil-water contact. However, in contrast to a groundwater setting, chemical interactions near the oil-water contact are commonly dominated by reduction instead of oxidation. For example, tar mats (concentrations of heavy oil that may overlie bottom water in a stratified petroleum reservoir) are sometimes associated with pyrite (iron sulfide) that precipitates as the petroleum zone is infiltrated by sulfate-reducing bacteria from below (Machel, 1987; Mason and Kirchner, 1992; Seeley, 1998). Reduced iron may also be incorporated into ferroan dolomite or other iron-bearing minerals (Schumacher, 1996; Parry et al., 2009). Because relatively high concentrations of ferrous iron may occur in oil field brines (e.g., Chidsey et al., 2007), the subsequent interaction of these strongly reducing brines with more oxidizing groundwater elsewhere in the formation is a potential mechanism for precipitating iron oxide.

Comparisons with Other Iron Oxide Precipitation Models

Previous authors have differentiated between two types of subsurface iron oxide horizons: ferricrete horizons formed in soils/sediments and ferruginous bedrock horizons produced in the deeper bedrock (McFarlane, 1976; Milnes et al., 1987; Wright et al., 1992). Ferruginous bedrock zones differ from pedogenic ferricretes in that they lack paleosol profiles, exhibit less variation in mineralogy (mostly hematite and goethite), display simpler fabrics, and have relatively unaltered host rock (Wright et al., 1992). Secondary iron oxide cements in the Navajo Sandstone meets each of these criteria and were likely precipitated within indurated bedrock.

Nodular ferric oxide horizons in the Permian Unidad Roja Superior in the Spanish Pyrenees have many similarities with those in the Navajo Sandstone and provide a useful comparison (Wright et al., 1992). Like the Navajo Sandstone, these horizons occur within high-permeability, fine- to medium-grained redbeds (in this case feldspathic arenite of volcanic origin) with some concretions occurring in partially to completely bleached sandstone. Although some horizons appear to be pedogenic, most are postulated to precipitate in a shallow groundwater setting, triggered by fluctuating groundwater levels (Wright et al., 1992). In addition to the Unidad Roja Superior, groundwater fluctuations are also proposed as a control for iron oxide precipitation in other settings, including mottled and discolored alluvial redbeds (Goldbery and Beyth, 1984), modern river sediments (Breit, 2001), fluvial-marine sediments (Charette and Sholkovitz, 2002; Tanner and Khalifa, 2009), perched aquifers (Driese et al., 2002), desert alluvium (Walker, 1976; Turner, 1980), and soils (McFarlane, 1976; Phillips, 2000; Zhang and Karathanasis, 1997; Autin and Aslan, 2001; Widdowson., 2007; Achyuthan and Fedoroff, 2008).

Other potential mechanisms for controlling iron oxide cementation are described in previous studies. Chan and others (2000) propose that localized concentrations of iron oxide and manganese oxide in sandstones formed as reduced, saline fluid bearing dissolved metal moved upward along faults and encountered shallower meteoric water. Hill and Polyak (2005) suggest that precipitation of hematite and goethite cements in the Grand Canyon may be triggered by temperature-induced mixing between ascending warm, reduced water and descending cold, oxidized water. Recent iron oxide concretions in sediments near acid-saline lakes in Australia are interpreted as having formed in response to pH and O_2 gradients in the shallow subsurface.

The examples of iron cycling in this southwest Utah study may also have relevance to the recent discovery of concretionary iron oxides on Mars. Hematite concretions on Mars are postulated to have formed in the saturated subsurface through the mixing of acid-saline brine with higher pH/Eh fluid introduced through groundwater recharge (Squyres and Knoll, 2005; McLennan et al., 2005). Iron oxide horizons in the Navajo Sandstone are similar in shape and appearance to a laterally extensive horizon on Mars (the Whatanga contact) that is composed of recrystallized evaporite cement and is interpreted as having formed in the capillary fringe of a paleo water table (Grotzinger et al., 2005; Appendix G). The above examples show that iron oxide can potentially precipitate in a variety of different subaqueous settings, with cement precipitation in each case triggered by the mixing of reactants though processes such as groundwater fluctuation, fluid migration, and localized diffusion.

Integration of Precipitation Models

One possible scenario for the formation of concentrated iron oxide horizons in the Snow Canyon SP area combines elements from several of the models outlined above and assumes that bleached rock in the Navajo Sandstone is the source of iron for subsequent cementation. The near-complete bleaching of both high and low permeability beds implies sustained chemical reduction, accompanied by large volumes of fluid (Parry et al., 2004; Beitler et al., 2005; Nielsen et al., 2009). Because bleached rock occupies the uppermost Navajo Sandstone, the entire formation was likely in the saturated subsurface when bleaching occurred. Although the timing of bleaching remains uncertain, it may be related to the expulsion of deep reduced fluids beginning with Sevier-age thrusting (compare with Eichhubl et al., 2004). For example, burial history modeling for the Iron Springs mining district to the north of Snow Canyon SP (Fig. 4.1) indicates that Paleozoic source rocks reached the thermal maturation window for hydrocarbon generation during Sevier-age deformation, with oil migrating upward along the Iron Springs thrust fault (Van Kooten, 1988). As chemically reducing fluid (hydrocarbon or other) infiltrated high permeability areas in the upper part of the Navajo Sandstone, it could have dissolved iron oxide grain coats and altered the composition of surrounding groundwater (e.g., Selley, 1998; Chidsey et al., 2007; Parry et al., 2009).

Detailed mapping of spatial relationships between bleached and iron enriched zones at Snow Canyon SP (Nielsen and Chan, 2009) shows that dissolved iron did not immediately re-precipitate as iron oxide along bleached boundaries in the upper part of the Navajo Sandstone (although some iron may have been incorporated locally into other iron-bearing minerals [Parry et al., 2009]). Instead, dissolved iron appears to have been transported away from the bleached zone by fluids. One possible triggering mechanism for iron oxide precipitation is the direct mixing of these iron-bearing fluids with unaltered groundwater below the bleached zone. However, it is unclear how oxygen consumed by reactions would be replenished at depths below the reducing zone.

Another possibility is that dissolved iron became widely dispersed within the formation and precipitated at a later stage in response to a change in subsurface chemistry. This overprinting of bleached rock with secondary iron oxide implies a transition from reducing to oxidizing conditions. Possible mechanisms for producing this transition on a large scale include fracturing of the formation (facilitating recharge by oxygenated meteoric water) and/or tectonic uplift and erosion (lowering groundwater levels and associated oxygen gradients). Although timing remains uncertain, these processes could have been associated with either Sevier-age lineament formation (Willis and Higgins, 1996), or Tertiary unroofing of the Navajo Sandstone (Flowers et al., 2008).

Applications

Upper Boundary of the Iron Enrichment Zone as a Marker Horizon

The upper boundary of the iron enrichment zone roughly parallels the top of the Navajo Sandstone and thus functions as a marker horizon. In areas such as Snow Canyon where the top of the Navajo Sandstone is missing, the boundary can be used as a rough field proxy for estimating the orientation of this upper formation surface. Boundary geometry can also be used to predict the location of concretionary lag deposits, which commonly occur where the land surface has eroded to just below the former elevation of an iron oxide horizon (Fig. 4.4B).

Reservoir Characterization and Modeling

The secondary precipitation of iron oxide minerals by migrating fluids selectively follows previously higher-permeability areas such as grainflow deposits in the eolian cross bedding (Fig. 4.8E). Upon cementation, these grainflow strata subsequently become low permeability barriers to further fluid flow in a process we refer to as "permeability inversion" (analogous to the larger geomorphic process of "valley inversion" commonly produced by basalt flows in southwestern Utah [Hamblin 1987; Higgins, 2003]). Permeability inversion is manifest by sheets and slabs of low-permeability ironstone that show concretions or other remnant structures indicative of former solute transport (e.g., Figs. 4.8E-F; 4.9). The localized inversion of permeability means that adjacent sandstones with similar depositional histories may now have vastly different reservoir qualities. For example, some primary red and white bleached sandstones have measured permeabilities of > 1,000 mD, whereas nearby ironstones may have permeabilities of < 10 mD (Table 4.4).

Permeability variations within an eolian sandstone result from a combination of primary heterogeneities associated with eolian bedsets and secondary heterogenetities produced by the precipitation of clays, iron oxide, and other authigenic cements (Uygur, 1980; Lindquist, 1988; Chandler et al., 1989; Tucker, 1991; Net, 2003). Because of these complexities, sandstone color is often an unreliable indicator of permeability. For example, the measured permeability of bleached (white and yellow) sandstones ranges from < 15 mD to > 1400 mD. Although bleaching fluids initially follow high-permeability bedsets, sustained bleaching alters both high and low-permeability bedsets over an entire zone (Nielsen et al., 2009). In addition, later precipitation of clays and other minerals creates additional heterogeneities in otherwise homogeneous-appearing white sandstone (Bowen et al., 2007). The most reliable indicator of permeability is the precipitation of secondary iron oxide cement, which (as opposed to primary grain coats) tends to bridge pore throats, and inhibit fluid flow (Table 4.4).

Permeability measurements from surface plugs in this study (Table 4.4) are generally higher than those from drilled cores (e.g., Lindquist 1988; Net, 2003), likely due to decreased confining pressure and surficial weathering. In contrast, measurements are mostly lower than those obtained using a portable field permeameter from comparable eolian strata in the Page Sandstone of Arizona (Chandler et al., 1989). Consistent with previous studies (Chandler et al., 1989; Selley, 1998), the present analysis shows that permeability in the Navajo Sandstone is generally lower when measured perpendicular to bedding (Table 4.5). Iron oxide cementation enhances this anisotropy because precipitation commonly follows primary permeability boundaries that are subhorizontally oriented in eolian sandstone.

Secondary iron oxide cementation in the Navajo Sandstone occurs both as sporadic, permeability-controlled areas in the lower part of the formation, as well as in concentrated cementation horizons along the upper boundary of the iron enrichment zone. These horizons are locally well-developed along areas up to ~2 m thick, and likely act as high impedance barriers to vertical fluid transmission. They also cut across primary bedding fabric and may disrupt reservoir continuity on a kilometer-scale, truncating primary permeability zones and altering fluid migration pathways. Interaction between these iron oxide horizons and other diagenetic, depositional, and structural barriers can locally segment or compartmentalize a reservoir, with the net result being discontinuous vertical permeability (Selley, 1998; Eichhubl et al., 2004).

Conclusions

Exceptional exposures of the Navajo Sandstone in southwestern Utah enable detailed study of regional patterns of concentrated iron oxide cementation and their impact on reservoir quality. Geospatial, geochemical and petrographic analysis of iron oxide cementation indicates that:

1. Most iron oxide precipitation features (spots, concretions, ironstone sheets, etc.) in the Navajo Sandstone of the southwestern Utah area occur within a broad zone in lower part of the formation. The upper boundary of this zone is commonly marked by concentrated iron oxide cementation, which forms laterally extensive horizons. Iron oxide in these concentrated horizons may locally follow high-permeability bedding features, but typically cuts across bedding fabric on a regional scale.
2. The upper boundary of the iron enrichment zone has a roughly planer (but gently undulating) geometry and subhorizontal orientation that differs only slightly (~2°) from the trend of the top of the Navajo Sandstone. Similarities between iron oxide cementation boundaries at Snow Canyon State Park and Zion National Park suggest these features were produced by similar geochemical processes, and may be spatially correlated.
3. The development of iron oxide horizons is a progressive process, with continued precipitation under favorable conditions resulting in more concentrated cementation and an eventual amalgamation of iron oxide features. Precipitation initially concentrates in high permeability bedforms which, upon further cementation, may become low permeability barriers that disrupt reservoir

continuity ("permeability inversion"). This can alter subsequent fluid migration pathways, resulting in discontinuous vertical permeability.

4. Multiple generations of iron oxide cement provide evidence of geochemical transitions in the subsurface that may be related to regional tectonic controls. Primary iron oxide grain coats likely have an early diagenetic origin, forming during deposition and/or early burial. Secondary pore-filling cements associated with concentrated iron oxide horizons represent a later diagenetic stage that predates Basin and Range extension.

In summary, concentrated iron oxide cementation in the lower Navajo Sandstone of southwestern Utah result from the complex interaction of sedimentologic, hydrodynamic, tectonic, and geochemical factors. These features occur on a regional scale and can result in discontinuous reservoir permeability. Thus, understanding the mechanisms that produce iron oxide cementation has broad implications for predicting fluid flow pathways within other this and other eolian reservoir systems.

Acknowledgements

This study was partially funded by the Utah Geological Survey under the "Characterization of Utah's Natural Gas Reservoirs and Potential New Reserves" initiative. We acknowledge the support of Tom Chidsey, Craig Morgan, Rick Allis, Robert Biek, and others at the Utah Geological Survey who provided support for the project. We also thank Kristin Comella at Snow Canyon State Park and Leslie Courtright of Zion National Park who provided research permits and recommendations for outcrop accessibility. Finally, we express our gratitude to Victor Heilweil with the U.S.

Geological Survey who provided well data and information on the hydrology of southwest Utah.

References

Achyuthan, H., and Fedoroff, N., 2008, Ferricretes in Tamil Nadu, Chennai, south-eastern India: From landscape to micromorphology, genesis, and paleoenvironmental significance, *in* Kapur, S., and Mermut, A., Stoops, G., eds., New trends in soil micromorphology: Berlin Heidelberg, Germany, Springer-Verlag, p. 111-136.

Antonellini, M.A., and Aydin, A., 1994, Effect of faulting on fluid flow in porous sandstones: Petrophysical properties: American Association of Petroleum Geologists Bulletin, v. 78, p. 355– 377.

Appelo, C.A.J. and Postma, D., 2006, Geochemistry, groundwater, and pollution: London, A.A. Balkema Publishers, Second Edition, 649 p.

Autin, W.J., and Aslan, A., 2001, Alluvial pedogenesis in Pleistocene and Holocene Mississippi River deposits: Effects of relative sea-level change: Geological Society of America Bulletin, v. 113, p. 1456–1466.

Back, W. and Barnes, I., 1965, Relation of electrochemical potentials and iron content to ground water flow patterns: U.S. Geological Survey Professional Paper 498C, 16 p.

Barcelona, M.J., Holm, T.R. Schock, M.R. and George, G.K., 1989, Spatial and temporal gradients in aquifer oxidation-reduction conditions: Water Resources Research, v. 25, p. 991- 1003.

Barge, L.M., Petruska, J., Chan, M, Potter, S., and Nealson, K., 2008, Formation of spherical precipitates in diffusion-controlled systems – a possible laboratory analogue for the Martian hematite concretions: Lunar and Planetary Science, v. 39, Abstract 1414.

Barker, D.S., 1995, Crystallization and alteration of quartz monzonite, Iron Springs Mining District, Utah: Relation to associated iron deposits: Economic Geology v. 90, p. 2197-2217.

Beitler, B., Parry, W.T., and Chan, M.A., 2003, Bleaching of Jurassic Navajo Sandstone on Colorado Plateau Laramide highs: Evidence of exhumed hydrocarbon supergiants?: Geology, v. 31, p. 1041–1044.

Beitler, B., Parry, W.T., and Chan, M.A., 2005, Fingerprints of Fluid Flow: Chemical Diagenetic History of the Jurassic Navajo Sandstone, Southern Utah, U.S.A.: Journal of Sedimentary Research, 2005, v. 75, p. 547–561.

Biek, R.F., 2003, Geology of Quail Creek State Park, Utah, *in* Sprinkel, D. A., Chidsey, T.C., Jr., and Anderson, P.B., eds., Geology of Utah's parks and monuments: Utah Geological Association Publication 28, p. 465-477.

Biek, R.F., Willis, G.C., Hylland, M.D., and Doelling, H.H., 2003, Geology of Zion National Park, Utah, *in* Sprinkel, D.A., Chidsey, T.C., and Anderson, P.B., eds., Geology of Utah's Parks and Monuments: Utah Geological Association Publication 28, p. 107–135.

Boving, T.B. and Grathwohl, P., 2001, Tracer diffusion coefficients in sedimentary rocks: correlation to porosity and hydraulic conductivity: Journal of Contaminant Hydrology, v. 53, p. 85-100.

Bowen, B.B., Martini, B.A., Chan, M.A., and Parry, W.T., 2007, Reflectance spectroscopic mapping of diagenetic heterogeneities and fluid-flow pathways in the Jurassic Navajo Sandstone: American Association of Petroleum Geology Bulletin, v. 91, p. 173–190.

Bowen, B.B., Benison, K.C., Oboh-Ikuenobe, F.E., Story, S. and Mormile, M.R., 2008, Active hematite concretion formation in modern acid saline lake sediments, Lake Brown, Western Australia: Earth and Planetary Science Letters, v. 268, p.52-63.

Breit, G.N., 2001, Early diagenetic ferric oxide accumulations formed along redox gradients; examples from modern and ancient fluvial sedimentary units: Geological Society of America Abstracts with Programs, v. 33, p. 281

Britch, S.J., Sherry, J.M., Venn, C., and Hallen, C.P., 2007, Geochemistry of Mineral Spring and its effect on Cold Run, World's End State Park, Sullivan County, Pennsylvania: Geological Society of America Abstracts with Programs, v. 39, p. 101.

Callebaut, F., Gabriels, D., Minjauw, W., and Boodt, M.D., 1982, Redox potential, oxygen diffusion rate, and soil gas composition in relation to water table level in two soils: Soil Science, v. 34, p. 149-156.

Chan, M.A., Parry, W.T., and Bowman, J.R., 2000, Diagenetic hematite and manganese oxides and fault-related fluid flow in Jurassic sandstones southeastern Utah: American Association of Petroleum Geology Bulletin, v. 84, p. 1281–1310.

Chan, M.A., Beitler B., Parry W.T., Ormo, J., and Komatsu, G., 2004, A possible terrestrial analogue for hematite concretions on Mars: Nature, v. 429, p. 731–734.

Chan, M.A., Ormo, J., Park, A.J., Stich, M., Sousa-Egipsy, V., and Komatsu, G., 2007, Models of iron oxide concretion formation: field, numerical, and laboratory comparisons: Geofluids, v. 7, p. 356–368.

Chandler, M.A., Kokurek, G., Goggin, D.J., and Lake, L.W., 1989, Effects of stratigraphic heterogeneity on permeability in eolian sandstone sequence, Page Sandstone, Northern Arizona: American Association of Petroleum Geologists Bulletin, v. 73, p. 658-668.

Chapin, D.M., Jr., 1998, Primary and secondary controls on permeability in a cross-stratified sandstone; implications for the correlation of diagenetic, structural and textural characteristics with laboratory based permeability upscaling measurements: American Association of Petroleum Geologists Bulletin, v.82, p. 2159.

Chernavskiia, D.S., Polezhaeva, A.A., and Müllerb, S.C., 1991, A model of pattern formation by precipitation, Physica D: Nonlinear Phenomena, v. 54, p. 160-170.

Charette, M.A. and Sholkovitz, E.R., 2002. Oxidative precipitation of groundwater-derived ferrous iron in the subterranean estuary of a coastal bay: Geophysical Research Letters v. 29, p. 1444.

Chidsey Jr., T.C., DeHamer, J.S., Hartwick, E.E., Johnson, K.R., Schelling, D.D., Sprinkel, D.A., Strickland, D.K., Vrona, J.P. and Wavrek, D.A., 2007, Petroleum geology of Covenant oil field, central Utah thrust belt, *in* Willis, G.C., Hylland, M.D., Clark, D.L,, and Chidsey Jr., T.C., eds., Central Utah—Diverse geology of a dynamic landscape: Utah Geological Association Publication 36, p. 273–296.

Christensen, P.R., Morris, R.V., Lane, M.D., Bandfield, J.L., and Malin, M.C., 2001, Global mapping of Martian hematite mineral deposits: Remnants of water-driven processes on early Mars: Journal of Geophysical Research, v. 106, p. 873– 885.

Clark, R.N., and Roush, T.L., 1984, Reflectance spectroscopy: Quantitative analysis techniques for remote sensing applications: Journal of Geophysical Research, v. 89, p. 6329–6340.

Clark, R.N., Swayze, G.A., Wise, R., Livo, E., Hoefen, T., Kokaly, R., Sutley, S.J., 2007, USGS digital spectral library splib06a: U.S. Geological Survey, Digital Data Series 231. <speclab.cr.usgs.gov> [accessed 8/15/2009]

Cornell, R.M. and Schwertmann, U., 2003, The iron oxides: structure, properties, reactions, occurrences and uses: Weinheim, Germany, Wiley-VCH, Second Edition, 573 p.

D'Amore, D.V., Stewart, S.R., Huddleston, J.H., 2004. Saturation, reduction, and the formation of iron–manganese concretions in the Jackson–Frazier Wetland, Oregon: Soil Science Society of America Journal, v. 68, p. 1012–1022.

Dapples, 1979, Diagenesis of sandstones, *in* Larsen, G. and Chilingar, G.V., eds., Diagenesis in Sediments and Sedimentary Rocks: New York, Elsevier, p. 31-97.

Davis, G.H., 1999, Structural geology of the Colorado Plateau region of southern Utah with special emphasis on deformation bands: Geological Society of America Special Paper 342, 167 p.

Dominico, P.A., 1990, Physical and chemical hydrogeology: New York, John Wiley and Sons, Inc., 824 p.

Drevor, J.I., 1982, The Geochemistry of natural waters: Englewood Cliffs, New Jersey, Prentice-Hall, 388 p.

Driese, S.G., Stiles, C.A., McKay, L.D., 2002, Mass-balance geochemistry of sedimentary rock saprolite; effects of pedogenesis on variable interbedded lithologies: Geological Society of America Abstracts with Programs, v. 34, p. 105.

Eichhubl, P., Taylor, W.L., Pollard, D.D. and Aydin, A., 2004, Paleo-fluid flow and deformation in the Aztec Sandstone at the Valley of Fire, Nevada-Evidence for the coupling of hydrogeologic, diagenetic, and tectonic processes: Geological Society of America Bulletin, v. 116, p. 1120-1136.

Fairbridge, R.W., 1979, Syndiagenesis-anadiagenesis-epidiagenesis: Phases in lithogenesis, *in* Larsen, G. and Chilingar, G.V., eds., Diagenesis in sediments and sedimentary rocks, 2: New York, Elsevier, p. 17-114.

Fetter, C.W., 1999, Contaminant hydrogeology: Upper Saddle River, New Jersey, Prentice Hall, Second Edition, 500 p.

Flowers, R.M., Wernicke, B.P., and Farley, K.A., 2008, Unroofing, incision, and uplift history of the southwestern Colorado Plateau from apatite (U-Th)/He thermochronology. Geological Society of America Bulletin, v. 120, p. 571-587.

Furniss, G., Hinman, N.W., Doyle, G.A., Runnells, D.D., 1999, Radiocarbon-dated ferricrete provides a record of natural acid rock drainage and paleoclimatic changes: Environmental Geology, v. 37, p. 102-106.

Garden, I.R., Guscott, S.C., Burley, S.D., Foxford, K.A., Walsh, J.J., and Marshall, J., 2001, An exhumed palaeo-hydrocarbon migration fairway in a faulted carrier system, Entrada Sandstone of SE Utah, USA: Geofluids, v. 1, p. 195-213.

George. J. and Varghese, G., 2002, Liesegang patterns: Estimation of diffusion coefficient and a plausible justification for colloid explanation: Colloid Polymer Science, v. 280, p. 131-1136.

Golden, D.C., Ming, D.W., Morris, R.V., Graff, T.G., 2007, Hydrothermal synthesis of hematite rich spherules: implications for diagenesis and hematite spherule formation in outcrops at Meridiani Planum, Mars: Lunar and Planetary Science XXXVIII, Abstract 2257.

Grotzinger, J.P., Arvidson, R.E., Bell, J.F., III, Calvin, W., Clark, B.C., Fike, D.A., Golombek, M., Greeley, R., Haldemann, A., Herkenhoff, K.E., Jolliff, B.L., Knoll, A.H., Malin, M., McLennan, S.M., Parker, T., Soderblom, L., Sohl-Dickstein, J., Squyres, S.W., Tosca, N.J., and Watters, W.A., 2005, Stratigraphy and sedimentology of a dry to wet eolian depositional system, Burns Formation, Meridiani Planum, Mars: Earth and Planetary Science Letters, v. 240, p. 11–72.

Hacker, D.B., Holm, D.K., Rowley, P.D., and Blank, H.R., 2002, Associated Miocene laccoliths, gravity slides, and volcanic rocks, Pine Valley Mountains and Iron Axis region, southwestern Utah, *in* Lund, W.R., ed., Field guide to geologic excursions in southwestern Utah and adjacent areas of Arizona and Nevada: U.S. Geological Survey Open-File Report 02-172, p. 236-283.

Halley, R.B., 1978, Estimating pore and cement volumes in thin section: Journal of Sedimentary Petrology; v. 48, p. 642-650.

Hamblin, W.K., 1987, Late Cenozoic volcanism in the St. George basin, Utah: Geological Society of America Centennial Field Guide – Rocky Mountain Section, p. 291-294.

Hanson, 1996, Hydrodynamics of magmatic and meteoric fluids in the vicinity of granitic intrusions, Geological Society of America Special Papers, v. 315, p. 251-259.

Heilweil, V.M., Freethey, G.W., Stolp, B.J., Wikowske, C.D., Wilberg, D.E., 2000, Geohydrology and numerical simulation of ground-water flow in the central Virgin River basin of Iron and Washington Counties, Utah: U.S. Geological Survey Technical Publication No. 116, 186 p.

Heilweil, V., 2009, U.S. Geological Survey, Written Communication, 10/8/2009.

Higgins, 2003, Geology of Snow Canyon State Park, Utah, *in* Sprinkel, D.A., Chidsey, T.C., Jr., and Anderson, P.B., eds., Geology of Utah's parks and monuments: Utah Geological Association Publication 28, 644 p.

Hill, C.A., Polyak, V.J., 2005, Progressive lowering of the water table in the Grand Canyon as recorded by cave and mine deposits: Geological Society of America Abstracts with Programs, v. 37, p. 16.

Hood, J. W., and D. J. Patterson, 1984, Bedrock aquifers in the northern San Rafael Swell area, Utah, with special emphasis on the Navajo Sandstone: State of Utah Department of Natural Resources Technical Publication No. 78, 128 p.

Hunt, G.R., and Ashley, R.P., 1979, Spectra of altered rocks in the visible and near infrared: Economic Geology, v. 74, p. 816-825.

Hurlow, H.A., 1998, The geology of the central Virgin River Basin, southwestern Utah, and its relation to ground-water conditions: Utah Geological Survey Water Resources Bulletin 26, 53 p., 6 plates.

Hunter, R.E., 1977. Basic types of stratification in small eolian dunes: Sedimentology, v. 24, p. 361-387.

James H.L., 1966, Chemistry of the iron-rich sedimentary rocks, *in* Fleischer M., ed., Data of geochemistry:, Washington D.C, U.S. Govt. Printing Office, Paper 440-W, Sixth Edition, 61 p.

Jepson, R.W., Ashcroft, G.L., Huber, A.L., Skogerbue, G.V., and Bagley, J.M., 1968, Hydrologic atlas of Utah: Logan, Utah, Utah Water Research Laboratory, 306 p.

Kandori, K., Sakai, J., Ishikawa, T., 2000. Definitive effects of chloride ions on the formation of spherical hematite particles in a forced hydrolysis reaction: Physical Chemistry Chemical Physics, v. 2, p. 3293–3299.

Kehew, A.E., 2001, Applied chemical hydrogeology: Upper Saddle River, New Jersey, Prentice Hall, 363 p.

Kimberley, M.M., 1994, Debate about ironstone: Has solute supply been surficial weathering, hydrothermal convection, or exhalation of deep fluids?: Terra Nova, v. 6, p. 116-132.

Kocurek, G., and Dott, R.H., 1981, Distinction and uses of stratification types in the interpretation of eolian sand: Journal of Sedimentary Petrology, v. 51, p. 579-595.

Konhauser, K.O., 1997, Diversity of bacterial iron mineralization: Earth-Science Reviews, v. 43, p. 91-121.

Kowallis, B.J., Christiansen, E.H., Deino, A.L., Zhang, C., and Everett, B.H., 2001, The record of Middle Jurassic volcanism in the Carmel and Temple Cap Formations of southwestern Utah: Geological Society of America Bulletin, v. 113, p. 373-387.

Krumbein, W.C., and Monk, G.D., 1942, Permeability as a function of the size parameters of unconsolidated sands: American Institute of Mining and Metallurgical Engineers Technical Publication 1492, p. 1-11.

Lindquist, S. J., 1988, Practical characterization of eolian reservoirs for development: Nugget Sandstone, Utah-Wyoming thrust belt, *in* Kocurek, G. ed., Late Paleozoic and Mesozoic eolian deposits of the Western Interior of the United States: Sedimentary Geology, v. 56, p. 515-339.

Lund, W.R., Hozik, M.J., and Hatfield, S.C., 2008, Paleoseismic investigation and long-term slip history of the Hurricane fault in southwestern Utah. Utah Geological Survey Publication 119, 81 p.

Machel, H.G., 1987, Some aspects of diagenetic sulphate-hydrocarbon redox reactions, *in* Marshall, J.D., ed., Diagenesis of sedimentary sequences: Geological Society Special Publication 36, p. 15-28.

Mallard, F., Hervant, F., 1999, Oxygen supply and the adaptations of animals in groundwater: Freshwater Biology, v. 41, p. 1-30.

Mason and Kirchner, 1992, Authigenic pyrite: evidence for a microbial origin of tar sand: Fuel, v. 71, p. 1403-1405.

Mazor, E., 2004, Chemical and isotopic groundwater hydrology, New York: Marcel Dekker, Inc., Third Edition, 453 p.

McFarlane, M.J., 1976. Laterite and landscape: London, Academic Press, 151 p.

McKee, E.H., Blank, H.R., and Rowley, P.D., 1995, Potassium-Argon ages of Tertiary igneous rocks in the eastern Bull Valley Mountains and Pine Valley Mountains, southwestern Utah, *in* Maldonado, F. and Nealey, L.D., eds., Geologic studies in the Basin and Range-Colorado Plateau transition in southeastern Nevada, southwestern Utah, and northwestern Arizona: U.S. Geological Survey Bulletin 2153, p. 241-252.

McLennan, S.M., and 31 others, 2005, Provenance and diagenesis of the evaporite-bearing Burns formation, Meridiani Planum, Mars: Earth and Planetary Science Letters. v. 240, p. 95-121.

Milnes, A.R., Bourman, R.P. and Fitzpatrick, F.W., 1987. Petrology and mineralogy of "laterites" in southern and eastern Australia and southern Africa: Chemical Geology, v. 60, p. 237-250.

Morris, R.V., Lauer, H.V., Lawson, C.A., Gibson, E.K. Jr., Nace, G.A., and Stewart, C., 1985, Spectral and other physiochemical properties of submicron powders of hematite, maghemite, maghemite, goethite, and lepidochrosite: Journal of Geophysical Research, v. 90, p. 3126-3144.

Moulton, F.C. and Pinnell, M.L., 2005, Stunning Utah oil, gas discovery focuses spotlight on Hingeline: Oil and Gas Journal, v. 103, p. 42-49.

Müller, S.C. and Ross, J., 2003, Spatial structure formation in precipitation reactions: Journal of Physical Chemistry A, v. 107, p. 7997-8008.

Net, L.I, 2003, Diagenesis and reservoir quality of the Eolian Nugget / Navajo Sandstone (Early Jurassic), Utah and Wyoming [Ph.D. thesis]: Austin, University of Texas, 182 p.

Nielsen, G.B., and Chan, M.A., 2009, Mapping and correlation of diagenetic coloration facies, Jurassic Navajo Sandstone, Snow Canyon State Park, Southwestern Utah, *in* Tripp, B., Krahulec, K., and Jordan, J.L., eds., Geology and geologic resources and issues of western Utah: Utah Geological Association Publication 38, p. 97-123.

Nielsen, G.B., Chan, M.A., and Petersen, E.U., 2009, Diagenetic coloration facies and alteration history of the Jurassic Navajo Sandstone, Zion National Park and vicinity, southwestern Utah, *in* Tripp, B.T., Krahulec, K, and Jordan, J.L., eds., Geology and geologic resources and issues of western Utah: Utah Geological Association Publication 38, p. 67-96.

Ortoleva, P., Merino, E., Moore, C., and Chadam, J., 1987, Geochemical self-organization I; reaction-transport feedbacks and modeling approach: American Journal of Science, v. 287, p. 979-1007.

Ostwald, W., Lehrbuch der Allgemeinen Chemie: Engelmann, Leipzig, Germany, 1897.

Parkhurst, D.L. and Appelo, C.A.J., 1999, User's guide to PHREEQC (version 2) – A computer program for speciation, batch-reaction, one-dimensional transport, and inverse geochemical calculations: U.S. Geological Survey, Water-Resources Investigations Report 99-4259, 312 p.

Parry, W.T., Chan, M.A., and Beitler, B., 2004, Chemical bleaching indicates episodes of fluid flow in deformation bands in sandstone: American Association of Petroleum Geologists Bulletin, v. 88, p. 1–17.

Parry, W.T., Chan, M.A., and Nash, B.P., 2009, Diagenetic characteristics of the Navajo Sandstone in the Covenant oil field, central Utah thrust belt: American Association of Petroleum Geologists Bulletin, v. 93, p. 1031-1061.

Phillips, J.D., 2000, Rapid development of ferricretes on a subtropical valley side slope. Geografiska Annaler, Series A, Physical Geography, v. 82, p. 69-78.

Pipiringos, G.N., and O'Sullivan, R.G., 1978, Principle unconformities in Triassic and Jurassic rocks, western interior U.S.A., preliminary report: U.S. Geological Survey Professional Paper 1035-A, 29 p.

Pirson, S.J., 1983, Geologic well log analysis: Houston, Texas, Gulf Publishing Company, 475 p.

Potter, S.L., 2009, Characterization of Navajo Sandstone Hydrous Ferric Oxide Concretions [M.S. Thesis], Salt Lake City, University of Utah, 180 p.

Prager, S., 1956, Periodic precipitation: Journal of Chemistry and Physics, v. 25, p. 279-283.

Price, M., 1998, Water table, *in* Herschy, R.W. Fairbridge, R.W., eds., Encyclopedia of Hydrology and Water Resources: Norwell, Massachusetts, Kluwer Academic Publishers, 803 p.

Rice, S.A., 1985, Diffusion-limited reactions, *in* Bamford, C.H., Tipper, C.F.H., and Compton, R.G., eds., Comprehensive Chemical Kinetics: New York, Elsevier, v. 25, 404 p.

Robson, S.G. and Banta, E.R., 2005, Ground water atlas of the United States – Arizona, Colorado, New Mexico, Utah: U.S. Geological Survey Hydrologic Investigations Atlas HA730-C, 32 p.

Rock-Color Chart Committee, 1991, Rock Color Charts: Boulder, Colorado, Geological Society of America, 10 p.

Rogers, C.M., Myers, D.A., and Engelder, T., 2004, Kinematic implications of joint zones and isolated joints in the Navajo Sandstone at Zion National Park, Utah: Evidence for Cordilleran relaxation: Tectonics, v. 23, TC1007.

Schumacher, D., 1996, Hydrocarbon-induced alteration of soils and sediments, *in* D. Shumacher, D. and Abrams, M.A., eds., Hydrocarbon migration and its near surface expression: American Association of Petroleum Geologists Memoir 66, p. 71-89.

Schwertmann, U. and Taylor, R.M., 1989, Iron oxides, *in* Dixon, J.B., and Weed, S.B., eds., Minerals in soil environments: Madison, Wisconsin, Soil Science Society of America, Second Edition, p. 379–438.

Schwertman, U. and Cornell, R.M., 2000, Iron oxides in the laboratory: preparation and characterization: New York, Wiley-VCH, Second Edition, 188 p.

Selley, R.C., 1998, Elements of petroleum geology: New York, Academic Press, Second Edition, 470 p.

Spangler, L.E., Naftz, D.L., and Peterman, Z.E., 1996, Hydrology, chemical quality, and characterization of salinity in the Navajo aquifer in and near the Greater Aneth oil field, San Juan County, Utah: U.S. Geological Survey Water-Resources Investigations Report 96-4155, 90 p.

Spiteri, C., Regnier, P., Slomp, C.P., and Charette, M.A., 2005, pH-Dependent iron oxide precipitation in a subterranean estuary, Journal of Geochemical Exploration, v. 88, p. 399–403.

Squyres, S.W., Grotzinger, J.P., Arvidson, R.E., Bell III, J.F., Calvin, W., Christensen, P.R., Clark, B.C., Crisp, J.A., Farrand, W.H., Herkenhoff, K.E., Johnson, J.R., Klingelhöfer, G., Knoll, A.H., McLennan, S.M., McSween Jr., H.Y., Morris, R.V., Rice Jr., J.W., Rieder, R. and Soderblom, L.A., 2004, In situ evidence for an ancient aqueous environment at Meridiani Planum, Mars: Science, v. 306, p. 1709-1714.

Squyres, S.W., Knoll, A.H., 2005, Sedimentary rocks at Meridinai Planum: origin, diagenesis, and implications for life on Mars. Earth Planetary Science Letters, v. 240, p. 1–10.

Tanner, L.H., Khalifa, M.A., 2009, Origin of ferricretes in fluvial-marine deposits of the Lower Cenomanian Bahariya Formation, Bahariya Oasis, Western Desert, Egypt: Journal of African Earth Sciences (in press).

Temgoua, E., Djeuda-Tchapnga, H.B.., Tanawa, E., Guenat, C., Pfeifer, H.R., 2005, Groundwater fluctuations and footslope ferricrete soils in the humid tropical zone of southern Cameroon: Hydrological Processes, v.19, p.3097-3111.

Tucker, M.E., 1991, Sedimentary petrology – an introduction to the origin of sedimentary rocks: Oxford, Blackwell Scientific Publications, Second Edition, 260 p.

Turner, P., 1980, Continental red beds: New York, Elsevier, 562 p.

Utah Geological Survey, 2009, Utah well and spring database. <http://geology.utah.gov/emp/geothermal/wells_springs_database.htm> [accessed 7/22/2009]

Uygur, K., 1980, Hydraulic and petrographic characteristics of the Navajo Sandstone in southern Utah [M.S. thesis], Salt Lake City, University of Utah, 134 p.

Van Kooten, G.K., 1988, Structure and hydrocarbon potential beneath the Iron Springs laccolith, southwestern Utah: Geological Society of America Bulletin, v. 100, p. 1533-1540.

Walker, T.R., 1975, Red beds in the western interior of the United States: U.S. Geological Survey Professional Paper 853, p. 49–56.

Walker, T.R., 1976, Hematite authigenesis in the Moenkopi Formation (Triassic Age), Colorado Plateau: A contribution to the origin of magnetism in red beds: Geological Society of America Abstracts with Programs, v. 8, p. 1158.

Walker, T.R., 1979, Red color in dune sand, *in* McKee, E.D., ed., A study of global sand seas: U.S. Geological Survey Professional Paper 1052, p. 61-68.

Weibel, R., 1998, Diagenesis in oxidising and locally reducing conditions — an example from the Triassic Skagerrak Formation, Denmark: Sedimentary Geology, v. 121, p. 259-276.

Weight, W.D., 2008, Hydrogeology field manual: New York, McGraw Hill, 751 p.

Widdowson, M., 2007, Laterite and ferricrete, *in* Nash, D.J., McLaren, S.J. eds., Geochemical sediments and landscapes: Malden, Massachusetts, Blackwell, p.46–94.

Wilkowske, C.D., Heilweil, V.M., and Wilberg, D.E, 1998, Selected hyrologic data for the central Virgin River Basin area, Washington and Iron Counties, Utah 1915-97: U.S. Geological Survey open-file report, 98-389, 53 p.

Willis, G.C., 1999, The Utah thrust system – an overview, *in* Sprangler, L.E., and Allen, J.J., eds., Geology of northern Utah and vicinity: Utah Geological Association Publication 27, p. 1-9.

Willis, G.C., and Higgins, J.M., 1996, Interim geologic map of the Santa Clara quadrangle, Washington County, Utah: Utah Geological Survey Open-File Report 339, scale 1:24,000, 87 p. text.

Willis, G.C., Biek, R.F., and Higgins, J.M., 1999, New $^{40}Ar/^{39}Ar$ ages of basalt flows in the lower Virgin River basin of southwest Utah – implications for volcanic, faulting, and downcutting histories: Geological Society of America Abstracts with Programs, v. 33, p. A-61.

Wray, W.D., and Pedersen, A.D., 2009, Iron resources and geology of the property of Palladon Ventures Ltd. in the Iron Mountain area, Iron County, Utah, *in* Tripp, B.T., Krahulec, K, and Jordan, J.L., eds., Geology and geologic resources and issues of western Utah: Utah Geological Association Publication 38, p. 157-167.

Wolfe, K.H. and Chilingarian, G.V., 1988, Ore-related diagenesis – an encyclopedic review, *in*, Chilingarian, G.V. and Wolf, K.H., eds., Diagenesis 1: New York, Elsevier, p. 25-554.

Wood, J.R. and Hewett, T.A., 1984, Reservoir diagenesis and convective fluid flow: American Association of Petroleum Geologists Memoir 37, p. 99-110.

Wright, V.P., Sloan, R.J., Valero Garcés, B., and Garview, L.A.J., 1992, Groundwater ferricretes from the Silurian of Ireland and Permian of the Spanish Pyrenees: Sedimentary Geology, v. 77, p. 37-47.

Yap, C.J., 1997, An assessment of isotopic equilibrium in goethites from a bog iron deposit and a lateritic regolith: Chemical Geology v. 135, p. 159-171.

Zhang, M., and Karathanasis, A.D., 1997, Characterization of iron-manganese concretions in Kentucky alfisols with perched water tables: Clays and Clay Minerals, v. 45, p. 428-439.

APPENDIX A

CODED MUNSELL COLORS FOR NAVAJO SANDSTONE SAMPLES

Table A.1

Munsell colors for diagenetic facies and subfacies

Diagenetic Facies	**Subfacies**	**Characteristic Munsell Colors**
Red Primary	-	• Moderate reddish orange (10R 6/6, 7/6)
Red/White Intermixed	-	• Moderate reddish orange (10R 6/6, 7/6) • Very pale orange (10YR 8/2)
Multicolored Local	Liesegang Banded	• Pale yellowish orange (10YR 8/6) • Moderate reddish orange (10YR 8/6) • Dark yellowish orange (10YR 6/6)
	Yellow/Orange Patchy	• Pale yellowish orange (10YR 8/6) • Moderate reddish orange (10YR 8/6) • Dark yellowish orange (10YR 6/6)
White Bleached	Tan	• Grayish orange (10YR 7/4)
	White Speckled	• Very pale orange (10YR 8/2) • Grayish brown (5YR 3/2)
	White	• Very pale orange (10YR 8/2)
	Yellow	• Dark yellowish orange (10YR 8/2) • Grayish orange (10YR 7/4) • Very pale orange (10YR 8/2)
Pink Altered	Uneven Red/Orange	• Moderate orange pink (5YR 7/4) • Moderate reddish orange (10R 6/6) • Pale reddish brown (10R 5/4) • Very pale orange (10YR 8/2)
	Ferruginous Lens	• Dusky yellowish brown (10YR 2/2)
Brown Ferruginous	Overprinted White	• Light brown (5YR 6/4) • Moderate brown (5YR 4/4) • Grayish black (N2)
	Overprinted Red	• Moderate brown (5YR 4/4) • Light brown (5YR 5/6)
	Green and Brown	• Grayish green (10GY 5/2) • Light brown (5YR 5/6)
	Ironstone	• Grayish brown (5 YR 3/2) • Moderate brown (5YR 4/4) • Dusky yellowish brown (10 YR 2/2)

Rock colors coded using the standardized Munsell system (Rock-Color Chart Committee, 1991). This system specifies colors based upon three dimensions: hue (designated with a number and a letter), value or "brightness" (range 0 for black to 10 for white), and chroma or "saturation" (range 0 for neutral gray to 30 for vivid colors).

References

Rock-Color Chart Committee, 1991, Rock color charts: Boulder, Colorado: Geological Society of America, 10 p.

APPENDIX B

BULK COMPOSITION (ICP-MS) DATA FOR THE NAVAJO SANDSTONE

Partially published in Utah Geological Survey, 2010, Open-File Report 561
Gregory B. Nielsen and Marjorie A. Chan
Used with permission.

Table B.1

Bulk composition (ICP-MS) of Navajo Sandstone samples from Snow Canyon State Park and vicinity.

#	Formation	Facies	Subfacies	Class	Subclass
1	Navajo Sandstone	Brown Ferruginous	Ironstone	Ironstone	
2	Navajo Sandstone	Brown Ferruginous	Ironstone	Ironstone	
3	Navajo Sandstone	Brown Ferruginous	Overprinted Red	Ferruginous Ss	Mixed
4	Navajo Sandstone	Brown Ferruginous	Overprinted Red	Ferruginous Ss	Secondary (overprinted)
5	Navajo Sandstone	Brown Ferruginous	Overprinted Red	Ferruginous Ss	Secondary (overprinted)
6	Navajo Sandstone	Brown Ferruginous	Overprinted Red	Ferruginous Ss	Secondary (overprinted)
7	Navajo Sandstone	Brown Ferruginous	Overprinted White	Ferruginous Ss	Secondary (replaced)
8	Navajo Sandstone	Multicolored Local	Yellow/Orange Patchy	Ferruginous Ss	Secondary (replaced)
9	Navajo Sandstone	Multicolored Local	Yellow/Orange Patchy	Ferruginous Ss	Secondary (replaced)
10	Navajo Sandstone	Red Primary	-	Ferruginous Ss	Primary
11	Navajo Sandstone	Red Primary	-	Ferruginous Ss	Primary
12	Navajo Sandstone	Red/White Intermixed	-	Bleached Ss	
13	Navajo Sandstone	Red/White Intermixed	-	Bleached Ss	
14	Navajo Sandstone	Red/White Intermixed	-	Ferruginous Ss	Primary
15	Navajo Sandstone	Red/White Intermixed	-	Ferruginous Ss	Secondary (mixed)
16	Navajo Sandstone	Red/White Intermixed	-	Ferruginous Ss	Secondary (mixed)
17	Navajo Sandstone	Red/White Intermixed	-	Ferruginous Ss	
18	Navajo Sandstone	Red/White Intermixed	-	Ferruginous Ss	
19	Navajo Sandstone	White Bleached	Tan	Ferruginous Ss	Secondary (replaced)
20	Navajo Sandstone	White Bleached	White	Bleached Ss	
21	Navajo Sandstone	White Bleached	Yellow	Bleached Ss	
22	Navajo Sandstone	White Bleached	Yellow	Bleached Ss	

Table B.1 continued

#	Locality	Area	Specimen ID	Brief Description
1	Sand Hollow	Concretion Knoll	Gr20050801-0	Dark, dense, concretionary ironstone.
2	Sand Hollow	Concretion Knoll	Gr20061213-1700	Very dense black ironstone.
3	Snow Canyon SP	Main Canyon	Gr20061218-1640	Red sandstone with dark oxidized outer surface.
4	Snow Canyon SP	"Butterfly Rock"	Gr20060402-1	Brown uniformly colored sandstone.
5	Snow Canyon SP	West Canyon	Gr20051208-3	Dark ferruginous sandstone with contorted banding.
6	Snow Canyon SP	West Canyon	Gr20060000-0	Brownish-red sandstone with poorly developed concretions.
7	Snow Canyon SP	SR 18 Trailhead	Gr20061219-1314A	White sandstone matrix with brown and black patches.
8	Snow Canyon SP	Three Ponds North	Gr20060401-2	Patchy yellow and orange sandstone.
9	Snow Canyon SP	White Rocks	Gr20051210-6B	Brightly colored patchy orange and yellow sandstone.
10	Snow Canyon SP	"Butterfly Rock"	Gr20060402-5	Uniform red sandstone.
11	Snow Canyon SP	Padre Canyon	Gr20060402-3	Red sandstone from flat-bedded base of Navajo Ss.
12	Snow Canyon SP	Three Ponds North	Gr20051001-6a	White sandstone from zone of intermixed red/white coloration.
13	Snow Canyon SP	Three Ponds North	Gr20060401-1	Yellow sandstone with gray bands.
14	Snow Canyon SP	Three Ponds North	Gr20060401-3	Mottled red sandstone
15	Red Cliffs Reserve	Bones Wash	Gr20061219-1504A	Purplish red sandstone (separated frompinstriped sample)
16	Red Cliffs Reserve	Bones Wash	Gr20061219-1504B	Light yellow sandstone (separated from pinstriped sample)
17	Snow Canyon SP	Three Ponds South	Gr20061218-1455A	Reddish sandstone from intermixed red/white zone.
18	Snow Canyon SP	Three Ponds South	Gr20061218-1455B	White sandstone from interlinear red/white outcrop.
19	Snow Canyon SP	North Rim	Gr20061214-1500	Tannish sandstone, reddish brown on weathered surface.
20	Snow Canyon SP	White Rocks	Gr20051210-5C	Completely bleached sandstone from area of zonal bleaching.
21	Snow Canyon SP	"Butterfly Rock"	Gr20050929-3	Yellow sandstone with small brownish-yellow specks.
22	Snow Canyon SP	White Rocks	Gr20060331-1	Uniform yellow sandstone.

Table B.1 continued

#	Fe_2O_3(T) %	MnO %	MgO %	CaO %	Na_2O %	K_2O %	TiO_2 %	P_2O_5 %	LOI %	Oxide Total %	Ag ppm	As ppm	Ba ppm	Be ppm	Bi ppm
1	19.32	0.10	0.09	0.79	0.05	0.47	0.02	0.10	3.09	98.52	< 0.5	208.00	109.00	4.00	4.70
2	29.9	2.529	0.11	0.15	0.08	0.93	0.027	0.08	4.85	100	< 0.5	27	1298	< 1	< 0.1
3	1.27	0.008	0.05	0.07	0.04	0.35	0.032	0.06	0.42	99.82	< 0.5	< 5	58	< 1	< 0.1
4	3.05	0.01	0.05	0.03	0.05	0.49	0.07	0.04	0.96	98.92	< 0.5	62.00	91.00	< 1	1.80
5	1.58	0.19	0.13	0.09	0.04	0.39	0.05	0.07	1.36	99.22	< 0.5	38.00	282.00	< 1	1.00
6	1.65	0.07	0.07	0.03	0.05	0.46	0.04	0.04	0.93	98.69	< 0.5	36.00	156.00	< 1	0.90
7	4.39	2.6	0.1	0.72	0.04	0.42	0.02	0.09	2.32	100.8	< 0.5	143	992	2	< 0.1
8	0.71	0.00	0.06	0.02	0.07	0.70	0.03	0.05	0.79	98.66	< 0.5	7.00	472.00	< 1	0.30
9	0.72	0.00	0.07	0.03	0.05	0.80	0.21	0.04	1.09	99.51	< 0.5	8.00	146.00	< 1	1.00
10	0.58	0.01	0.05	0.02	0.05	0.53	0.05	0.04	0.63	98.67	< 0.5	< 5	108.00	< 1	0.20
11	0.57	0.00	0.07	0.03	0.05	0.55	0.03	0.03	0.31	98.84	< 0.5	< 5	89.00	< 1	0.50
12	0.45	0.00	0.03	0.02	0.06	0.44	0.03	0.04	0.53	98.77	< 0.5	< 5	92.00	< 1	0.40
13	0.31	0.02	0.04	0.05	0.04	0.33	0.02	0.04	0.48	98.51	< 0.5	< 5	69.00	< 1	0.30
14	0.73	0.01	0.05	0.02	0.05	0.44	0.02	0.04	0.68	99.44	< 0.5	9.00	75.00	< 1	< 0.1
15	1.6	0.012	0.06	0.06	0.07	0.74	0.069	0.02	0.56	99.86	< 0.5	< 5	151	< 1	< 0.1
16	1.43	0.023	0.1	0.09	0.08	1.05	0.204	0.02	0.96	99.01	< 0.5	< 5	201	< 1	< 0.1
17	0.97	0.008	0.09	0.02	0.04	0.88	0.162	0.04	0.99	100.3	< 0.5	< 5	145	< 1	< 0.1
18	0.6	0.004	0.03	0.02	0.09	0.22	0.023	0.03	0.45	100.7	< 0.5	< 5	66	< 1	< 0.1
19	0.88	0.006	0.08	0.04	0.1	0.92	0.066	0.04	1.25	100	< 0.5	10	194	< 1	< 0.1
20	0.20	0.00	0.06	0.02	0.07	1.04	0.11	0.04	0.89	99.65	< 0.5	< 5	175.00	< 1	0.60
21	0.47	0.00	0.05	0.03	0.07	0.81	0.05	0.05	0.68	99.22	< 0.5	6.00	137.00	< 1	0.70
22	0.45	0.00	0.05	0.02	0.07	0.74	0.04	0.04	0.61	99.29	< 0.5	22.00	168.00	< 1	0.40

Table B.1 continued

#	Co ppm	Cr ppm	Cs ppm	Cu ppm	Dy ppm	Er ppm	Eu ppm	Ga ppm	Gd ppm	Ge ppm	Hf ppm	Ho ppm	In ppm	La ppm	Lu ppm	Mo ppm	Nb ppm
1	33.00	< 20	0.50	20.00	1.65	0.77	0.46	2.00	1.74	9.70	0.70	0.30	< 0.1	3.41	0.10	11.00	0.50
2	137	< 20	0.6	20	4.23	1.79	1.78	6	5.54	1	0.9	0.71	< 0.1	4.78	0.206	6	0.7
3	1	< 20	0.4	< 10	0.36	0.24	0.103	2	0.34	1	1.2	0.08	< 0.1	2.59	0.045	< 2	0.6
4	2.00	< 20	0.90	< 10	0.66	0.46	0.19	3.00	0.67	3.00	2.10	0.14	< 0.1	4.02	0.09	< 2	1.10
5	10.00	20.00	1.00	40.00	0.86	0.48	0.28	3.00	1.03	1.30	0.90	0.16	< 0.1	6.83	0.07	< 2	0.90
6	5.00	< 20	1.00	20.00	0.58	0.35	0.22	3.00	0.64	1.30	0.90	0.12	< 0.1	4.10	0.05	< 2	0.70
7	69	70	0.6	< 10	0.98	0.5	0.389	5	1.01	1.4	0.7	0.19	< 0.1	2.21	0.062	< 2	0.4
8	< 1	< 20	0.80	< 10	0.55	0.31	0.21	2.00	0.63	1.50	0.70	0.10	< 0.1	3.44	0.05	< 2	0.60
9	< 1	< 20	0.80	< 10	1.05	0.77	0.30	3.00	1.07	1.00	8.90	0.23	< 0.1	6.65	0.16	2.00	2.80
10	< 1	< 20	0.70	< 10	0.54	0.31	0.17	2.00	0.58	1.00	1.00	0.11	< 0.1	3.46	0.05	< 2	0.70
11	3.00	< 20	1.20	< 10	0.35	0.22	0.08	1.00	0.34	0.80	1.00	0.07	< 0.1	2.19	0.04	< 2	0.50
12	1.00	30.00	0.40	20.00	0.44	0.24	0.16	1.00	0.53	1.00	0.70	0.08	< 0.1	2.93	0.04	< 2	0.50
13	< 1	< 20	0.40	< 10	0.32	0.21	0.09	1.00	0.33	0.80	0.60	0.07	< 0.1	2.26	0.03	< 2	0.30
14	< 1	< 20	0.60	< 10	0.44	0.26	0.15	2.00	0.54	1.20	0.60	0.09	< 0.1	2.87	0.04	< 2	0.40
15	2	< 20	0.9	10	0.61	0.38	0.176	4	0.58	1.2	1.9	0.12	< 0.1	3.65	0.07	< 2	1.3
16	2	510	1.4	10	0.98	0.68	0.269	5	0.85	1.3	7.6	0.21	< 0.1	5.5	0.149	< 2	3
17	1	< 20	1.4	< 10	0.92	0.69	0.312	4	0.89	1.2	6.9	0.21	< 0.1	4.64	0.144	< 2	2.3
18	< 1	110	0.5	< 10	0.4	0.24	0.109	2	0.4	1.1	0.6	0.08	< 0.1	2.49	0.037	< 2	0.5
19	1	90	0.8	< 10	0.59	0.37	0.217	5	0.62	1.3	1.4	0.12	< 0.1	4.94	0.058	< 2	1.1
20	< 1	< 20	0.80	< 10	0.73	0.48	0.29	3.00	0.82	1.00	3.70	0.15	< 0.1	4.93	0.09	< 2	1.60
21	< 1	30.00	0.80	< 10	0.63	0.34	0.20	2.00	0.64	1.00	1.30	0.12	< 0.1	3.87	0.05	< 2	0.90
22	< 1	< 20	0.70	< 10	0.55	0.30	0.22	2.00	0.65	1.00	0.80	0.10	< 0.1	3.42	0.05	< 2	0.70

Table B.1 continued

#	Ni ppm	Pb ppm	Pr ppm	Rb ppm	Sb ppm	Sc ppm	Sm ppm	Sn ppm	Sr ppm	Ta ppm	Tb ppm	Th ppm	Tl ppm	Tm ppm	U ppm	V ppm	W ppm
1	90.00	21.00	0.89	12.00	4.30	22.00	1.37	< 1	20.00	0.04	0.31	1.17	0.28	0.11	0.98	43.00	< 0.5
2	110	23	1.31	23	< 0.2	22	4.48	2	106	0.05	0.87	1.63	0.48	0.236	1.12	71	5.1
3	< 20	< 5	0.55	9	< 0.2	< 1	0.42	2	16	0.06	0.06	0.82	0.13	0.039	0.31	< 5	1.3
4	< 20	11.00	0.84	15.00	7.80	5.00	0.68	< 1	68.00	0.10	0.11	0.99	0.30	0.08	1.76	21.00	20.80
5	< 20	9.00	1.49	14.00	0.80	2.00	1.13	7.00	52.00	0.10	0.15	1.63	1.84	0.07	0.82	16.00	11.50
6	< 20	18.00	0.92	15.00	1.90	2.00	0.74	3.00	72.00	0.08	0.10	0.99	2.25	0.06	0.87	12.00	4.00
7	60	5	0.61	13	< 0.2	4	1.01	3	125	0.07	0.17	0.65	16.1	0.067	2.93	38	18.2
8	< 20	11.00	0.84	20.00	1.30	< 1	0.71	< 1	105.00	0.08	0.10	0.84	0.17	0.05	0.20	< 5	1.50
9	< 20	20.00	1.47	24.00	1.20	2.00	1.11	< 1	76.00	0.28	0.17	1.79	0.37	0.13	1.12	35.00	4.20
10	< 20	7.00	0.83	17.00	1.10	< 1	0.67	< 1	82.00	0.08	0.09	0.89	0.13	0.05	0.23	< 5	2.40
11	< 20	< 5	0.47	14.00	0.90	< 1	0.38	< 1	13.00	0.06	0.06	0.76	0.10	0.04	0.27	< 5	< 0.5
12	< 20	9.00	0.73	12.00	2.10	< 1	0.59	2.00	87.00	0.12	0.08	0.83	0.09	0.04	0.15	< 5	< 0.5
13	< 20	17.00	0.54	8.00	0.50	< 1	0.42	< 1	13.00	0.06	0.05	0.70	0.22	0.03	0.18	< 5	< 0.5
14	< 20	6.00	0.68	12.00	0.90	< 1	0.60	< 1	85.00	0.07	0.08	0.75	0.10	0.04	0.16	< 5	1.70
15	< 20	6	0.77	23	< 0.2	< 1	0.59	2	24	0.12	0.1	1.13	0.23	0.062	0.3	7	< 0.5
16	< 20	7	1.17	34	< 0.2	1	0.85	3	34	0.29	0.15	1.53	0.29	0.116	0.58	10	< 0.5
17	< 20	9	1.08	26	< 0.2	1	0.96	2	123	0.23	0.15	1.39	0.18	0.115	0.49	8	0.7
18	< 20	< 5	0.55	9	0.2	< 1	0.43	3	62	0.05	0.07	0.84	0.07	0.039	0.18	< 5	< 0.5
19	< 20	8	1.06	26	< 0.2	< 1	0.75	< 1	73	0.12	0.1	1.36	0.47	0.057	0.27	12	< 0.5
20	< 20	14.00	1.13	30.00	0.70	< 1	0.95	< 1	108.00	0.15	0.13	1.16	0.25	0.08	0.42	< 5	1.30
21	< 20	9.00	0.90	23.00	0.50	< 1	0.73	< 1	112.00	0.08	0.11	0.88	0.16	0.05	0.23	< 5	6.00
22	< 20	12.00	0.83	22.00	1.30	1.00	0.76	< 1	80.00	0.07	0.10	0.87	0.24	0.05	0.22	8.00	1.20

Table B.1 continued

#	Yb ppm	Zn ppm	Zr ppm
1	0.64	230.00	34.00
2	1.4	420	33
3	0.28	< 30	49
4	0.56	30.00	90.00
5	0.44	30.00	33.00
6	0.36	< 30	38.00
7	0.4	170	22
8	0.31	< 30	23.00
9	0.97	< 30	383.00
10	0.33	< 30	40.00
11	0.24	< 30	39.00
12	0.23	< 30	26.00
13	0.23	< 30	24.00
14	0.26	< 30	23.00
15	0.42	< 30	72
16	0.86	< 30	319
17	0.84	< 30	288
18	0.26	< 30	21
19	0.38	< 30	58
20	0.55	< 30	152.00
21	0.34	< 30	56.00
22	0.30	< 30	33.00

Table B.2

Bulk composition of Navajo Sandstone samples from Zion National Park.

#	Formation	Facies	Subfacies	Class	Subclass
23	Navajo Sandstone	Brown Ferruginous	Green and Brown	Ferruginous Ss	Secondary (overprinted)
24	Navajo Sandstone	Brown Ferruginous	Overprinted Red	Ferruginous Ss	Mixed
25	Navajo Sandstone	Brown Ferruginous	Overprinted Red	Ferruginous Ss	Secondary (overprinted)
26	Navajo Sandstone	Brown Ferruginous	Overprinted Red	Ferruginous Ss	Secondary (overprinted)
27	Navajo Sandstone	Brown Ferruginous	Overprinted Red	Ferruginous Ss	Secondary (overprinted)
28	Navajo Sandstone	Multicolored Local	Liesegang-Banded	Ferruginous Ss	Secondary (mixed)
29	Navajo Sandstone	Multicolored Local	Yellow/Orange Patchy	Ferruginous Ss	Secondary (replaced)
30	Navajo Sandstone	Pink Altered	Ironstone Lens	Ironstone	
31	Navajo Sandstone	Pink Altered	Uneven Red/Orange	Ferruginous Ss	Secondary (mixed)
32	Navajo Sandstone	Pink Altered	Uneven Red/Orange	Ferruginous Ss	Secondary (replaced)
33	Navajo Sandstone	Red Primary	-	Ferruginous Ss	Primary
34	Navajo Sandstone	Red/White Intermixed	-	Ferruginous Ss	
35	Navajo Sandstone	Red/White Intermixed	-	Ferruginous Ss	
36	Navajo Sandstone	White Bleached	White Speckled	Ferruginous Ss	Replaced
37	Navajo Sandstone	White Bleached	Yellow	Ferruginous Ss	

Table B.2 continued

#	Locality	Area	Specimen ID	Brief Description
23	Zion NP	Canyon Overlook Trail	Gr20070318-1319	Sandstone with intermixed green and brown coloration.
24	Zion NP	Taylor Creek Canyon	Gr20061216-1454	Fairly uniform red sandsonte with some
25	Zion NP	Angel's Landing Trail	Gr20061220-1318	Spotty brown sandstone from near Fe enrichment boundary.
26	Zion NP	Canyon Overlook Trail	Gr20070318-1320	Spotty brown sandstone from just below Fe boundary.
27	Zion NP	East Rim Trail	Gr20061214-1147	Uniform reddish sandstone with numerous small brown spots.
28	Zion NP	East Rim Trail	Gr20061214-1517	Bright pink and yellow Liesegang-banded sandstone.
29	Zion NP	Canyon Overlook Trail	Gr20070318-1202	Patchy gray and orange sandstone.
30	Zion NP	Angel's Landing Trail	Gr20061220-1438	Dense concretionary ironstone lens.
31	Zion NP	East Rim Trail	Gr20061214-1355	Pink sandstone with localized areas of darker cementation.
32	Zion NP	Canyon Overlook Trail	Gr20070318-1235	White sandstone with small orange specs.
33	Zion NP	Taylor Creek Canyon	Gr20061216-1552	Uniform red sandstone.
34	Zion NP	Hop Valley	Gr20070317-1413A	Uniform red sandstone from intermixed red/white zone.
35	Zion NP	Hop Valley	Gr20070317-1413B	White bleached with brown specks from intermixed r/w zone.
36	Zion NP	East Rim Trail	Gr20061214-1603	Tannish-white sandstone with small brown specks.
37	Zion NP	East Rim Trail	Gr20061214-1621	Yellow and brownish yellow sandstone.

Table B.2 continued

#	Fe_2O_3(T) %	MnO %	MgO %	CaO %	Na_2O %	K_2O %	TiO_2 %	P_2O_5 %	LOI %	Oxide Total %	Ag ppm	As ppm	Ba ppm	Be ppm	Bi ppm
23	1.54	0.09	0.69	12.38	0.05	0.62	0.015	0.02	10.82	99.91	< 0.5	< 5	120	< 1	< 0.1
24	1.33	0.006	0.12	0.09	0.08	1.42	0.113	0.05	0.88	99.96	< 0.5	< 5	215	< 1	< 0.1
25	1.77	0.01	0.02	0.03	0.07	1.51	0.061	0.03	0.28	99.87	< 0.5	< 5	188	< 1	< 0.1
26	1.13	0.096	0.14	11.31	0.09	2.05	0.081	0.1	9.39	100.1	< 0.5	< 5	272	< 1	< 0.1
27	0.8	0.036	0.08	0.07	0.22	2.72	0.161	0.06	1	99.46	< 0.5	10	338	< 1	< 0.1
28	1.4	0.01	0.06	0.12	0.08	1.1	0.034	0.02	0.25	100.4	< 0.5	< 5	164	< 1	< 0.1
29	2.57	0.018	0.03	0.04	0.2	1.39	0.038	0.03	-0.24	96.72	< 0.5	< 5	171	< 1	< 0.1
30	13.22	0.041	0.09	0.04	0.04	0.42	0.038	0.06	2.35	100.2	< 0.5	266	64	2	< 0.1
31	1.18	0.011	0.04	0.03	0.18	1.84	0.032	0.03	0.29	99.99	< 0.5	< 5	236	< 1	< 0.1
32	0.72	0.004	0.03	0.04	0.44	1.8	0.108	0.04	0.25	98.19	< 0.5	< 5	204	< 1	< 0.1
33	0.77	0.004	0.08	0.06	0.06	1.2	0.037	0.03	0.65	100.1	< 0.5	< 5	163	< 1	< 0.1
34	0.7	0.006	0.04	0.02	0.04	0.5	0.025	0.02	0.21	100.3	< 0.5	< 5	52	< 1	< 0.1
35	1.87	0.009	0.06	0.21	0.3	1.42	0.084	0.15	-0.15	95.77	< 0.5	< 5	129	< 1	< 0.1
36	1.24	0.008	0.07	0.04	0.09	1.54	0.061	0.03	0.16	99.88	< 0.5	< 5	257	< 1	< 0.1
37	0.69	0.004	0.04	0.02	0.15	1.12	0.032	0.01	0.52	98.07	< 0.5	6	23150	< 1	< 0.1

Table B.2 continued

#	Co ppm	Cr ppm	Cs ppm	Cu ppm	Dy ppm	Er ppm	Eu ppm	Ga ppm	Gd ppm	Ge ppm	Hf ppm	Ho ppm	In ppm	La ppm	Lu ppm	Mo ppm	Nb ppm
23	2	< 20	0.3	< 10	0.42	0.27	0.095	2	0.39	0.8	0.5	0.09	< 0.1	1.76	0.042	< 2	0.4
24	1	< 20	1.2	< 10	0.87	0.53	0.337	4	0.94	1.1	3.2	0.17	< 0.1	5	0.092	< 2	1.8
25	2	30	0.6	10	0.35	0.29	0.101	4	0.28	1.3	2.1	0.08	< 0.1	1.87	0.056	< 2	1.1
26	2	60	0.8	< 10	0.6	0.39	0.228	3	0.65	0.8	2	0.13	< 0.1	3.11	0.064	< 2	1.4
27	2	70	1	10	0.91	0.62	0.315	5	0.89	1.3	5.3	0.19	< 0.1	4.93	0.123	< 2	2.1
28	1	< 20	0.6	< 10	0.54	0.3	0.203	2	0.63	1	0.8	0.11	< 0.1	3.11	0.045	< 2	0.7
29	3	< 20	0.6	20	0.45	0.26	0.146	2	0.44	1.1	0.9	0.09	< 0.1	2.52	0.043	< 2	1
30	10	170	0.5	10	0.88	0.52	0.222	3	0.77	2.5	0.9	0.18	< 0.1	5.9	0.071	5	0.8
31	2	< 20	0.9	< 10	0.57	0.32	0.24	4	0.63	1.1	0.7	0.11	< 0.1	3.52	0.048	< 2	0.8
32	< 1	120	0.8	< 10	0.76	0.49	0.231	3	0.74	1.1	4.5	0.16	< 0.1	4.32	0.103	< 2	1.7
33	< 1	140	0.8	< 10	0.45	0.27	0.174	3	0.49	1.1	1	0.09	< 0.1	3.2	0.043	< 2	0.7
34	< 1	120	0.3	< 10	0.3	0.2	0.054	2	0.26	0.9	0.8	0.06	< 0.1	1.96	0.035	< 2	0.6
35	2	< 20	0.5	10	0.47	0.33	0.124	3	0.45	1.1	3.4	0.1	< 0.1	2.6	0.07	< 2	1.3
36	2	< 20	0.9	10	0.65	0.38	0.247	4	0.69	1.2	1.6	0.13	< 0.1	4.11	0.063	< 2	1.2
37	< 1	100	0.8	< 10	0.44	0.27	0.274	3	0.44	1.1	1.2	0.09	< 0.1	3.05	0.044	< 2	0.7

Table B.2 continued

#	Ni ppm	Pb ppm	Pr ppm	Rb ppm	Sb ppm	Sc ppm	Sm ppm	Sn ppm	Sr ppm	Ta ppm	Tb ppm	Th ppm	Tl ppm	Tm ppm	U ppm	V ppm	W ppm
23	< 20	< 5	0.43	23	< 0.2	< 1	0.34	1	21	0.03	0.07	0.58	< 0.05	0.039	0.28	< 5	< 0.5
24	< 20	8	1.18	41	< 0.2	1	1.04	2	35	0.17	0.15	1.2	0.23	0.082	0.46	6	< 0.5
25	< 20	6	0.37	33	< 0.2	< 1	0.27	2	21	0.11	0.05	1.12	0.18	0.047	0.41	7	0.6
26	< 20	7	0.79	44	< 0.2	< 1	0.68	2	40	0.14	0.1	1.11	0.19	0.061	0.7	6	< 0.5
27	< 20	< 5	1.19	57	< 0.2	2	0.95	2	48	0.24	0.15	1.25	0.3	0.1	0.63	11	< 0.5
28	< 20	< 5	0.74	25	< 0.2	< 1	0.61	1	18	0.07	0.1	0.86	0.16	0.043	0.41	< 5	< 0.5
29	< 20	< 5	0.57	29	< 0.2	< 1	0.48	2	19	0.07	0.07	0.87	0.14	0.039	0.47	< 5	< 0.5
30	30	8	1.23	10	0.7	3	0.84	2	31	0.07	0.14	2.5	0.09	0.074	11.4	38	1.1
31	< 20	7	0.86	41	< 0.2	1	0.67	2	25	0.08	0.1	0.93	0.21	0.049	0.92	8	< 0.5
32	< 20	< 5	1	40	< 0.2	4	0.79	2	23	0.18	0.12	1.34	0.19	0.08	0.64	24	< 0.5
33	< 20	< 5	0.71	29	< 0.2	< 1	0.53	2	24	0.08	0.08	0.82	0.17	0.042	0.28	< 5	1.2
34	< 20	< 5	0.39	11	< 0.2	< 1	0.27	3	7	0.06	0.05	0.82	0.06	0.032	0.28	< 5	< 0.5
35	< 20	< 5	0.61	27	< 0.2	< 1	0.48	2	19	0.13	0.08	1.05	0.13	0.053	0.42	12	< 0.5
36	< 20	8	0.93	42	< 0.2	< 1	0.78	2	33	0.12	0.11	1.04	0.24	0.059	0.57	7	< 0.5
37	< 20	6	0.63	30	< 0.2	1	0.47	2	100	0.55	0.07	0.88	0.18	0.043	0.37	7	0.6

Table B.2 continued

#	Yb ppm	Zn ppm	Zr ppm
23	0.26	< 30	21
24	0.57	< 30	138
25	0.34	< 30	86
26	0.41	< 30	84
27	0.73	< 30	224
28	0.28	< 30	34
29	0.26	< 30	43
30	0.45	60	34
31	0.32	< 30	34
32	0.58	< 30	195
33	0.28	< 30	41
34	0.22	< 30	26
35	0.38	< 30	152
36	0.4	< 30	66
37	0.29	30	35

. APPENDIX C

SOXHLET EXTRACTION, GAS CHROMATOGRAPHS,

AND HYDROCARBON GAS PHASE ANALYSIS

Partially published in Utah Geological Survey, 2010, Open-File Report 561
Gregory B. Nielsen and Marjorie A. Chan

Table C.1

Soxhlet extraction yields for bleached and unbleached samples from the Navajo Sandstone and underlying Kayenta Formation

#	Formation	Sample Description	Rock (g)	Extract (g)	Yield (mg/g)	Yield (wt%)
1	Navajo Ss.	Uniform reddish sandstone.	137.8802	0.0006	0.004	0.0004
2	Navajo Ss.	White bleached sandstone	221.3850	0.0016	0.007	0.0007
3	Navajo Ss.	White bleached sandstone (surficial alteration to gray)	65.4970	0.0006	0.009	0.0009
4	Navajo Ss.	White bleached sandstone	158.4657	0.0039	0.025	0.0025
5	Navajo Ss.	White bleached sandstone (surficial alteration to gray)	218.0183	0.0033	0.015	0.0015
6	Navajo Ss.	Yellow/white bleached sandstone	193.7021	0.0018	0.009	0.0009
7	Kayenta Fm.	Uniform reddish sandstone.	170.1763	0.0018	0.011	0.0011
8	Kayenta Fm.	Partially bleached red and white siltstone	171.7691	0.0032	0.019	0.0019
9	-	Laboratory blank	-	0.0002	-	-
10	-	Laboratory blank	-	0.0000	-	-

Extraction performed using methylene chloride solvent. Small amounts of unidentified organic material was extracted from all samples (both bleached and unbleached), but yields are very low.

Figure C.1
Gas chromatographs for organic compounds extracted from samples from the Navajo Sandstone and Kayenta Formation at Snow Canyon SP (pA = electrical response in picoamps and min = time in minutes). Analyses by the Energy and Geoscience Institute at the University of Utah. Signatures have n-alkane peaks that may be associated with thermogenic hydrocarbon, but these are largely masked by other signatures that likely represent recent environmental and/or human organic contaminants. If degraded hydrocarbon is present, it likely occurs across facies and only in trace amounts. (A) Sample 1 - uniform reddish Navajo Sandstone with surficial alteration to gray (sample 1). (B) Sample 2 – white bleached Navajo Sandstone. (C) Sample 3 - white bleached Navajo Sandstone with surficial alteration to gray. (D) Sample 4 - white bleached Navajo Sandstone. (E) Sample 5 - white bleached Navajo Sandstone with surficial alteration to gray. (F) Sample 6 - yellow/white bleached Navajo Sandstone. (G) Sample 7 - uniform reddish Navajo Sandstone. (H) Sample 8 - partially bleached red and white siltstone from the Kayenta Formation. (I) Sample 9 laboratory blank. (J) Sample 10 laboratory blank.

A.

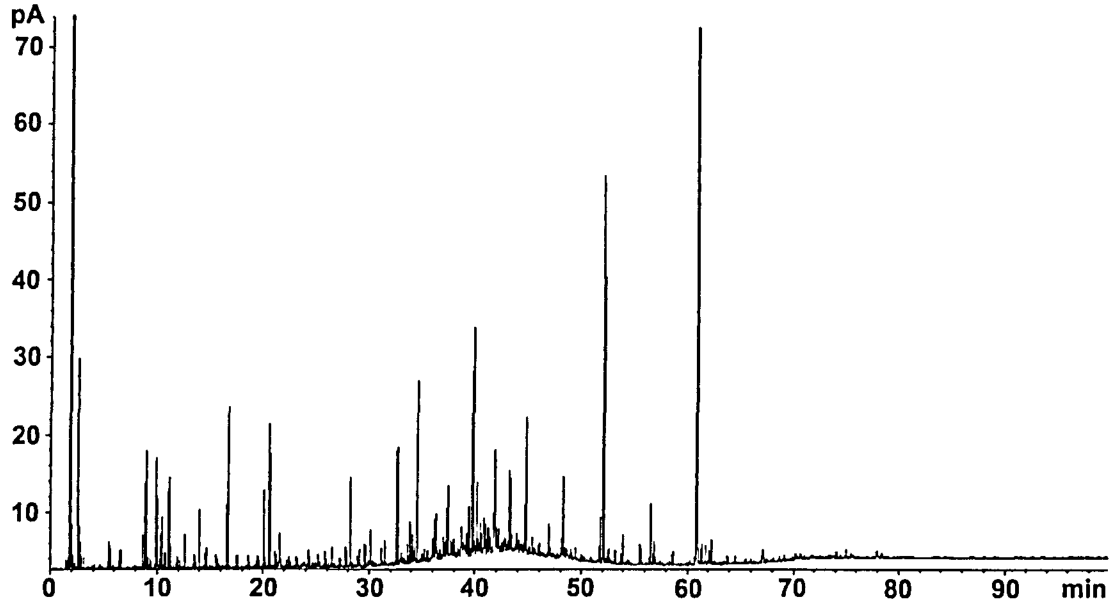
pA
70
60
50
40
30
20
10
0
10
20
30
40
50
60
70
80
90
min

B.

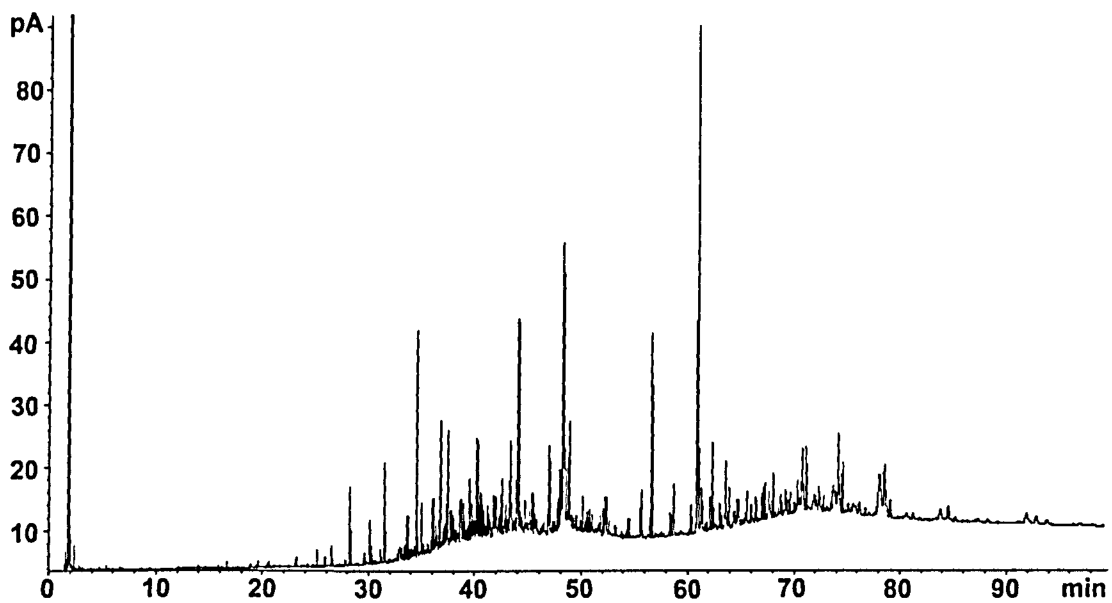
pA
80
70
60
50
40
30
20
10
0
10
20
30
40
50
60
70
80
90
min

C.

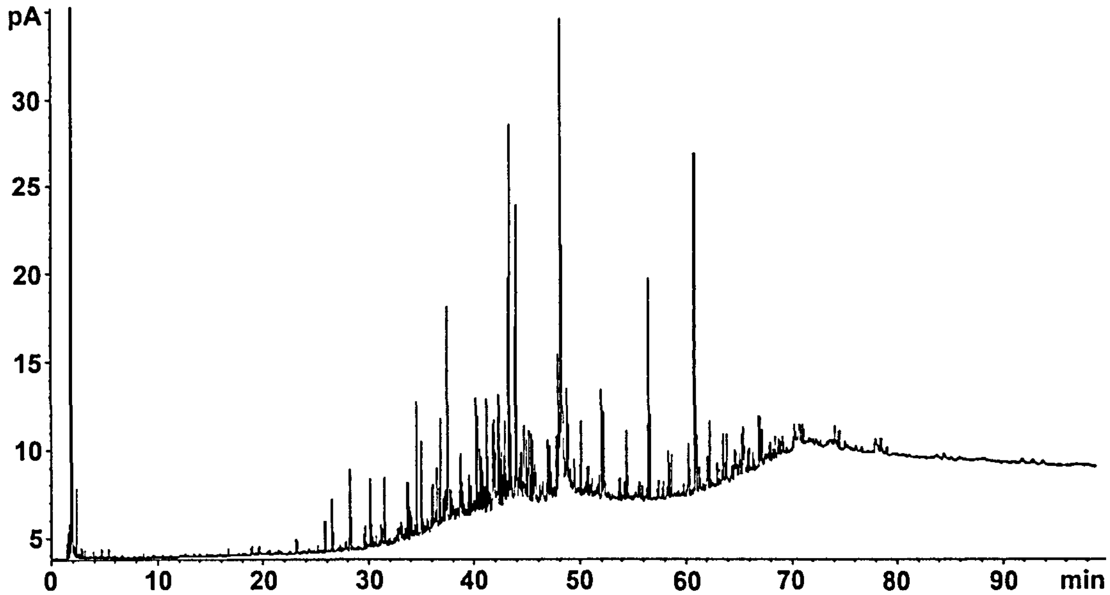

D.

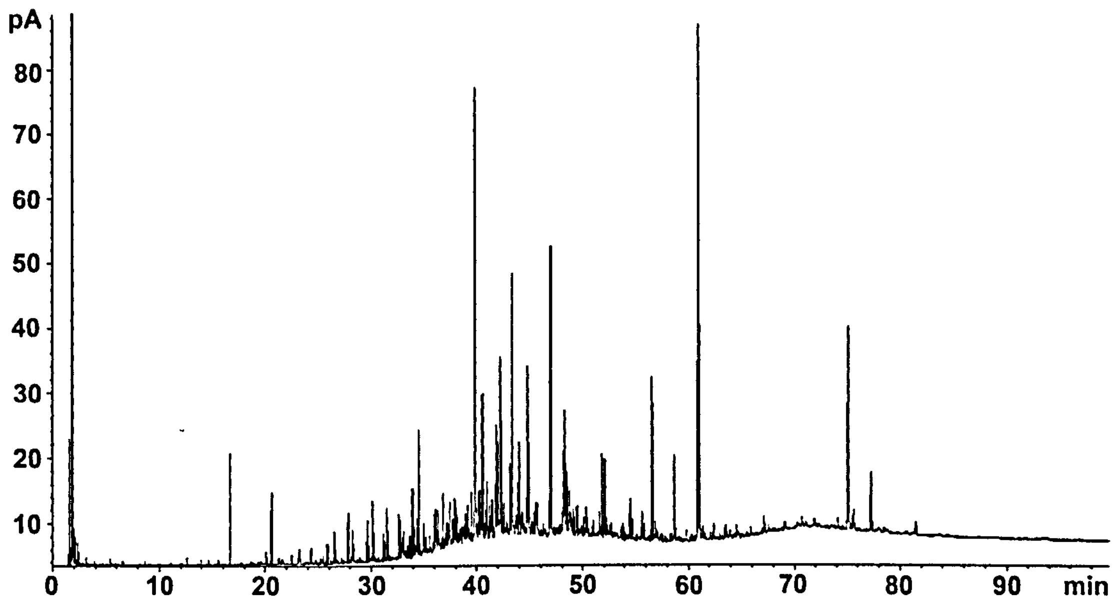

Figure C.1 continued

E.

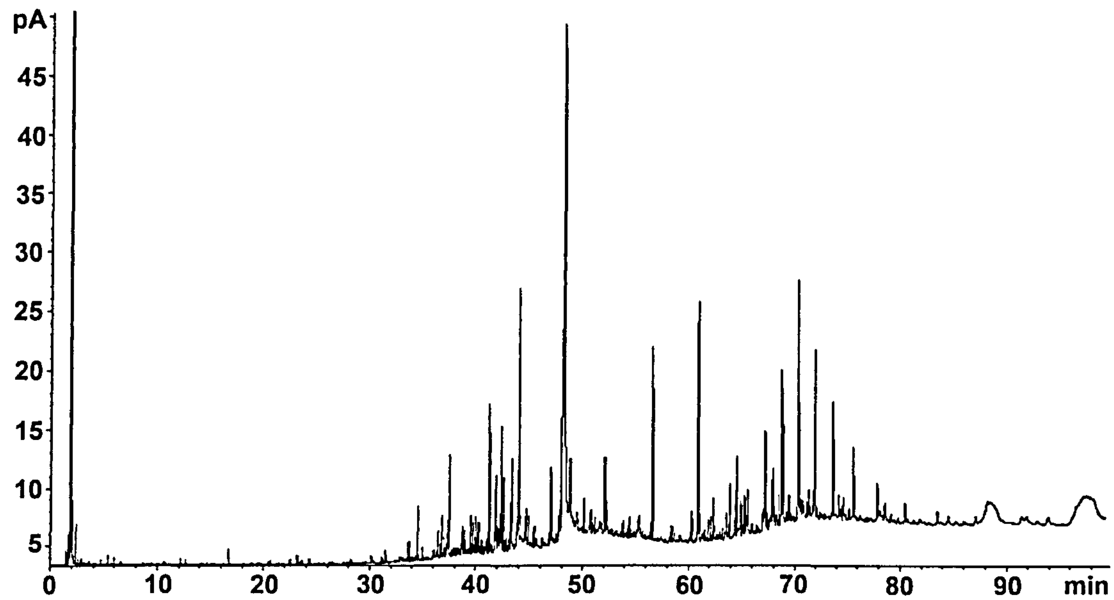

F.

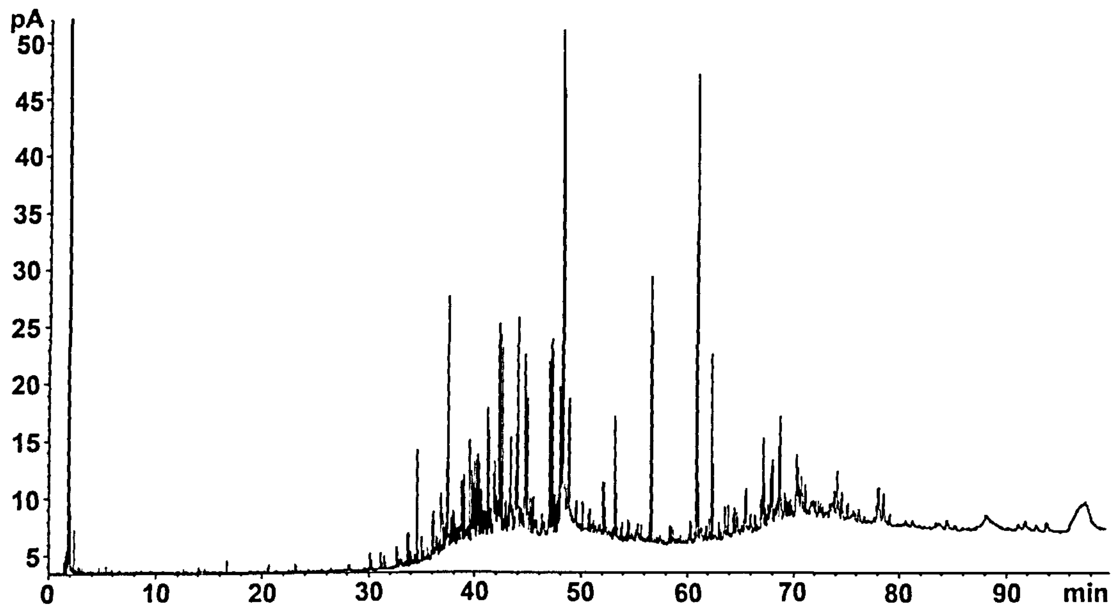

Figure C.1 continued

G.

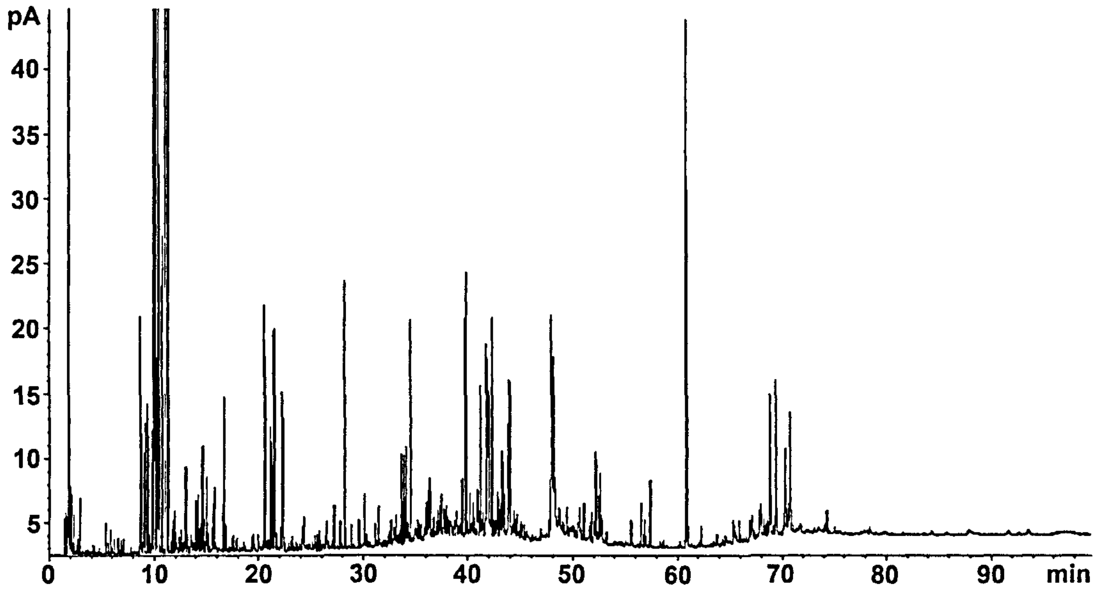

H.

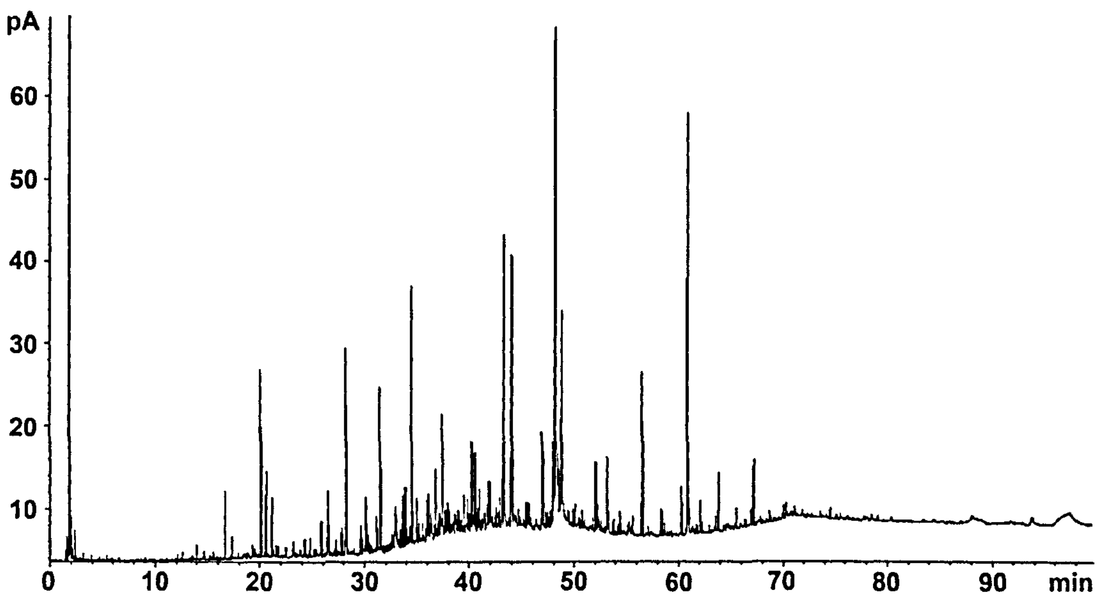

Figure C.1 continued

I.

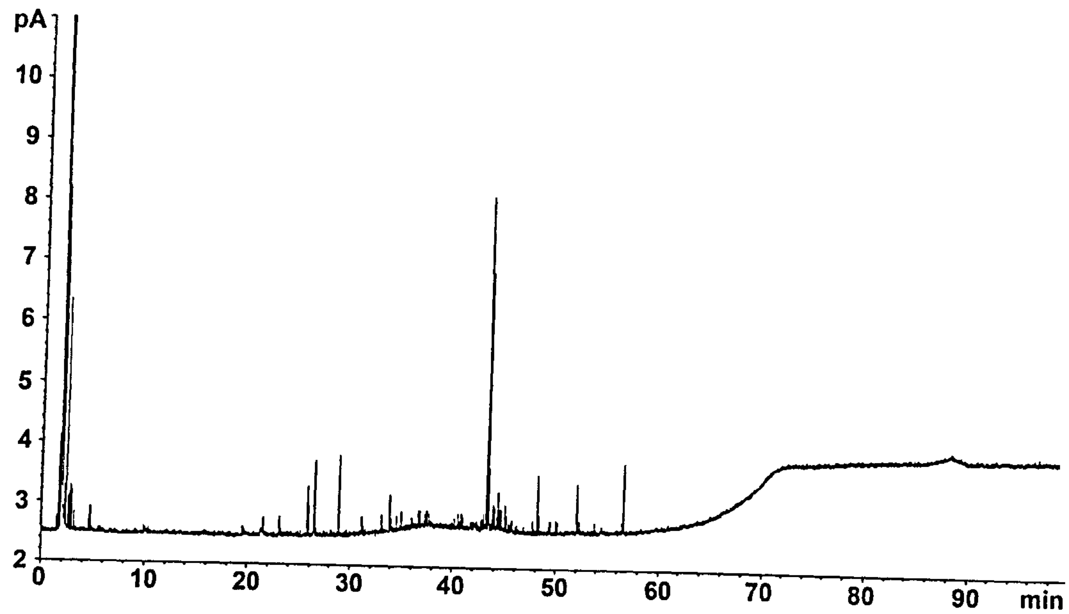

J.

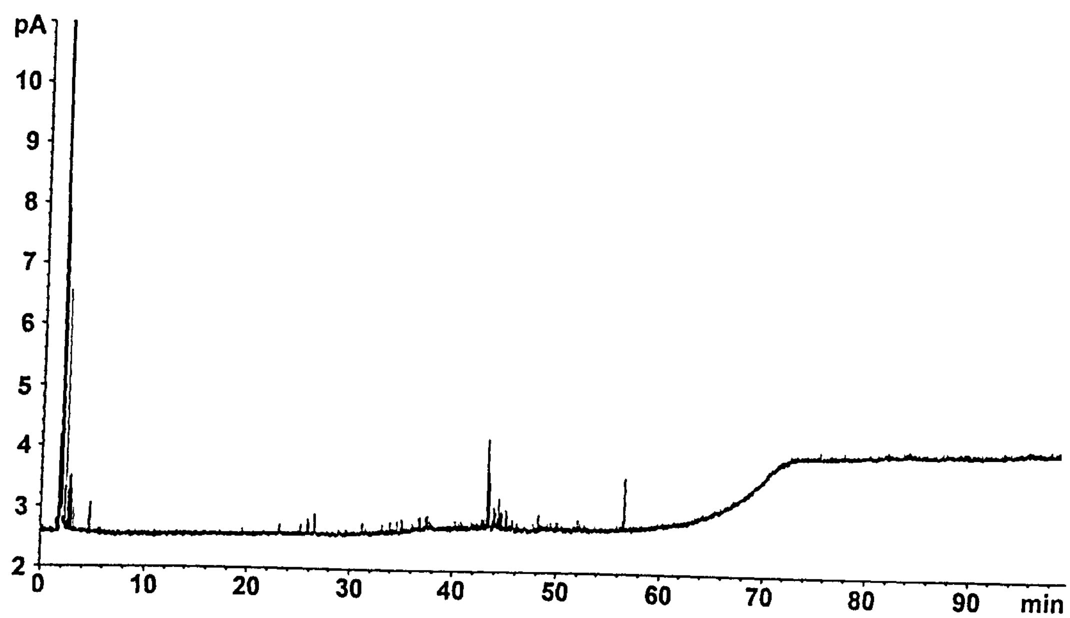

Figure C.1 continued

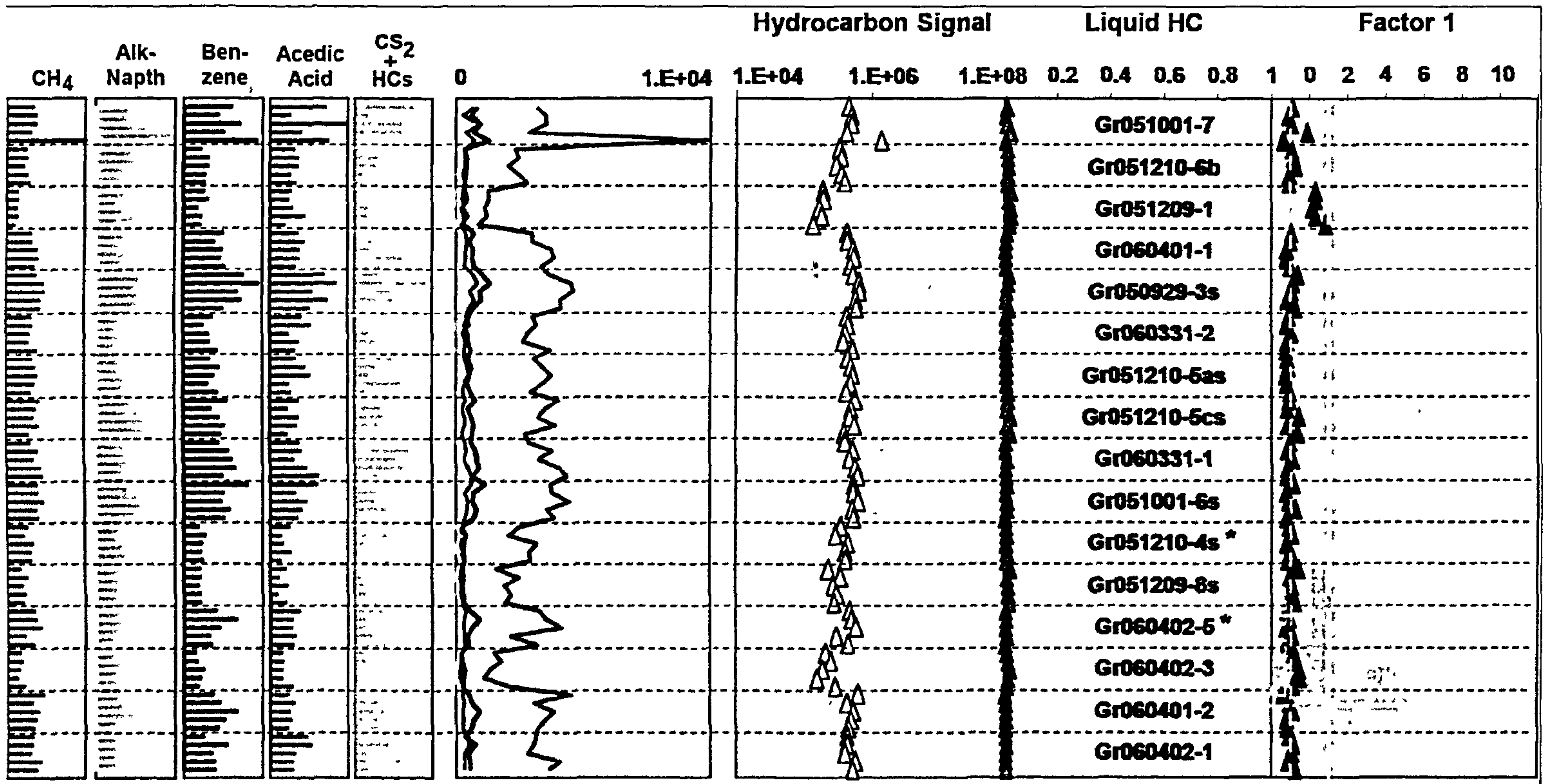

Figure C.2
Hydrocarbon gas phase analysis of 16 variably colored Navajo Sandstone samples (80 total analyses) from the Snow Canyon SP area. Data courtesy of David A.Wavrek, of Petroleum Systems International, Inc (Wavrek et al., 2004). Panel 1 shows signals for five key indicators with each track at full scale. Values for the indicators are normalized in panel 2. The strongest signals across samples were produced by methane. Panel three shows that the overall hydrocarbon signal is low to very low with minor concentrations of hydrocarbon that occurs as dry gas.

References

Wavrek, D.A., Coleman, D., Pelphrey, S., Hall, D., Tobey, M., and Jarvie, D.M., 2004, Got gas? Innovative technologies for evaluating complex reservoir zones: American Association of Petroleum Geologists Bulletin, v. 13, p.145.

APPENDIX D

BLEACHING RELATIONSHIPS

AT ZION NATIONAL PARK

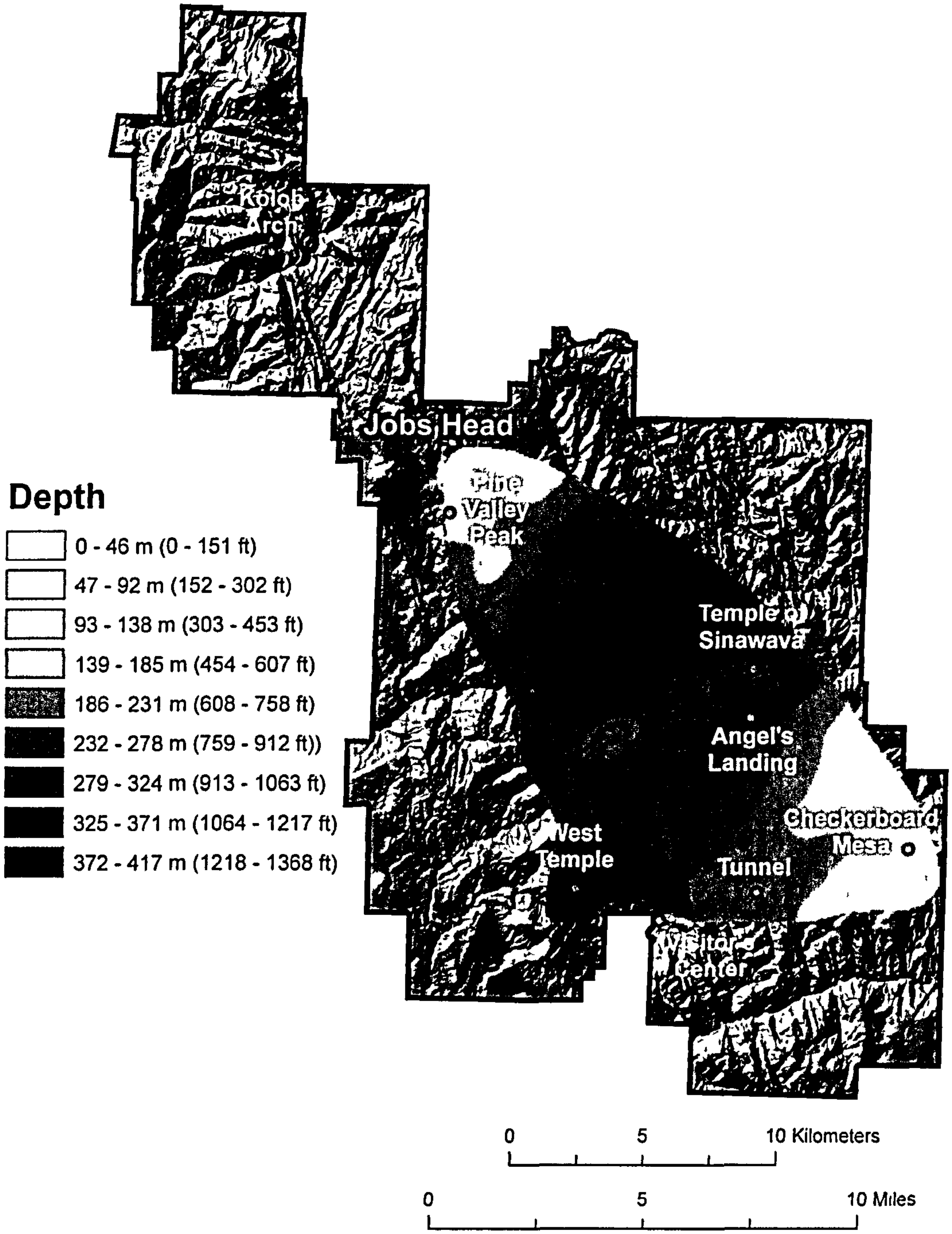

Figure D.1

Depth to which bleached rock extends in the upper part of the Navajo Sandstone at Zion NP. Measured as the depth of the boundary between the pink and white diagenetic coloration facies below the calculated trend surface for the top of the Navajo Sandstone. Kriging surface generated using ESRI ArcMap (n=1130; S_{est} = 14 m). Note that the base of bleaching becomes shallower and then pinches out in the Pine Valley peak area.

Figure D.2

Views of the subtle pattern of increasing diagenetic alteration moving southward through Zone 2 in Zion NP (Fig. 2.1). (A) Northern part of zone is characterized by uniform reddish coloration (1) with faint, isolated bleaching bands (2 and 3). Locality: Kolob Canyons. (B) Middle of zone has relatively even pigmentation in the upper part of the formation (4) and uneven coloration with localized bleaching in the lower formation (5). Locality: La Verkin Creek Canyon near Kolob Arch. (C). Southern zone displays uneven, patchy coloration throughout the unit (6). Locality: Jobs Head. (7) The White Throne Member of the Temple Cap Formation in Zone 2 has a reddish brown color (Fig. 2.19B).


A
1
2
3
4
5
C
6
7

APPENDIX E

DATA AND FIGURES FOR THE JURASSIC KAYENTA AND TEMPLE CAP FORMATIONS

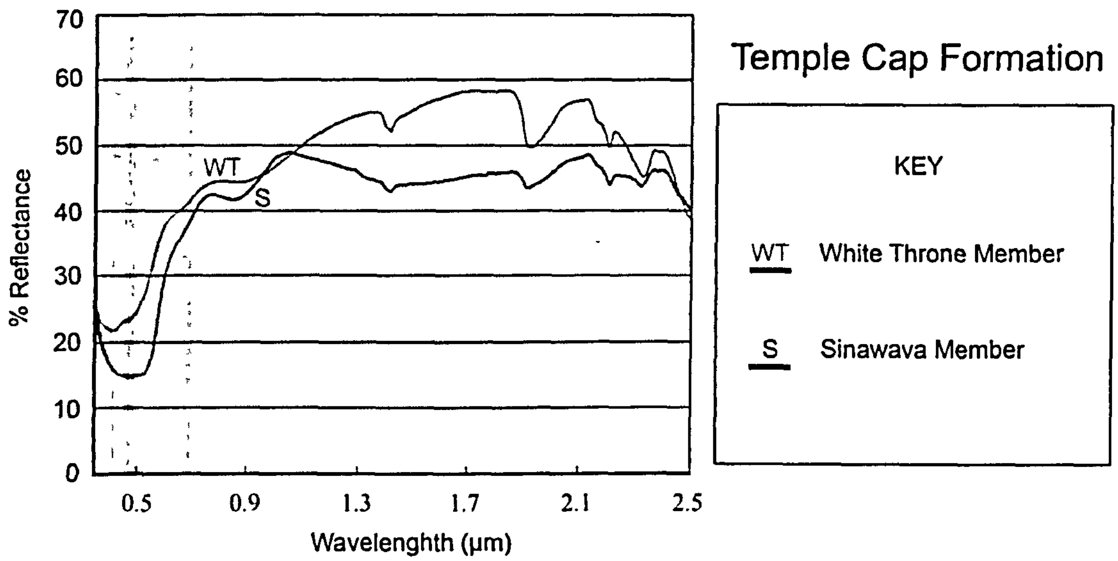

Figure E.1
Visible and infrared reflectance spectroscopy for the Temple Cap formation. Samples were evaluated in the lab using artificial illumination. Strong absorption near 0.9 μm for the Sinawava member is indicative of iron oxide, which also occurs in the White Throne member but at lower concentrations. Absorption at approximately 2.3 μm represents carbonate which is abundant in the formation (Clark et al., 2007).

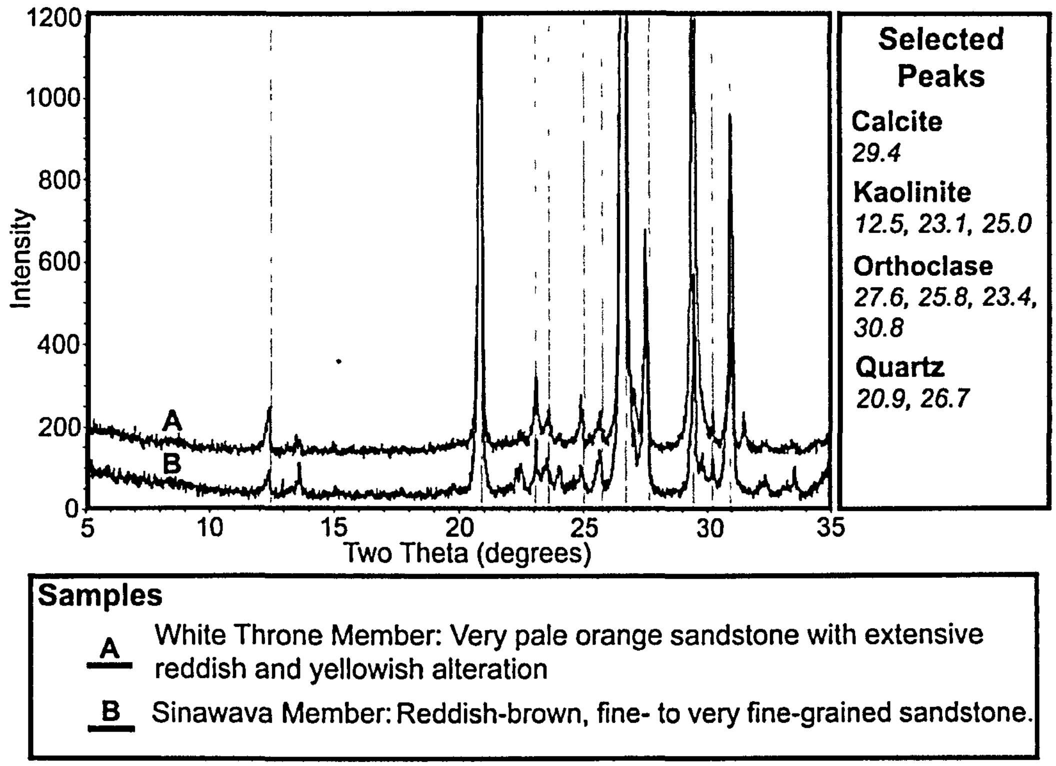

Figure E.2

Superimposed X-Ray Diffraction (XRD) patterns for the Sinawava (lower) and White Throne (upper) members of the Temple Cap Formation. Intensity patterns have been artificially offset by 100 units to separate them visually.

Table E.1

Bulk composition (ICP-MS) for samples from the Kayenta and Temple Cap Formations.

#	Formation	Member	Locality	Area	Specimen ID	Brief Description
38	Kayenta Formation	-	Snow Canyon SP	Padre Canyon.	Gr20051209-1b	Unbleached red siltstone.
39	Kayenta Formation	-	Snow Canyon SP	Padre Canyon	Gr20051209-1a	Bleached pale green siltstone.
40	Temple Cap Fm	Sinawava	Zion NP	East Rim Trail	Gr20061214-1625	Reddish-brown sandstone.
41	Temple Cap Fm	White Throne	Zion NP	East Rim Trail	Gr20061214-1626	Multicolored sandstone.

Table E.1 continued

#	Fe_2O_3(T) %	MnO %	MgO %	CaO %	Na_2O %	K_2O %	TiO_2 %	P_2O_5 %	LOI %	Oxide Total %	Ag ppm	As ppm	Ba ppm	Be ppm	Bi ppm
38	1.72	0.03	2.99	3.52	0.15	2.52	0.47	0.11	7.48	99.87	< 0.5	5.00	300.00	< 1	1.10
39	0.43	0.06	3.19	4.13	0.14	2.37	0.35	0.09	7.86	99.95	< 0.5	5.00	308.00	< 1	0.60
40	1.13	0.049	2.46	5.97	0.08	2.41	0.095	0.07	8.05	99.15	< 0.5	< 5	283	< 1	< 0.1
41	0.69	0.037	2.12	11.72	0.08	1.23	0.046	0.04	12.15	100.3	< 0.5	< 5	195	< 1	< 0.1

Table E.1 continued

#	Co ppm	Cr ppm	Cs ppm	Cu ppm	Dy ppm	Er ppm	Eu ppm	Ga ppm	Gd ppm	Ge ppm	Hf ppm	Ho ppm	In ppm	La ppm	Lu ppm	Mo ppm	Nb ppm
38	3.00	30.00	4.10	< 10	3.08	1.96	0.68	7.00	3.04	1.00	11.80	0.63	< 0.1	17.50	0.33	< 2	7.00
39	12.00	< 20	3.30	< 10	2.24	1.38	0.60	6.00	2.48	1.00	9.20	0.45	< 0.1	13.40	0.25	< 2	5.30
40	3	< 20	1.4	< 10	1.11	0.7	0.367	5	1.17	1.1	2.2	0.23	< 0.1	6.76	0.115	< 2	1.8
41	1	100	0.8	10	0.6	0.39	0.211	3	0.64	0.8	1.8	0.13	< 0.1	4.12	0.068	< 2	0.9

Table E.1 continued

#	Ni ppm	Pb ppm	Pr ppm	Rb ppm	Sb ppm	Sc ppm	Sm ppm	Sn ppm	Sr ppm	Ta ppm	Tb ppm	Th ppm	Tl ppm	Tm ppm	U ppm	V ppm	W ppm
38	< 20	12.00	4.11	63.00	< 0.2	5.00	3.11	< 1	87.00	0.63	0.52	4.87	0.36	0.32	1.99	35.00	0.80
39	< 20	12.00	3.33	61.00	1.00	4.00	2.68	< 1	76.00	0.49	0.39	3.79	0.46	0.22	1.94	17.00	0.50
40	< 20	7	1.53	51	< 0.2	2	1.21	2	43	0.18	0.2	1.91	0.26	0.109	0.36	8	2.3
41	< 20	< 5	0.89	28	< 0.2	< 1	0.71	2	40	0.09	0.1	0.91	0.15	0.061	0.31	7	1.1

Table E.1 continued

#	Yb ppm	Zn ppm	Zr ppm
38	2.16	< 30	472.00
39	1.50	40.00	371.00
40	0.74	< 30	91
41	0.42	< 30	72

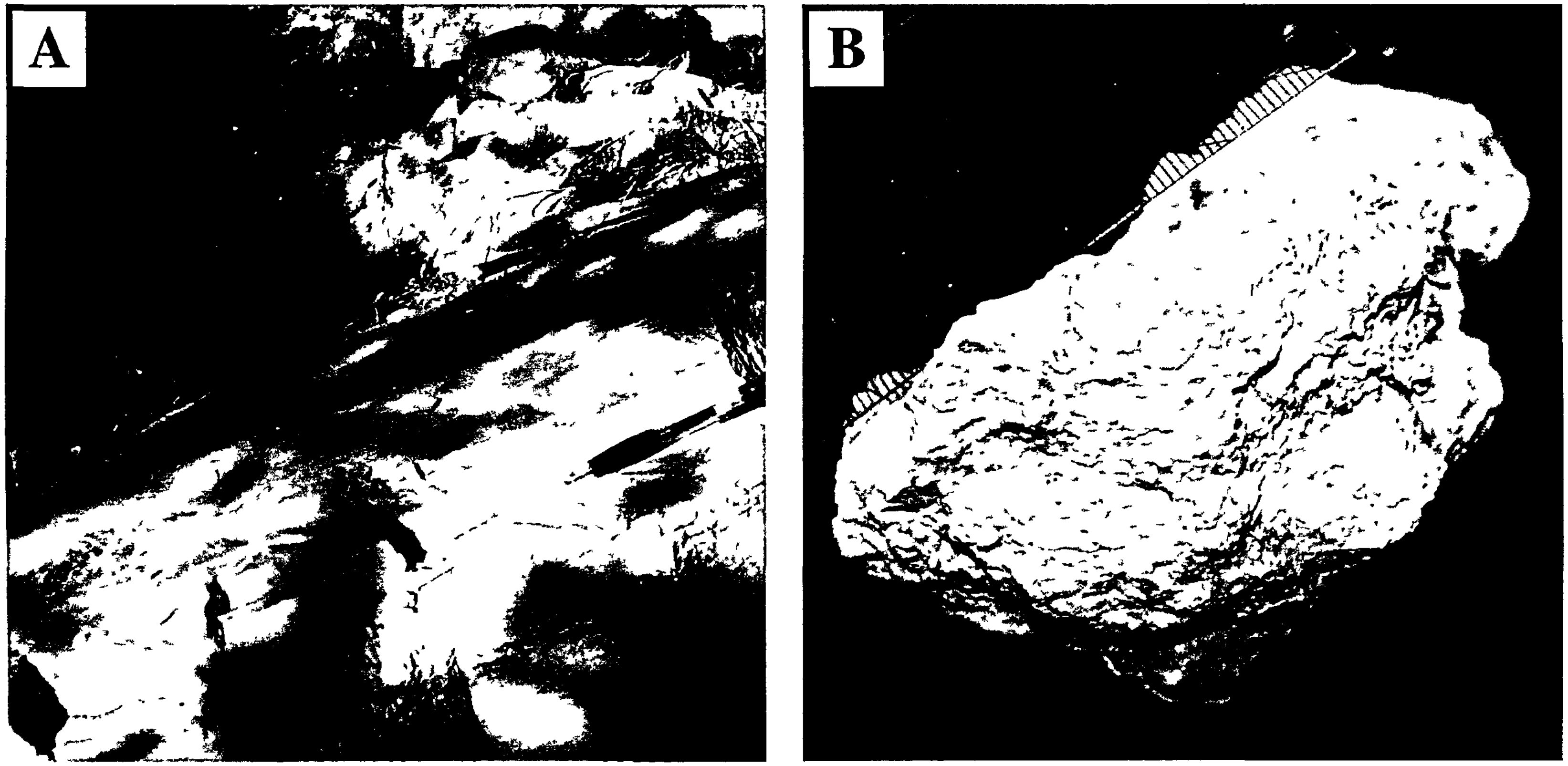

Figure E.3
Bleaching of the Lower Jurassic Kayenta formation of Padre Canyon at Snow Canyon SP (Fig. 3.4). (1) Narrow zone of bleached sandstone follows primary bedding. (B) Reduction spots (~ 1 cm in diameter) have a pale greenish-yellow color. Reduction spots are common in the Kayenta Formation of Padre Canyon but were not observed in the overlying Navajo Sandstone.

References

Clark, R.N., Swayze, G.A., Wise, R., Livo, E., Hoefen, T., Kokaly, R., Sutley, S.J., 2007, U.S. Geological Survey digital spectral library splib06a: U.S. Geological Survey, Digital Data Series 231. <http://speclab.cr.usgs.gov/spectral-lib.html> [accessed 8/30/2007]

APPENDIX F

MINERALOGY AND IMAGES OF OVERPRINTED SANDSTONE FOR SNOW CANYON STATE PARK

Partially published in Utah Geological Survey, 2010, Open-File Report 561
Gregory B. Nielsen and Marjorie A. Chan

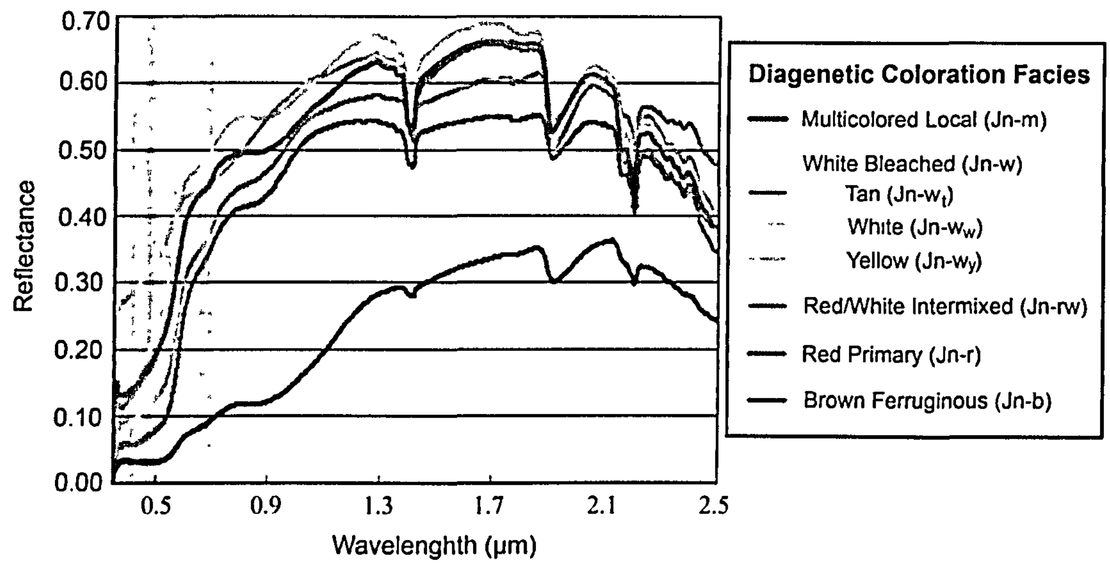

Figure F.1

Composite visible and infrared reflectance spectroscopy for each diagenetic coloration facies at Snow Canyon SP (n = 53 variably colored samples). Samples were evaluated in the field using a portable reflectance spectrometer. Artificial illumination was used to provide consistency and eliminate atmospheric effects. Strong absorption near 0.9 µm is indicative of iron oxide. The absorption band at 2.2 µm is typical of clay minerals with the doublet indicating the mineral kaolinite. Prominent bands near 1.4 µm and 1.9 µm are also characteristic of clays. The overall similarity in reflectance patterns indicates similar mineralogy, whereas differences in band depth reflect variations in the abundance and spatial distribution of these minerals.

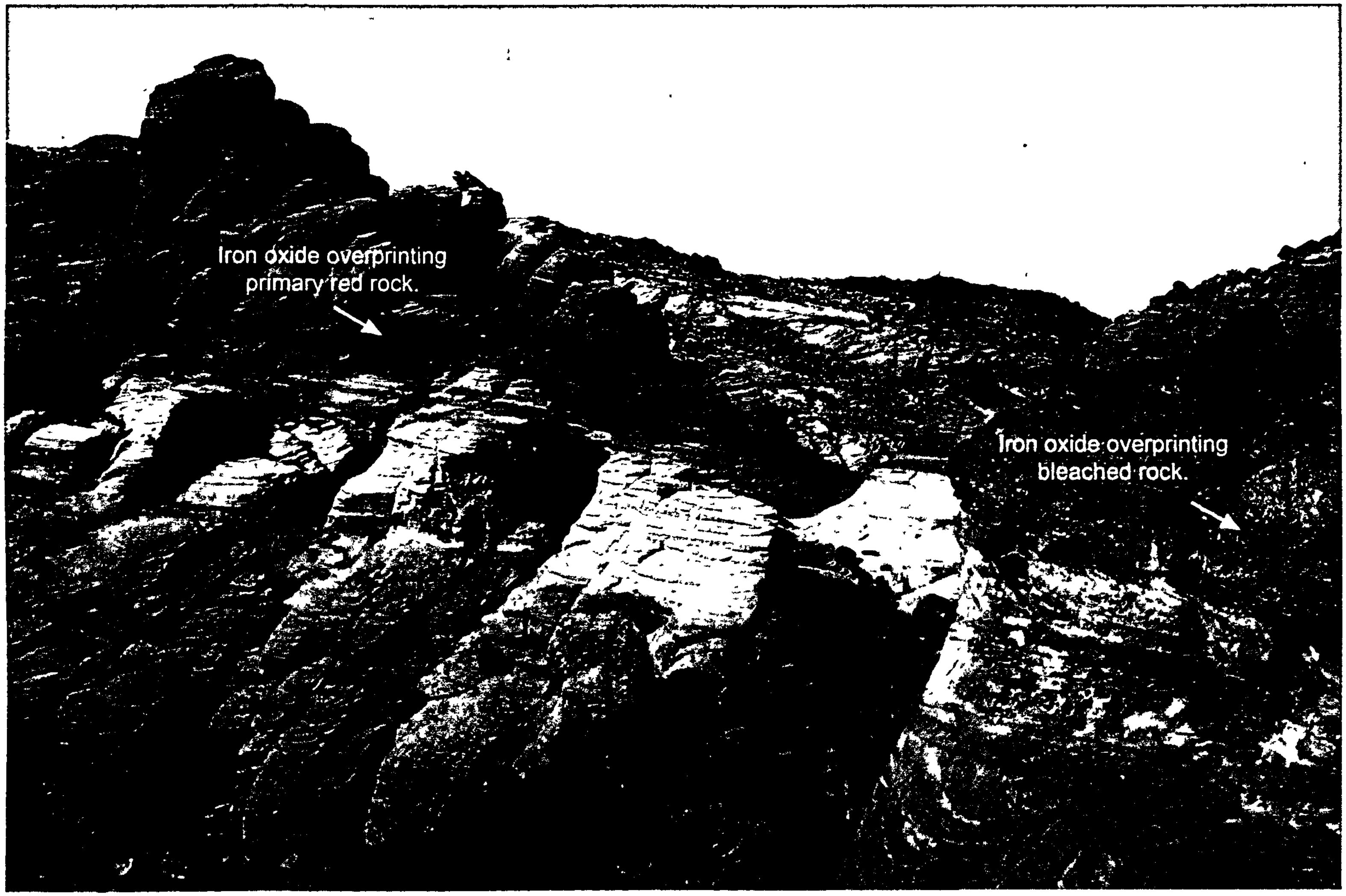

Figure F.2
Dark-colored iron and manganese oxide cement overprints both unbleached and bleached Navajo Sandstone at Snow Canyon SP (SR-18 trailhead). Black basalt caps ridges and occurs as large blocks in the ravine.

Figure F.3
Bright secondary coloration overprints bleached rock near the West Canyon lineament at Snow Canyon SP (Fig. 3.4).
Author in foreground.

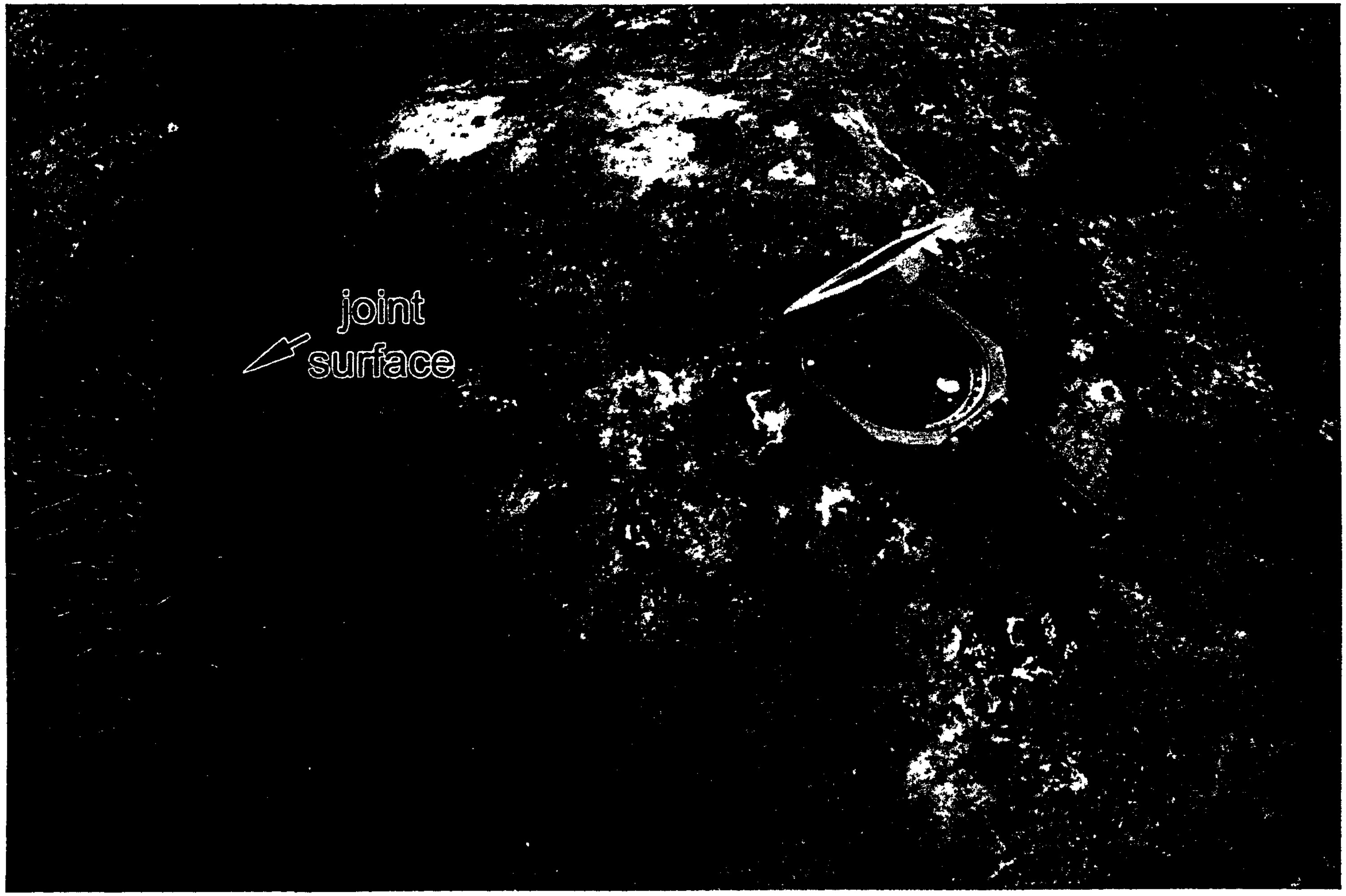

Figure F.4
Detail of joint-controlled cementation and bright secondary coloration near location 4 in Fig. 3.4. Joint surface is coated with a thin coat of dark-colored iron or manganese oxide.

APPENDIX G

COMPARISONS BETWEEN IRON OXIDE CEMENTATION FEATURES IN SOUTHWESTERN UTAH AND SIMILAR DIAGENETIC FEATURES ON MARS

Initial remote detection of hematite by the Mars Global Surveyor at Meridiani Planum on Mars was followed in 2004 by the discovery of small (~1-5 mm) hematite spherules on the surface by the Opportunity rover (Christensen et al., 2000; Squyres et al., 2004). Chemical modeling and comparison with terrestrial analogs suggests they are concretions similar to those in the Navajo Sandstone, and were also produced by fluid-related diagenesis (Chan et al., 2004; Chan et al., 2007; Golden et al., 2007). Like concretions on Earth, those on Mars occur scattered across the surface as lag deposits as well as in situ within nearby outcrops of dominantly eolian sandstone (the Burns Formation, Grotzinger et al., 2005). Despite these similarities, the Burns Formation differs from the Navajo Sandstone in that it is sourced by basalts and sulfate-rich evaporites and was likely saturated with saline brines (Grotzinger et al., 2005). Thermal emission spectrometry indicates that hematite on Mars is widely distributed within a sedimentary unit covering ~300,000 km^2 at Meridiani Planum (Christensen et al., 2001; Hynek, 2004), much larger than the 150+ km^2 estimated extent of concentrated iron oxide cementation in SW Utah. Interpretations based on the nature and distribution of hematite deposits on Mars should be viewed as tentative: as of early 2009 the Opportunity rover had travelled a total distance of ~15 km and the best vertical outcrop exposures encountered thus far (in Victoria Crater) have thicknesses of less than ~30 m.

Hematite concretions in the Burns Formation are postulated to have formed in the phreatic zone during periods of groundwater recharge. In contrast to the Navajo Sandstone where iron may have been transported for substantial distances, iron on Mars was likely produced in situ by breakdown of ferric iron sulfate (jarosite) under fairly stagnant hydrodynamic conditions (Squyres and Knoll, 2005; Marion et al., 2006). Precipitation is believed to have occurred as a result of the mixing of this acid-saline brine with higher pH/more oxidizing fluid introduced into the system through groundwater recharge (McLennan et al., 2005). Unlike the distinct cementation zones that occur in the Navajo Sandstone of SW Utah, concretions imaged in the Burns Formation thus far are dispersed throughout most of the formation. Although the size and concentration of these concretions varies by both locality and stratigraphic level, the distribution is relatively unaffected by bedding and facies boundaries (Squyres et al., 2004; McLennan et al., 2005; Squyres et al., 2007). This may reflect precipitation in relatively shallow sediment that was still unlithified and poorly compacted (Bowen et al., 2008), similar to the high-permeability conditions in which iron oxide became uniformly distributed throughout the Navajo Sandstone to form primary grain coats. In contrast, secondary ferruginized horizons in the Navajo Sandstone likely precipitated in indurated bedrock within a deeper subsurface setting.

The diagenetic history of the Burns Formation encompasses multiple episodes of groundwater recharge with both depositional and diagenetic features having a possible relationship to water table fluctuations (Grotzinger et al., 2005; McLennan et al., 2005). Within Endurance crater, water table level is postulated as a possible control for both a deflation surface that separates the lower and middle units (the Wellington contact [Grotzinger et al., 2005]) and a planar zone of recrystallized evaporite cement that forms a diagenetic boundary between the middle and upper units (the Whatanga contact [Grotzinger et al., 2005]). Iron oxide concretions overprint deposits of all three Burns subunits and extend to the top of the bedrock section, indicating that precipitation must have occurred during a period of high regional groundwater level (Grotzinger et al., 2005). Although the evaporitic mineralogy of the Whatanga contact differs from that of iron oxide horizons in the Navajo Sandstone, its planar geometry, subhorizontal orientation, concentrated area of cementation directly below the boundary, and sharp upper contact with overlying lighter-colored sandstone strongly resemble cementation horizons in the Navajo Sandstone (Fig. 4.11; compare with Figs. 4.4C-D, 4.5, 4.10). These similarities may warrant further examination of how cementation horizons form and their potential correlation with groundwater fluctuations.

Figure G.1
Cropped and split panorama of the diagenetic Whatanga contact (arrows) in the Burns Formation on Mars. Imaged by the NASA Opportunity Rover (sol 287 to 294, approximate true-color rendering combining Pancam with 430 nm, 530 nm, and 750 nm filters, viewed spans ~140°). This contact is interpreted by Grotzinger (2005) as a diagenetic reaction front boundary produced at or near the water table. Although mineralogy differs (not iron oxide), geometry and other characteristics are similar to reaction front horizons in the Navajo Sandstone (e.g. Figs. 4.4B and 4.10). Adapted from composite panoramic image by NASA / JPL / Cornell (marsrovers.jpl.nasa.gov).

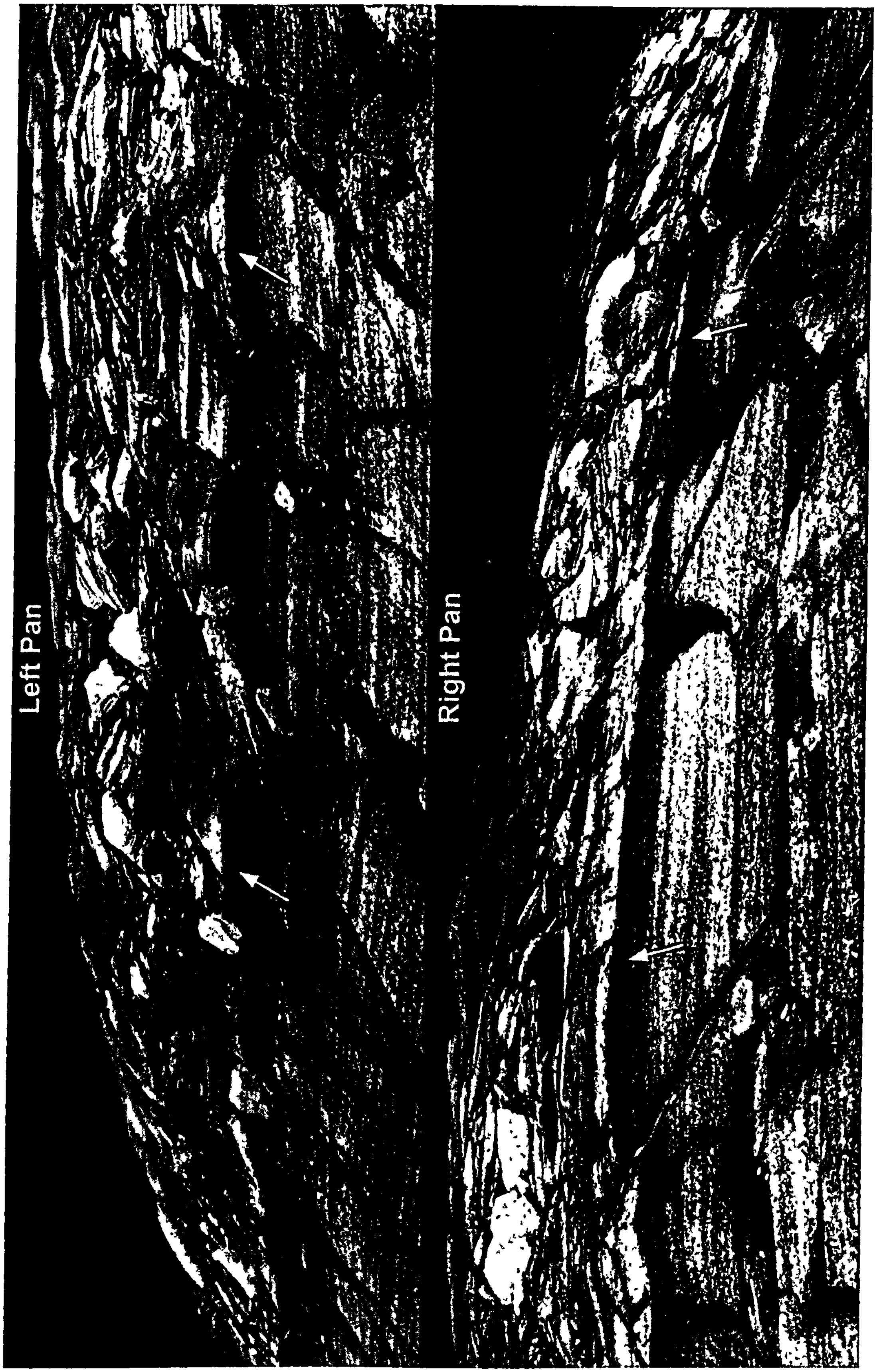
Left Pan
Right Pan

References

Bowen, B.B., Benison, K.C., Oboh-Ikuenobe, F.E., Story, S. and Mormile, M.R., 2008, Active hematite concretion formation in modern acid saline lake sediments, Lake Brown, Western Australia: Earth and Planetary Science Letters, v. 268, p.52-63.

Chan, M.A., Beitler B., Parry W.T., Ormo, J., and Komatsu, G., 2004, A possible terrestrial analogue for hematite concretions on Mars: Nature, v. 429, p. 731–734.

Chan, M.A., Ormo, J., Park, A.J., Stich, M., Sousa-Egipsy, V., and Komatsu, G., 2007, Models of iron oxide concretion formation: field, numerical, and laboratory comparisons: Geofluids v. 7, p. 356–368.

Christensen, P.R., Bandfield, J.L., Clark, R.N., Edgett, K.S., Hamilton, V.E., Hoefen, T., Kieffer, H.H., Kuzmin, R.O., Lane, M.D., Malin, M.C., Morris, R.V., Pearl, J.C., Pearson, R., Roush, T.L., Ruff, S.W., and Smith, M.D., 2000, Detection of crystalline hematite mineralization on Mars by the Thermal Emission Spectrometer: Evidence for near-surface water: Journal of Geophysical Research, v. 105, p. 9623–9642.

Christensen, P. R., Morris, R.V., Lane, M.D., Bandfield, J.L., and Malin, M.C., 2001, Global mapping of Martian hematite mineral deposits: Remnants of water-driven processes on early Mars: Journal of Geophysical Research, v. 106, p. 873-885.

Golden, D.C., Ming, D.W., Morris, R.V., Graff, T.G., 2007, Hydrothermal synthesis of hematite rich spherules: implications for diagenesis and hematite spherule formation in outcrops at Meridiani Planum, Mars: Lunar and Planetary Science XXXVIII, Abstract 2257.

Grotzinger, J.P., Arvidson, R.E., Bell, J.F., III, Calvin, W., Clark, B.C., Fike, D.A., Golombek, M., Greeley, R., Haldemann, A., Herkenhoff, K.E., Jolliff, B.L., Knoll, A.H., Malin, M., McLennan, S.M., Parker, T., Soderblom, L., Sohl-Dickstein, J., Squyres, S.W., Tosca, N.J., and Watters, W.A., 2005, Stratigraphy and sedimentology of a dry to wet eolian depositional system, Burns Formation, Meridiani Planum, Mars: Earth and Planetary Science Letters, v. 240, p. 11–72.

Hynek, B.M., 2004, Implications for hydrologic processes on Mars from extensive bedrock outcrops throughout Terra Meridiani: Nature, v. 431, p. 156-159.

Marion, G.M., Kargel, J.S., and Catling, D.C., 2006, Modeling ferrous/ferric iron chemistry with application to Martian surface geochemistry: Lunar and Planetary Science, v. 37, Abstract 1898.

McLennan, S.M., and 31 others, 2005, Provenance and diagenesis of the evaporite-bearing Burns formation, Meridiani Planum, Mars: Earth and Planetary Science Letters. v. 240, p. 95-121.

Squyres, S.W., Grotzinger, J.P., Arvidson, R.E., Bell III, J.F., Calvin, W., Christensen, P.R., Clark, B.C., Crisp, J.A., Farrand, W.H., Herkenhoff, K.E., Johnson, J.R., Klingelhöfer, G., Knoll, A.H., McLennan, S.M., McSween Jr., H.Y., Morris, R.V., Rice Jr., J.W., Rieder, R. and Soderblom, L.A., 2004, In situ evidence for an ancient aqueous environment at Meridiani Planum, Mars: Science, v. 306, p. 1709-1714.

Squyres, S.W., Knoll, A.H., 2005, Sedimentary rocks at Meridinai Planum: origin, diagenesis, and implications for life on Mars. Earth Planetary Science Letters, v. 240, p. 1–10.

Squyres, S.W., and many others, 2007, Recent results from the Mars Exploration Rover Opportunity at Victoria Crater: Houston, Texas, Lunar and Planetary Institute Contribution, Seventh International Conference on Mars, Abstract 3030.

COLOR PLATE A

Geologic map and coloration facies of the Jurassic Navajo Sandstone, Snow Canyon State Park and areas of Red Cliffs Desert Reserve, Washington County, Utah: scale 1:10,000.

Published in Utah Geological Survey, 2010, Open-File Report 561
Gregory B. Nielsen and Marjorie A. Chan
Used with permission.

Letters on map refer to sample locations in Appendix B.

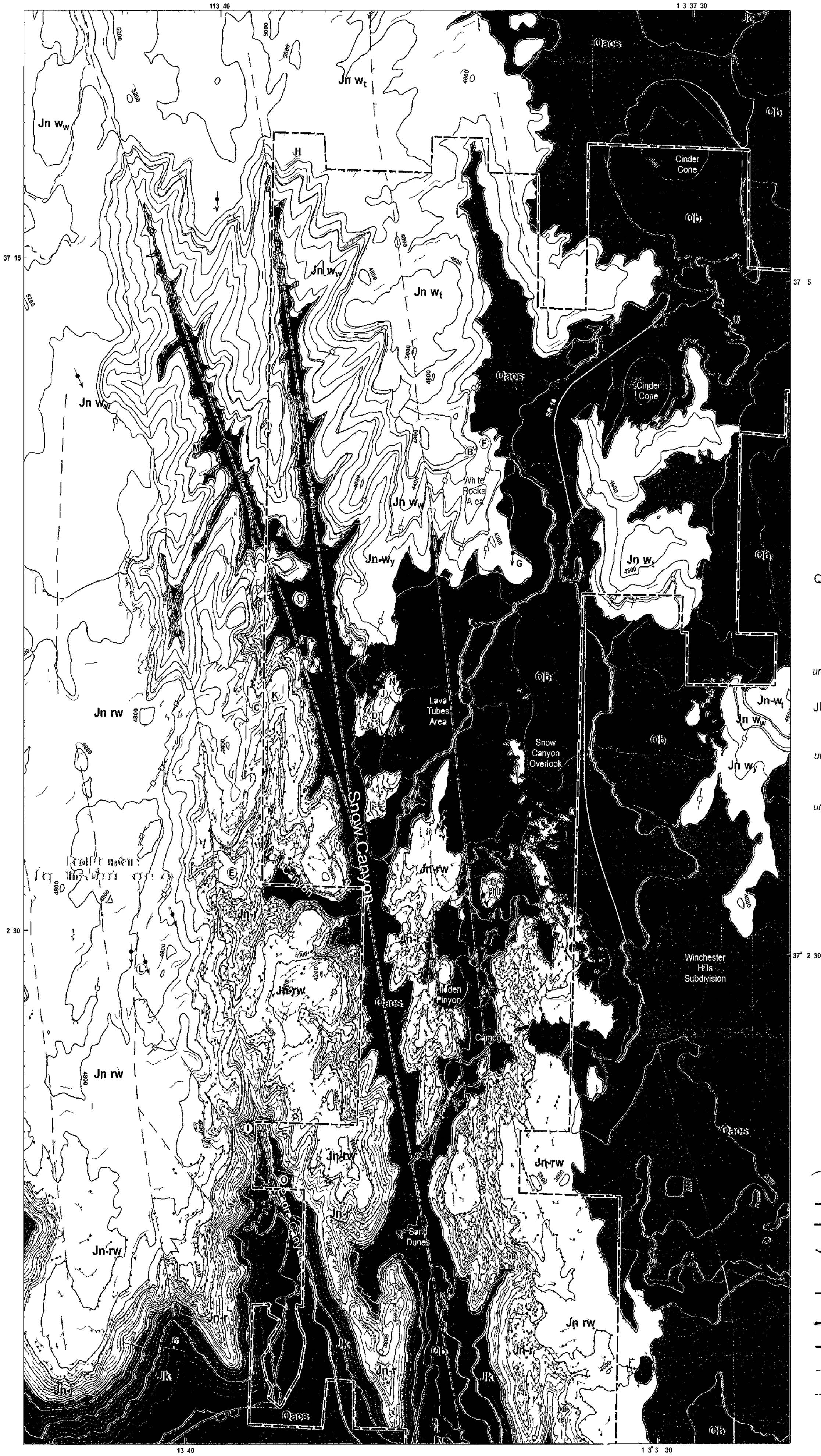

GEOLOGIC MAP AND COLORATION FACIES OF THE JURASSIC NAVAJO SANDSTONE SNOW CANYON STATE PARK AND AREAS OF RED CLIFFS DESERT RESERVE WASHINGTON COUNTY UTAH

2010

by
Gregory B N elsen
and
Marjor e A Chan

Sca e 10 000
heq a appo ma 0 5m e
C o e a 50 ee a d200 e

0 0 5 025 05 0 5 M es

0 0 25 025 05 0 5 K me e

N

UTAH

EXPLANATION

QUATERNARY

Quaternary Alluvium Colluvium Sand

Quaternary Basalts

unconform ty

JURASSIC

Jc Carmel Formation

unconform ty?

Jtc Temple Cap Formation (not exposed in mapped a ea)

unconform ty

Navajo Sandstone

Wh te Bleached Fac es

Jn wt Tan Subfac es

Jn ww Wh te Subfac es

Jn wy Yellow Subfac es

Red/Wh te Interm xed Fac es

Jn rw

Red Pr mary Fac es

Jn r

Brown Fe ruginous Fac es

Jk Kayenta Formation (Uppe Membe)

MAP SYMBOLS

Contact

Strike and Dip of Bedding

Strike of Vertical or Subvertical Joint

Lineament (used for large widely spaced joints or faults)

Eolian Paleocurrent (arrow points in direct on of flow not corrected for regional dip)

State Park Boundary

State Highway

Local Road

Small Road/Subdivision

Ⓐ Sample locations referenced in this report